

Copyright
by
Alejandro Escalona
2003

The Dissertation Committee for Alejandro Escalona Certifies that this is the approved version of the following dissertation:

**Regional Tectonics, Sequence Stratigraphy and Reservoir
Properties of Eocene Clastic Sedimentation, Maracaibo Basin,
Venezuela**

Committee:

William L. Fisher, Supervisor

Paul Mann, Co-Supervisor

William E. Galloway

Robert H. Tatham

Carlos Torres-Verdin

**Regional Tectonics, Sequence Stratigraphy and Reservoir
Properties of Eocene Clastic Sedimentation, Maracaibo Basin,
Venezuela**

by

Alejandro Escalona, B.Sc.

Dissertation

Presented to the Faculty of the Graduate School of

The University of Texas at Austin

in Partial Fulfillment

of the Requirements

for the Degree of

Doctor of Philosophy

The University of Texas at Austin

December, 2003

Dedication

To my wife, Sylvia

To my son and daughter

To my mother, who is always there for me

Acknowledgements

I would like to thank all of those that participated directly or indirectly in the development of this research. First of all I am very grateful to my supervisors: Dr. William Fisher and Dr. Paul Mann for all their guidance, patience and friendship. I also want to thank the rest of my committee members for all the technical support: Dr. William Galloway, Dr. Carlos Torres-Verdin and Dr. Robert Tatham.

I acknowledge Centro Internacional de Educación y Desarrollo (CIED), Petróleos de Venezuela (PDVSA) and the Universidad Central de Venezuela (UCV), in particular to: Maria Josefina Lazo, Inirida Rodriguez, Felipe Audemard and the group of “Estudios Integrados Centro Lago” for their financial support and for providing the data used in this study.

I thank to the UT Department of Geological Sciences and the UT Institute for Geophysics for providing me the facilities to conduct this study. I thank Veronica Castillo for kindly providing the results of her unpublished UT dissertation (Castillo, 2001). I thank Dr. Mike Hudec at the UT Bureau of Economic Geology for assistance with structural restorations. I thank Arturo Contreras for assistance in synthetic seismograms.

Finally, I thank my wife, Sylvia, who provided me the unconditional support necessary to finish this dissertation.

**Regional Tectonics, Sequence Stratigraphy and Reservoir
Properties of Eocene Clastic Sedimentation, Maracaibo Basin,
Venezuela**

Publication No. _____

Alejandro Escalona, Ph.D.

The University of Texas at Austin, 2003

Supervisors: William L. Fisher and Paul Mann

The Maracaibo basin of Venezuela is one of the most prolific hydrocarbon basins in the world. During the Paleogene, oblique collision between the Caribbean and South American plates produced a 4-km-thick wedge of clastic sediments, where over 40 billion barrels of hydrocarbons have been produced.

Previous studies in the Eocene interval are focused either at a large regional scale or a field-size reservoir scale. Integration between both scales of observation has not been previously done, and, as a consequence, the effect of regional tectonics is not considered in the small-scale stratigraphic record. The aim of this dissertation is to study the interplay of tectonic and stratigraphic variables that controlled the Eocene sedimentation in the Maracaibo basin, and to establish a geologic model that incorporates data from a regional to reservoir scale.

Interpretation of 2-D and 3-D seismic data in the central and eastern Maracaibo basin reveals two major tectonic features formed during Paleogene collision between the Caribbean and the South American plates: 1) a late Paleocene-early Eocene foreland basin; and 2) a middle-late Eocene lateral ramp fault. The lateral ramp fault forms a paleogeographic facies boundary separating a less faulted and folded shelf area to the west from a fold-thrust belt to the east.

In the Eocene Maracaibo shelf area, intraplate deformation occurs by N-NE-striking left-lateral faulting with pull-apart basins localized at fault stepovers. Three-dimensional seismic time slice interpretation of more than 2000 km² of 3-D seismic data allows mapping of the Icotea pull-apart basin. Extension of the Icotea pull-apart basin is localized on pre-existing NW-SE-striking normal faults, formed by Paleocene-Eocene plate flexure during the foreland basin period.

Detailed sequence stratigraphic interpretation of the central Maracaibo basin was carried out using 330 wells and 3-D visualization methods that combined well and 3-D seismic data techniques providing greater vertical and lateral resolution (pseudo-seismic). These data reveal that Eocene clastic sedimentation is controlled by tectonic subsidence and to a lesser degree by changes in sediment supply and eustasy.

Hydrocarbon reservoirs of the central Maracaibo basin are concentrated in distributary channels and tidal sand bar facies on structural highs produced by strike-slip motion of N-NE-striking faults. Depositional environments and fluid content of Eocene reservoirs are inferred from cross sections based on closely spaced well logs.

Table of Contents

List of Tables.....	xiii
List of Figures	xiv
CHAPTER 1	1
Introduction and overview of dissertation.....	1
CHAPTER 2	7
Eocene structure and stratigraphy along an exhumed lateral ramp fault, eastern Maracaibo Basin, Venezuela	7
2.1 Introduction	7
2.2 Regional setting.....	11
2.3 Previous interpretations of the Maracaibo basin	14
1. Tear fault, lateral ramp or transversal fault model	14
2. Foreland basin model	19
2.4 Database and methodology used in this study	21
Database:	21
Methodology:	21
2.5 Major Eocene stratigraphic and structural features of central and eastern Maracaibo basin	23
Eocene elastic wedge:	23
Fault inversion:.....	25
Eocene sub-basins:	25
Burro Negro fault zone:.....	27
Oligocene-Miocene sub-basins and areas of chaotic reflectors:.....	32
The Paleocene unconformity:.....	34
The Eocene unconformity:	34
Tectonic loading:.....	35

The Oca fault Zone:.....	36
2.6 Eocene Barinas Basin.....	36
2.7 Discussion	37
Tectonic escape in northern Venezuela.....	37
Pre-collisional paleogeography in northern Venezuela	39
Model for the Paleogene tectonic evolution of the Maracaibo basin	39
A. Late Paleocene - early Eocene.....	39
B. Middle – late Eocene	41
C. Late Eocene-Oligocene.....	41
D. Late Tertiary	42
Comparison of lateral ramps faults in western and eastern Venezuela	43
2.8 Conclusions and recommendations	45
CHAPTER 3	48
Three-dimensional structural architecture and evolution of an Eocene pull-apart basin, central Maracaibo basin, Venezuela	48
3.1 Introduction	48
3.2 Plate tectonic setting of the Maracaibo basin.....	51
3.3 Late Neogene to present geologic setting of the Maracaibo basin.....	52
3.4 Late Paleocene-Eocene geologic setting of the Maracaibo basin	54
3.5 Database and methodology	56
3.6 Subsurface seismic units in the central Maracaibo basin.....	60
A) Paleozoic orogenic phase (pre-sequence A):.....	60
B) Late Jurassic rifting phase (Sequence A ~ 208 to 131 my.):	60
C) Cretaceous and Paleocene passive margin phase (Sequence B ~ 131 to 66-54 my.):	62
D) Late Paleocene to late Eocene collisional phase (Sequence C ~66-54 to 49-36 my.):.....	62

E) Oligocene-Recent convergent margin, Maracaibo syncline (Sequence D 36-25 my. to Recent):	63
3.7 Description of the Icoatea pull-apart basin	65
Interpreted isochron and edge detection maps	65
Seismic time slices	67
Seismic time slices at 2200 ms and 2600 ms	67
Seismic time slices at 3400 ms and 3800 ms	68
3.8 Extension of the Icoatea sub-basin and minimum amount of strike-slip displacement	73
3.9 Discussion	77
3.10 Conclusions	85
CHAPTER 4	87
Sequence stratigraphy analysis of Eocene clastic foreland basin deposits in central Lake Maracaibo using high resolution well correlation and 3-D seismic data	87
4.1 Introduction	87
4.2 Study area	90
4.3 Database	90
4.3.1 3-D seismic data:	92
4.3.2 Well data	92
4.4 Objectives, methodology and theoretical considerations	93
4.4.1 Core data	94
4.4.2 Parasequence, parasequence set, genetic sequence and sequence	99
4.4.3 Pseudo-seismic transform technique	103
Pseudo seismic transform code	104
4.4.4 Seismic interpretation	108
4.5 Sequence stratigraphy	110
4.5.1 One dimensional stratigraphic analysis	111
4.5.2 Facies associations	114

4.5.3 Two-dimensional stratigraphic analysis.....	116
4.5.4 Three dimensional stratigraphic analysis.....	120
Genetic sequence 1.....	124
Genetic sequence 2.....	126
Genetic sequence 4.....	128
Sequence 6.....	130
4.5.5 Seismic stratigraphy.....	132
4.6 Regime variables.....	141
4.6.1 Eustasy.....	141
4.6.2 Sediment supply.....	146
4.6.3 Subsidence.....	147
1. Late Paleocene ~ 60 my.....	148
2. Early Eocene ~54 my.....	148
3. Early-middle Eocene ~49 my.....	151
4. Middle-late Eocene ~40 my.....	151
5. Late Eocene-Oligocene ~35-25 my.....	152
4.7 Comparison with other areas of the Maracaibo basin.....	152
4.8 Orinoco delta analog (Eastern Venezuela).....	155
4.9 Summary and discussion: Integrated evolution of the study area.....	160
4.10 Conclusions.....	163
CHAPTER 5	166
Reservoir properties.....	166
5.1 Introduction.....	166
5.2 Comments on petroleum systems.....	168
Source rocks:.....	168
Migration and trapping:.....	171
5.3 Main reservoirs in central Lake Maracaibo.....	172
5.4 High resolution sequence stratigraphic correlation.....	173

5.5 Well and seismic data correlation	178
5.5.1 Petrophysical properties of the reservoirs	178
5.5.2 Acoustic properties of well and seismic data: Implications for interwell correlation using seismic data	180
Seismic properties and synthetic seismograms	180
Crossplots	182
Seismic and well data resolution implications	185
Tuning	186
Stratal slices	190
5.6 Conclusions	193
CHAPTER 6	195
Conclusions	195
Future work	198
Appendices	199
Appendix 1: Core data	199
Appendix 2: Code for pseudo-seismic transform in Matlab	205
References	208
Vita	222

List of Tables

Table 4.1. GR facies associations for the study area.....	115
---	-----

List of Figures ¹

Figure 2.1. A) Topographic/bathymetric map showing six main tectonic belts observed in the northern margin of South America. B) Satellite gravity map showing the six tectonic belts, basement structural map and main depocenters of Cretaceous-Cenozoic sedimentary rocks.	8
Figure 2.2. Surface geologic map of the Maracaibo basin region and seismic time slice at a depth of 3.4 seconds beneath the Lake Maracaibo area *.....	12
Figure 2.3. Isopach map of Eocene clastic sedimentary rocks in the Maracaibo and Barinas basins.....	15
Figure 2.4. Paleogeographic maps of the Maracaibo basin.....	16
Figure 2.5. Two previous interpretations of Paleogene tectonics and sedimentation in the Maracaibo basin *.....	17
Figure 2.6. Fence diagram showing the structural and stratigraphic architecture of the central and eastern part of the Maracaibo basin and the location of the main faults in the map view *.....	22
Figure 2.7. A) Regional seismic transect 1. B) Detail of boxed area shown in Figure 2.7A *.....	24
Figure 2.8. A) Regional E-W transect 4. B) Detailed of boxed area shown on Figure 2.8A. C) Seismic line SW-NE.....	26
Figure 2.9. Radar image and regional seismic time slice at 3400 ms, in the Maracaibo basin area *.....	28
Figure 2.10. A) Location map of the detailed study area of the NE Maracaibo basin. B) Surface geological map of NE Maracaibo basin corresponding to the boxed are shown in Figure 2.10A. C) Transect 1. D) Transect 3. E) Transect 2 *.....	29
Figure 2.11. Tectonic reconstruction of northern South America during the Cenozoic: A) Paleocene-early Eocene; B) Middle – late Eocene; C) Late Eocene-Oligocene-Miocene; D) and Present-day distribution of Eocene depocenters following 100 km of right-lateral strike-slip motion along the Boconó fault *.....	40
Figure 2.12. Comparison of similar lateral ramp fault deformation of different ages. A) Interpreted seismic line in the Maturin sub-basin across the Urica lateral ramp fault. B) Interpreted seismic line across the northern part of the Burro Negro fault, Maracaibo basin *.....	44
Figure 3.1. A). Major crustal provinces of the Caribbean region. B) The inferred position of the leading edge of the Great arc.....	50

¹ * These figures are fold outs (11” x 17”).

Figure 3.2. Surface geologic map of the Maracaibo basin region and seismic time slice at 1 second beneath the floor of the Lake Maracaibo *	53
Figure 3.3. Interpreted regional seismic time slices at 3400 ms level showing the main structural styles in the Eocene, Paleocene, Cretaceous and Pre-Cretaceous stratigraphic levels *	55
Figure 3.4. A) Location of the 3-D seismic data cube used in this study. B) Illustration of five representative seismic time slices taken at 1 second time intervals through the 3-D seismic cube volume C) 3-D view of the seismic cube showing an interpreted seismic time slice at 2200 ms.	58
Figure 3.5. General stratigraphic column used for the area of study *	61
Figure 3.6. A) Uninterpreted east-west regional seismic line. B) Interpreted seismic line showing the main structural and stratigraphic features of the Lake Maracaibo area *	64
Figure 3.7. A) Isochron map of the top of sequence B (Paleocene unconformity). B) Edge detection map of the top of sequence B (Paleocene unconformity). C) Isochron map of sequence C (Eocene).	66
Figure 3.8. A) Uninterpreted seismic line 3800. B) Interpreted seismic line *	69
Figure 3.9. A) Uninterpreted and interpreted seismic time slice at 3400 ms. B) Uninterpreted and interpreted seismic time slice at 3800 ms *	70
Figure 3.10. A) Uninterpreted seismic line 3000. B) Seismic line interpretation *	72
Figure 3.11. Fence diagram showing the structural architecture of the central part of the Maracaibo basin, including the Icotea pull-apart basin *	74
Figure 3.12. A) Uninterpreted longitudinal seismic line through the Icotea pull-apart basin. B) Depth-converted and interpreted seismic line. C) Entire section restored to the top of the Paleocene using vertical shear. D) South of fault F (future Icotea pull-apart basin) restored using 60° antithetic shear method. North of fault F the section was restored with vertical shear *	75
Figure 3.13. 3-D seismic time slice succession showing different structural styles in the study area within second-order sequences *	79
Figure 3.14. 3-D diagrams showing the structural and stratigraphic evolution of the study area from Jurassic rifting (lower diagram) to present-day (upper diagram) *	80
Figure 4.1. A) Location of the 2000 km ² study area in the central Maracaibo basin showing data coverage used for this stratigraphic analysis. B) More than 300 wells were used.	91
Figure 4.2. Lithologic facies used in core data description	95

Figure 4.3. A) W12 well log with facies and environment descriptions based on lithofacies of Fig. 4.2. B and C) Heterolithic facies showing flaser bedding, mud drapes and herringbone sedimentary structures indicating tidal influence. D) Medium-to-fine grained sandstone interpreted as distributary channel fill *	98
Figure 4.4. A) Log response of parasequences. B) Stacking patterns in parasequence sets and well log expression	100
Figure 4.5. A) Conventional well-to-well log correlation, using GR and Resistivity logs. B) Example of a seismic line showing lateral continuity of reflections due to the amount of traces used. C) Stratigraphic pseudo-seismic section (modified from Carr et al., 1995). D) Structural pseudo-seismic section (this study) *	105
Figure 4.6. A) Well basemap. B) 3-D pseudo-seismic grid over the basemap showing direction of cross-lines and in-lines. C) Enlarged section of a part of the grid showing well selection for the 3-D pseudo-seismic.	107
Figure 4.7. A) Methodology for seismic cube flattening and generation of seismic time slices. B) Methodology for generation of stratal slices relative to an interpreted horizon.	109
Figure 4.8. A) Type log of the study area with one-dimensional stratigraphic interpretation before this study, and B) Type log of the study area with one-dimensional stratigraphic interpretation from this study *	112
Figure 4.9. Pseudo-seismic N-S cross-line 16: A) Uninterpreted. B) Structural interpretation and main surfaces. C) Stratigraphic interpretation with datum surface MFS2. D) Facies interpretation with datum on surface MFS2 *	117
Figure 4.10. Pseudo-seismic E-W line 25: A) Uninterpreted. B) Structural interpretation and main surfaces. C) Stratigraphic interpretation with datum surface MFS2. D) Facies interpretation with datum on surface MFS2 *	118
Figure 4.11. 3-D pseudo-seismic fence diagram including crossline 14, in-lines 15, 25 and 45, and net sand isopach map of parasequence set A. Datum is MFS2.	121
Figure 4.12. 3-D pseudo-seismic facies interpretation illustrated by a fence diagram using crosslines 11, 16 and 19. Datum is given by MFS2.	123
Figure 4.13. Parasequence sets net-to-gross maps and net sand isopach fence maps of sets A, B, C and D (genetic sequence 1) *	125
Figure 4.14. Parasequence sets net-to-gross maps and net sand isopach fence maps of sets E, F, G and H (genetic sequence 2) *	127
Figure 4.15. Parasequence sets net-to-gross maps and net sand isopach fence maps of sets L, M, N and O (genetic sequence 4) *	129

Figure 4.16. Sequence 6 net-to-gross map.	131
Figure 4.17. Example of a synthetic seismogram from well W26.	133
Figure 4.18. A) Uninterpreted seismic crossline. B) Interpreted seismic crossline showing different stratigraphic sequences *	135
Figure 4.19. A) Uninterpreted seismic line. B) Interpreted seismic line showing different stratigraphic sequences *	136
Figure 4.20. A) Partially interpreted seismic time slices flattened relative to SB1. B) Partially interpreted flattened time slice at 12 ms above SB1. C) Time slice interpretation. D) Net sand isopach map of set A *	139
Figure 4.21. A) Composite sea level charts, including transgressive-regressive cycles of Hardenbol et al. (1998), composite oxygen isotope record of Abreu and Anderson (1998) and eustatic curve of Haq et al. (1988). B) Enlarged composite Eocene composite sea level charts from Fig. 4.21A.	144
Figure 4.22. Subsidence plots generated for the Maracaibo basin.	149
Figure 4.23. Subsidence evolution of the Maracaibo basin during the Paleogene and its effect on stratigraphic architecture.	150
Figure 4.24. A) Comparison of parasequence sets in the area of study with other studies in Lake Maracaibo. B) Net sand map of set G compared with equivalent unit C4X mapped by Ambrose et al. (1995). C) Net sand map of sequence 6 compared with sub-unit A of Maguregui (1990).	154
Figure 4.25. Orinoco delta physiography: A) Location of the Orinoco delta with respect to the Maracaibo basin. B) Orinoco delta, major distributaries, and sub-zones. C) Main depositional elements and geometries of an area of the Orinoco delta. D) Funnel shape and depositional environments in the main distributary channel *	156
Figure 4.26. Comparison of depositional systems of the Orinoco delta with depositional systems interpreted in the study area *	158
Figure 4.27. Evolution of the study area from the Eocene to the Oligocene. Interplay between: Subsidence and eustatic sea level history *	162
Figure 5.1. Giant hydrocarbon oil fields in the Maracaibo basin and major faults.	169
Figure 5.2. Profile derived from interpreted E-W seismic line in Figure 3.6. The section shows the main structural and stratigraphic features of the Maracaibo Basin and its petroleum system *	170
Figure 5.3. Central Lake Maracaibo structural maps indicating net sand distribution and areas with high resistivity values.	174
Figure 5.4. A) Structural GR pseudo-seismic line 25. B) Structural deep-resistivity pseudo-seismic line 25.	176

Figure 5.5. A) Structural GR pseudo-seismic cross line 17. B) Structural deep-resistivity pseudo-seismic cross line 17.	177
Figure 5.6. A) Facies petrophysical properties from core data in well W12. B) Crevasse splays and tidal bars have an average of 20% porosity and 300 md. C) Fluvial channels and distributaries have an average of 19 % porosity and permeability varies from 160 to 700 md *.....	181
Figure 5.7. A) Synthetic seismogram of well W12. B) Extracted wavelet, frequency and phase from the seismic data. C) Quality control between the seismic data and the extracted wavelet.	183
Figure 5.8. A) Synthetic seismogram of well W16. B) Extracted wavelet, frequency and phase from the seismic data. C) Quality control between the seismic data and the extracted wavelet.	184
Figure 5.9. A) Crossplot and synthetic seismogram of genetic sequence 5 in well W12. B) Crossplot and synthetic seismogram of genetic sequence 4 in well W12. C) Crossplot and synthetic seismogram of genetic sequence 3 in well W16. D) Crossplot and synthetic seismogram of genetic sequence 4 in well W16.	187
Figure 5.10. A) Crossplots at well and seismic resolution and synthetic seismogram of genetic sequence 2 in well W12. GR and acoustic impedance logs are displayed with the seismic frequency. B) Crossplots at well and seismic resolution and synthetic seismogram of genetic sequence 4 in well W16. GR and acoustic impedance logs are displayed with the seismic frequency *.....	188
Figure 5.11. A) Net sand map of set M. B) Seismic line showing the possible reservoir. C) Amplitude map of the top of the reservoir. D) Sandstone thickness vs. amplitude.	191
Figure 5.12. A) Net sand map of set A in the neighborhood of Wells W26 and W27. B) Synthetic seismogram of well W27, showing the main reservoir. C) Seismic interpretation of the reservoir using stratal slices. D) Slice 8 ms above the Paleocene unconformity *.....	192

CHAPTER 1

Introduction and overview

Venezuela has the fifth largest hydrocarbon reserve in the world with more than 30 known giant hydrocarbon fields with proven hydrocarbon reserves greater than 70 billion bbl (as compiled by Mann et al., in press; BP 2002). Most of these giant fields occur in the onland foreland basins (Maracaibo, Barinas and Eastern Venezuela basins), south of the presently active Caribbean-South America strike-slip plate boundary.

Northern South America experienced Late Jurassic-early Cretaceous rifting from southern North America and the Yucatan block followed by prolonged Cretaceous subsidence in a passive margin setting (Bartok, 1993; Pindell et al., 1998; Mann, 1999b). The passive margin phase was interrupted by progressive west-to-east collision of the Caribbean arc with the passive margin in late Cretaceous in Colombia (Cooper et al., 1995); in Paleogene in the Maracaibo basin region (Pindell and Barrett, 1990; Lugo and Mann, 1995); and in Neogene in the area of eastern Venezuela and Trinidad (Erlich and Barrett, 1992; Pindell et al., 1998; Babb and Mann, 1999b; Di Croce et al., 1999) (Fig. 3).

The structural evolution of the Maracaibo basin is complex because of multiple tectonic events occurring from the Jurassic to Present. For this reason, characterization of Cretaceous-Miocene hydrocarbon reservoirs is challenging. During the early-middle Eocene, the Misoa Formation was deposited within the Maracaibo foreland basin (Lugo and Mann, 1995; Parnaud et al. 1995b). The

lower-middle Eocene in the Lake Maracaibo area is a deltaic complex (Zambrano et al., 1971; Van Veen, 1972), with significant tidal influence (Maguregui, 1990).

The Maracaibo basin has previously been the subject of previous studies of, its tectonic origin (e.g. Audemard, 1991; Lugo and Mann, 1995; Parnaud et al., 1995), and its Cretaceous-Miocene reservoirs (e.g. Maguregui, 1990; Ambrose et al., 1995). Depositional systems based on chronostratigraphic units are essential to fully understand the sedimentation patterns within the Maracaibo basin. Interpretation of the Maracaibo basin geology and petroleum systems, with its structural complexity and vertical and lateral stratigraphic heterogeneities, requires a deep understanding of the different processes that affect stratigraphic sequences, such as eustasy, sediment supply and subsidence. Detailed analysis of the stacking patterns in a sequence stratigraphic framework can improve the description of reservoir architecture and facies content down to the bedset scale (Carter et al., 1997). But, stratigraphic interpretation involves analysis of the regional evolution of the basin, and mechanisms of depocenter formation.

The main goal of this project is to document the Eocene stratigraphic and structural evolution of the Maracaibo basin, from the plate tectonic scale to the reservoir scale. High-resolution sequence stratigraphy and seismic interpretation form the basis of this study. A principal objective of this study is to use a dense well database control to offset the vertical resolution limitations of the 3-D seismic reflection data.

This dissertation is structured in four main chapters, where each chapter considers a particular geological problem in the basin at a different scale of

observation. The data available for this study include 3-D and 2-D seismic data of a representative area of the central Maracaibo basin, more than 330 wells with suitable wireline log data and a review of previous studies.

These chapters are organized as follow:

- Chapter 2 discusses two different tectonic models proposed for the thick Eocene depocenter located along the northeastern margin of the Maracaibo basin. The first model proposes that the northeast sedimentary wedge was controlled by a large lateral ramp fault (Burro Negro fault), separating SE-directed, but independently moving thrust sheets, whereas the second model proposes that the depocenter is a foreland basin controlled by southwestward-directed overthrusting during late Paleocene-middle Eocene collision between the Caribbean and South American plates. The present configuration of the basin and faults is more supportive of a tear or lateral ramp fault origin than other interpretations.

- Chapter 3 discusses three-dimensional seismic mapping of interpretative subsurface time slices 3. The main objective of this chapter is to place constraints on the structure of the Icotea fault and its stratigraphic control of the Icotea pull-apart basin, located at a left-step on the fault. These 3-D data provide an excellent observational basis for understanding the structural history of three sets of regionally-extensive faults and testing two models for the formation of pull-apart basins in general.

Interpretation of the sense of displacement along the Icotea fault is controversial. It has been interpreted as a left-lateral strike-slip, thrust with a

right-lateral oblique-slip component, and inverted normal fault lacking strike-slip displacement.

The structural and stratigraphic architecture of the Icoatea basin interpreted from five time slices through the basin and its flank areas supports the simple pull-apart model for the Eocene opening of the Icoatea basin. The amount of extension along the Icoatea fault is consistent with some previous estimates of minor left-lateral displacement (0.8 to 2.25 km), but is inconsistent with either low-angle or high-angle thrusting during Eocene time, as inferred from previous interpretations of widely spaced 2-D seismic lines. The normal faults that formed the pull-apart basin reactivated pre-existing faults due to plate flexure during the foreland stage that affected the Maracaibo shelf.

- Chapter 4 focuses on the stratigraphic record of the central Maracaibo basin by interpreting the main Eocene chronostratigraphic surfaces and clastic depositional cycles. This analysis assumes that the Eocene sedimentary record of the basin was formed as a foreland basin during an oblique collisional event between the Caribbean and South American plates (Chapters 2 and 3). High rates of subsidence controlled the formation of the main depocenter and long term relative sea-level. Sediment supply and eustasy were less important than tectonics in controlling the stratigraphic framework.

In contrast to previous stratigraphic interpretations done in the Maracaibo basin, this chapter uses visualization methods applied to 3-D seismic data and large numbers of wells to maximize lateral correlations and interpretation methods (pseudo-seismic transform technique of Carr et al., 1995). Seismic data

resolution and quality are not satisfactory to rely entirely on seismic stratigraphic analysis and to confidently perform well-to-well correlations. The Eocene stratigraphic succession in the study area is characterized by an aggradational package overlain by regressive and transgressive cycles in a retrogradational trend and a regressive sequence capped by the Eocene unconformity. The lack of erosional sequence boundaries reveals that the Maracaibo basin shelf was not sub-aerially exposed during the early and most of the middle Eocene.

Fluvial and tidal processes dominate Eocene facies architecture. Further effort is required to better understand the lateral and vertical distribution of the depositional systems and the interplay between forebulge, shelf and deep basin.

- Chapter 5 consists of two parts: an overview of the distribution of the Eocene reservoirs in the central Lake Maracaibo area, and a feasibility analysis for correlating seismic and petrophysical properties of the rocks. The objective of this chapter is to estimate the degree to which the spatial continuity of the 3-D seismic data can be used in combination with the vertical resolution of the well data in predicting poorly imaged interwell reservoir areas. Prediction of reservoir facies and the petrophysical properties is very poor in the interwell areas.

Main reservoirs are concentrated in distributary channels and tidal sand bar facies, which originate good quality fluid flow units. Even though lithology and fluid content can be differentiated by acoustic impedance in the well logs, the low vertical resolution of the seismic data available (25 Hz dominant frequency), is unable to resolve the lateral and vertical continuity of the reservoirs. Most of

the reservoirs are below the limit of resolution of the seismic data for the study area.

CHAPTER 2

Eocene structure and stratigraphy along an exhumed lateral ramp fault, eastern Maracaibo Basin, Venezuela

2.1 INTRODUCTION

A “tear fault” is defined as a steep to vertical fault with horizontal motion, located in the hanging wall of a low-angle overthrust fault (Bates and Jackson, 1984). Its strike is generally perpendicular to that of the overthrust. Linzer et al. (1995) applied the term “tear faults” as displacement transfer structures in the Alps, where oblique convergence to the foreland basin resulted in *en-echelon* arrays of thrust faults displaced by dextral strike-slip faults. Both thrust and tear fault systems are kinematically connected to each other. Possible geological controls on the location of transfer structures are: Sub-thrust basement faults, basement rooted faults and/or stratigraphic variations (Thomas, W. A., 1990). Mann (1999a) proposed that areas of the Caribbean-arc continental collision resulted in several examples of tear faults. He used the term “lateral ramp” as a transtensional, strike-slip fault that formed as tears between collided and uncollided parts of the diachronously forming, circum-Caribbean fold-thrust belt.

In northern Venezuela, a west-to-east younging pattern of thrusts and lateral ramp faults are developed along the Caribbean–South American margin (Fig. 2.1A). In the present day, these lateral ramps and thrusts are inactive or reactivated by mainly EW plate motion (Pérez et al., 2001; Trenkamp et al., 2002). Younger faults in eastern Venezuela have been studied by Munro and

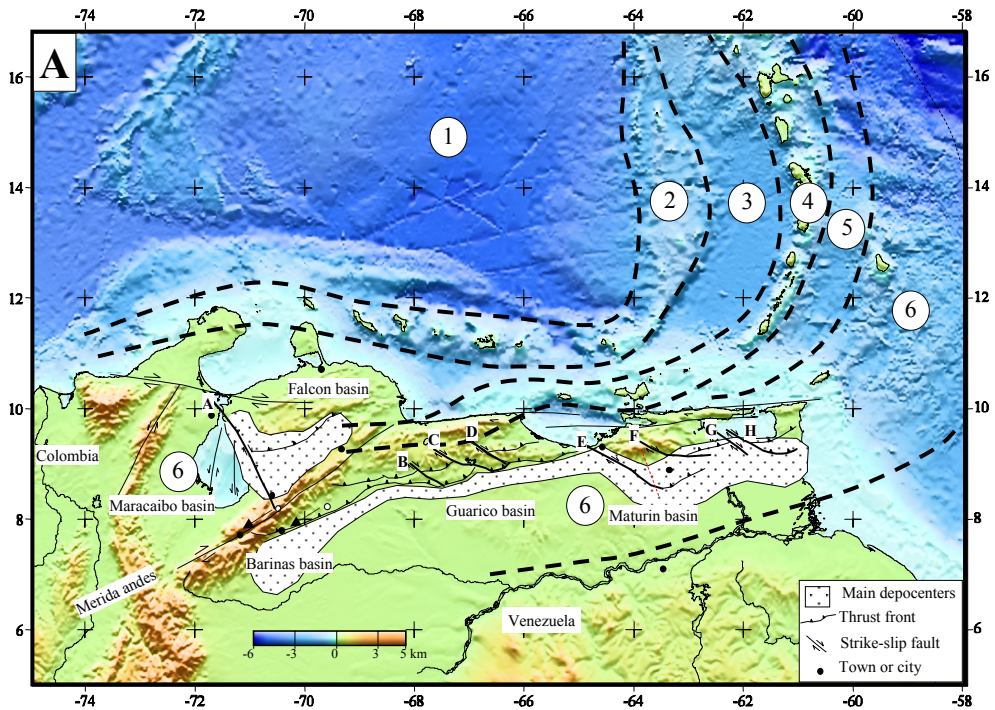


Figure 2.1. A) Topographic/bathymetric map showing six main tectonic belts observed in the northern margin of South America (modified from Stephan (1985), and Babb and Mann (1999)): 1) Venezuela basin, 2) Aves Ridge-Dutch Antilles, 3) Grenada Basin-Bonaire volcanic basin-Falcon basin, 4) Lesser Antilles arc-Cordillera e la Costa, 5) Tobago basin-Carupano basin, and 6) Barbados accretionary prism, Major Cenozoic sedimentary basins, major thrusts, lateral ramps and strike-slip faults. Major lateral ramps faults are: A-Burro Negro fault, B, C and D-Cordillera de la Costa lateral ramps, E- Urica fault, F- San Francisco fault, G- El Soldado fault, and H- Los Bajos fault.

Figure 2.1 continues

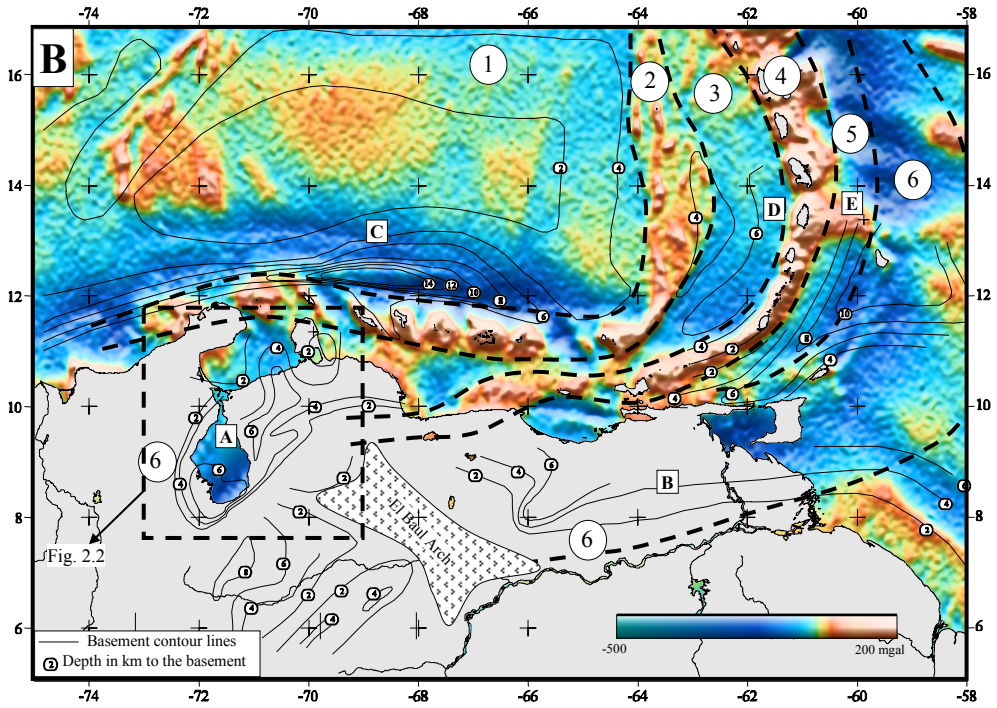


Figure 2.1. B) Satellite gravity map from Sandwell and Smith (1997) showing the six tectonic belts, basement structural map and main depocenters of Cretaceous-Cenozoic sedimentary rocks.

Smith (1984), Parnaud et al. (1995a), Roure et al. (1997) and Di Croce et al. (1999). Lateral ramp faults in eastern Venezuela are typically buried beneath thick, fluvial and shallow marine sediments, or exposed in the Serranía del Interior range of eastern Venezuela or Trinidad. In western Venezuela, lateral ramp faults and thrusts are exposed by later tectonic inversion related to Neogene motion along the Maracaibo block and the Neogene North Andean orogeny in the Falcón basin area. Topographic/bathymetry maps (Fig. 2.1A) and Geosat marine free-air gravity data (Fig. 2.1B) reveals that the structure of the northern South America and Caribbean margin is composed of a regular pattern of elongated volcanic-arc-related and basins that are compressed against the South American continental margin. These collapsed terranes are continuous features formed with the intraoceanic Caribbean island arc. The Lesser Antilles segment of the Caribbean volcanic arc is unopposed in its progressive, eastward displacement over Atlantic oceanic crust (Fig. 2.1).

In this chapter, I focus on the Burro Negro fault zone, an exhumed Eocene age lateral ramp fault partially exposed along the eastern edge of the Maracaibo basin. The main objective of this chapter is to illustrate the overall structure of the Burro Negro zone fault and the two different areas of the Eocene sedimentation that it separates (Maracaibo shelf to the west, and Maracaibo deep basin to the east). This study is the first time a compilation of outcrop and subsurface observations derived from previous works and regional seismic data were used into a complete regional interpretation.

2.2 REGIONAL SETTING

During late Paleocene to Eocene time, oblique collision between the Caribbean plate and the northwestern continental margin of South America produced a complex wedge of Paleogene clastic sediments and accretionary terranes in the northeastern part of the Maracaibo basin (Kellogg, 1984; Lugo, 1991; Audemard, 1991; Parnaud et al, 1995b; Mann, 1999b). This oblique collisional event, that was diachronous from west to east, severely modified the configuration of lithologic facies belts along the South America passive margin. The Maracaibo basin developed a thick (> 4 km) Eocene depocenter in the north-northeast of the present-day Maracaibo basin (Fig. 2.2). The shape of post-Eocene sedimentary rocks of the basin was influenced by the uplift of the main mountain ranges (Mérida Andes and Sierra de Perijá) from the Oligocene to Present.

Figure 2.2 shows the present-day configuration of the Maracaibo basin. The basin is an elongate intermontane depression bounded by the NE-trends of the Mérida Andes and Sierra de Perijá. The Oca fault is interpreted as a dextral strike-slip fault, with estimates of Oligocene-Recent lateral offset ranging from 20 to 100 km (Rod, 1956; Kellogg, 1984). The Mérida Andes bounds the basin to the south, and its topographic axis is closely controlled by the Boconó fault, also interpreted as a right-lateral strike-slip fault (Schubert, 1982). Toward the east the Maracaibo depression is bounded by the Trujillo Mountains, located east of the Burro Negro and Ballenato faults. These parallel faults strike northwest-southeast and terminate near the Valera fault. East of the Trujillo Mountains are the Lara nappes forming an anticlinorium striking northeast-southwest (Stephan,

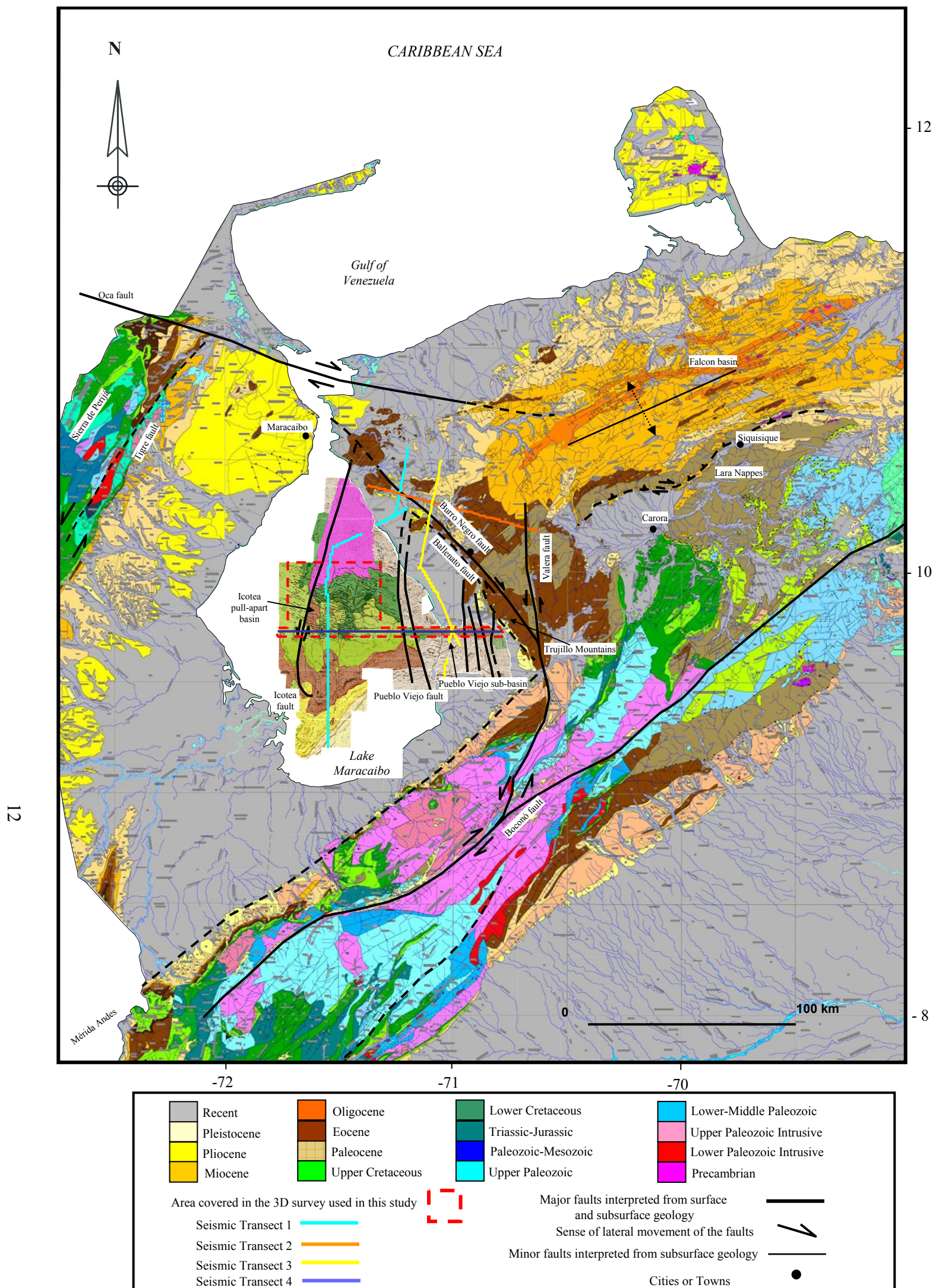


Figure 2.2. Surface geologic map of the Maracaibo basin region (modified from Borges, 1984) and seismic time slice at depth of 3.4 seconds beneath the Lake Maracaibo area. The present-day topographic and geological configuration of the Maracaibo basin is controlled by uplift of the Mérida Andes and Sierra de Perijá. Interpreted regional seismic time slice at 3.4 seconds shows the main structural styles in the Eocene, Paleocene, Cretaceous and Pre-Cretaceous stratigraphic levels (modified from Castillo, 2001). All sequences are dipping towards the south or southeast. An asymmetric, Eocene pull-apart basin formed along the Eocene Icoatea left-lateral fault. The Burro Negro fault bounds the present-day Maracaibo basin to the northeast. The Lara nappes are located east and northeast of the Burro Negro fault. The dashed boxed located in the central part of Lake Maracaibo is the area covered by the 3D seismic survey presented in this chapter. The color lines represent the regional 2D seismic transects also presented in this chapter.

1977, Kellogg, 1984, Mathieu, 1989). The Lara nappes are composed of Paleocene-Eocene sandstones and shales, igneous and bioclastic olistoliths of Cretaceous age (Mathieu, 1989). The present-day stress field analysis (Colmenares and Zoback, in press) reveals that western Venezuela is undergoing NW-SE shortening as a result of plate convergence between the South American and Caribbean plates.

Interpretation of a regional seismic time slice at 3400 ms, comprising most of the Lake Maracaibo area and part of the eastern coastal plain of the lake, intersect Cretaceous to Miocene rocks (Fig. 2.2). Prominent structural features seen on this seismic time slice include N-NE-striking faults (e.g. Icotea and Pueblo Viejo faults) that terminate before reaching the southern Maracaibo basin (Castillo, 2001). These faults originated as Jurassic half-grabens and were reactivated as strike-slip faults during the Eocene. Another family of east-west-striking faults is observed, mainly in the central part of the Maracaibo basin. These faults have been previously interpreted as a flexural response to the subsidence of the South American plate due to load of the Caribbean plate during the Paleogene (Roure et al., 1997; Castillo, 2001; Chapter 3). Major regional unconformities interpreted in the Maracaibo basin include the Pre-Cretaceous-Cretaceous unconformity, the Paleocene unconformity, the Eocene unconformity, and the middle Miocene unconformity.

The emplacement of the Lara nappes followed oblique collision between the Caribbean and South America plates, forming a more than 4 km thick foreland basin during the Paleogene in the N-NE areas of the Maracaibo basin. An isopach

map of the Eocene on Figure 2.3 shows several important features of this Eocene basin: 1) Thickening toward the NE part of the Maracaibo basin, 2) appearance of localized depocenters along the trace of N-NE trending faults (Chapter 3), 3) thickness changes along the Burro Negro fault; and 4) the Barinas Basin located in the south of the Maracaibo basin has no more than 500 m (~1500 feet) of Eocene rocks (González de Juana et al., 1980).

Due to late Tertiary uplift of the Mérida Andes preservation of Paleogene rocks in the mountain range separating the Maracaibo and Barinas basins is poor. Paleographic maps of the Maracaibo basin reveal that the Paleogene shelf edge trended to the northwest along the northeastern coast of the present-day Maracaibo Lake (González de Juana et al., 1980; Mathieu, 1989; Lugo, 1991; Parnaud et al., 1995b) (Fig. 2.4).

2.3 PREVIOUS INTERPRETATIONS OF THE MARACAIBO BASIN

Two models for the Paleogene tectonic evolution of the Maracaibo basin and the development of the deep Eocene depocenter located in the northeast-east part of the basin have been proposed by previous workers (Fig. 2.5):

1. TEAR FAULT, LATERAL RAMP OR TRANSVERSAL FAULT MODEL (Stephan, 1977; Stephan, 1985; Mathieu, 1989; Fig. 5A): This model proposes that the Maracaibo Eocene depocenter developed parallel to a tear fault or lateral ramp fault striking NW-SE. Right-lateral strike-slip displacement along the tear fault allowed independent motion of the thrust front east of the tear fault (Lara Nappes) (Fig. 2.5A). Oblique Caribbean-South America convergence led to

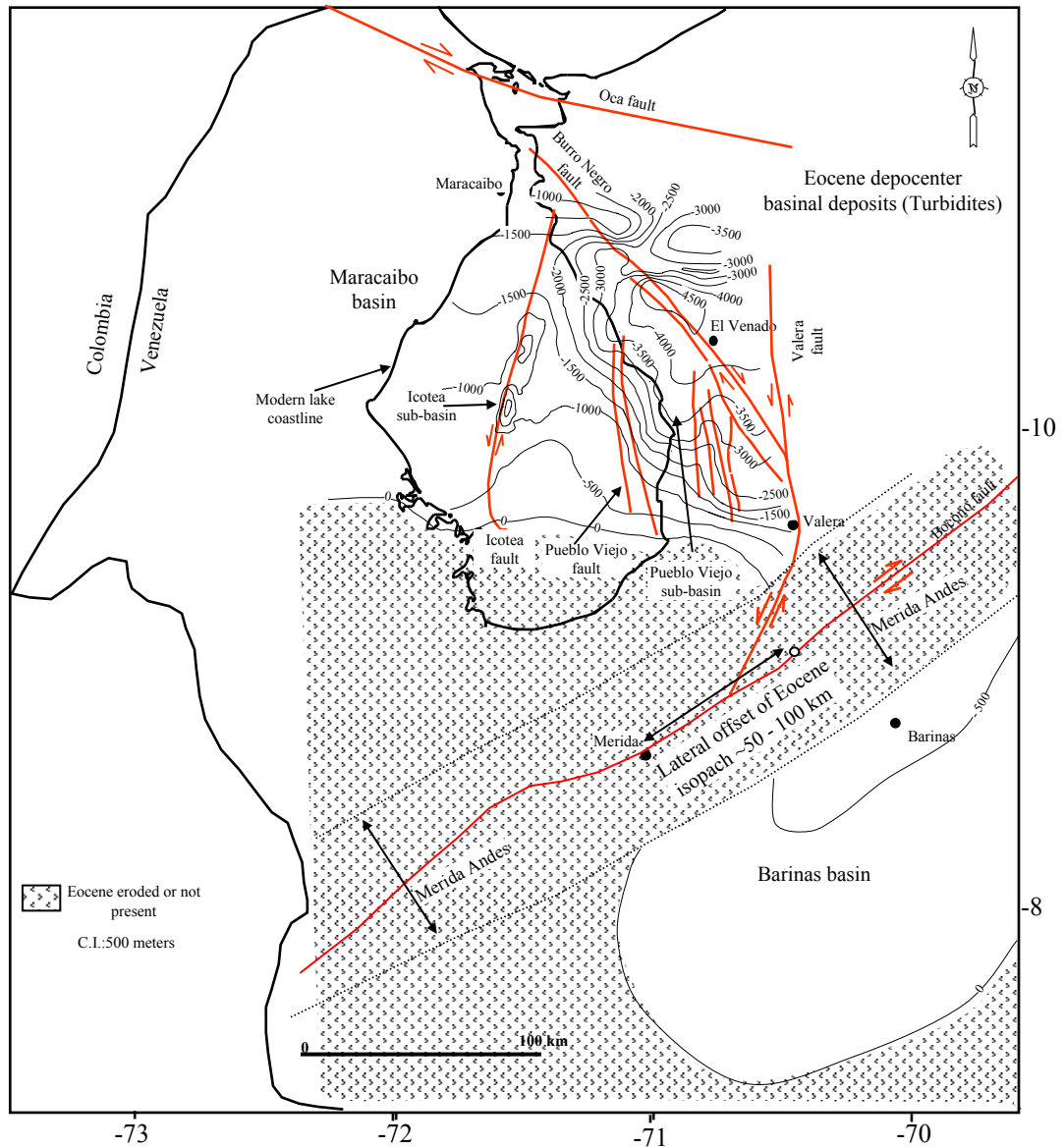


Figure 2.3. Isopach map of Eocene clastic sediment rocks in the Maracaibo and Barinas basins (modified from Zambrano et al. (1971) and Gonzáles de Juana et al. (1980)). Major faults in the Eocene are shown in red. Main depocenters in the Maracaibo basin are located along the Icoatea, Pueblo Viejo and Burro Negro faults zones.

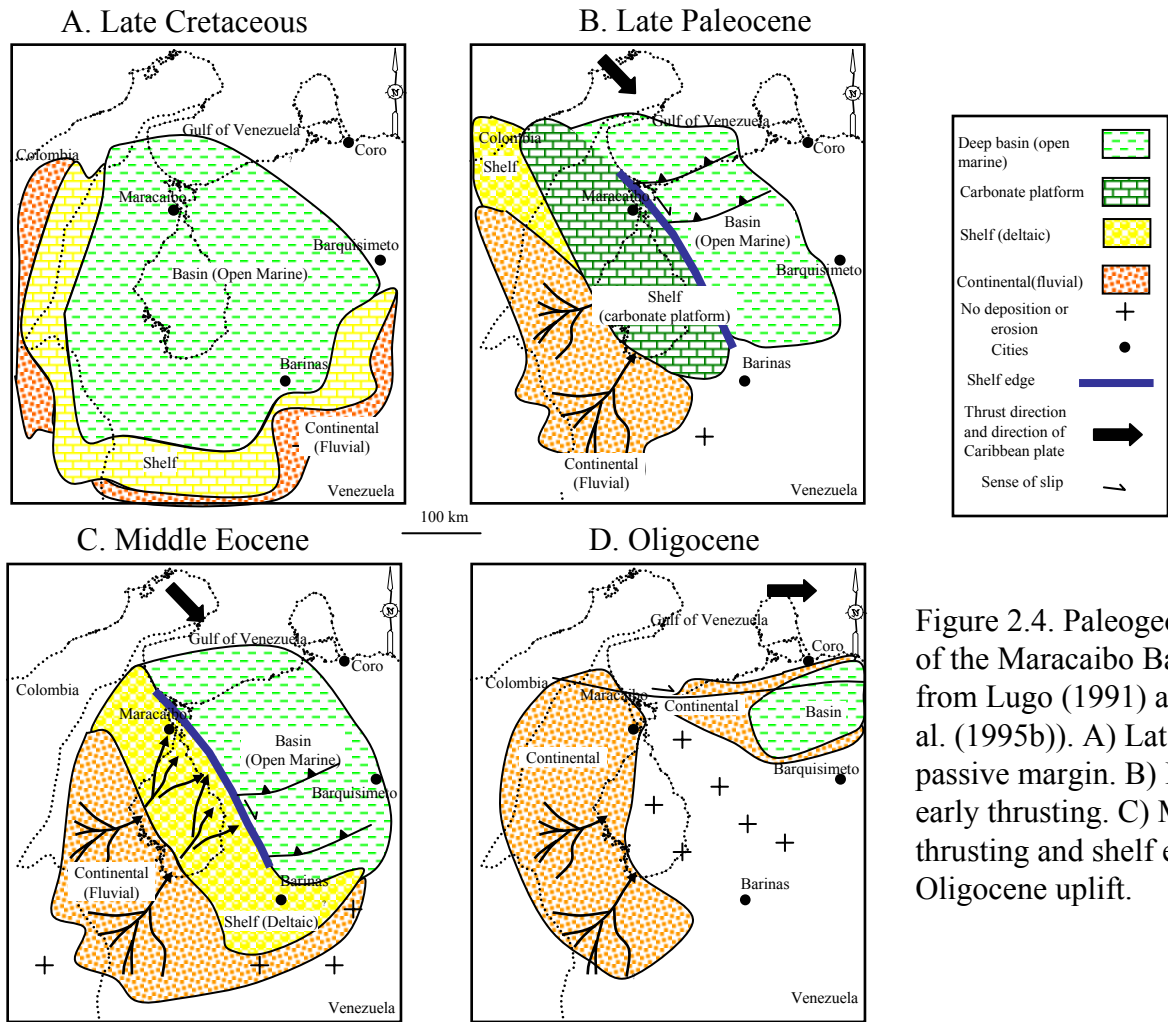


Figure 2.4. Paleogeographic maps of the Maracaibo Basin (modified from Lugo (1991) and Parnaud et al. (1995b)). A) Late Cretaceous passive margin. B) Late Paleocene early thrusting. C) Middle Eocene thrusting and shelf edge. D) Oligocene uplift.

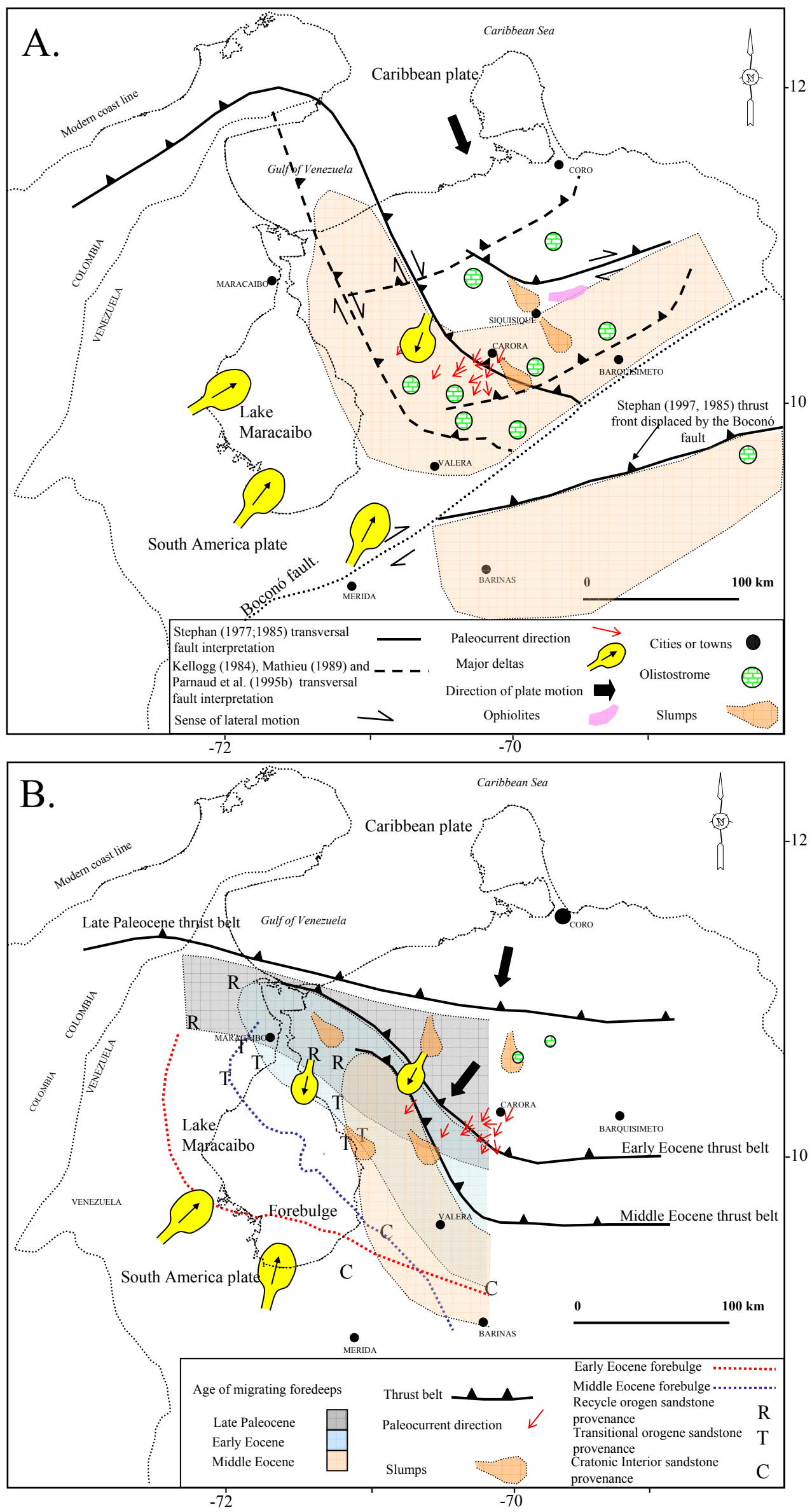


Figure 2.5. Two previous interpretations of Paleogene tectonics and sedimentation in the Maracaibo basin: A) Tear fault or “transversal fault” model of Stephan (1985); and B) Foreland basin model of Lugo and Mann (1995).

emplacement of the Lara nappes toward the southeast (Stephan, 1977; Kellogg, 1984, Stephan, 1985; Mathieu, 1989; Parnaud et al., 1995b). Parnaud et al. (1995b) propose a side thrust front or a lateral ramp thrust front in the northeastern margin of the Maracaibo basin instead of a tear or strike-slip fault. This model is based on the following observations (Fig. 2.5A):

- Orientation of Paleocene and Eocene folds between N45° and N60° in the E-NE area of the Maracaibo basin indicates right-lateral shear along the lateral fault (Burro Negro fault) (Kellogg, 1984; Mathieu, 1989).

- A complete absence of olistoliths and SW-NE folds in the Eocene rocks west of the Burro Negro fault indicates that this lateral ramp fault separated two areas of different deformation style (Mathieu, 1989).

- Early to middle Eocene rocks prograding from SW to NE have distal facies toward the NE parts of the basin (Stephan, 1977). A shelf edge located along the trend of the Burro Negro fault zone represents the paleogeographic boundary between shallow and deep water sedimentary environments (González de Juana et al., 1980). Paleocurrents flow shows a NE to SW direction for turbidites of the Eocene Trujillo formation east of the Burro Negro fault (Mathieu, 1989).

- Offset of more than 100 km of the front of the Lara nappes is interpreted, east of the Maracaibo basin. Major thrusting occurred during the Paleocene-Eocene.

- The Barinas middle-late Eocene depocenter seems to be offset between 50 to 100 km to the SW from the Maracaibo basin equivalent Eocene

depocenter located along the trend of the Burro Negro fault zone. Stephan (1977) interpreted the leading edge thrust front of the Lara nappes to be located south of the Mérida Andes in the Barinas Basin and displaced toward the southwest by more than 50 km of Neogene right-lateral offset on the Boconó fault zone (Fig. 2.6B).

2. FORELAND BASIN MODEL (Audemard, 1991; Lugo and Mann, 1995; Fig. 5B): A thrust fault was located in the northern part of the basin and created an Eocene foredeep that paralleled the thrust front. The thrust front migrated southeastward and culminated with the emplacement of the Lara nappes (Stephan, 1985). The source of clastic sediments changed in the Eocene foredeep from the southwest (proto-Magdalena or proto Orinoco-rivers; Díaz de Gamero, 1996) toward the northeast (Audemard, 1991; Lugo and Mann, 1995; Castillo, 2001).

This model is based on the following observations (Fig. 2.5B):

- A thick Eocene depocenter (> 4 km) developed along the eastern margin of the lake (Audemard, 1991; Lugo and Mann, 1995; Parnaud et al. 1995). Because the area of isopach mapping by Lugo (1991), Audemard (1991) and Lugo and Mann (1995) just reached the eastern margin of the Lake Maracaibo, there is scarce information available for the Eocene isopach beyond the northeastern margin of the Lake.

- A thrust belt is located northeast of the Maracaibo basin. Lugo (1991) proposed that the thrust front was located north of the town of Carora and was advancing to the S-SW over the area of the Maracaibo basin. Audemard (1991)

pointed out that the thrust front is evident in the NE part of the Maracaibo basin, but it advanced through time toward the SE.

- Cretaceous slumps and olistoliths in the Eocene rocks surrounding the town of Carora have been mapped (Renz, 1981).

- Paleocurrents from Eocene turbidite outcrops in the Carora area indicate paleo flow directions from NE to SW (Mathieu, 1989; Lugo, 1991).

- N-NE provenance for Eocene clastic rocks in the E-NE part of the basin has been interpreted (Lugo, 1991; Castillo, 2001). Parnaud et al. (1995b) and Castillo (2001) also described a S-SW source of the early-middle Eocene rocks and a W-EW source for middle and late Eocene rocks in the Maracaibo basin. Provenance studies by Lugo (1991) indicate a continental source from the south during this period.

- A flexural bulge with absence of Eocene clastic sedimentary rocks is located in the southern part of the Lake Maracaibo (Lugo, 1991; Audemard, 1991; Parnaud et al., 1995b).

- Subsidence plots for Eocene clastic rocks in the eastern margin of Lake Maracaibo, from Lugo (1991) and Castillo (2001) reveal rapid rates of subsidence during the Paleocene-early Eocene following abrupt uplift during middle and late Eocene.

- Lugo and Mann (1995) proposed southwest-prograding clinofolds in Eocene clastic rocks in the N-NE area of the Maracaibo basin. Clinofolds are middle to late Eocene in age.

2.4 DATABASE AND METHODOLOGY USED IN THIS STUDY

DATABASE: This study uses 2000 km² of 3-D seismic data, located at the center of the Maracaibo basin along with approximately 500 km of 2-D seismic lines (Fig. 2.2). The 3-D seismic data were collected by PDVSA, S.A. (Venezuela national oil company) during the 1980's. Regional seismic time slices, produced by merging all available 3-D seismic surveys of the Lake Maracaibo area were also used in this study (Castillo, 2001). Five deep exploratory wells located in the central and eastern parts of the basin were used in this study to constraint ages of lithologies of seismic sequences (Fig. 2.2). Seismic sequences are described in detail in chapter 3 of this dissertation.

METHODOLOGY: Four regional seismic transects (1-4) were constructed using 2-D and 3-D seismic lines (Fig. 2.6) and conventional seismic interpretation was carried out. Synthetic seismograms were generated to improve the correlations between seismic reflectors and well data. Interpretation of the main, regionally continuous seismic reflections and reflection terminations were correlated to synthetic seismograms and wells. The main unconformity-based sequences were delineated in the basin, and an Eocene isopach map was generated using interval velocities derived from sonic logs of the five wells located in central Lake Maracaibo (Fig. 2.3). Velocities used for depth conversion were: Pre-Cretaceous: 6.2 km/sec; Lower Cretaceous: 5.0 km/sec; Upper Cretaceous and Paleocene: 2.8 km/sec; Eocene: 4.0 km/sec; Oligocene-Present: 3.1 km/sec. Interpretive subsurface seismic time slice maps were constructed using age data, unconformity-based sequences, and detailed structural

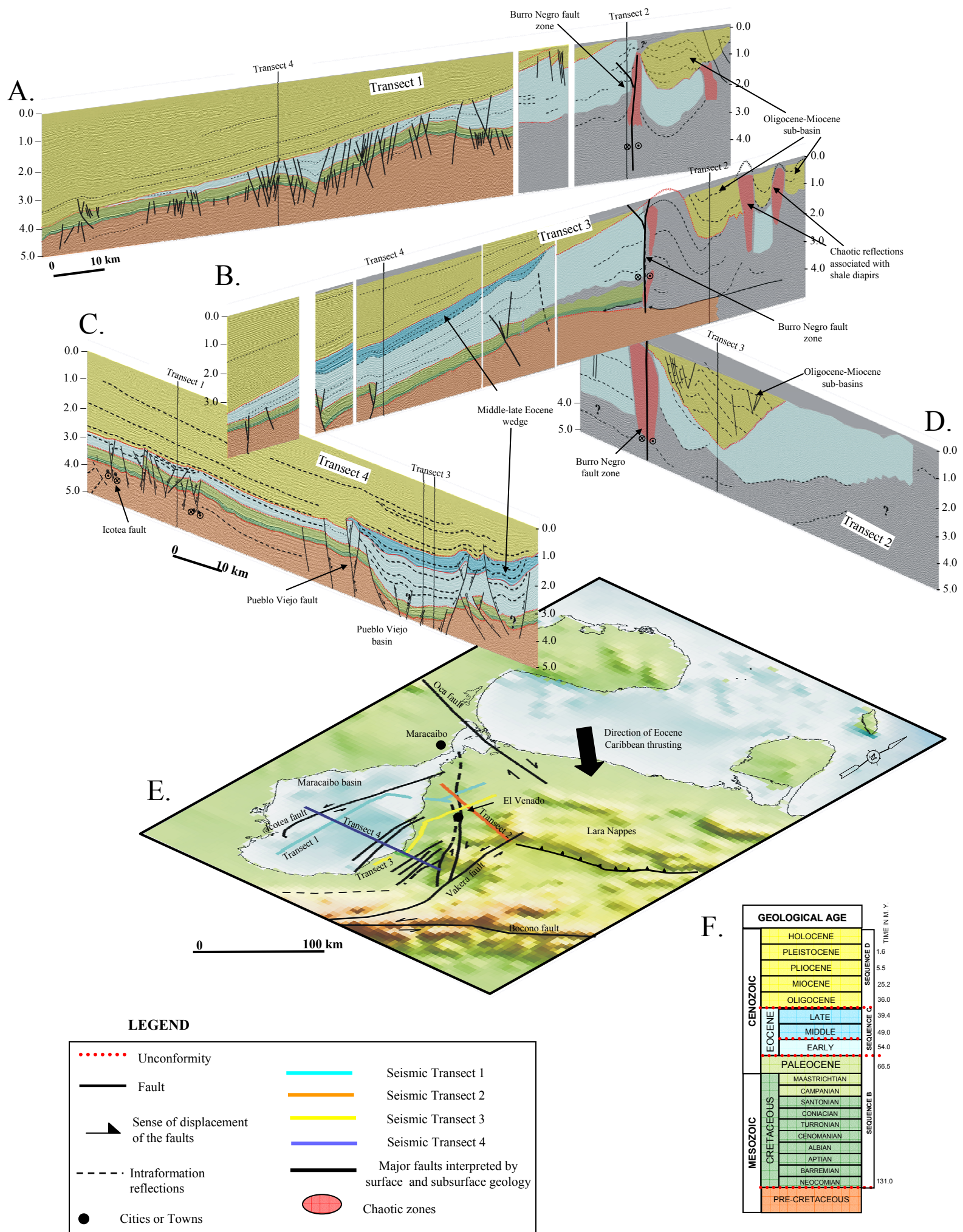


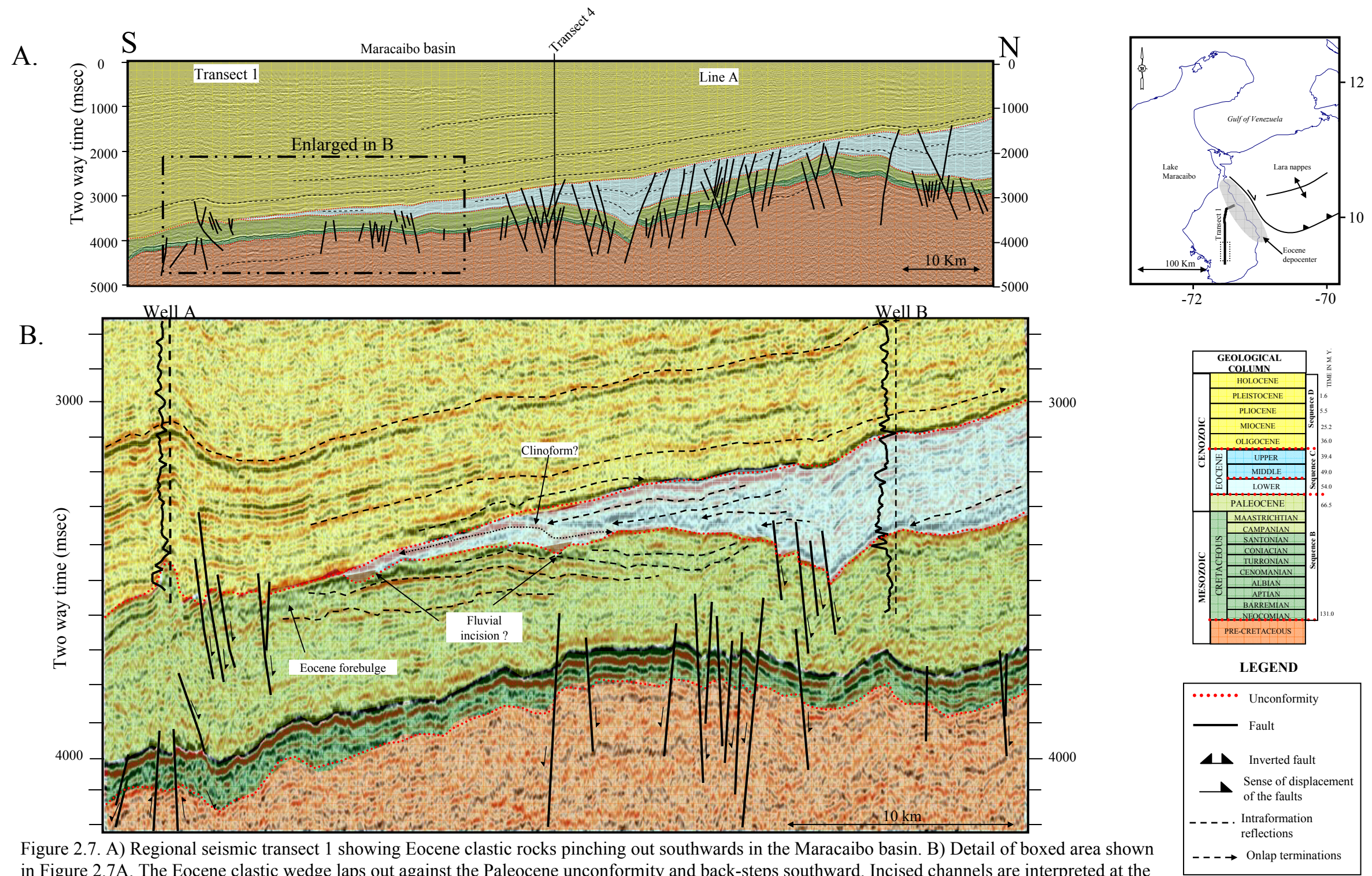
Figure 2.6. Fence diagram showing the structural and stratigraphic architecture of the central and eastern part of the Maracaibo basin and location of the main faults in the map view: 1) Pre-Oligocene rocks are folded east of the Burro Negro fault (A,B and D), 2) Eocene pinches out in center Lake Maracaibo (A and B), 3) The Eocene thickens toward the north and east (A, B and C), and 4) The middle and late Eocene wedge is confined to the eastern part of the basin, between the Burro Negro and Pueblo Viejo faults, within the inverted Pueblo Viejo sub-basin (C).

observations from 3-D seismic and regional seismic time slices (Castillo, 2001; Escalona and Mann, 2003a; Chapter 3 this dissertation).

2.5 MAJOR EOCENE STRATIGRAPHIC AND STRUCTURAL FEATURES OF CENTRAL AND EASTERN MARACAIBO BASIN

In order to describe the main structural and stratigraphic features of the Maracaibo basin during the Paleogene a fence diagram, using 2-D seismic transects, was constructed (Fig. 2.6). This fence diagram provides a three dimensional view of the stratal geometries in distinct Paleogene depocenters in the central and northeastern parts of the Maracaibo basin. Main observations are:

EOCENE CLASTIC WEDGE: The early Eocene wedge pinches out in the central part of the present-day Lake Maracaibo, and thickens up to more than 4 km toward the northeast (Transect 1 in Figs. 2.6A and 2.7). Figure 2.7 shows an interpretation from the N-S transect 1 showing the early Eocene wedge in the southern part of the basin (Fig. 2.6A). To the south, the Eocene wedge onlaps against a folded Paleocene high (forebulge and/or basal unconformity). Internal reflections on Figure 2.7B show truncations of the underlying Paleocene reflections against the early Eocene section. Back-stepping onlap of Eocene sequences toward the south is interpreted and reflections within the Eocene section suggest subaerial exposure of the late Paleocene rocks, with possible fluvial incision. Clinoform progradation toward the N and NE is inferred (Figs. 2.7 and 2.8) is supported by interpretation of the main depocenters in the northern parts of the Maracaibo basin.



FAULT INVERSION: At the end of the late Eocene, inverted structures formed along the eastern margin of the Lake Maracaibo (Figs. 2.6C and 2.8, transect 4). This inversion is also observed along the Icotea fault (Chapter 3; Escalona and Mann, 2003b), suggesting that E-W compression was produced as the final stage of the folding and emplacement of the Lara nappes in the eastern part of the basin, east of the Burro Negro fault, which major vergence was to the SE.

EOCENE SUB-BASINS: Two main sub-basins are interpreted in the Eocene Maracaibo shelf: 1) The Icotea pull-apart basin at a left-step along the Icotea fault indicates between 0.8 to 2.3 km of left-lateral strike-slip and it is explain in detail in Chapter 3; and 2) The Pueblo Viejo basin, that is an inverted rift basin located near the eastern margin of the Lake Maracaibo. This basin is bounded by the Pueblo Viejo fault on the west and probably the Burro Negro fault on the east (Transect 4, Figs. 2.6C and 2.8). The Pueblo Viejo basin is a deep Eocene depocenter containing more than 3 km (10000 feet) of Eocene rocks (Fig. 2.4). This basin thickens toward the north following the trace of the Pueblo Viejo fault (Transect 3, Fig. 2.6B). Inversion of the basin occurred at the end of the late Eocene and during the Miocene (Fig. 2.6C).

The Pueblo Viejo basin was infilled by two different Eocene episodes (Fig. 2.6B, C and 2.8): The early Eocene and the middle-late Eocene. The early Eocene section onlaps the Paleocene unconformity toward the west, and reflections suggest clinoforms prograding east (Figs. 2.8B and 2.8C). Instead, the middle-late Eocene section pinches out toward the west, downlapping over the

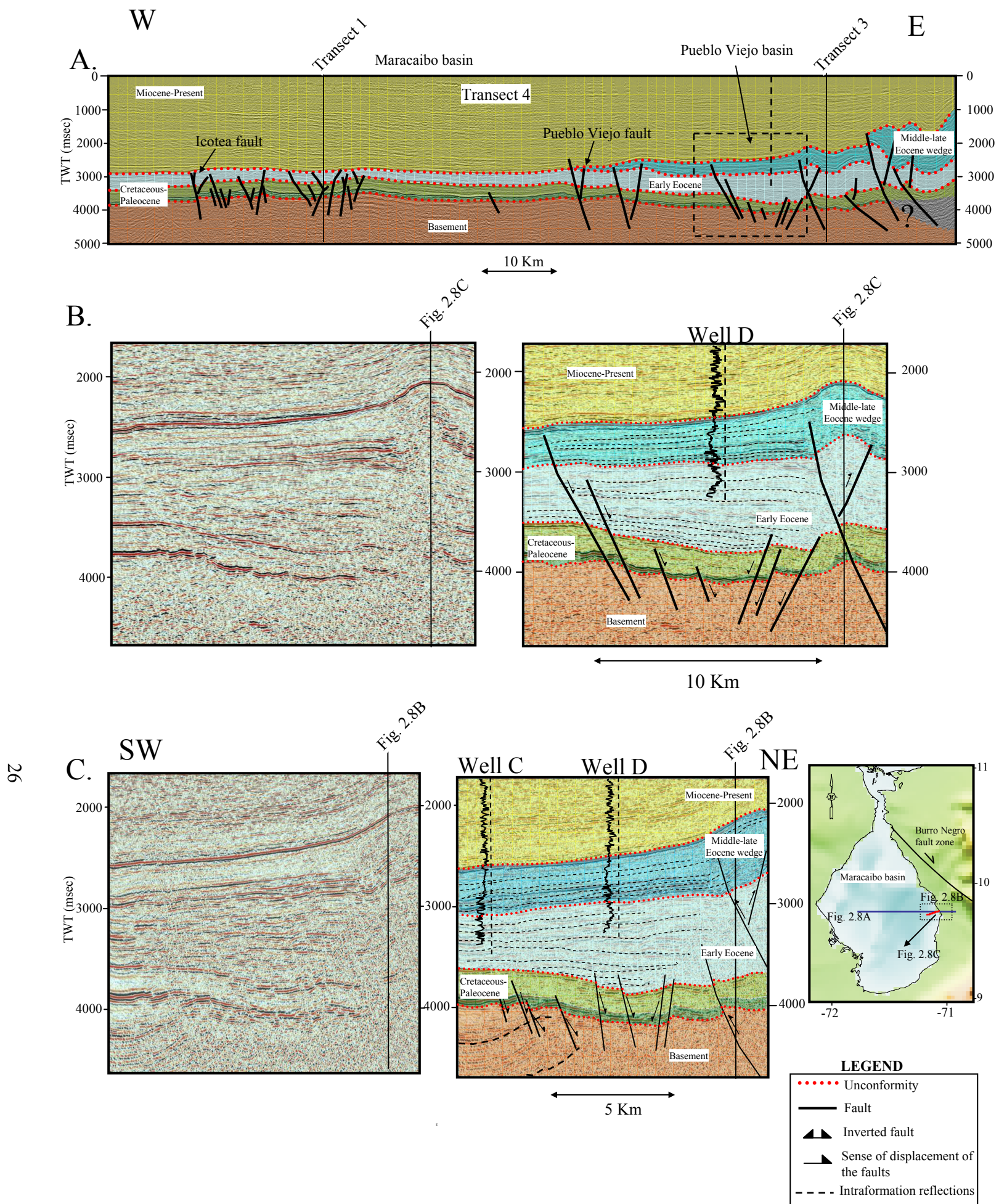


Figure 2.8. A) Regional E-W transect 4 showing thickening of lower Eocene clastic rocks towards the eastern Maracaibo basin and overlapping of the middle and upper Eocene clastic wedge. The Miocene to present section thickens towards the west. B) Detailed of boxed area shown on Figure 2.8A. Gamma ray log of well D shows the main stratigraphic patterns of Eocene clastic rocks. Clinoforms are shown by dashed lines. C) Seismic line SW-NE. Gamma Rays logs of wells C and D indicate lower Eocene wedge to prograde eastward, whereas middle and upper Eocene section becomes less sandy westward.

early-middle Eocene boundary (interpreted by well control and as a continuous seismic reflection), suggesting progradation toward the west. Also, the early Eocene section has a lower percentage of sandstone (low Gamma Ray) toward the east (Well D, Fig. 2.8B), whereas the middle and upper Eocene becomes less sandy toward the west (Wells C and D, Fig. 2.8C).

BURRO NEGRO FAULT ZONE: Surface expression of the Burro Negro fault can be observed and interpreted in the radar image shown in Figure 2.9. The fault is located to the E-NE of the basin and strikes NW-SE following the axis of the Trujillo Mountains. Field observations by Mathieu (1989) on map view show the Burro Negro fault as a linear fault with associated *en echelon* folds striking E-W (Fig. 2.9). In cross section the fault is interpreted as a high angle fault dipping toward the NE with an associated low angle fault defining the Burro Negro fault zone, representing the western topography front of the Trujillo Mountains. Based on these field observations, Mathieu (1989) interpreted the Burro Negro fault as a right-lateral strike-slip fault with undetermined amount of offset

On seismic data the Burro Negro fault is a chaotic reflection zone (Fig. 2.10). Its linear trace and high dip angle on seismic lines is consistent with the surface mapping of Mathieu (1989). It remains a high angle fault to a time of at least 3 to 4 seconds (Fig. 2.10C and 2.10D).

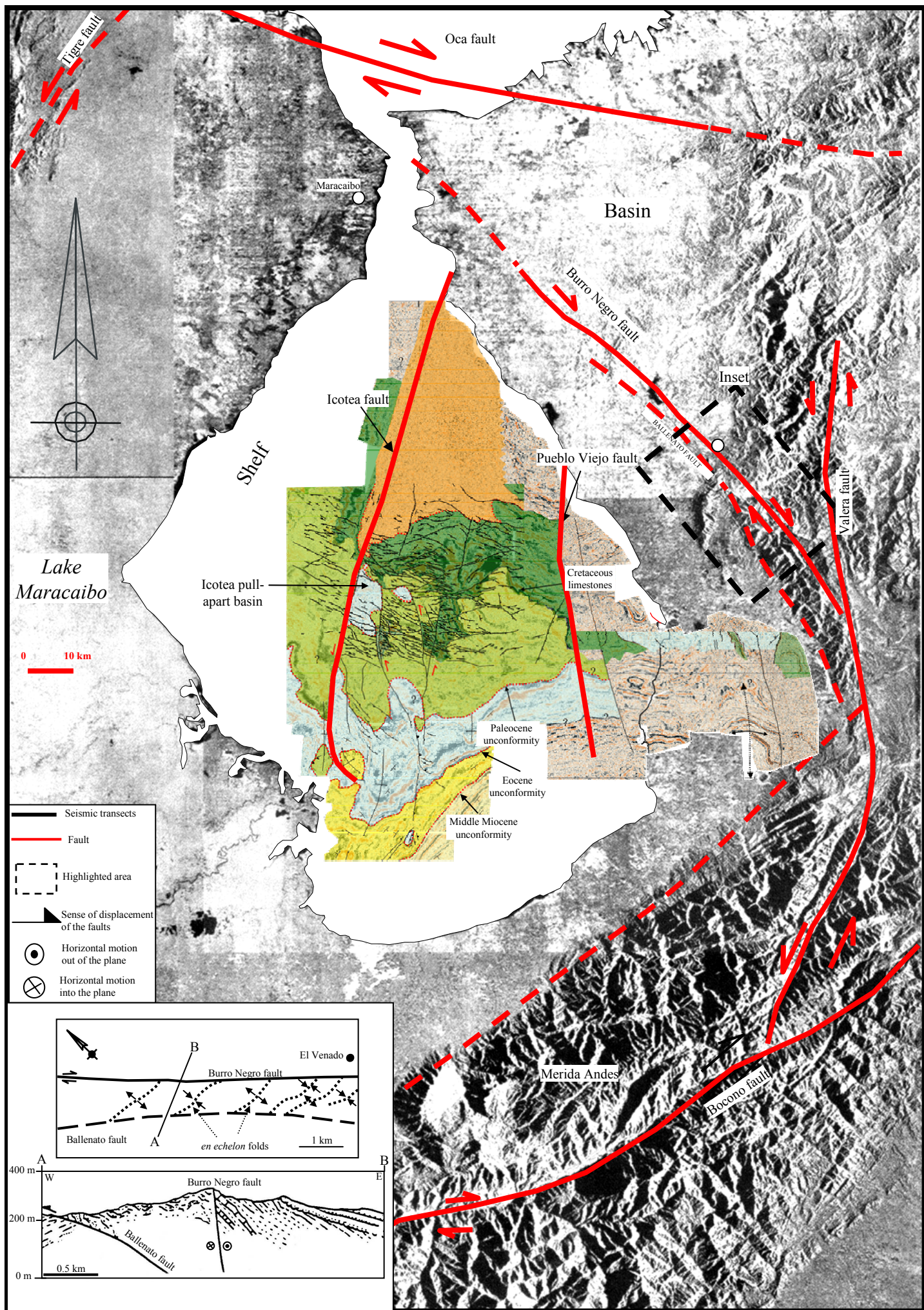


Figure 2.9. Radar image and regional seismic time slice at 3400 ms, in the Maracaibo basin area. Main faults shown are: Boconó, Valera, Burro Negro, Tigre, Icoatea, Pueblo Viejo and Oca. Other features indicated are the Icoatea and Pueblo Viejo sub-basins in the Eocene Maracaibo shelf. Map view interpretation shows the Burro Negro fault as a dextral strike-slip fault with associated *en-echelon* folds. A cross-section interpretation of outcrop mapping shows its sub-vertical dip (modified from Mathieu, 1989).

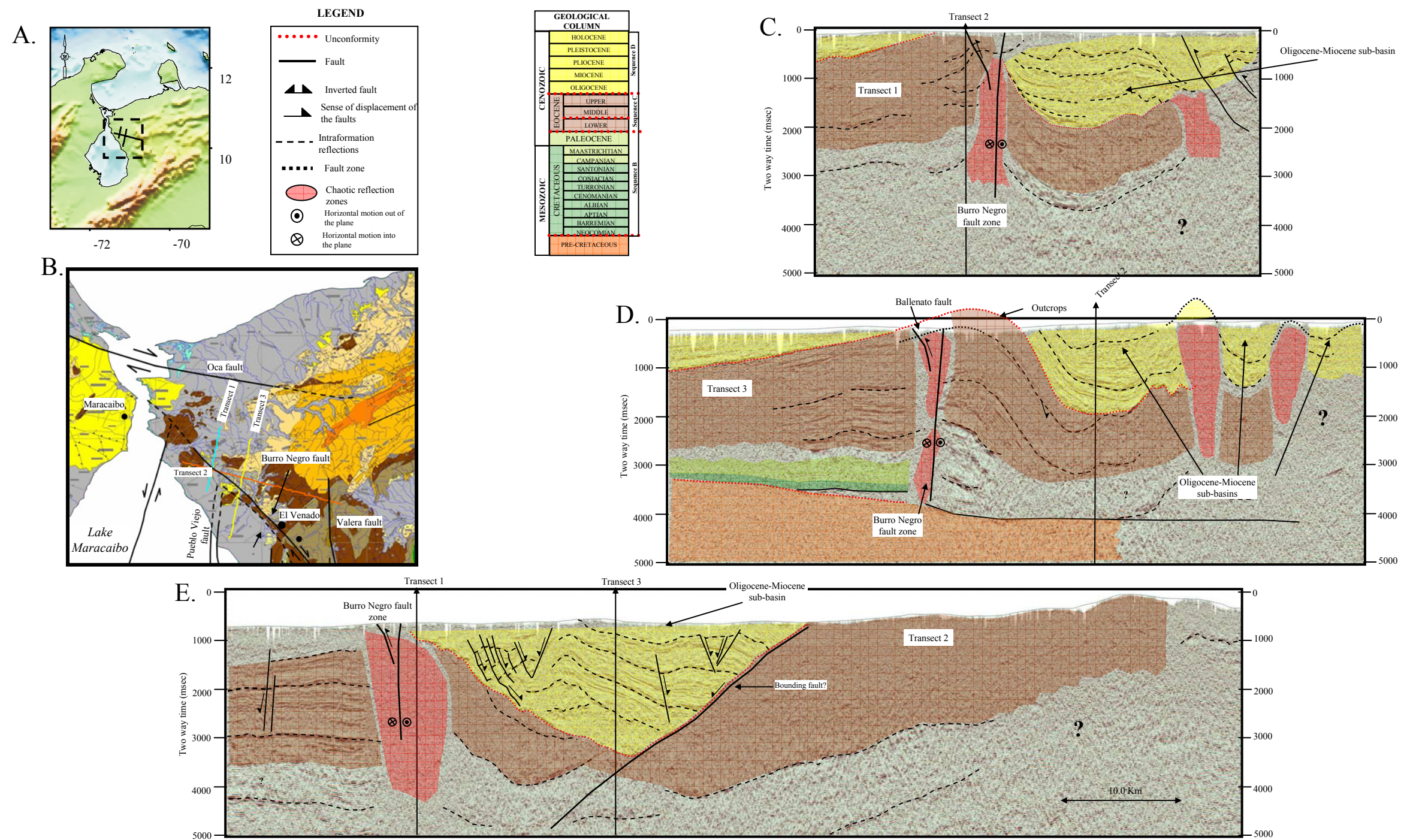


Figure 2.10. A) Location map of the detailed study area of the NE Maracaibo basin. B) Surface geological map of NE Maracaibo basin corresponding to the boxed are shown in Figure 2.10A. C) Transect 1. Burro Negro sub-vertical fault zone. Note that the Oligocene- Miocene sub-basin is folded; South of the Burro Negro fault zone the Eocene and the thin Miocene clastic wedge are dipping southward with few faults and folds. D) Transect 3, similar to Figure 2.10C. E) Transect 2. The Burro Negro fault zone bisects the line in two parts. To the east, an Oligocene- Miocene sub-basin formed and a west-dipping normal fault.

The Burro Negro fault zone divides the eastern Maracaibo basin into two different structural provinces: The folded Eocene with Oligocene–Neogene sub-basins to the northeast and the stable Eocene wedge, with divergent reflections toward the south (Fig. 2.6 and 2.10). This change in tectonic regime occurred later than the early Eocene and before the Oligocene, because of orientation of folds west of the Burro Negro fault during the Eocene indicates NW shortening (Mathieu, 1989; Fig. 2.6). The orientation of Oligocene-Neogene basins interpreted from the surface geological map in Figure 2.2, and by Boesi and Goddard (1991) also suggest ENE-WSW folding.

To the south of the Burro Negro fault, Eocene rocks form a wedge of rocks that thin up toward the south and pinch out against the Paleocene unconformity (Fig. 2.6 and 2.10). In this area, deformation is transtensional related to the formation of pull-apart basins along N-NE-striking inverted faults (e.g. Icotea and Pueblo Viejo faults). Extension is mainly toward the NE as interpreted from the NW-SE striking faults (Chapter 3; Escalona and Mann, 2003b). To the north of the Burro Negro fault zone folding and thrusting of the pre-Oligocene rocks is observed (Transects 1, 2 and 3 in Fig. 2.6). The thrust front migrated E-SE and produced two pulses of coarse clastic sedimentation interpreted by Stephan (1977). The clastic main depocenters were located in front of the fold thrust belts (to the SE), east of the Burro Negro fault zone (Mathieu, 1989). Uplifted Paleocene and Eocene rocks served as a source for the middle-late Eocene clastic wedge located in the Pueblo Viejo basin area, and probably nourished adjacent areas to the south and west (Mathieu, 1989). The presence of

ophiolitic rocks within the deformed Paleocene-Eocene belt east of the Maracaibo basin (Lara nappes) suggest thin skinned obduction of fragments of the Caribbean plate over the South America margin (Stephan, 1977).

The Burro Negro fault coincides with the platform margin of northwestern South America and a re-entrant of the deep open marine basin of the proto-Caribbean during the Paleogene (Lugo, 1991; Parnaud et al, 1995b; Fig. 2.4). Gonzáles de Juana et al. (1980) defined a hinge zone located along the Trujillo Mountains, following the trace of the Burro Negro fault zone (Fig. 2.2, 2.9B and 2.10). Late Paleocene-Eocene paleogeographic reconstructions (Fig. 2.4) in the Maracaibo basin by exploratory wells, outcrop and seismic data (Gonzáles de Juana et al., 1980; Mathieu, 1989; Parnaud, 1995b) agreed that this hinge zone represents a stratigraphic boundary between the shallow marine environments to the south (platform province) and basinal environments, with the presence of slumps and turbidites, north of the Burro Negro fault area. Folding of these sediments north of the Burro Negro fault zone by the continuing advance of the Caribbean plate from the northwest over South America induced the formation of slumps interpreted by Stephan (1977) and Mathieu (1989) in the deep basin.

Pindell and Kennan (in press) interpreted the paleogeography of western Pangea from Jurassic rifting to the present. Their main observations are that Jurassic rifting produced a serrated crustal margin in northern Venezuela, with rift segments oriented approximately N70° and separated by left-lateral transfer faults striking ~ N140°. Present-day rift related faults in the Maracaibo basin are oriented between N10° to N60° (e.g. Icotea fault, Pueblo Viejo fault Tigre fault

and Boconó fault, Fig. 2.2). The Boconó and Tigre fault are oriented $\sim N60^\circ$ and probably would correlate to the main crustal margin orientation proposed by Pindell and Kennan (in press), whereas the Burro Negro fault, which is oriented $\sim N140^\circ$, would correlate to a Jurassic transfer fault.

Considering the previous discussion, it can be concluded that the Burro Negro fault defines the platform edge between the deep basin located to the N-NE and the Maracaibo platform to the S-SW. The shape of the margin may reflect a transfer fault inherited from Jurassic rifting (Pindell and Kennan, in press). The Jurassic transfer fault was reactivated by oblique collision of the Caribbean plate and formed the Burro Negro fault as a lateral ramp fault. Using Mann's (1999a) definition, the Burro Negro fault acted as a lateral ramp fault separating collided and uncollided parts of a diachronously forming fold-thrust belt.

OLIGOCENE-MIOCENE SUB-BASINS AND AREAS OF CHAOTIC REFLECTORS: Development of Oligocene-Miocene syntectonic sub-basins (Roure et al., 1997) along the syncline axis of the folds is observed on transects 1, 2 and 3 (Figs. 2.6A, B and D), north of the Burro Negro fault zone. These sub-basins are bounded by chaotic reflections defining their main fold axis including the area along the Burro Negro fault (Fig. 2.6 and 2.10). Eocene clastic rocks crop out east and west of transect 2, as well as the Oligocene and Miocene sub-basins (Surface geologic map in Figs. 2.2 and 2.10B). The trend of these sub-basins is WSW-ENE, paralleling the folds and thrusts north of the Burro Negro fault zone (Fig. 2.2 and 2.10B).

Chaotic zones separating the Oligocene-Neogene sub-basins interpreted on seismic lines in Figure 2.10 show similar features to those observed at highly fracture fault zones or shale diapirs. Chatellier et al. (1998) first proposed the presence of an Eocene shale diapir in northeastern Maracaibo basin based on the presence of near-vertical beds and shale diapirs features seen in cores, wells and seismic data. The presence of shale diapirs indicates the existence of overpressured shales. Sedimentary loading from rapid sedimentation, tectonic loading and hydrocarbon generation are some of the primary conditions needed to generate overpressured sediments and diapirism (Barber et al., 1986). These conditions are plausible along the oblique collisional Eocene margin between the Caribbean and South American plates. Active diapirism occurs in northern Colombia, the eastern Venezuela basin, the Orinoco delta, and Trinidad (Aslan et al., 2001).

Rapid mud sedimentation in front of the thrust belt deep basin areas of the Maracaibo basin (north of the Burro Negro fault) from the Cretaceous to the early Eocene provide the right geologic setting for Eocene shale diapirism. The presence of olistoliths east of the Burro Negro fault has been attributed to slumping in front of the thrust front (Stephan, 1977; Mathieu, 1989). However, surface expression of these features can be similar to chaotic deposits composed of blocks in a shale matrix in shale diapir provinces (Barber et al., 1986).

From the seismic data shown in Figure 2.10, I interpreted the chaotic zones as highly faulted and shale diapirs zones, where basinal shale is overpressured by Eocene compression. Field analysis, well information, and

denser seismic lines grid is needed in order to understand better the geometry and composition of these chaotic zones in the eastern Maracaibo basin.

THE PALEOCENE UNCONFORMITY: It represents the basal unconformity between the Eocene foredeep and the previously tilted passive margin (Di Croce et al., 1999). A Flexural bulge (uplift) is formed as a response of downwarping continental lithosphere due to tectonic loading of an active thrust front (Allen and Homewood, 1986; Giles and Dickinson, 1995), and the bulge uplift is a minor feature compared to the size of the basin as a whole (Crampton and Allen, 1995). In the Maracaibo basin the forebulge was previously mapped by Parnaud et al. (1995b) and is revealed by the Eocene isopach where thickness becomes zero (Fig. 2.4). Southward migration of younger sedimentary rocks onlapping the Paleocene unconformity reflects migration of the forebulge toward the south as subsidence increases, caused by tectonic loading in the northern Maracaibo basin (Lugo and Mann, 1995). Internal reflectors within the Eocene suggest previous unconformities surfaces, which may represent either eustatic changes or previous tectonic pulses that filled this area with continental to shallow marine deposits.

THE EOCENE UNCONFORMITY: It is present beneath most of the Maracaibo basin. Missing time across the unconformity increases toward the south, where Miocene rocks overlay Paleocene rocks (Fig. 2.7). To the north of the Burro Negro fault, early to middle Eocene rocks are overlain by Oligocene and Neogene rocks (Figs. 2.6 and 2.10), whereas in the east middle and probably late Eocene rocks are overlaid by Neogene rocks (Fig. 2.6 and 2.8).

By middle Eocene most of the Maracaibo basin was exposed. Isostatic rebound and cessation of tectonic loading over the basin are the final stage of a foreland basin, producing a regional unconformity (Emery and Myers, 1996). This regional unconformity suggests a final stage for the foreland basin in the Maracaibo area. The basin was nourished mainly from the south and southwest by a main clastic system during the early Eocene (Fig. 2.4 and 2.8).

TECTONIC LOADING: It is responsible for generating the deep depocenter (foredeep) and uplift of the continental lithosphere (forebulge). The early Eocene deep depocenter, located in the N-NE of the Maracaibo basin, is related to tectonic loading produced by the Caribbean-South American plates Paleogene collision in western Venezuela (interpreted from subsidence plots by Lugo (1991) and Lugo and Mann (1995)). The only field evidence of the thrust belt that formed the foreland basin and the orogenic event is a complex sequence of Paleocene and Eocene turbiditic rocks with some ophiolite fragments located northeast and east of the Burro Negro fault (Stephan, 1977; Stephan, 1985; Mathieu, 1989; Fig. 2.5). This evidence supports the early-middle Eocene depocenter, but there is no evidence of late Paleocene-early Eocene thrusting, north of the Maracaibo basin. Considering that collision between the Caribbean and South American plates moved diachronously from west to east, the location of the late Paleocene-early Eocene thrust front must be N-NW of the Maracaibo basin (north of the Oca fault), where there is no present-day surface evidence and little published data in the area. More field work and subsurface studies are needed in this area.

THE OCA FAULT ZONE: It is located north of the Maracaibo basin is part of the complex strike-slip boundary between the Caribbean and South America plates. Its horizontal motion during the late Tertiary is relative small (less than 100 km, Rod (1956) and Kellogg (1984). The Burro Negro fault intersects the Oca fault near the northern margin of the Lake Maracaibo. More intensive work of the Oca fault, using well and seismic data will help to better decipher the evolution of the basin in this area, and understand the tectonic configuration of the Maracaibo basin during the early Paleogene.

2.6 EOCENE BARINAS BASIN

The Eocene depocenter in the Barinas area is restricted to the middle Eocene and thickness can reach up to 1 km (3000 feet) (Fig. 2.3). Location of this depocenter is located between 50 to 100 km southwest of the Maracaibo basin middle Eocene depocenter. The two depocenters are presently separated by the 80-km-wide Mérida Andes.

Strike-slip motion along the Boconó fault is interpreted to have begun during the late Tertiary. Present-day motion is calculated to be around 7-10 mm/yr, and lateral displacements of Holocene glacial moraines indicate lateral displacement between 60-100 meters (Schubert, 1982; Audemard et al., 1999). Total horizontal displacement is still controversial but most authors agree that is more than 30 km and less than 100 km (Rod, 1956; Stephan, 1977; Schubert, 1982; Kellogg, 1984; Audemard et al., 1999). Furthermore, Stephan (1997) interpreted the leading edge of the Lara nappes to be south of the Mérida Andes,

and that the thrust front was separated from the Lara nappes by 80 km of horizontal motion along the Boconó fault (Fig. 2.5B).

Considering dextral motion along the Boconó fault, the Eocene Barinas depocenter was located 50 to 100 km northeast of its present position relative to the Maracaibo basin. By removing this displacement, the western edge of the Barinas Basin depocenter aligns to the Burro Negro fault south of the leading edge thrust front of the Lara nappes as interpreted by Stephan (1977; 1985). The amount of the strike-slip motion along the Boconó fault is still controversial at the northeast and southwest ends of the fault (Stephan, 1977; Mann and Burke, 1984). Also direct evidence for the stratigraphic link between the Maracaibo and Barinas Eocene depocenters have been removed by erosion and uplift of the Mérida Andes during the late Cenozoic.

2.7 DISCUSSION

TECTONIC ESCAPE IN NORTHERN VENEZUELA

Tectonic escape is a strike-slip dominated motion produced of colliding continental or arc material toward a nearby oceanic margin or free face (Mann et al., 1995). The tectonic escape takes place when changes in the direction of plate convergence as the plate underwent terminal collision in one direction is reoriented toward a free face by shearing the plate and accreting or forming microplates in the collided zone (Mann et al., 1995). Direction of reorientation is controlled by location of oceanic versus continental crust in front of the orogenic belt (Hippolyte et al., 1999). This process leads to rotation and creation of strike-

slip faults bounding the mobile thrust belt toward a direction where lithosphere can be subducted, and obduction of accretionary terranes along the continental margin.

Oblique collision between the Caribbean and South America plates from the Paleogene to Present has evolved from an obliquely convergent zone to a more strike-slip boundary along the northern coast of Venezuela as explained later in the tectonic model reconstructions (Fig. 2.11). This change through time, from west to east, implies that the Caribbean plate is escaping or migrating toward the east with respect to South America (Pérez et al., 2001; Trenkamp et al., 2002).

Figure 2.1A shows a series of lateral ramp faults and thrusts that have been interpreted along the northern margin of Venezuela (Stephan, 1985; Babb and Mann, 1999b). These lateral ramp faults, that contributed to obduction of accretionary terranes along northern South America, strike more to the SE in western Venezuela (i.e. Burro Negro fault), whereas in eastern Venezuela and Trinidad their strike has a more eastward component (i.e. Urica fault) (Fig. 2.1A). This change in strike along the South America margin reflects the change in direction through time of the oblique collision between the Caribbean and South American plates, as the Caribbean plate escapes toward the east. Accretionary terranes along the Venezuela Caribbean mountain ranges include the Lara Nappes, the Tinaco-Tinaquillo complex, The Loma de Hierro ophiolite and the Villa de Cura paleo-arc complexes (Stephan, 1977; Mathieu, 1989).

PRE-COLLISIONAL PALEO GEOGRAPHY IN NORTHERN VENEZUELA

The Paleogeographic shape of the northern South America continental margin was inherited from Jurassic rifting, and appears to have controlled the oblique collision between the Caribbean and South America plates (Pindell and Kennan, in press). Transfer faults connected the Jurassic rifted margin and controlled the location of re-entrants along the continental margin. I propose that these re-entrants were later reactivated as lateral ramps by west–east directed oblique collision of the Caribbean plate with the northern margin of South America, and allowed accretion of obducted terranes. The lateral ramp faults change strike angle from SE to more E in general, as the Caribbean plate escapes eastward and a free face stage is reached to the east of the collisional zone.

MODEL FOR THE PALEOGENE TECTONIC EVOLUTION OF THE MARACAIBO BASIN

An integrated reconstruction of the evolution of the Maracaibo basin during the Paleogene is summarized in Figure 2.11. Three main stages can be described as follow:

A. LATE PALEOCENE - EARLY EOCENE (Fig. 2.11A): The Maracaibo basin began to downwarp as a response of tectonic loading in the north and northeast as the Caribbean plate starts to collide with northern South America. Eocene clastic input from the south and southwest infill the basin and onlap over the Paleocene platform as tectonic loading continues. A flexural bulge formed in the central part of the basin and migrated southwards as a response of the thrust

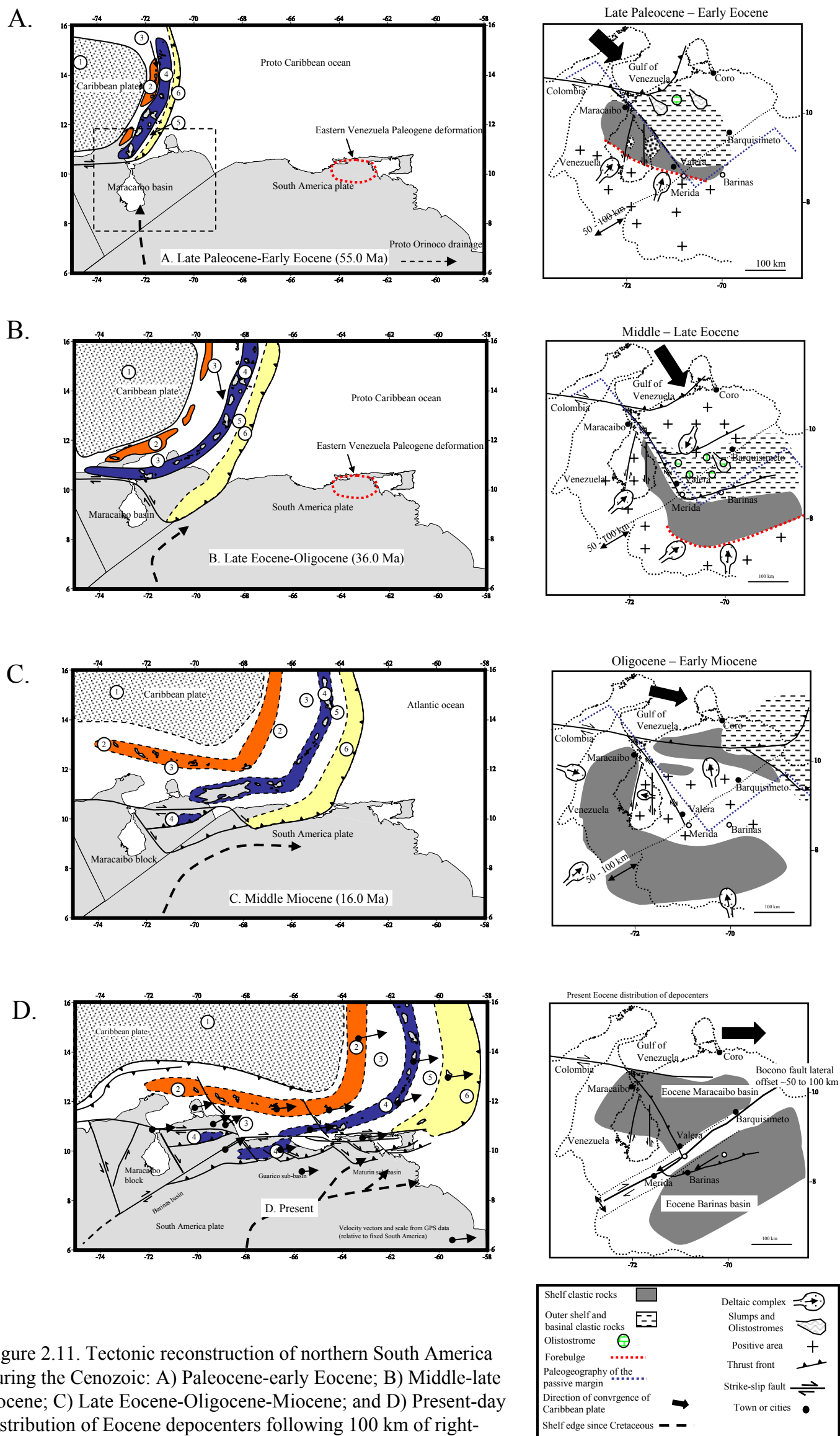


Figure 2.11. Tectonic reconstruction of northern South America during the Cenozoic: A) Paleocene-early Eocene; B) Middle-late Eocene; C) Late Eocene-Oligocene-Miocene; and D) Present-day distribution of Eocene depocenters following 100 km of right-lateral strike-slip motion along the Boconó fault.

belt located in the north-northwest. Early Eocene rocks onlap the forebulge. N-NE striking faults (Icotea and Pueblo Viejo fault) were reactivated as left-lateral strike-slip faults developing pull-apart basins along their traces allowing NW shortening. The platform margin was located along the Burro Negro fault zone at the western margin of the Trujillo Mountains (Fig. 2.11A).

B. MIDDLE – LATE EOCENE (Fig. 2.11B): Tectonic loading ended in central and south Maracaibo basin and produced a regional unconformity by tectonic rebound. The thrust front began to move southeastward and was bounded to the west by the Burro Negro fault in the northeastern part of the basin. This fault, inherited from a Jurassic transfer fault, acted as a lateral ramp fault with right-lateral strike-slip motion. A depocenter developed along the trace of the Burro Negro fault and along the trace of the reactivated Pueblo Viejo fault. Depocenters were developed in front of the thrust front, which was migrating southeastward by 100 km east of the Burro Negro fault. Simultaneous, folding and uplift of the Paleocene and Eocene rocks in front of the thrust front provided the source of sediments for the existent depocenters toward the southwest, south and southeast. The Barinas region subsided as a response of the tectonic loading caused by the leading edge of the Lara nappes. The forebulge was located toward the south and clastic input was from the south.

C. LATE EOCENE-OLIGOCENE (Fig. 2.11C): Collision of the Caribbean plate moved SE-E by tectonic escape that induced right-lateral strike-slip motion in the area. Coeval folding continued east of the Burro Negro fault. The thrust front reached its final stage in the southeast (Barinas area). In the Maracaibo

basin, strike-slip motion moved the thrust front toward the east inducing pull-apart basin formation in the Falcón area (NE of the Maracaibo basin) above previously obducted accretionary terranes. Major right-lateral strike-slip motion was probable located north of the Falcon basin (Wheeler, 1963; Muessig 1984; Boesi and Goddard, 1991). Shortening directions interpreted in the Falcón basin changed from NNW-SSE during the late Eocene to WNW-ESE in the Oligocene-Miocene (Mathieu, 1989), and appear to be the same during the Pliocene to Present (Audemard et al., 1999). Isostatic rebounding exposed the Eocene Maracaibo and Barinas basins. Syntectonic sedimentation occurred in the syncline axis of the NE trending folds east of the Burro Negro faults, and west of the Icotea fault. Interpretation of changes in the compression direction from Eocene to Present supports a more west-east strike-slip motion by the Oligocene-Miocene, where the collisional thrust front moved toward eastern Venezuela.

D. LATE TERTIARY (Boconó fault; Fig. 2.11D): Uplift of the Mérida Andes during the late Tertiary separated the Maracaibo basin from the Barinas Basin. Later lateral motion along the Boconó fault displaced the Maracaibo basin toward the northeast relative to the Barinas Basin. Horizontal offset of both depocenters range from 30 to 100 km. The Burro Negro fault and the leading edge thrust front fault are also offset.

COMPARISON OF LATERAL RAMPS FAULTS IN WESTERN AND EASTERN VENEZUELA

Eastern Venezuela exhibits a similar pattern of lateral ramp faults to those seen in the Maracaibo basin. The Urica fault, located in the Maturin sub-basin, northeastern Venezuela (Fig. 2.1A) shows a similar structural and stratigraphic setting to that of the Burro Negro fault in the Maracaibo basin (Fig. 2.12). Figure 2.12A shows an interpreted seismic line through the Urica fault (Munro and Smith, 1984; Location in Figs. 2.1 and 2.12A). The fault is interpreted as a left-lateral strike-slip fault, separating the Maturin sub-basin into a zone of compression to the northeast, from one of tension to the southwest (Munro and Smith, 1984). By the middle Miocene the Urica fault and the leading edge of the thrust front separated shelf deposits from deep marine basin (Di Croce, 1995). Figure 2.12B shows an interpreted seismic line through the Burro Negro fault located in the Maracaibo basin. As seen for the Urica fault, the Burro Negro fault separates an extensional zone to the southwest from a compressional zone to the northeast. Other similar features between the two lateral ramp faults are chaotic reflections interpreted as mud diapirs located in the compressional zone of the Urica fault, formation of syntectonic sub-basins bounded by chaotic reflections, and more continuous even reflections toward the tensional zone southwest of both faults.

A main difference between both regions is their age (Eocene vs. Miocene) and later inversion of the Maracaibo basin depocenters. Following oblique

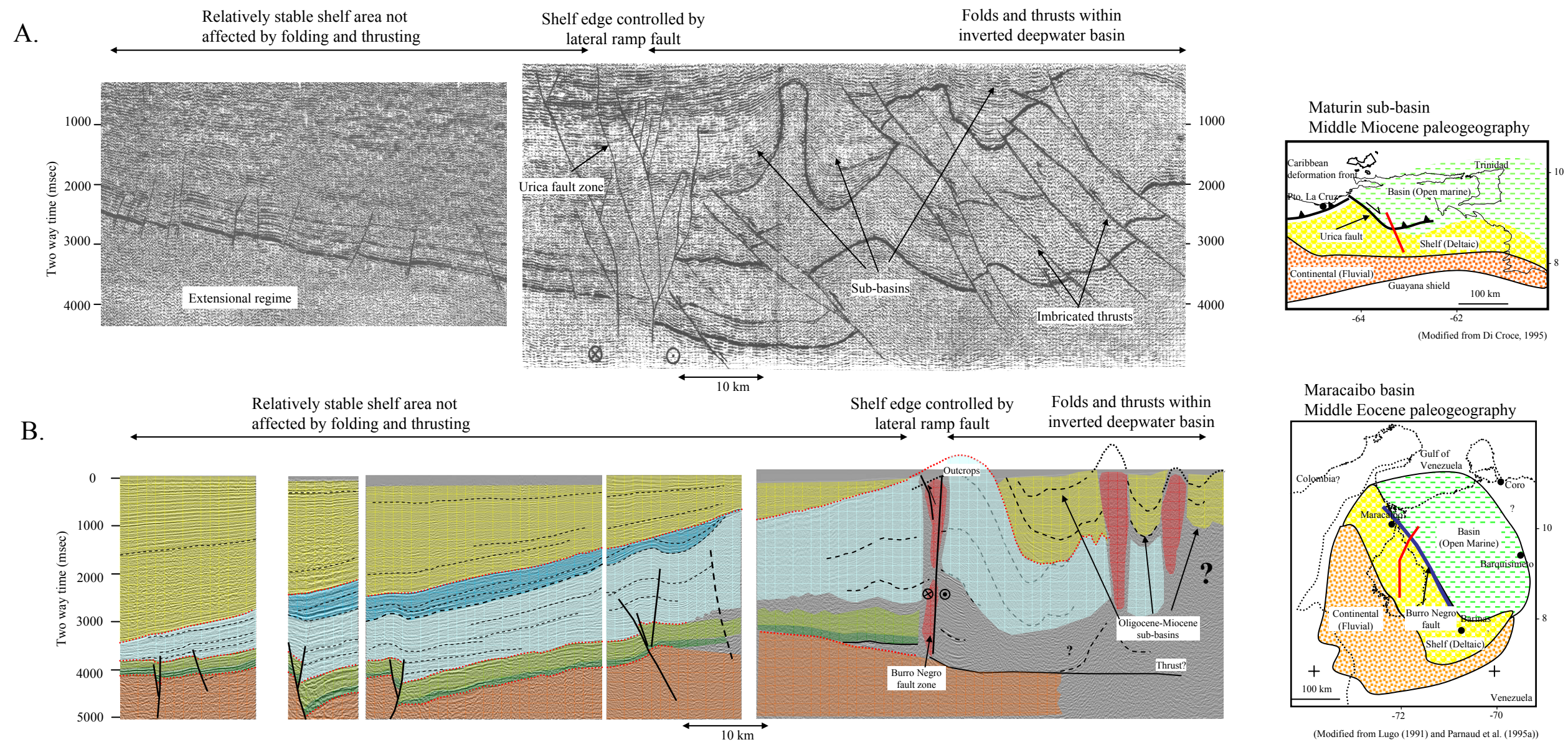


Figure 2.12. Comparison of similar lateral ramp fault deformation of different ages. A) Interpreted seismic line in the Maturin sub-basin across the Urica lateral ramp fault separating a stable platform to the west from a deformed deepwater basin and diapirs to the east. Main phase of deformation is Miocene (modified from Munro and Smith, 1984). B) Interpreted transect across the northern part of the Burro Negro fault, Maracaibo basin, from this study. The Burro Negro lateral ramp fault separates a stable platform to the west from a deformed deepwater basin and diapirs to the east. Main phase of deformation is Eocene.

collision between the Caribbean and northwestern South America in the Maracaibo basin area, uplift of the Mérida Andes occurred from late Oligocene through Recent. Andes uplift led to development of a foredeep to the south of the basin and switched the depocenter from the northeast-east during the Eocene to the south during the Miocene (Castillo, 2001). In contrast, the Maturin sub-basin has not been inverted by later tectonic events. Another difference can be observed in the trends: the Burro Negro fault strikes more to the south-southeast ($\sim N140^\circ$), whereas the Urica fault strikes more to the east-southeast ($\sim 120^\circ$) (Fig 2.1A).

The more east-directed strike of the Urica fault than the Burro Negro fault suggests major strike-slip motion between the Caribbean and South America plate by the time that Miocene collision took place in eastern Venezuela. Also, development of the exhumed and inverted Falcón basin as a pull-apart basin during the Oligocene-Miocene resembles the present-day Cariaco pull-apart basin. Analysis of this areas falls beyond the scope of this study, and further study is necessarily in order to have a more integrated interpretation of the collisional evolution between northern South America and the Caribbean plates.

2.8 CONCLUSIONS AND RECOMMENDATIONS

Interpretation of 2-D and 3-D seismic data in central and eastern Maracaibo basin, and analysis of the two different models proposed for the Paleogene evolution in the basin, allowed me to develop the following conclusions:

- The Maracaibo basin records several deformations during the collision between the Caribbean and the South America plates in the Paleogene:

- a. Late Paleocene-early Eocene: A foreland basin formed with its main depocenter located north and northeast of the basin. A forebulge formed in the southern part of the basin. Pre-existing N-NE trending faults were reactivated.

- b. Middle-late Eocene: Strike-slip motion through a lateral ramp fault controlled the middle-late Eocene depocenters and directed the thrust front toward the SE, ending the foreland basin stage in most of the Maracaibo basin. Major Eocene depocenters were located along the trace of the tear fault. Folding of Paleogene rocks within the SE diverted thrust front produced Oligocene and Neogene sub-basins within the fold synclines.

- The Burro Negro fault represents the platform break in the Maracaibo basin from Cretaceous to Eocene. The fault separates an unthrust, asymmetrical shallow to deep basin from a thrust area of deepwater sedimentary rocks. It was inverted as a tear fault or lateral ramp fault allowing SE motion of the leading edge Caribbean deformation front, east of the Maracaibo basin. When offset along the Boconó fault is removed the lateral ramp-thrust geometry of the Burro Negro fault connects the Eocene depocenters of the Maracaibo and Barinas basins. Because the Burro Negro fault forms a line of separation between shallow to outer shelf rocks to the SW and deep marine rocks to the NE, these paleogeographic boundaries suggest that the serrated aspect of the margin was inherited from Mesozoic rift structures and was subsequently reactivated by Eocene and younger

thrusting. Field work is necessarily in order to determine motion and age of the fault. This will help to support the evolution model proposed in this dissertation.

- The presence of chaotic reflections zones NE of the Burro Negro fault reveals complex structural features which may have been formed by overpressured shales. Further surface and sub-surface analysis of this area is recommended to understand the cause of these chaotic zones.

- Oligocene-Neogene sub-basins are a sub-surface continuation of those observed in the surface in the northeast parts of the Maracaibo basin.

- The Barinas basin formed as a part of the SE thrust front controlled by the Burro Negro fault. Later Andean uplift and right-lateral motion along the Boconó fault separated the main depocenters of both basins.

- Interpretation of the Burro Negro fault, located in the Maracaibo basin and the Urica fault located in the Maturin sub-basin revealed similar geological features. Both faults separated tensional stable shelf areas from highly deformed fold thrust belts. Both faults acted as tear faults or lateral ramps that allowed SE motion of the thrust front.

- This study supports the inherited, serrate paleogeographic shape of the South America continental passive margin as proposed by Pindell and Kennan (in press).

CHAPTER 3

Three-dimensional structural architecture and evolution of an Eocene pull-apart basin, central Maracaibo basin, Venezuela ¹

3.1 INTRODUCTION

The origin, evolution and recognition of strike-slip faults and pull-apart basins have been widely studied in experimental models (Hempton and Neher, 1986; McClay and Dooley, 1995; Gölke and Cloetingh, 1994), as well as in the field using outcrops (Wilcox et al., 1973; Reading, 1980; Rodgers, 1980; Mann et al., 1983; Aydin and Nur, 1985) and in the subsurface using well and seismic data (Christie-Blick and Biddle, 1985; Harding et al., 1985; Wood et al., 1994). Two models are proposed to explain the formation and evolution of transtensional basins along strike-slip faults: 1) Formation of transtensional rhombohedral “pull-apart basins” at stepovers, or discontinuities, along traces of strike-slip faults (Mann et al., 1983; Naylor et al., 1986; Sylvester, 1988; Gölke and Cloetingh, 1994; McClay and Dooley, 1995); 2) Formation of more elongate and rift like basins produced by fault-normal extension simultaneous with strike-slip motion (Ben-Avraham and Zoback, 1992;).

The pull-apart model predicts that the two longitudinal sides of the basin are bounded by strike-slip faults, and basin-transverse faults are dominantly normal. Lengthening of the basin is accomplished by accumulated strike-slip displacement along the “master” strike-slip faults, which link transverse normal

¹ In Marine and Petroleum Geology, 2003, with co-author P. Mann

faults at the ends of the basin (Mann et al, 1983; McClay and Dooley, 1995). In contrast, the fault-normal extension model is based on the interpretation that pull-apart basins are bounded on one side by strike-slip faults and on the other by normal faults striking sub-parallel to the transform. This juxtaposition of sub-parallel strike-slip and normal faults suggests that both strike-slip and normal faulting processes occur together as a result of crustal weakness around the entire faulted zone (Ben-Avraham and Zoback, 1992).

The 30,000 km² Maracaibo basin, located in northwestern South America (Fig. 3.1A), records a complex geologic evolution history lasting from the Late Jurassic to the present (Lugo and Mann, 1995; Parnaud et al., 1995b). One of the main structural elements of the basin is the linear ~100 km long, N-S striking Icotea fault. Studies regarding the sense of displacement along the Icotea fault is controversial and has been interpreted as left-lateral strike-slip with 7.5 to 18 km of offset (Krause, 1971; Lugo, 1991; León et al., 1999), thrust with a right-lateral oblique-slip component (Munro, 1985; Audemard, 1991) and inverted normal fault lacking strike-slip displacement (Castillo, 2001).

Models of formation of transtensional basins along strike-slip faults, as well as the motion along the Icotea fault, are poorly constrained because previous interpretations have been restricted by the use of widely spaced 2-D seismic lines. Three dimensional seismic data covering an area of approximately 2000 km² collected during hydrocarbon exploration of the Maracaibo basin were used to place constraints on the three-dimensional structural architecture and evolution of the Icotea sub-basin. The objectives in this chapter are to:

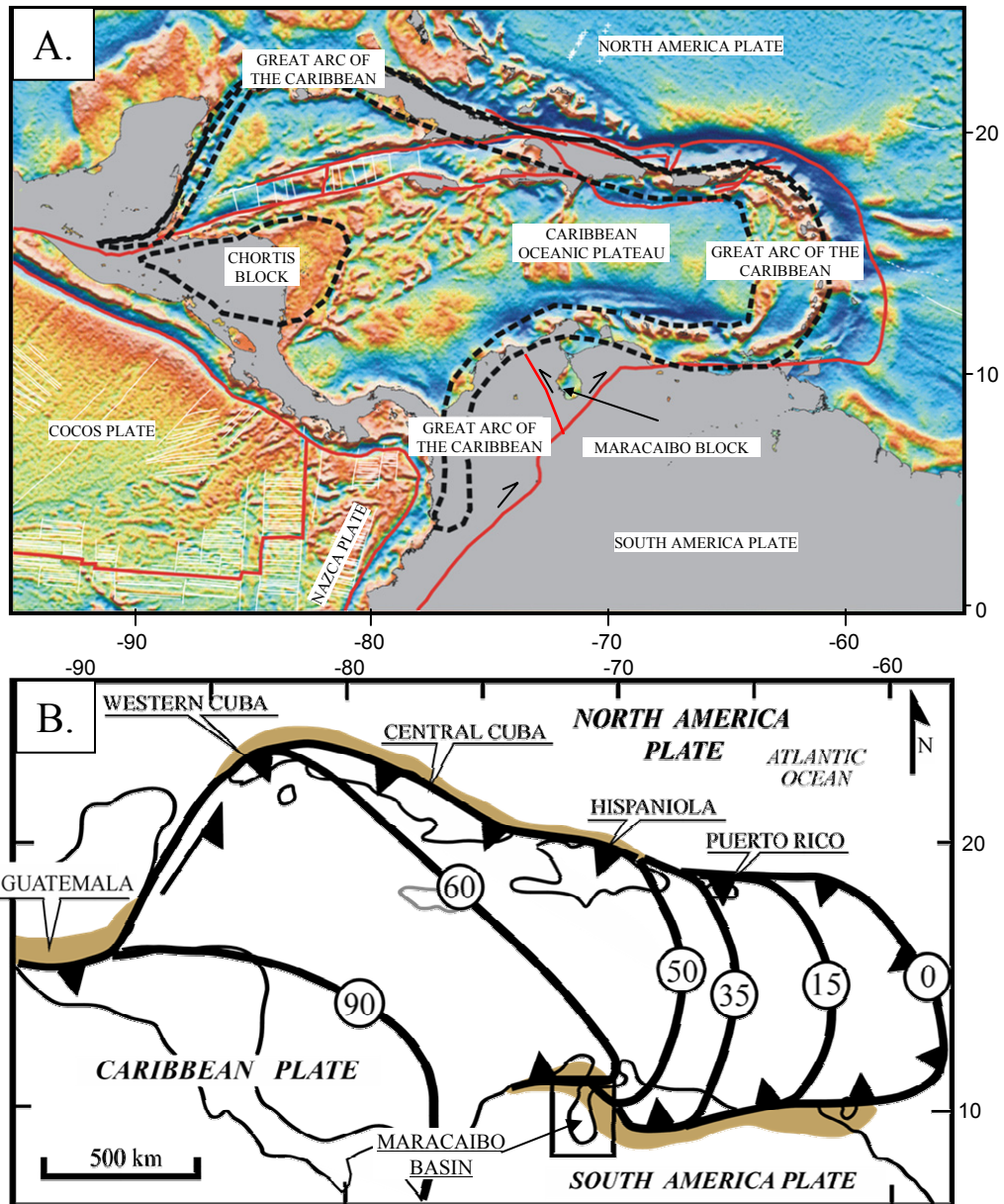


Figure 3.1. (A). Major crustal provinces of the Caribbean region: Precambrian-Paleozoic Chortis block; Cretaceous oceanic plateau of the central Caribbean; Early Cretaceous-Recent Great Arc; and passive margins of North and South America. Red lines indicate active plate boundaries (modified from Mann, 1999b). (B) Inferred position of the leading edge of the Great arc at: 90 Ma - Late Cretaceous; 60 Ma- Paleocene; 50 Ma- Eocene; 35 Ma- Oligocene; 15 Ma- Miocene; 0 Ma- Recent (modified from Lugo and Mann, 1995).

1. Provide a complete fault description of the evolution of the Icotea pull-apart basin within its Eocene, oblique collision-related, tectonic framework,
2. Quantify the amount of normal fault displacement that formed the basin using vertical and antithetic shear methods. Both methods yield minimum estimates for the horizontal displacement along the Icotea fault that can be compared to estimates by previous workers; and
3. Determine which basin-forming model (pull-apart vs. transform-normal extension) best fits observations from 3-D seismic data.

3.2 PLATE TECTONIC SETTING OF THE MARACAIBO BASIN

The geology of the Maracaibo basin, located in northwestern South America, is dominated by complex Mesozoic-Cenozoic interactions between North American, South American and Caribbean plates (Fig. 3.1). The basin records an evolution from the separation and rifting between North America and South America during the Jurassic, followed by migration of the Caribbean plate to its present position since the late Paleocene (e.g., Lugo and Mann, 1995).

Most workers now accept that the Caribbean region originated in the eastern Pacific and was transported into its present position between North and South American plates along large-offset strike-slip faults and oblique subduction zones (Burke, 1988; Pindell and Barrett, 1990; Mann, 1999b) (Fig. 3.1A). The age of collisional deformation and sedimentary overlap between the Caribbean plate and the passive margin of southern North America and northern South America is diachronous, with older Late Cretaceous-Paleocene deformation in western

Colombia and Yucatan Peninsula, and younger Oligocene-Recent deformation in the east in northeastern South America (Fig. 3.1B).

The major pulse of tectonically driven subsidence in the central and eastern margin of the Maracaibo basin occurred during an oblique collisional event between the Caribbean and South American plates (Pindell and Barret, 1990; Lugo, 1991; Lugo and Mann, 1995; Castillo, 2001). Prior to the collision event, the margin was a passive margin characterized by slow, thermally related subsidence following Jurassic rifting between North and South America, interpreted by the presence of rift related rocks in the Maracaibo basin (Audemard, 1991; Lugo, 1991; Lugo and Mann, 1995; Roure et al., 1997; Castillo, 2001).

3.3 LATE NEOGENE TO PRESENT GEOLOGIC SETTING OF THE MARACAIBO BASIN

The Maracaibo basin is an actively subsiding, triangular, intermontane basin occupying an area of western Venezuela where the northern Andes bifurcates into a western branch (Sierra de Perijá) and an eastern branch (Mérida Andes) (Fig. 3.2). The topography and elongate geologic outcrop patterns of both ranges adjacent to the Maracaibo basin are closely controlled by northwest to northeast transpressional strike-slip faults (e.g., Boconó fault).

GPS results indicate that the triangular area bounded by these faults and including the Maracaibo basin (“Maracaibo block” of Mann and Burke, 1984) is actively moving north-northeast relative to the rest of the South American plate (Pérez et al., 2001; Trenkamp et al., 2002). Present-day plate motion includes a

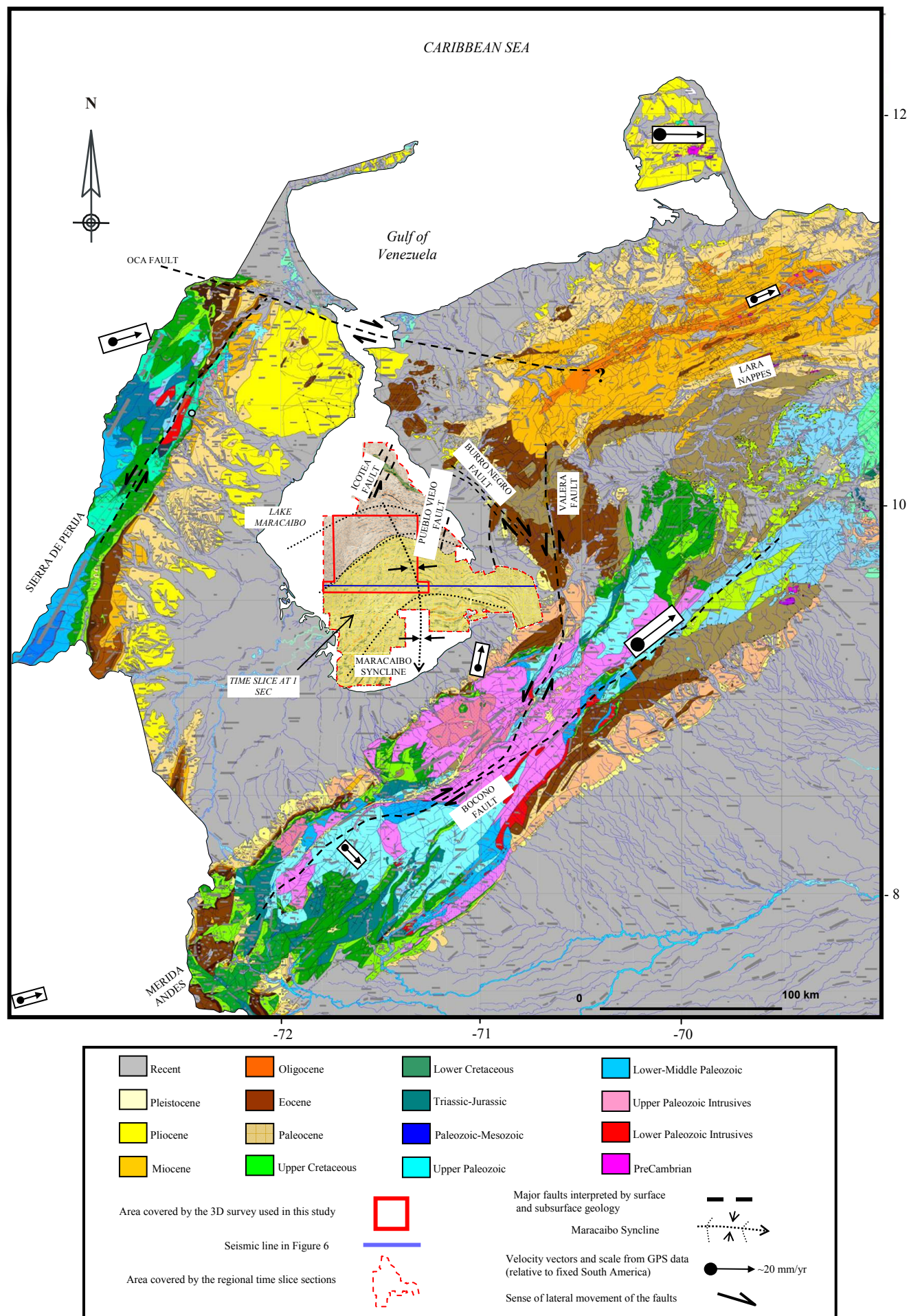


Figure 3.2. Surface geologic map of the Maracaibo basin region (modified from Borges, 1984) and seismic time slice at 1 second beneath the floor of the Lake Maracaibo. The present-day topographic and geologic configuration of the basin is controlled by uplift of the Mérida and Sierra de Perijá mountain ranges and by formation of the Miocene-Recent Maracaibo syncline. GPS velocity vectors from Trenkamp et al. (2002) and Pérez et al. (2001) indicate direction and relative rate of displacement of the Maracaibo block to the N-NE relative to the rest of South American plate. N-NE-striking, pre-Oligocene faults characterize the subsurface of Lake Maracaibo (Icoetea and Pueblo Viejo faults). The Burro Negro fault bounds the present Maracaibo basin by its northeastern boundary. The boxed area of 3D seismic study is located in the central part of Lake Maracaibo.

large component of late Neogene east-west-oriented convergent motion across the Maracaibo block and surrounding mountain ranges that is thought to be related to the collision of the Panama arc against the northwestern corner of South America (Taboada et al., 2000).

Figure 3.2 shows the present-day surface geology of the Maracaibo basin and an interpreted seismic time slice at 1.0 second beneath the floor of Lake Maracaibo from Castillo (2001). Lake Maracaibo, with a maximum water depth of approximately 30 m, forms a shallow topography depression in the central part of the basin. The lake occupies approximately 30% of the total area of the basin (Fig. 3.2). Subsurface deformation within Lake Maracaibo at the 1.0-second level intersects the stratigraphic level from late Miocene to Pleistocene. These Neogene rocks dip into a north-south-oriented syncline (“Maracaibo syncline” of Castillo, 2001) while the surrounding surface geology shows a combination of northeast fault and fold trends (Fig. 3.2). The Maracaibo syncline probably reflects active east to west convergence as discussed by Taboada et al. (2000) and Trenkamp et al. (2002).

3.4 LATE PALEOCENE-EOCENE GEOLOGIC SETTING OF THE MARACAIBO BASIN

During the late Paleocene and Eocene, the geologic and structural setting of the Maracaibo basin was very different from the late Neogene to present setting previously described. Figure 3.3 shows an interpretation of a seismic time slice at 3.4 seconds in the present-day geography of Lake Maracaibo, intersecting Cretaceous to Miocene rocks. Prominent structural features interpreted include the

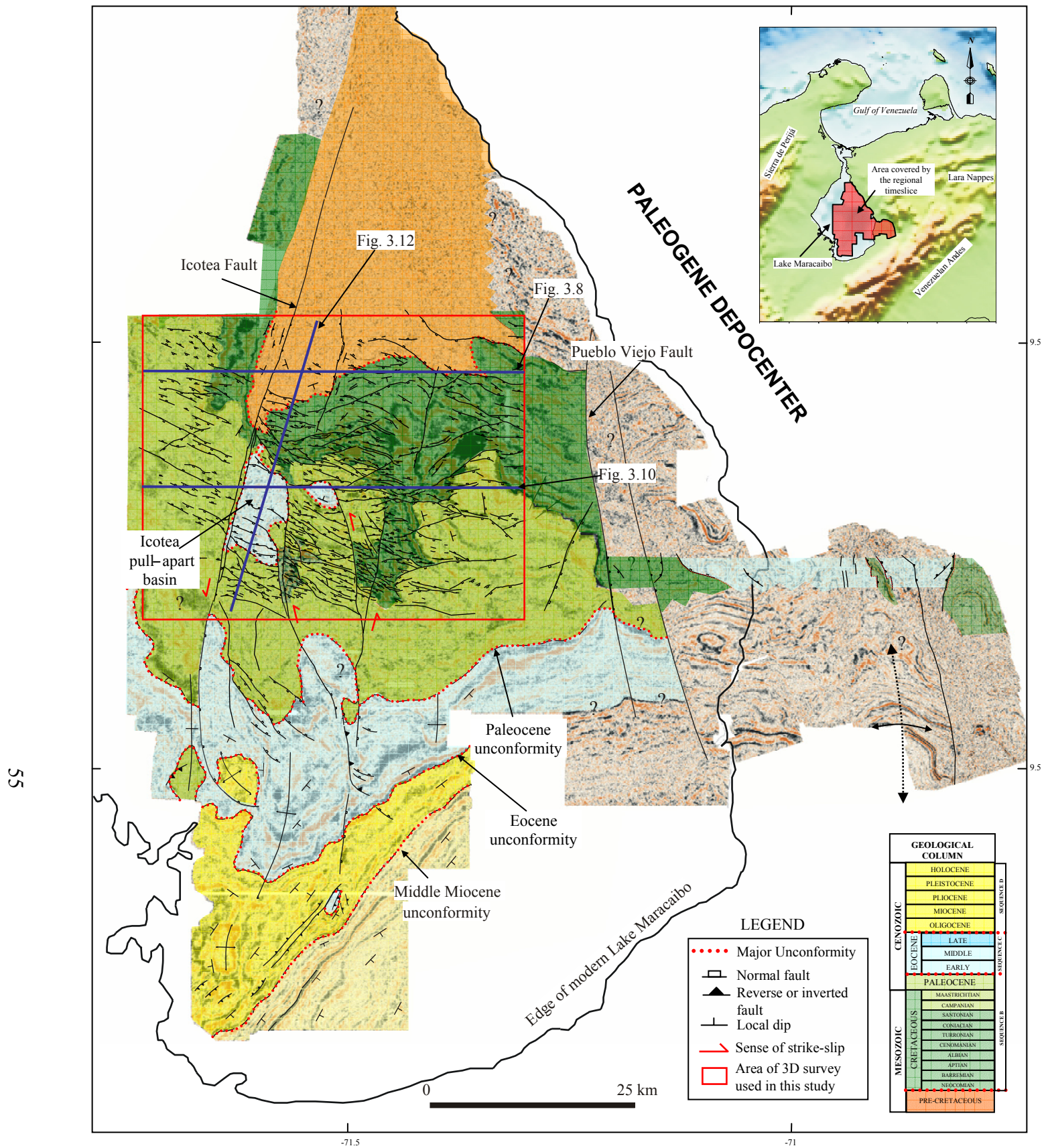


Figure 3.3. Interpreted regional seismic time slice at 3400 ms level showing the main structural styles in the Eocene, Paleocene, Cretaceous and Pre-Cretaceous stratigraphic levels (modified from Castillo, 2001). All seismic sequences in the boxed area shown in detail in Figure 3.5. N-NE and NW-SE striking faults are also shown. The Eocene Icoatea pull-apart basin formed by 0.8 to 2.2 km of left-lateral strike-slip displacement on the Icoatea fault zone.

remarkably linear and sub-parallel N-striking Icotea and Pueblo Viejo faults. Most of the N-striking faults terminate before reaching the southern area of Lake Maracaibo (Castillo, 2001).

Another important family of east-west-striking faults is observed, mainly in the central area of the lake (Fig. 3.3). These faults are less continuous, but more numerous and closer spaced. These faults have been previously interpreted as a flexural response to the subsidence of the South American plate due to the collision with the Caribbean plate (Roure et al., 1997; Castillo, 2001). The fault dips of the EW fault family are mainly to the north and northeast. Other major features interpreted on Figure 3.3 are regional unconformities present in the Maracaibo basin (e.g., Pre-Cretaceous-Cretaceous unconformity, Paleocene unconformity, Eocene unconformity, and a middle Miocene unconformity).

The location of an Eocene depocenter at a left-step along the Icotea fault, interpreted on Figure 3.3, supports the previous interpretation that the fault is left-lateral in nature, and that the depocenter is a pull-apart basin formed at a left-step in the fault traces (Krause, 1971; Naylor et al., 1986; Lugo, 1991; León et al., 1999). The disappearance of most faults and stratigraphic thickness anomalies above the Eocene regional unconformity indicates that most strike-slip movement and associated basins within the Maracaibo basin were confined to Eocene time.

3.5 DATABASE AND METHODOLOGY

DATABASE: This study uses 2000 km² of 3-D seismic data, located at the center of the Maracaibo basin (Figs. 3.3 and 3.4). Location and orientation of the

lines and crosslines within the 3-D survey are shown in Figure 3.4. Regional seismic time slices, produced by merging 3-D seismic surveys that cover most of the Lake Maracaibo area (Castillo, 2001), were incorporated (Figs. 3.2 and 3.3). Well logs located on the eastern part of the 3-D survey were also incorporated to provide age and lithologic control (Fig. 3.4).

METHODOLOGY: Conventional interpretation of 3-D seismic data was carried out. Generation of synthetic seismograms using well logs to provide improved correlations between seismic reflectors and well data was followed by interpretation of the main, regionally-continuous seismic reflections and reflection terminations (Fig. 3.5). The main unconformity-based sequences were delineated in the basin, and isochron maps and a discontinuity map were generated to identify major and subtle changes in thickness and to detect fault discontinuities from changes in dip and reflection character. Interpretive subsurface time slice sections were constructed from the 3-D seismic survey, which incorporates age data, unconformity-based sequences, and detailed structural observations. This approach allows a systematic analysis of the major deformation events that make up a basin, following the methods of Brown (1996) and Castillo (2001) (Fig. 3.4). Regional seismic time slices modified from Castillo (2001) were used to place regional constraints on the area covered for the 3-D seismic survey. Finally, I conducted a structural fault restoration using the vertical shear and 60° antithetic shear of a seismic line longitudinally through the Icotea basin.

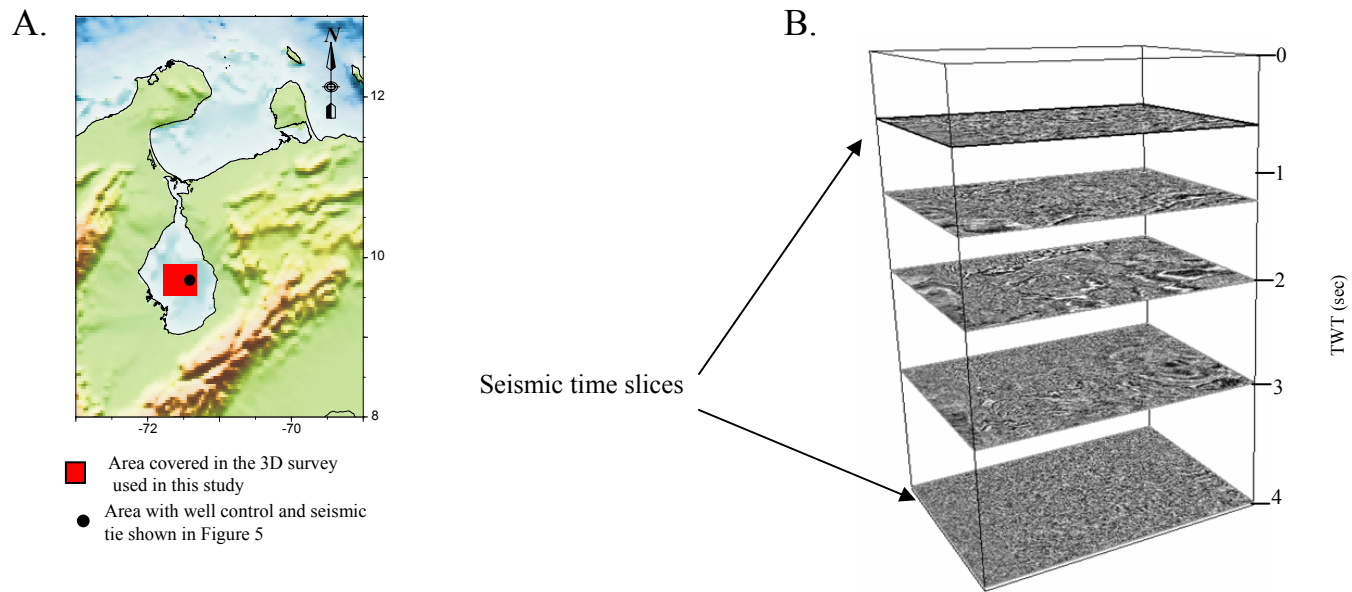


Figure 3.4. A) Location of the 3-D seismic data cube used in this study. B) Illustration of five representative seismic time slices taken at 1 second time intervals through the 3-D seismic cube volume.

Figure 3.4 continues

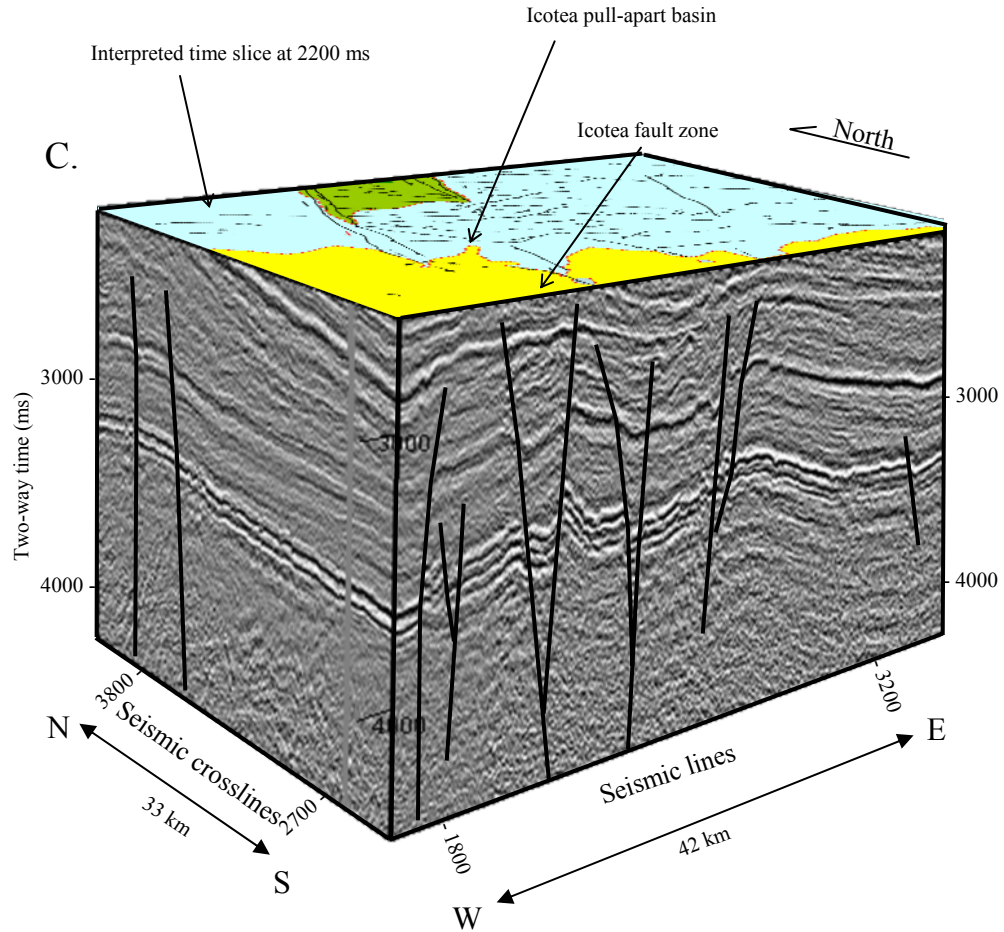


Figure 3.4. C) 3-D view of the seismic cube showing an interpreted seismic time slice at 2200 ms.

3.6 SUBSURFACE SEISMIC UNITS IN THE CENTRAL MARACAIBO BASIN

MAIN SEISMIC SEQUENCES: Four major, tectonostratigraphic sequences (A-D), based on major regional unconformities in the Maracaibo basin, were interpreted in the area. Their distinct log response and seismic character is summarized in Figure 3.5. Following the sedimentary sequence cycle hierarchy devised by Vail et al. (1977), the stratigraphic record of the central Maracaibo basin consists of one Mesozoic-Recent first-order cycle, with a duration of approximately 200 my. Sequence classification in Figure 3.5 is modified slightly from Lugo and Mann (1995), Parnaud et al. (1995b) and Castillo (2001):

A) PALEOZOIC OROGENIC PHASE (PRE-SEQUENCE A): Metamorphic basement rocks beneath the Maracaibo basin which crop out in the adjacent Perijá and Mérida Andes were deformed during the Appalachian-Ouachita-Marathon collision between the Gondwana and Laurentia continental blocks.

B) LATE JURASSIC RIFTING PHASE (SEQUENCE A ~ 208 TO 131 MY.): Linear, north-northeast striking faults, originated as normal faults bounding Late Jurassic half-grabens and were reactivated as strike-slip and reverse faults during the Paleogene (Lugo and Mann, 1995; Parnaud et al., 1995b; Roure et al., 1997). Sedimentary rocks derived from the erosion of continental rift blocks include upper Jurassic alluvial and lacustrine sedimentary rocks of the La Quinta Formation (Fig. 3.5). These rocks are poorly known in the Maracaibo basin due to their great depth beneath the overlying Cretaceous and Cenozoic rocks, but have been mapped from outcrops in the surrounding mountain ranges (Schubert et al., 1979; Gónzales de Juana et al., 1980).

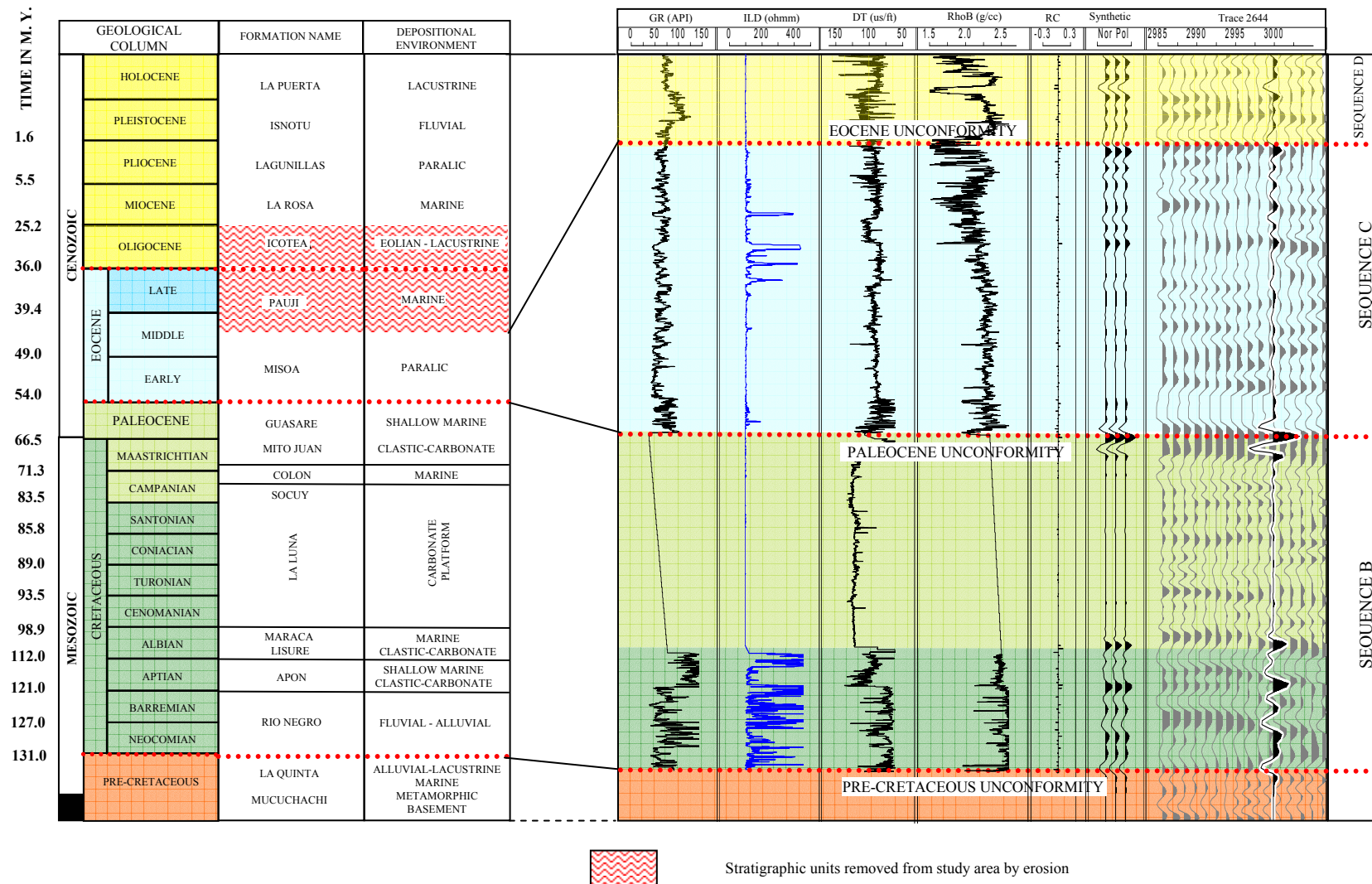


Figure 3.5. General stratigraphic column used for the area of study. Typical well log and seismic response for the three main second-order sequences defined in this study are shown. Middle Eocene-Oligocene deposits are not present in the area of study, based on palynological data. Formation names, ages and depositional environments compiled from Lugo and Mann (1995), Parnaud et al. (1995b) and Castillo (2001). Time scale from Gradstein et al. (1995).

C) CRETACEOUS AND PALEOCENE PASSIVE MARGIN PHASE (SEQUENCE B ~ 131 TO 66-54 MY.): Following rifting, a Lower Cretaceous–Paleocene, mixed clastic-carbonate platform formed across the present-day Maracaibo basin. Thermal subsidence led to sediment accumulation and tectonic quiescence resulted in an absence of significant structures during this period (Lugo and Mann, 1995). Prominent reflectors in this sequence include the base of sequence B (formed by impedance contrast at carbonate-basement rocks or carbonates-red beds) and the top of sequence C (impedance contrast at carbonate-clastic contact), attributed to a Paleocene unconformity (Fig. 3.5).

D) LATE PALEOCENE TO LATE EOCENE COLLISIONAL PHASE (SEQUENCE C ~66-54 TO 49-36 MY.): Oblique collision between the Caribbean plate and the northwestern margin of South America produced a complex wedge of clastic sediments and accretionary terranes in the northeastern part of the Maracaibo basin (Lara nappes of Stephan, 1977; Fig. 3.2). This collisional deformation began in the Maracaibo basin and becomes younger toward the east (Pindell and Barrett, 1990; Lugo and Mann, 1995; Mann, 1999b) (Fig. 3.1). This collisional phase in the Maracaibo area can be subdivided into different periods:

Period 1: During the Late Cretaceous and Paleocene, the Caribbean plate started to collide with the north-western part of the Maracaibo basin (Fig. 3.1B), but most of the Maracaibo basin area remained as a passive margin with only a few inverted or newly-developed convergent or strike-slip structures. This period is interpreted by Lugo and Mann (1995) and Parnaud et al. (1995b) as the passive

to active-margin transition with the development of a foredeep along the NE edge of the Maracaibo basin.

Period 2: Late Paleocene to middle Eocene, development of a foreland basin (Lugo and Mann, 1995; Parnaud et al., 1995b) related to continuation of the oblique collision between the Caribbean plate and the South American plate. Figure 3.6 shows an EW seismic line with the main tectonic elements of the Paleogene Maracaibo basin, including: 1) a westward-thinning, asymmetric clastic wedge of early to late Eocene; 2) a partially inverted graben within the basin (Pueblo Viejo sub-basin); and 3) the Icotea pull-apart basin, close to the area where the Eocene sediment rocks pinch out. Paleogene collision is characterized by SE migration of the depocenter through time, as shown in isopach maps in Lugo and Mann (1995) (Fig. 3.3). A complex angular unconformity formed during the end of this period (Fig. 3.6) was probably produced by a combination of collision-related folding and thrusting and the formation of a flexural bulge due to vertical loading (Audemard, 1991; Lugo, 1991; Parnaud et al, 1995; Chapter 2). This unconformity is called the Eocene unconformity (Fig. 3.5).

E) OLIGOCENE-RECENT CONVERGENT MARGIN, MARACAIBO SYNCLINE (SEQUENCE D 36-25 MY. TO RECENT): This phase of basin development is characterized by the uplift of the Sierra de Perijá and the Mérida Andes. The formation of the N–S Maracaibo syncline (Castillo, 2001) is the final stage of this evolution, and controls the present-day geographic configuration of the basin (Fig. 3.2). The main convergent structural style developed (in addition to the

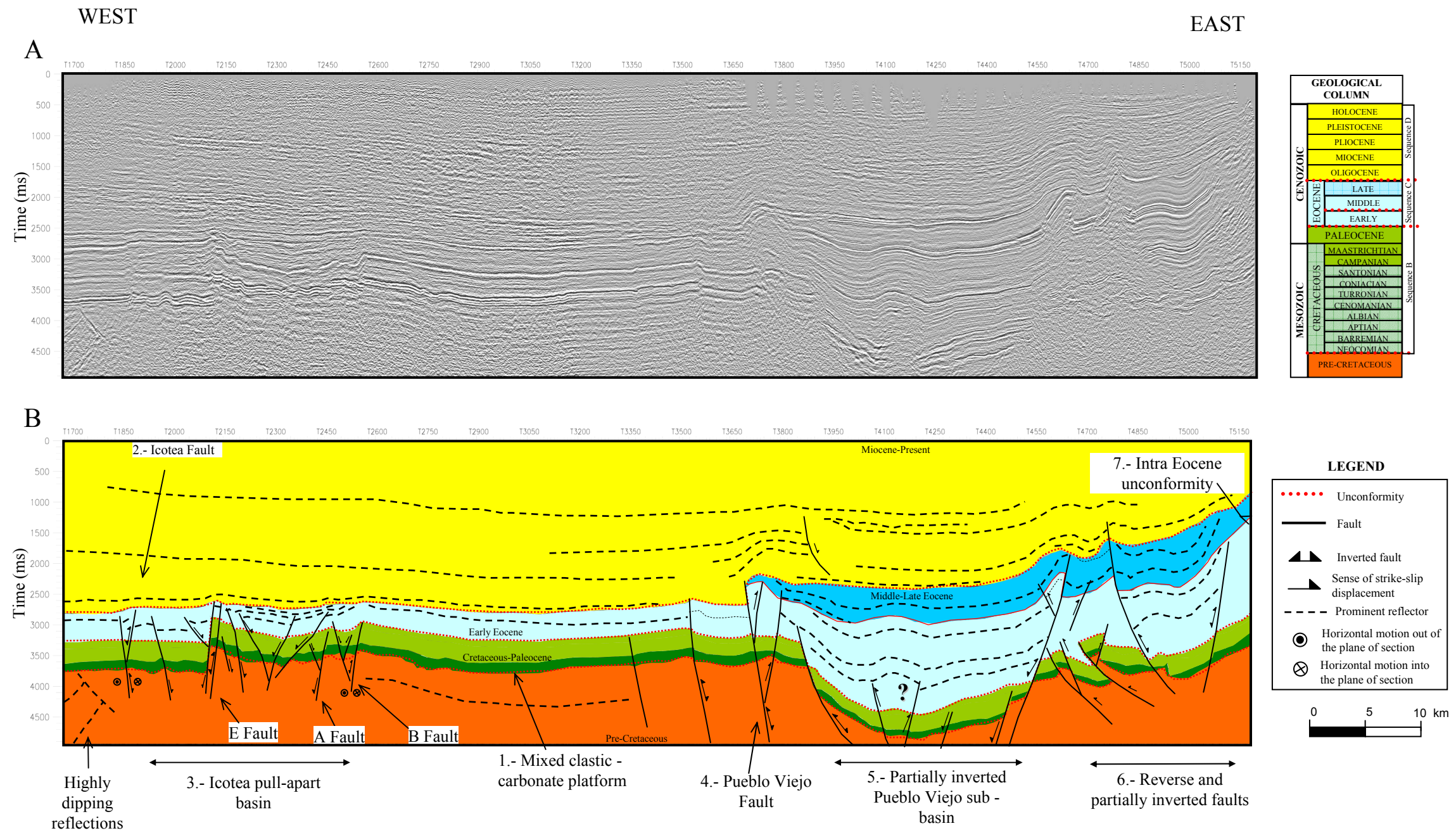


Figure 3.6. A) Uninterpreted east-west regional seismic line (Location on Fig. 2). B) Interpreted seismic line showing the main structural and stratigraphic features of the Lake Maracaibo area: 1) Stable mixed clastic-carbonate platform during the Cretaceous and Paleocene; 2) Ico tea fault; 3) Ico tea sub-basin; 4) Pueblo Viejo fault; 5) partially inverted Pueblo Viejo sub-basin; 6) inverted oblique-slip fault and; 7) Early-middle Eocene unconformity.

Maracaibo syncline) is the inversion of Eocene structures in the central part of the basin during the Oligocene and early Miocene (Figure 3.6), and uplift of the Sierra the Perijá and the Mérida Andes along thrust systems near the bases of mountain fronts (Audemard, 1991; Duerto, 1998; Castillo, 2001). This period of basin development is of less interest to this study since the Icotéa strike-slip fault became largely inactive by Oligocene time.

3.7 DESCRIPTION OF THE ICOTEA PULL-APART BASIN

Interpreted isochron and edge detection maps

An isochron map of the uppermost Paleocene unconformity is presented in Figure 3.7A. An asymmetrical depression (Icotéa pull-apart basin), and a major elongate uplift, north and east of the sub-basin, bounded by N-NE striking faults, is seen on the isopach map. Edge-detection maps of the top of the Cretaceous limestone and the Paleocene unconformity (Fig. 3.7B) highlight the three main fault families in the area of the pull-apart:

- N-NE-striking faults (Icotéa, A, B, C, D, E faults)
- NE-SW-striking faults, evident only in the top of the Cretaceous limestone
- NW-SE-striking faults (F fault)

The isochron map between the top of the Cretaceous limestone and the Paleocene unconformity reflects a constant time thickness, but areas along the NW striking faults show subtle thickness variations. This observation suggests

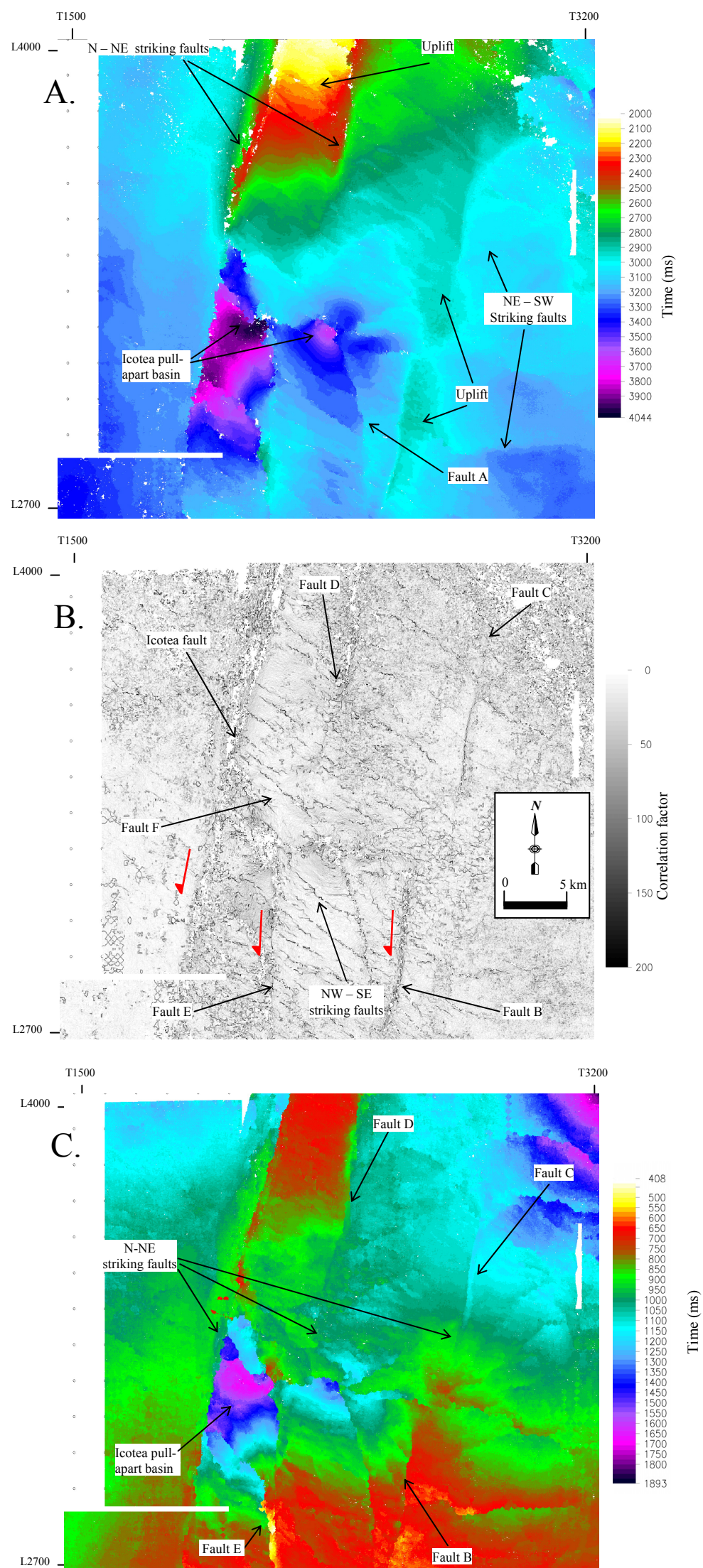


Figure 3.7. A) Isochron map of the top of sequence B (Paleocene unconformity). The asymmetrical depression and uplifted areas is still recognized. B) Edge detection map of the top of sequence B (Paleocene unconformity): two main fault trends, N-NE and NW-SE, are observed. The NE-SW fault trend is not evident, but the NW-SE faults are better seen on both maps. C) Isochron map of sequence C (Eocene): A thick section of Eocene sedimentary rocks is filling the depression (Icotéa sub-basin) interpreted in Figure 3.7A. Eocene sedimentary rocks thin across uplifted areas, but thickening of the Eocene sedimentary sequence occurs toward the NE.

that the basin was deformed by late Paleocene NE–SW faults, probably formed during extension related to flexural loading (Castillo, 2001).

The isochron map between the Eocene and the Paleocene unconformity (Fig. 3.7C) shows abrupt changes in thickness of sequence C. The asymmetrical development of the Icoatea pull-apart basin and its related uplifts controlled these abrupt thickness changes. Sequence C shows a general wedge shape, thinning to the south and thickening to the northeast, but the main area of deformation and subsidence occurs in the area between the N–NE-striking faults (Icoatea and B faults) (Fig. 3.7C). The deformed pull-apart basin area is characterized by an asymmetrical depression filled with Eocene rocks in the area adjacent to the east of the Icoatea fault and by thinning in the uplifted areas.

Seismic time slices

The structure of the Neogene and older sedimentary rocks in the Lake Maracaibo basin shows the southward-plunging Maracaibo syncline (Fig. 3.2). Areas in the central part of the basin show more complex structures during Eocene time (Fig. 3.3). I document the Maracaibo syncline and more complex, deeper structures using five deeper time slices:

Seismic time slices at 2200 ms and 2600 ms

At these intervals, the Maracaibo syncline deforms the Oligocene–Miocene section (sequence D). For the Eocene (sequence C) and Cretaceous–Paleocene (sequence B), the syncline is disrupted by a major anticline plunging southward. The anticline is bounded by NNE–SSW-striking faults in the northern part of the seismic time slice (Figs. 3.13A and 3.13B). Sequence D shows faulting

deformation at the level of the Eocene unconformity, whereas sequences B and C are affected by folding. Furthermore, NW-SE striking faults interpreted in the time maps are recognized beneath sequence D.

Seismic line 3800 (Fig. 3.8) cuts through the main structural features observed in seismic time slices at 2200 ms and 2600 ms. Line 3800 shows a major uplift affecting all sequences from pre-Cretaceous sedimentary rocks (acoustic basement) to the early stages of sequence D (Fig. 3.8). Sequence B, in general, has the same thickness across the whole study area. Sequence C thins in the uplifted area, where truncation is interpreted from seismic reflection terminations (Fig. 3.8B). Thickening occurs at both sides of the uplift, and lap terminations are observed over the basal unconformity. Sedimentation of sequence C appears to be syntectonic.

Seismic time slices at 3400 ms and 3800 ms

Seismic time slice at 3400 ms shows a major asymmetrical pull-apart basin controlling sequence C of Eocene age (Fig. 3.9A). The pull-apart basin is bounded by uplifted areas along the N-NE fault trend. The major stratigraphic thickening appears to be controlled by the Icotea fault, although faults A, B and E are locally important in subdividing the pull-apart basin in different Eocene depocenters (Fig. 3.9A). NE-striking normal faults become evident in sequence B, whereas faults striking NW are recognized throughout the area, and in all the sequences except in the seismic time slice at 2200 ms.

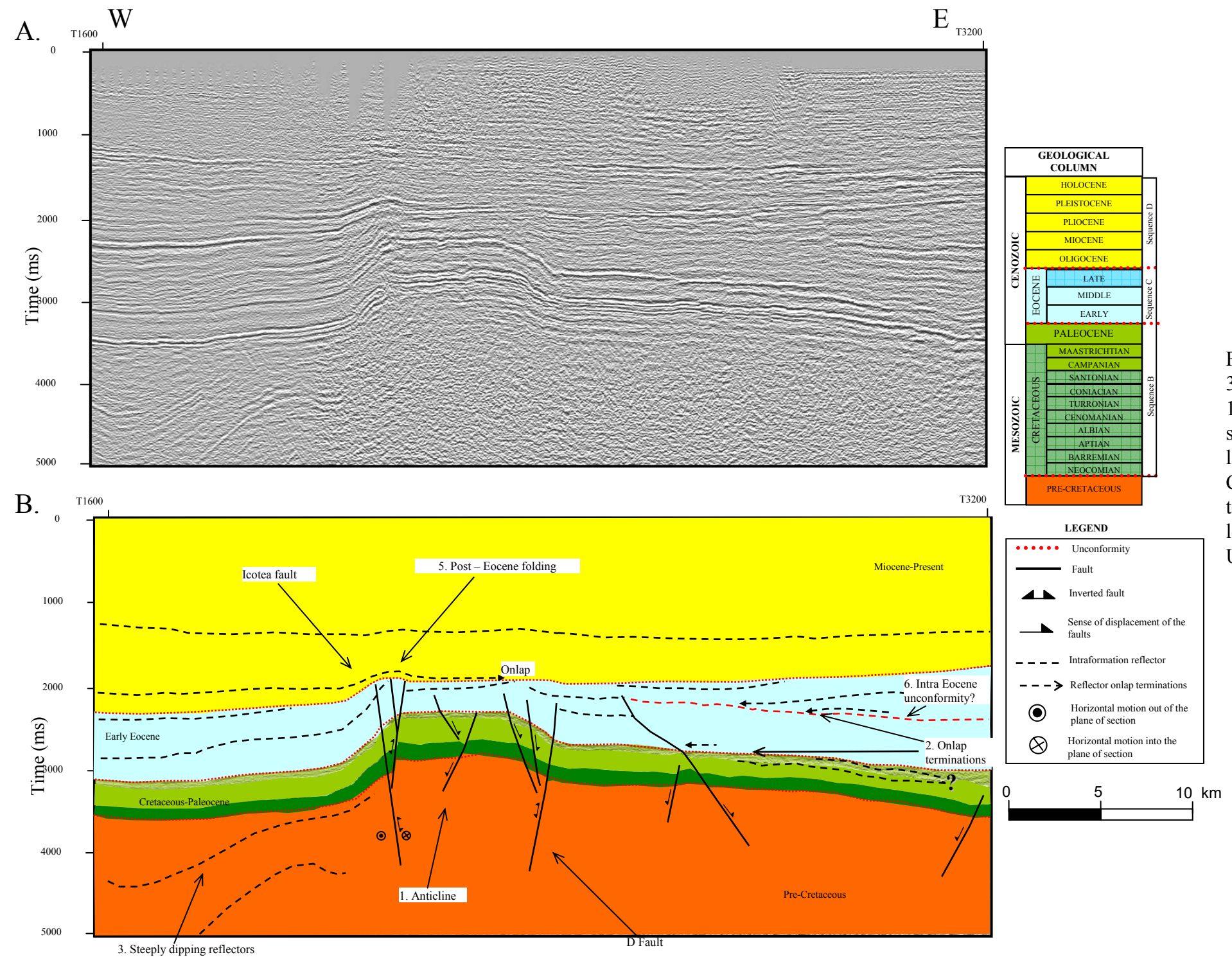


Figure 3.8. A) Uninterpreted seismic line 3800. B) Interpreted seismic line showing: 1) the main anticline observed in the seismic time slices at 2200 and 2600 ms; 2) lap terminations and truncation of sequence C; 3) pre-Cretaceous reflections; 4) syn-tectonic sedimentation of sequence C; 5) lower sequence D deformation; 6) Unconformities within Eocene sequence C

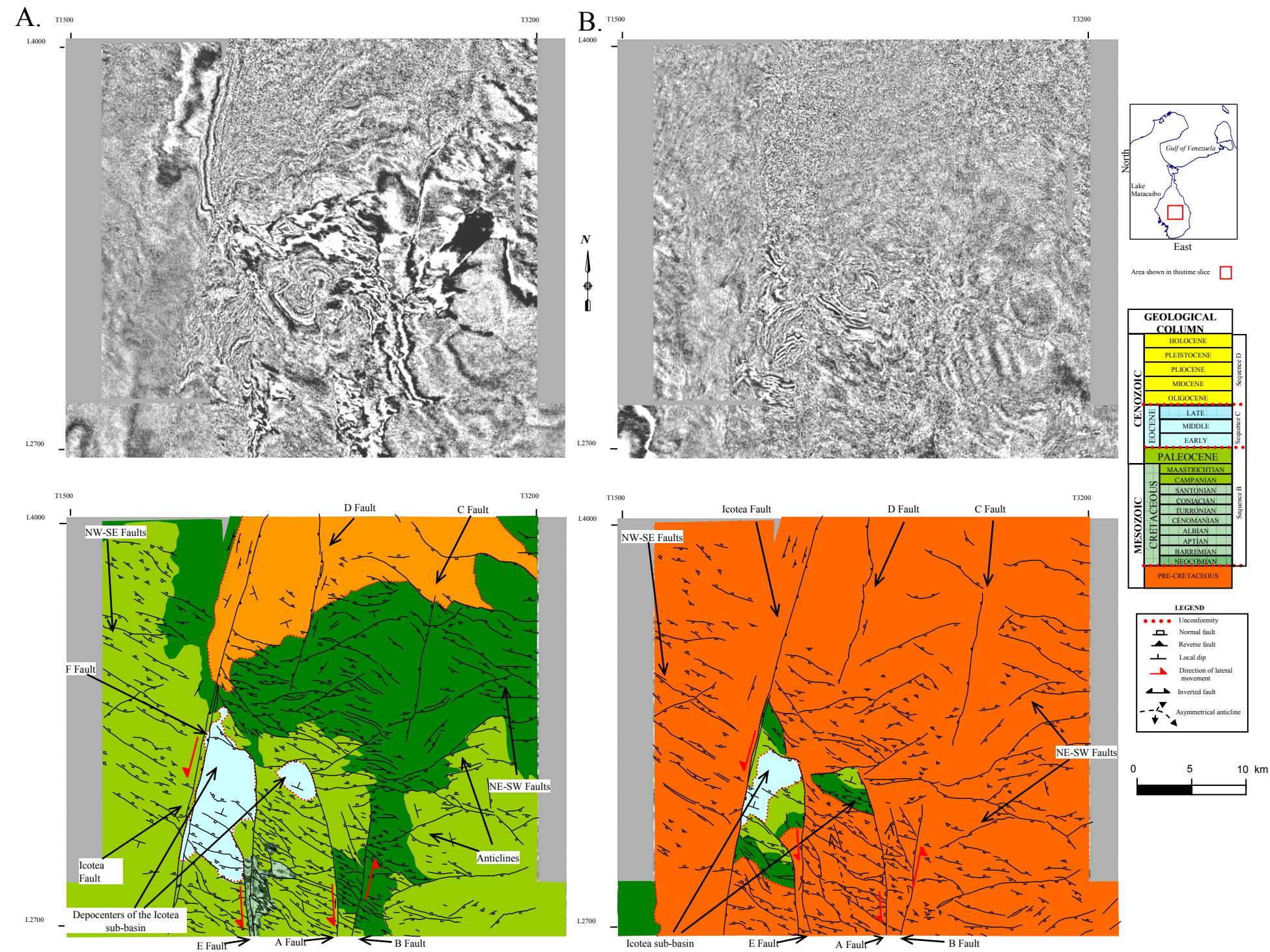


Figure 3.9. A) Uninterpreted and interpreted seismic time slice at 3400 ms. Three main trends of faults are interpreted: N-NE, NW-SE and NE-SW. The Icoatea pull-apart basin is evident, and sinistral strike-slip motion of the N-NE faults is interpreted. B) Uninterpreted and interpreted seismic time slice at 3800 ms. The Icoatea pull-apart basin is encased within the basement and bounded by the Icoatea fault to the west, faults A and B to the east, and fault F to the north. Reservoir rocks of sequence C are possibly in contact with source rock of sequence B. Prevalence of three main trending fault directions and the development of the pull-apart basin and related uplifted areas is controlled by the N-NE striking faults.

The seismic time slice at 3800 ms highlights the main fault trends already interpreted in the overlying seismic time slices (Fig. 3.9B). At 3800 ms, these faults also cut the pre-Cretaceous sequence (acoustic basement), which is the main stratigraphic unit present at this level. The Icoatea pull-apart basin, containing sequences B and C, is enclosed in pre-Cretaceous rocks and extends between the Icoatea fault and fault A. The lower part of sequence B (source rock) is in fault contact with sequence C, which is the main reservoir rock in the Maracaibo basin (Fig. 3.9B) (Gonzales de Juana et al., 1980).

Seismic line 3000 cuts transversally through the major depocenter of the Icoatea pull-apart basin in sequence C (Fig. 3.10). The main boundaries of the depocenter are fault B and the Icoatea fault. Asymmetry of the depocenters is characteristic of Icoatea the pull-apart basin, even at its deepest level (Fig. 3.10). This asymmetric geometry is controlled by differential displacement of the N-NE master striking faults. Syntectonic deposition is inferred from lower Eocene growth strata of sequence C during the early Eocene. Middle and upper Eocene rocks are likely not to have been preserved. An abrupt change from the deep pull-apart basin to the adjacent uplift is controlled by fault F, a major NW-SE fault (Fig. 3.9A). Sequence B, as interpreted in the time maps and seismic lines, has an overall constant thickness. In contrast, sequence D is affected by reactivation of underlying structures during its early stages of deposition and, in general, thickens to the S-SW (Fig. 3.7).

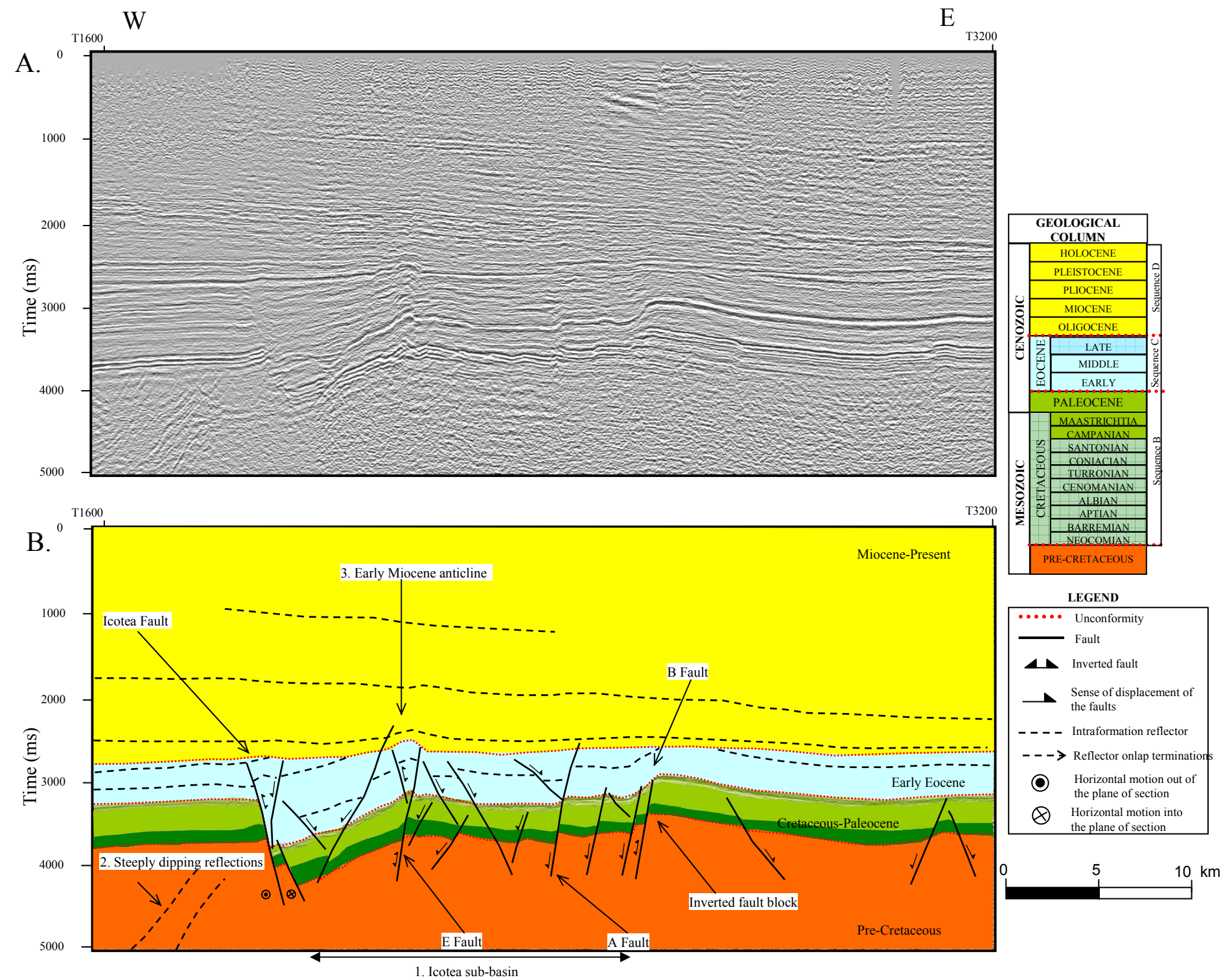


Figure 3.10. A) Uninterpreted seismic line 3000. B) Seismic line interpretation: 1) Asymmetrical Icotea pull-apart basin bounded by the Icotea fault and fault B; 2) Pre-Cretaceous reflections truncated by sequence B; and 3) Deformation in the lower part of sequence D.

Figure 3.11 illustrates the basin geometry described above in the form of a seismic fence diagram. Outside the main area of deformation controlled by the N-NE fault trend, sequence C thickens toward the N-NE, whereas sequence D thickens toward the S-SW (between seismic crosslines 1800 and 2800). These thickness variations reflect the change in position of the main depocenters of the Maracaibo basin from N-NE in the Eocene to the south during the Miocene. The western side of the area shows the NW–SE faults mainly dying out in sequence C (seismic crossline 1800), and major faults dipping northwards (Fig. 3.10A). In contrast, the eastern side (seismic crossline 2800) shows an increase in the inclination of the reflections of sequences C and D (Fig. 3.10A) Sequence C is more affected by NW-SE-striking faults inside the area of deformation, asymmetry of the pull-apart basin fill along with the juxtaposition of the basin and the surrounding anticlines (Figs. 3.9B, 3.13D and 3.13E).

3.8 EXTENSION OF THE ICOTEA SUB-BASIN AND MINIMUM AMOUNT OF STRIKE-SLIP DISPLACEMENT

Pull-apart basin length depends on the horizontal offset of the master strike-slip faults, which is transferred into extensional offset of the basin-transverse faults (e.g., fault F) (Figs. 3.9A and 3.11A). Transverse normal faults allow pull-apart basin lengthening, and their extension occurs in a direction parallel to the lateral offset.

Figure 3.12A shows an arbitrary longitudinal seismic line through the Icotea pull-apart basin and parallel to the direction of strike-slip motion as the

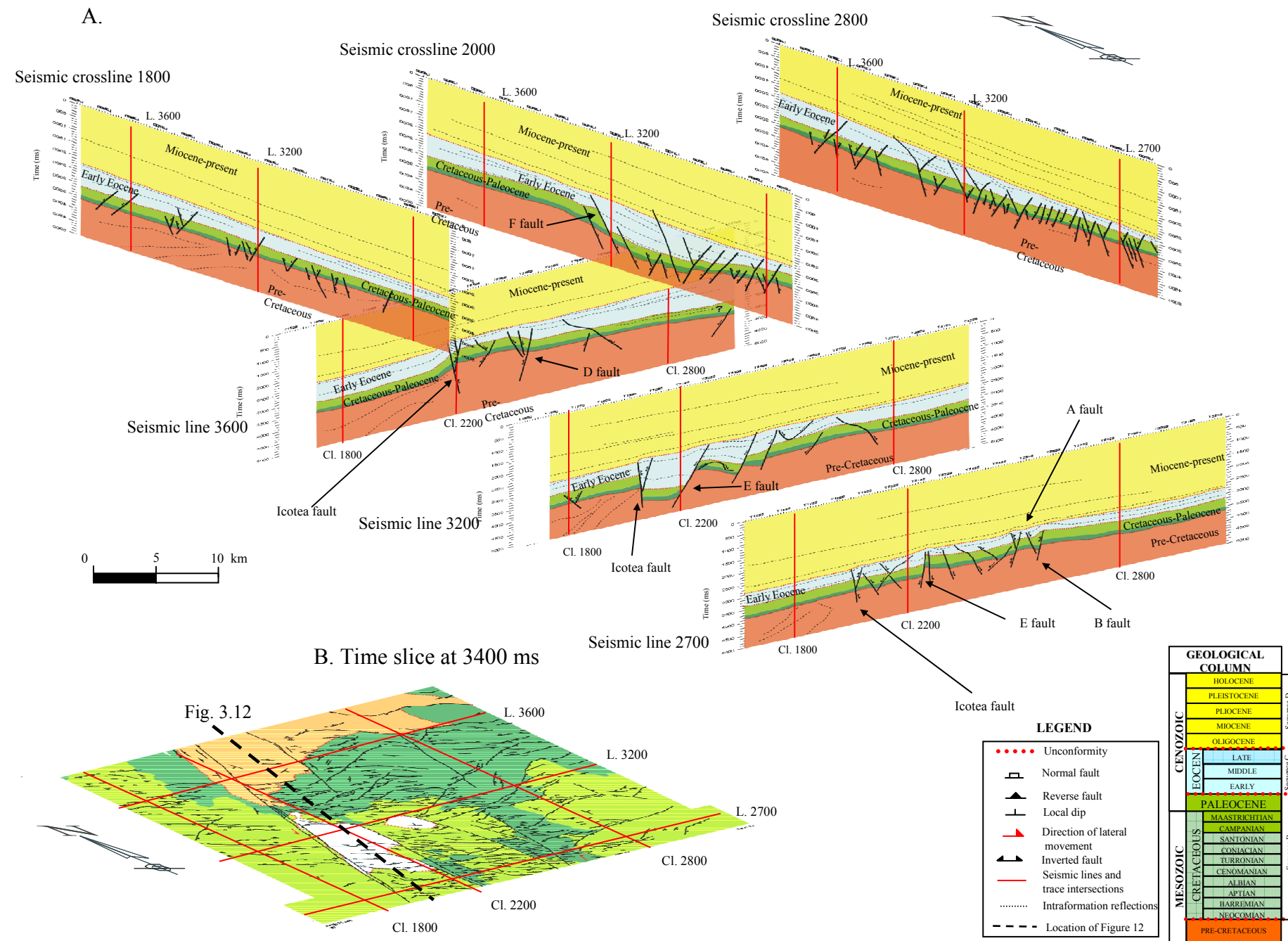
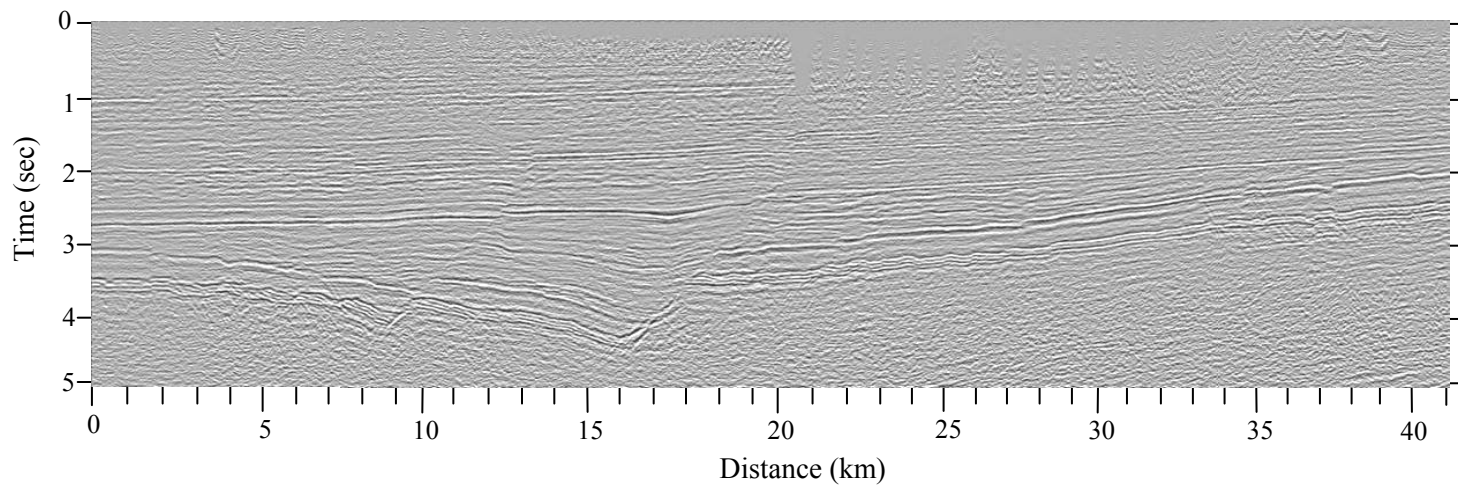


Figure 3.11. Fence diagram showing the structural architecture of the central part of the Maracaibo basin, including the Icoatea pull-apart basin. East and west of the pull-apart basin fewer faults are observed. NW-SE faults are attributed to flexure of the South American plate during Paleogene loading of the Caribbean plate over South America. The calculated extension west of the Icoatea fault in the flexural area is approximately 0.5 km.

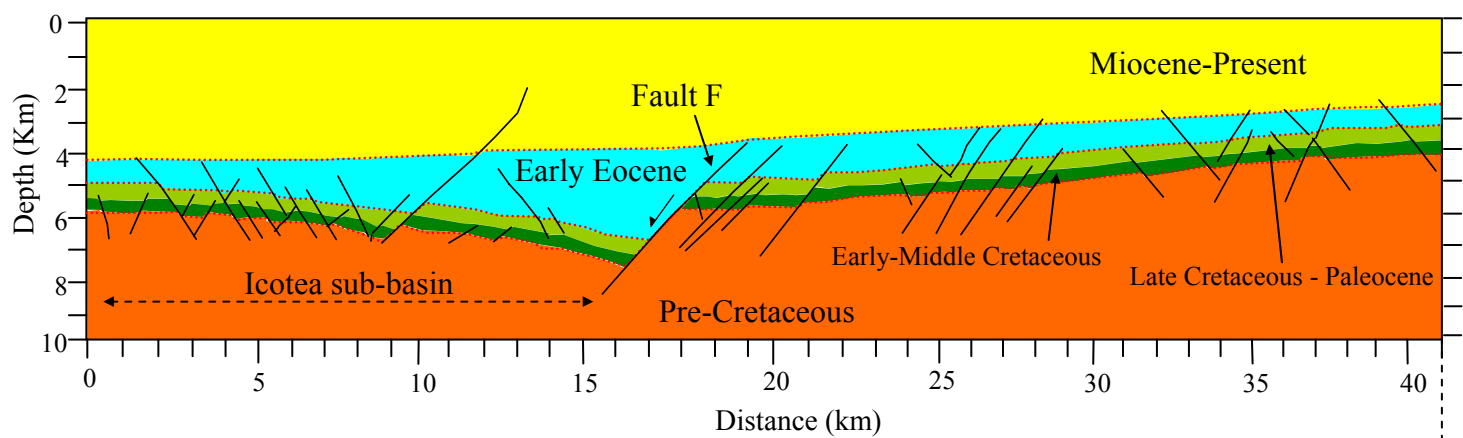
SW

NE

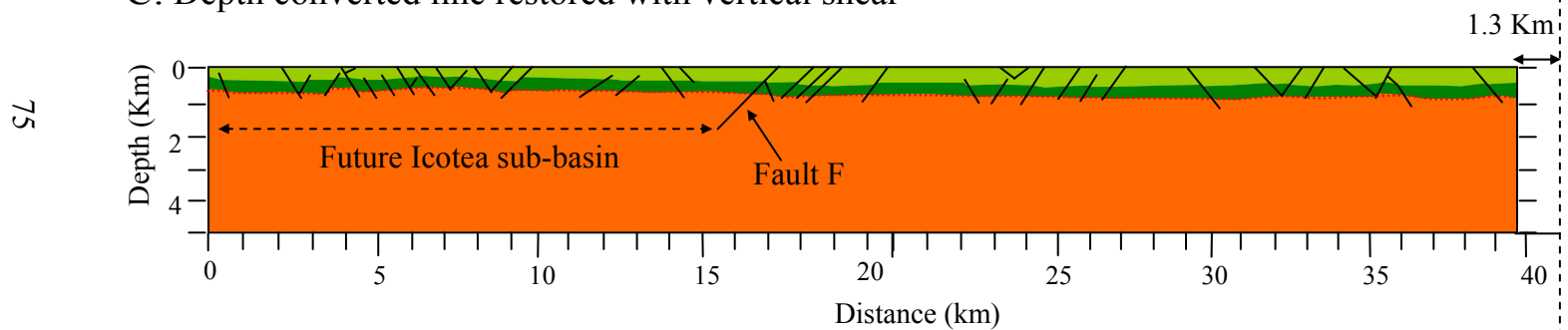
A. Seismic line across transverse normal faults of the Icotea pull-apart basin (Fig. 3.11B)



B. Seismic line converted to depth



C. Depth converted line restored with vertical shear



D. Depth converted line restored with antithetic shear

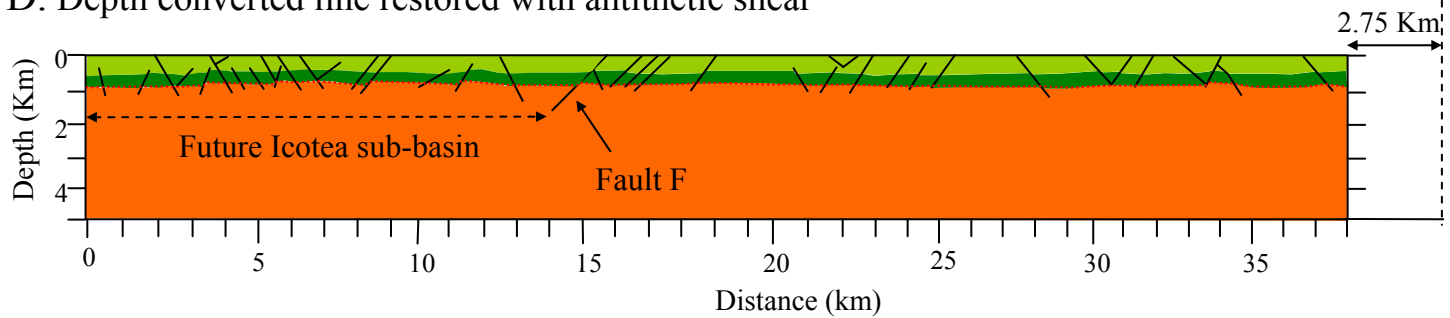


Figure 3.12. A) Uninterpreted longitudinal seismic line through the Icotea pull-apart basin. B) Depth-converted and interpreted seismic line. Interval velocities derived from well velocities were used for the depth conversion (Pre-Cretaceous: 6.2 km/sec; Lower Cretaceous: 5.0 km/sec; Upper Cretaceous and Paleocene: 2.8 km/sec; Eocene: 4.0 km/sec; Oligocene-Present: 3.1 km/sec). C) Entire section restored to the top of the Paleocene using vertical shear method yields 1.3 km of extension. D) South of fault F (future Icotea pull-apart basin) restored using 60° antithetic shear method. North of fault F the section was restored with vertical shear. Calculated extension is 2.75 km. Estimated minimum slip along the Icotea fault varies from 0.8 and 2.25 km.

Icotea fault (Fig. 3.11B). This line was used to make a structural restoration at the top of the Paleocene in order to calculate the total extension produced by transverse normal faults. The seismic line was converted to depth (Fig. 3.12B) using interval velocities for the different sequences, derived from sonic logs (Fig. 3.5 and 3.12).

Two types of shear were used to restore the faulted, depth converted seismic section in Figure 3.12B (Xiao and Suppe, 1992): 1) Vertical shear, where the hanging-wall material drops down vertically to fill the void (Fig. 3.12C), and 2) antithetic shear, where collapse takes place in a non-vertical direction, (antithetic to fault F, Fig. 3.12D) along the surface to be restored and the adjacent fault block (Worrall and Snelson, 1989). Shear angles measured in the laboratory using clay box experiments range between 60° and 70° for different rock types (Xiao and Suppe, 1992). A 60° maximum fault dip angle was used in the vertical shear model. This angle is similar to the measure dip angles of antithetic faults within the Icotea basin (Fig. 3.12). Vertical shear was applied to the western block of fault F (Fig. 3.12D) because the western block does not exhibit significant extension.

The longitudinal section restored with vertical shear has a total extension of 1.3 km (Fig. 3.12C), whereas the Icotea pull-apart basin restored with antithetic shear has a total extension of 2.75 km (Fig. 3.12D). However, upper Paleocene-Eocene rocks were also extended by flexural-loading during oblique collision between the Caribbean plate and the northern South America plates (Castillo, 2001) (Figs. 3.9 and 3.11). Therefore, this previous extensional event needs to be

calculated, in order to better estimate the amount of extension provided by basin transverse faults within the Icotea pull-apart basin. I calculated a total extension of 0.5 km in the area east of the Icotea fault, where sequence C is less deformed (Figs. 3.11A and 3.11B, seismic crossline 1800). This minor extension provides an estimate for regional extension related to the flexural loading event.

Therefore, extension localized within the ~15-km-long Icotea pull-apart basin ranges between 0.8 and 2.25 km. This amount of extension is a minimum estimate of the amount of left-lateral strike motion along the Icotea fault. Maximum contribution of extension calculated in the restoration is obtained from fault F. This fault defines the northern boundary of the Icotea basin (Figs. 3.7A, 3.9A and 3.12B).

3.9 DISCUSSION

As previously proposed by Audemard (1991), Lugo and Mann (1995), Parnaud et al. (1995b), and Castillo (2001), the Maracaibo basin formed as an oblique foreland basin during the late Paleocene (latest stage of seismic sequence B) and Eocene (all the deposition of seismic sequence C) (Fig. 3.5, Chapter 2). Deformation ended by Oligocene times following the migration of the Caribbean-South America collision zone to eastern Venezuela (Fig. 1B). Main NE-striking, wedge-like depocenters were located in the north and northeastern parts of the basin (Fig. 3.3). Formation of the Icotea pull-apart basin occurred during the early Eocene and possibly extended into the middle and late Eocene, because possible younger growth strata of sequence C may have been removed by the Eocene

unconformity (Figs. 3.6, 3.8 and 3.10). A more precise age of origin is not possible.

Figure 3.13A-E summarizes the main structural stages of the Icotea pull-apart basin derived from interpretation of 3-D seismic data. The seismic time slice succession demonstrates that the pull-apart basin is controlled by N-NE-striking master strike-slip faults, strike-slip offset is Eocene in age, and transverse-normal faults control localized extension within the basin (Fig. 3.13D). Seismic time slices also revealed that the pull-apart basin represents an anomalously thick (~3 km) Eocene sequence C, in contrast to the surrounding thinner (~1km) distribution of Eocene sequence C in this area of the Maracaibo basin (Fig. 3.12B), as seen on isochron maps (Fig. 3.7) and regional time slices (Fig. 3.3).

The late Paleocene extensional regime pre-dating the formation of the Icotea pull-apart basin is produced by flexural loading of the late Paleocene-early Eocene foreland basin northeast of the Maracaibo basin. Convergence inversion of preexisting normal faults has remained the dominant tectonic process, except locally within the Icotea pull-apart basin. Reactivation of the preexisting N-NE-striking Cretaceous faults during the Paleogene, as left-lateral strike-slip faults led to the formation of the Icotea pull-apart basin. Extension within the pull-apart basin was controlled by transverse faults as a simple stepover or pull-apart, rather than by fault-normal extension (Ben-Avraham and Zoback, 1992).

Evolution of the three different fault trends described in this paper and their role in the formation of the Icotea pull-apart basin is described below and is shown schematically in Figure 3.14:

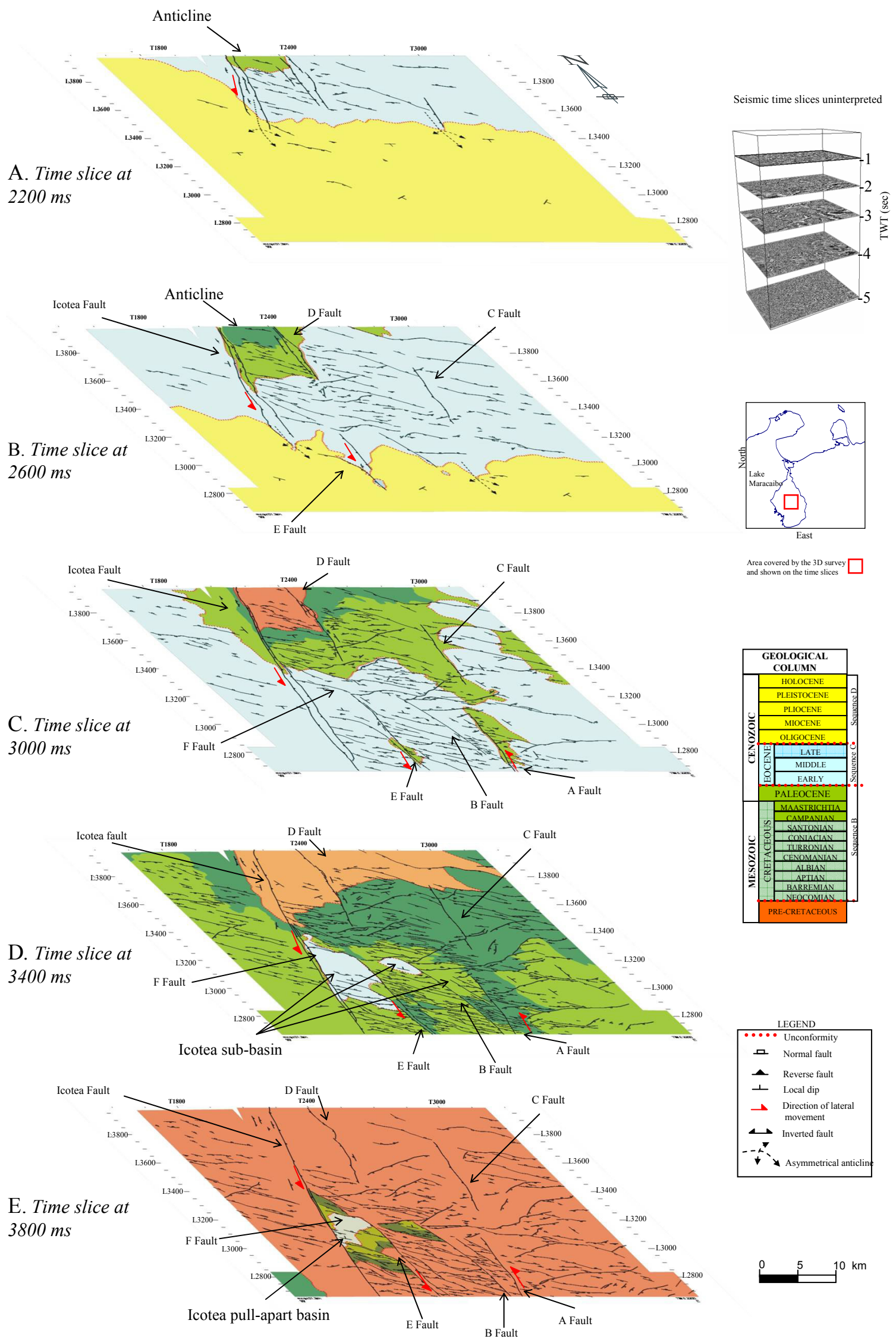


Figure 3.13. 3D seismic time slice succession showing different structural styles in the study area within second-order sequences. The Icotéa pull-apart basin appears as a prominent main geological feature in seismic time slices at 3400 and 3800 ms levels.

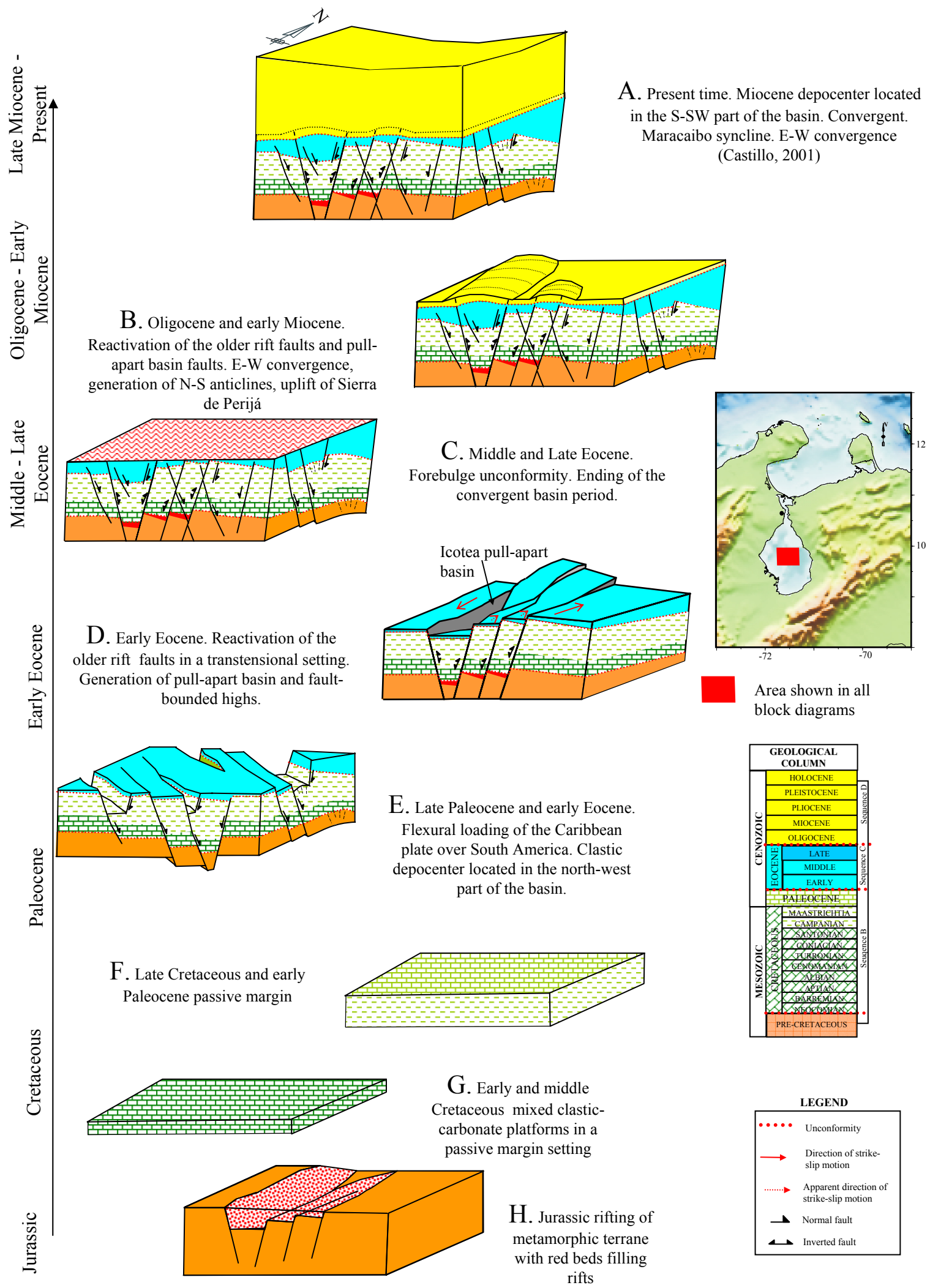


Figure 3.14. 3D diagrams showing the structural and stratigraphic evolution of the study area from Jurassic rifting (lower diagram) to present-day (upper diagram).

1) NNE–SSW faults (Icotea fault and faults A, B, C and D): These faults constitute the main structural elements of the study area, and are interpreted to have formed during the Jurassic-Cretaceous rifting (Lugo and Mann, 1995; Castillo, 2001) (Fig. 3.14H).

Reactivation of the Icotea fault and other N-NE-striking faults occurred during the early Eocene, when the oblique collision between northwest South America and the Caribbean plate reached its climax in the northeastern edge of the Maracaibo basin.

There are several previously proposed and conflicting interpretations of the age and sense of displacement of the Icotea fault. Lugo (1991) used widely spaced 2-D seismic data, and interpreted the Icotea basin as a pull-apart basin, formed by left-lateral strike-slip movement of the Icotea fault and fault E. In this study, the Icotea sub-basin has been interpreted as bounded by the Icotea fault to the west, and by fault B to the east, as interpreted from the hypocenters identified in isochron maps (Fig. 3.7) and seismic time slices (Fig. 3.9). My interpretation proposed that the most likely process that would develop a sub-basin within the central part of the Maracaibo basin during the Paleogene is left-lateral strike-slip of the N-NE trending faults (e.g., Icotea, A, B faults, Fig. 3.13), by transferring displacement as normal extension to the NW-SE trending faults (e.g., fault F, Fig. 3.12).

Inversion is caused by basin compression-transpression, producing uplift and partial upward extrusion of the basin (Cooper et al., 1989). The final component of inversion is compression, strike-slip or oblique-slip, and depends

on the changing azimuth of maximum principal compressional stress and the direction of original basin trend through time (Lowell, 1995).

During the Eocene evolution of sequence C of the Maracaibo basin (Fig. 3.5), the convergence migrated from north to almost east and followed the trend of the foredeep. Convergence generated a strike-slip-controlled, early Eocene inversion of the N-NE trending faults. These faults continued to invert during the middle Eocene as the regional depocenter migrated eastward (Lugo and Mann, 1995) (Fig. 3.3).

As a product of convergent inversion, the western block of the Icotea fault moved south relatively to the eastern block to form a left-lateral strike-slip fault (Fig. 3.14D). Either normal or reverse dip-slip motion accompanying strike-slip motion will produce basins or uplifts parallel or within the fault zone (Ryan and Coleman, 1992). Between 0.8 to 2.3 km of displacement along the Icotea fault formed the Icotea pull-apart basin (Fig. 3.12).

A gradual change from transpression to compression, produced by migration of the convergence from north to southwest, induced the development of uplifts north and east of the sub-basin. Positive areas subjected to localized erosion were developed in the areas surrounding the pull-apart basin (Figs. 3.8 and 3.10).

A main NW-striking normal fault (Fault F) bounds the northern edge of the Icotea pull-apart basin and separates its deep basin from an uplifted area (Figs. 3.9A and 3.12B). The pull-apart basin is asymmetrical with a deeper area to the west, and to the east is segmented by N-NE faults (Faults E, A and B) (Fig. 3.10).

This observation suggests different displacement of the N–NE faults involved during the formation of the pull-apart basin, rather than the type of asymmetry suggested by the fault-parallel extension model proposed by Ben-Avraham and Zoback (1992). Experimental models of Gölke and Cloetingh (1994) suggest that pull-apart asymmetry becomes more pronounced with proximity to the more active strike-slip fault. In this interpretation, pull-apart basin deepening occurs progressively toward the fault characterized by the largest amount of lateral displacement, as I suggest for the Icotea fault.

Another inversion period is also proposed for the N-NE-striking faults (Fig. 3.14B). This inversion occurred during the Oligocene–early Miocene (lower portion of sequence D). Inversion is inferred from gentle anticlines along the N-NE faults (Figs. 3.8B and 3.10B). Inversion seems to be related to the Sierra de Perijá uplift west of the basin during the Oligocene and middle Miocene. This uplift was the main source of clastic sediments in the Maracaibo basin during Oligocene-middle Miocene (Audemard, 1991).

2) NW-SE normal faults: Castillo (2001) proposed the formation of these faults as a response of the downward flexure of the South American plate due to load of the Caribbean plate during late Paleocene–middle Eocene convergence. Bradley and Kidd (1991) concluded that normal faults will develop as a flexural extension deformation and resulted from the bending of convex side of a flexed lithospheric plate in collisional settings.

Following the evolution of the Maracaibo basin during the Paleogene, these late Paleocene faults parallel the late Paleocene–early Eocene depocenters

(Lugo and Mann, 1995). These Paleocene-Eocene depocenters formed as a response of the oblique collision between the Caribbean and South America plates. The faults are mostly parallel with the NW-trending thrust front, and dip NE toward the foreland area (Fig. 3.3). The NW-SE-striking normal faults formed contemporaneously to the late Paleocene-Eocene inversion of the N-NE striking faults (e.g. Icotea, A, B, C and D faults).

A major change in the main fault dip direction, from dominantly northward in the west, to dominantly southward in the east, is observed in Figure 3.11A. Faults on the eastern side of the study area have greater throw (Fig. 3.11A, seismic crossline 3000). This difference in throw appears to be controlled by strike-slip motion of the N-NE convergence from front north to east during the middle Eocene. The block west of the Icotea fault was isolated from the effects of the latest stages of the collision during the middle and late Eocene, when the depocenter was located to the east of the basin. The block east of the Icotea fault, located adjacent to the eastern depocenter, modified its orientation as a result of changes from transpression to increasing convergence in the area (Figs. 3.3 and 3.11A).

Early Eocene inversion of the N-NE-striking faults occurred during the formation of the late Paleocene-early Eocene NW-SE-striking faults, which linked the two faults systems. The left-lateral strike-slip movement of the N-NE faults reactivated the pre-existing NW normal faults, thus controlling the geometry and extension of the pull-apart basin. Outside the pull-apart basin, extension of the NW-SE faults is relatively minor (Fig. 3.11A).

3) NE-SW faults: These faults are mainly mapped in the Cretaceous and Paleocene level time slices. These faults probably formed during the Permian (Appalachian-Ouachita-Marathon orogeny). More regional mapping and better seismic resolution of deep structures is needed to corroborate this idea. Reactivation of NE-SW-striking faults occurred during the Eocene.

3.10 CONCLUSIONS

I interpreted the evolution of three different fault trends of Cretaceous-Cenozoic unconformity-bounded seismic stratigraphic sequences along the Icotéa left-lateral strike-slip fault zone in the central part of the Maracaibo basin. The main conclusions include the following:

- The three fault trends within the study area include:
 - * N-NE faults, during the late Paleocene-Eocene (including the Icotéa fault and parallel faults A, B, C, D and E). These faults are reactivated pre-existing Jurassic faults and show left-lateral and reverse movement. Strike-slip displacement was driven by NW-SE directed oblique collision of the Caribbean plate against the northern South American plate.
 - * NW-SE-striking, small-offset normal faults: These faults formed during the late Paleocene during downward flexure of the central Maracaibo basin (South American plate) as a result of southeastward loading of the Caribbean plate. Strike-slip movement along the N-NE-

striking faults locally reactivated these faults as normal faults to form the Icotea pull-apart basin.

* NE-SW-striking faults: Normal faults formed during pre-Cretaceous rifting between North America and South America, and were reactivated during late Paleocene-Eocene oblique collision between the Caribbean and South America.

- The Icotea pull-apart basin formed in Eocene times between the Icotea and B faults as a result of transfer of left-lateral strike-slip motion between the Icotea and A, E and B faults. The pull-apart model explains the formation of the small, deep basin formed as a ~10 km wide left-step in the strike-slip faults zone.

- The Icotea fault can be classified as a crustal intraplate fault (Sylvester, 1988) restricted to the crust. The Icotea fault transfers horizontal slip to the other N-NE faults, as a result of crustal block motion caused by convergence. Normal displacement for the Icotea pull-apart basin on 23 basin transverse faults was measured in a range between 0.8 and 2.25 km. Normal displacement is localized on pre-existing NW-SE-striking faults formed by 0.5 km of plate flexure. Down-to-the-west, asymmetry within the Icotea pull-apart indicates greater vertical throw on the Icotea fault on the western edge of the basin than faults B, C and D on the eastern side.

- No evidence was seen for significant E-W extension of the basin that would support the origin of the basin by a mechanism of fault-normal extension (Ben-Avraham and Zoback, 1992). Instead, all extension is concentrated on basin-transverse normal faults oriented at a high angle to the strike-slip “master faults”.

CHAPTER 4

Sequence stratigraphic analysis of Eocene clastic foreland basin deposits in central Lake Maracaibo using high resolution well correlation and 3-D seismic data

4.1 INTRODUCTION

The stratigraphic record of any sedimentary basin is controlled by three variables: eustasy, subsidence and sediment supply. In foreland basins, high rates of subsidence characterize the main thrust depocenter, which is formed by downwarping the foreland plate by loading. As an elastic response to thrust loading, peripheral upwarping occurs distal opposite to the depocenter (at the distal margin of the foreland basin), and forms a “forebulge” (Crampton and Allen, 1995; Chapter 2). Sediment supply feeds the foreland basin from either the flexed plate (craton) or overriding thrust belt. Eustasy and sediment supply control the short-term stratigraphic framework, superimposed over low frequency tectonosequences. The basal unconformity of the foreland tectonosequence is formed by erosion of the progressive migrating forebulge or tilted passive margin Di Croce et al. (1999). The upper unconformity of foreland basins is formed by tectonic rebound as the tectonic loading dissipates (White et al., 2002).

The Eocene sedimentary record of the Maracaibo basin was formed in a foreland basin setting during an oblique collisional event between the Caribbean and South American plates (Lugo and Mann, 1995; Chapter 2; Escalona and Mann 2003a). As a result of this collisional event, a major depocenter developed

in the northwestern area of the basin. The source of Eocene clastic sediments was from the south during the early-middle Eocene. During the middle-late Eocene, source areas remain in the south or were in the E-NE in the Pueblo Viejo sub-basin area (Lugo and Mann, 1995; Escalona and Mann, 2003a; Chapter 2).

Sequence stratigraphic analysis in the Maracaibo basin has been based either on regional or detailed reservoir-scale studies. Regional studies utilize widely separated wells to define the main bounding surfaces (Lugo, 1991), whereas detailed reservoir-scale interpretations focus on small areas without considering the regional evolution of the basin (Maguregui, 1990; Ambrose et al., 1995; León, 1997). Depositional environments in the Eocene of the Maracaibo basin were highly variable and include fluvial, deltaic and marginal marine settings with tidal influence (Maguregui, 1990; Ambrose et al., 1995). Seismic data resolution and quality are not sufficient to make lateral correlations between widely spaced wells. Previous studies by Maguregui (1990), Lugo (1991), Ambrose et al. (1995) and León (1997) among others, generally did not consider the early-middle Eocene period as a greenhouse climatic setting where eustatic changes have small amplitudes, and did not analyze the interaction between the rate of subsidence, eustatic sea level change and sediment supply.

Well data depict vertical stratigraphic variations in detail, but lateral correlation is dependent on the amount of wells available. The use of a dense well database covering a large area can improve lateral stratigraphic correlations, but conventional interpretation methods are inefficient when working with hundreds of wells (Carr et al, 1995). The 3-D pseudo-seismic transform technique of Carr et

al. (1995) uses visualization methods applied to 3-D seismic data along with large numbers of wells. The objective is to maximize lateral correlations and improve interpretations.

The main objective of this study is to use a dense well database (330 wells) combined with 3-D pseudo-seismic transform and 3-D seismic data for a representative area of the Eocene foreland basin setting of the Maracaibo basin to:

- Generate a high resolution sequence stratigraphic framework in order to enhance vertical and lateral correlations in a three-dimensional view.

- Determine the utility of the 3-D pseudo-seismic log displays in a structurally complex, deeply buried clastic stratigraphy. The pseudo-seismic approach has previously been applied to shallow water carbonate reservoirs (Carr et al, 1995), and regional 2-D cross sections in shallow clastic deposits (Ralph and Mitchum, 1997).

- Understand the interplay between subsidence, eustasy and sediment supply in a sequence stratigraphic framework. This approach takes into account the basin as a foreland basin, whose main sediment supply was from intracratonic areas to the south rather than from the fold-thrust belt to the northeast (Chapter 2).

- Generate maps and evolutionary models for the Eocene clastic section in the central Maracaibo basin.

- Integrate 3-D seismic and the pseudo-seismic to enhance lateral correlations between widely spaced wells.

4.2 STUDY AREA

Selected for this study is a 500 km² area in the central Maracaibo basin (Fig. 4.1) and it is covered by a dense grid of well data on an average of 600 well spacing and more than 2000 km² of 3-D seismic data (Fig. 4.1).

Oil fields in the study area were discovered in the 1960's, and production comes mainly from the Eocene sedimentary rocks located on structural highs along NW-SE trending strike-slip faults. Few wells produce from Cretaceous carbonates and Miocene clastic intervals. The Eocene section for the central Maracaibo basin represents an ideal interval for application of new methodologies and concepts of correlations because of the abundant data and the stratigraphic and structural complexity of the Eocene basin fill (Chapters 2 and 3).

4.3 DATABASE

The data used in this study consist of approximately ~2000 km² of conventional 3-D seismic reflection data, wireline logs of over 330 wells, and lithologic descriptions of approximately 1600 m (5000 feet) of discontinuous cores taken from 9 wells. The database was collected by the Venezuelan state oil company (PDVSA, S.A) and made available to me for this study. The 3-D seismic data and well information (including logs) were provided in digital format, and were loaded into a Landmark interpretation system at the Department of Geological Sciences, The University of Texas at Austin.

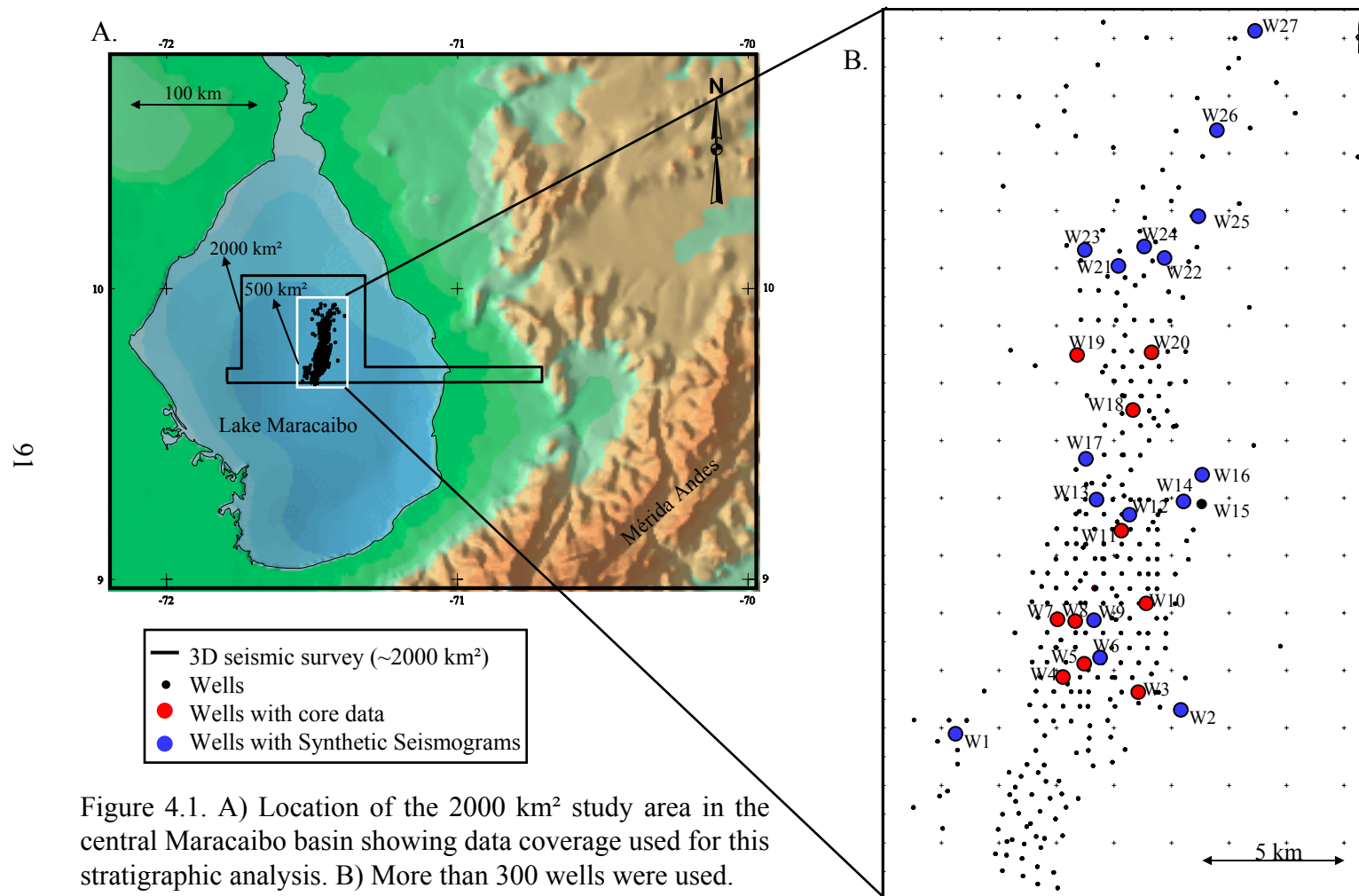


Figure 4.1. A) Location of the 2000 km² study area in the central Maracaibo basin showing data coverage used for this stratigraphic analysis. B) More than 300 wells were used.

4.3.1 3-D seismic data:

3-D seismic reflection data used in this study were originally part of a merged seismic volume that included most of the 3-D seismic surveys collected by PDVSA, S.A. in the Maracaibo basin during the late 80's and the 90's. Seismic data consist of 2000 km², 5 seconds of two-way travel time data, sampled at 4 ms, and with bin size of 30 meters (Fig. 4.1). The data available were in an 8-bit display format limiting their usefulness for more detailed quantitative analysis. For the Eocene interval, the dominant frequency is between 20-35 Hz, giving a minimum estimated vertical resolution of about 40 m (~120 feet) and lateral resolution of 200 m (~600 feet). These resolution estimates are also dependent on processes such as deconvolution and migration (Gil and Trautnitz, 1995).

4.3.2 Well data

The well data base used in this study contains more than 300 wells (Fig. 4.1). Most wells reach depths greater than 3 km (~10000 feet) into Eocene reservoirs, because these are the most prolific reservoirs in the area (International Reservoir Technologies, Inc., 1997; PDVSA E&P Occidente and Veba Oil, 1998). Few wells reach the Cretaceous carbonate interval, which lies at depths over 5 km (~15000 feet). The wells form a NE-SW-trend belt which follows the main structural highs controlled by strike-slip faults bounding the Icotea pull-apart basin to the east (Chapter 2 and 3; Escalona and Mann, 2003b). The

minimum well spacing in the Eocene producing interval is 600 meters due to governmental drilling regulations.

All wells used in this study have wireline logs that include gamma ray, spontaneous potential and a suite of resistivity logs. About 20% of the wells also include sonic, density and neutron logs. Only nine wells have core data in the Eocene producing interval and two wells have core plugs (Fig. 4.1). In addition, descriptions available for this study include sedimentological, paleontological, palynological and conventional analysis. These reports were done by the Instituto de Investigaciones Petroleras de La Universidad del Zulia and S.A. Consultores C.S.C (see Appendix 1 for more detail on core description). Most of the cores described in these reports are archived at the PDVSA core facility, located in La Concepción, Estado Zulia, Venezuela.

Check-shots, or time-depth curves, used in this study include 17 wells. Most wells that have sonic and density logs were used to generate synthetic seismograms.

4.4 OBJECTIVES, METHODOLOGY AND THEORETICAL CONSIDERATIONS

The objective of this study is to define the high frequency sequence stratigraphic framework of the central Maracaibo basin and to delineate the architecture of Eocene clastic reservoirs within the study area by utilizing core, well and 3-D seismic data. The method is to generate maps and models of the different Eocene stratigraphic units that allow a better understanding of the interplay between the regime variables and the resultant sequence stratigraphy.

This approach is necessary because the 3-D seismic data available have poor vertical resolution, and the core information is from widely separated wells.

4.4.1 Core data

I incorporated core observations when possible to better define Eocene paleoenvironments, to calibrate log curves, and to provide age control. Most of the core data are located in the central part of the study area and does not constrain the southern and northern areas (Fig. 4.1). None of the cores are continuous and in general do not sample the lower and upper sections of the Eocene interval.

Seven common core lithofacies are interpreted and are color coded on Figure 4.2 (based on Instituto de Investigaciones Petroleras de La Universidad del Zulia and S.A. Consultores C.S.C, see Appendix 1 for core description). These facies can be described in three main groups as following:

Sandstone facies: range from coarse to fine grained and are dominated by cross-stratification, wavy lamination and abundant coal and plant debris (coarse, medium an fine grained sandstones; Fig. 4.2). Microtidal influence is observed mostly in the fine-grained sandstones represented by uni- and bi-directional, small-scale ripples, and wavy lamination. Depositional environments are interpreted to be fluvially dominated (i.e., distributary channels) and with limited tidal influence (i.e., tidal bars).

Heterolithic facies: range from sandstone to shale-dominated deposits and is the most common facies interpreted from cores (heterolithic, mainly

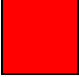

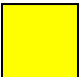

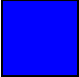
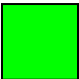
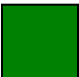
Sandstone facies		Coarse grained sandstone: Cross-stratification
		Medium grained sandstone: Abundant cross-stratification, wavy lamination, thin coal layers, massive bedding.
		Fine grained sandstone: Predominantly cross-stratification, parallel lamination, wavy lamination, tabular lamination, ripples, coal and plant debris, thin coal layers.
Heterolithic facies		Heterolithic, predominantly sandstone (shales and sandstones): Thin layers, cross and parallel laminations. Flaser bedding, wavy lamination, ripples, coal and plant debris.
		Heterolithic mixed shale and sandstone: Wavy parallel and flaser, parallel lamination, ripples, coal laminae, and plant debris.
		Heterolithic, predominantly shale: Thin parallel, flaser and wavy lamination, ripples, plant debris, and thin coal layers.
Shale facies		Shale: Parallel and wavy lamination, massive, ripples, plant debris and thin coal layers.

Figure 4.2. Lithologic facies used in core data description

sandstones; heterolithic; heterolithic, mainly shales; Fig. 4.2). Sedimentary structures include flaser bedding, wavy lamination, uni- and bi-directional ripples, and coal and plant debris. Depositional environments are interpreted as microtidal dominated with terrestrial influence (i.e., tidal bars, tidal channels, and tidal flats).

Shale facies: Is rare in the logs and are characterized by parallel and wavy lamination, massive bedding, ripples, and plant and coal debris. Depositional environments include lower delta plain to open marine.

Age control in wells is based on pollen analysis, as depositional environments are transitional between continental, coastal and shallow-marine (Rull, 2002). Palynology considers the ranges of palynomorphs as chronostratigraphic markers and is useful when traditional marine fauna cannot be used. The prevalent vegetation type based on pollen and salinity ratio of marine and freshwater fossils is used to define environment and age (Rull, 2002). Rull (2002) studied the palynology of the Maracaibo basin and classified the age of Eocene sedimentary rocks in several pollen zones. The early Eocene of the Maracaibo basin is represented by a single pollen zone that ends at 49.5 my (zone 17, *Rugutricolporites Felix*). This zone is identified in core data from the study area (Fig. 4.3A).

The middle Eocene has been divided into several pollen zones; two are recognized in the study area. The first zone ranges from 49.5 my to ~46.5 my (zone 18, *Echitricolporites Felix*); and the second one ranges from ~46.5 my to 44 my (zone 19, *Retitricolpites Magnus*) (Rull, 2002). Zone 19 has been identified in

two wells and reduces the accuracy for using this zone. Zone 19 has been mostly eroded in the south and central parts of the study area, because rocks of this age have been mostly eroded at the Eocene unconformity.

An early Miocene zone has been identified overlying zone 18 and 19 (Eocene on age). The time gap between the early Miocene and middle Eocene rocks accounts for more than 20 my years of non-deposition or erosion (middle-late Eocene, and the Oligocene intervals). This gap in time is defined as the Eocene unconformity which has been regionally interpreted in the Maracaibo basin (Lugo and Mann, 1995; Parnaud et al, 1995b; Castillo, 2001; Escalona and Mann, 2003b; Chapters 2 and 3).

Figure 4.3 shows an example of a core analysis of well W12 (see Fig. 4.1 for well location). Facies description (based on Instituto de Investigaciones Petroleras de La Universidad del Zulia and S.A. Consultores C.S.C reports, see Appendix 1 and Fig. 4.2), well logs (GR-Gamma ray, ILD-Deep induction resistivity and RhoB-density), chronostratigraphic boundaries defined by palynology and core photos from León (1997) are also shown. Observations from logs (Fig. 4.3A) and core photos (Figs. 4.3B and C), indicate the heterolithic facies dominates, representing tidal-influenced coastal plain and shallow marine environments. Fluvial facies are located within the main progradational units and usually have a blocky, low GR response. In addition, the Eocene unconformity is identified by palynological analysis and by changes in the GR and ILD logs. None of the wells with core data penetrated the Paleocene unconformity, which is assumed to be ~54 my based on previous regional work and seismic correlations

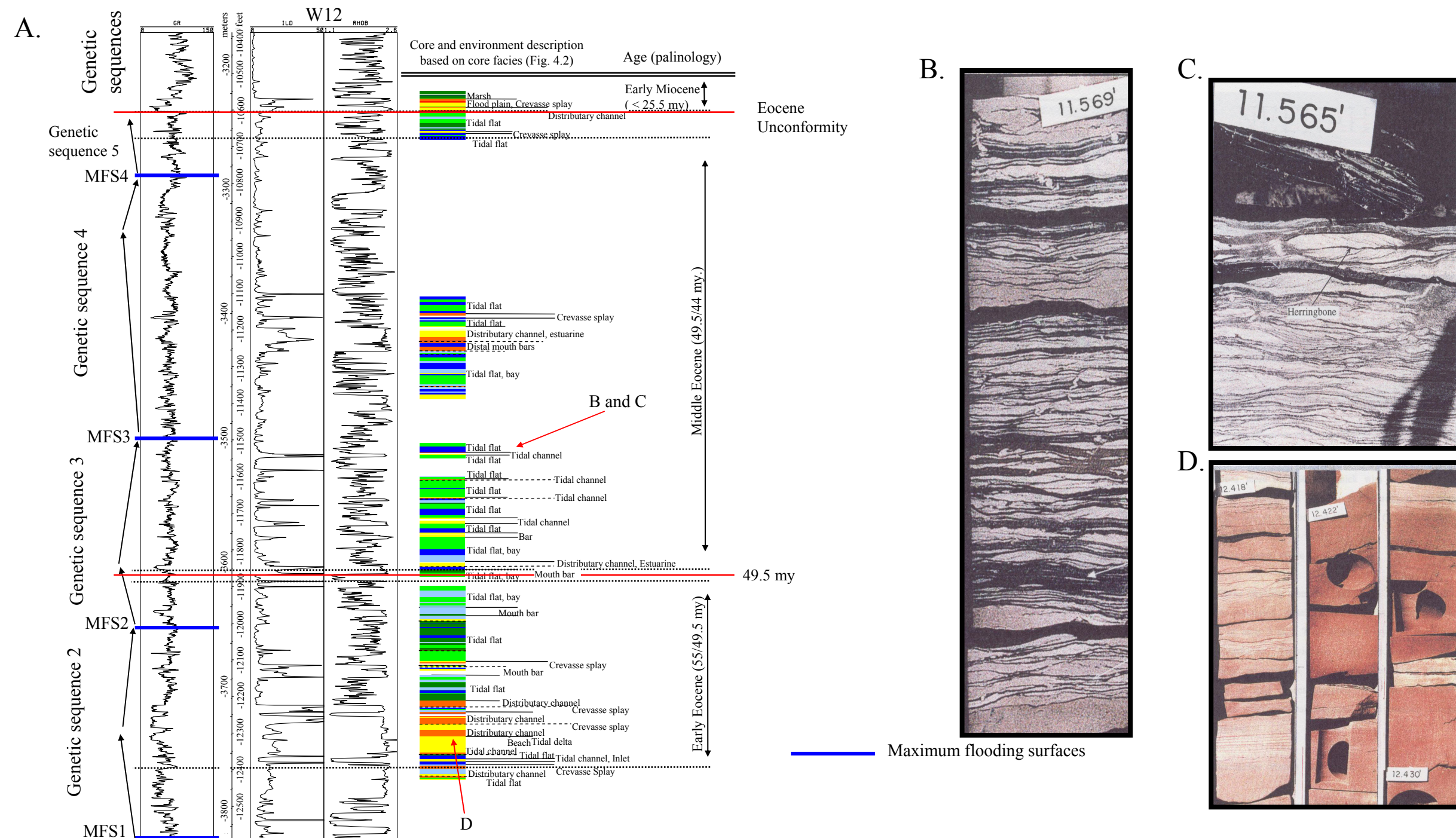


Figure 4.3. A) W12 well log (GR-gamma ray, ILD-deep induction and RhoB-density) with facies and environment descriptions based on lithofacies of Figure 4.2. Age defined by palynology and major regressive-transgressive cycles are shown. B and C) Heterolithic facies showing flaser bedding, mud drapes and herringbone sedimentary structures indicating tidal influence. D) Medium-to-fine grained sandstone interpreted as distributary channel fill. (Modified from S.A. Consultores CSC (1992) and León (1997)).

(Lugo, 1991; Parnaud et al. 1995b; Castillo, 2001; Escalona and Mann, 2003b; Chapters 2 and 3). Appendix 1 lists other wells with core data analysis.

4.4.2 Parasequence, parasequence set, genetic sequence and sequence

Sequence stratigraphic interpretation is based on stacking patterns and identification of transgressive and regressive cycles at different scales observed in the well logs by using 1-D, 2-D and 3-D stratigraphic analysis. These vertical cycles were interpreted using stratigraphic concepts including parasequence, parasequence set, and two kinds of sequences: genetic sequence and depositional sequence. Definition of these concepts is appropriate in order to understand their applicability and usefulness for this study.

Parasequence: A relatively conformable succession of genetically related beds or bedsets bounded by marine-flooding surfaces and their correlative surfaces (Van Wagoner et al., 1990) (Fig. 4.4).

Parasequence set: A succession of genetically related parasequences forming distinctive stacking patterns and commonly bounded by major marine-flooding surfaces and their correlative surfaces (Van Wagoner et al., 1990) (Fig. 4.4).

Genetic sequence: A package of sediment recording a significant episode of basin margin outbuilding and basin filling, bounded by periods of widespread basin-margin flooding (Galloway, 1989; Galloway and Hobday, 1996).

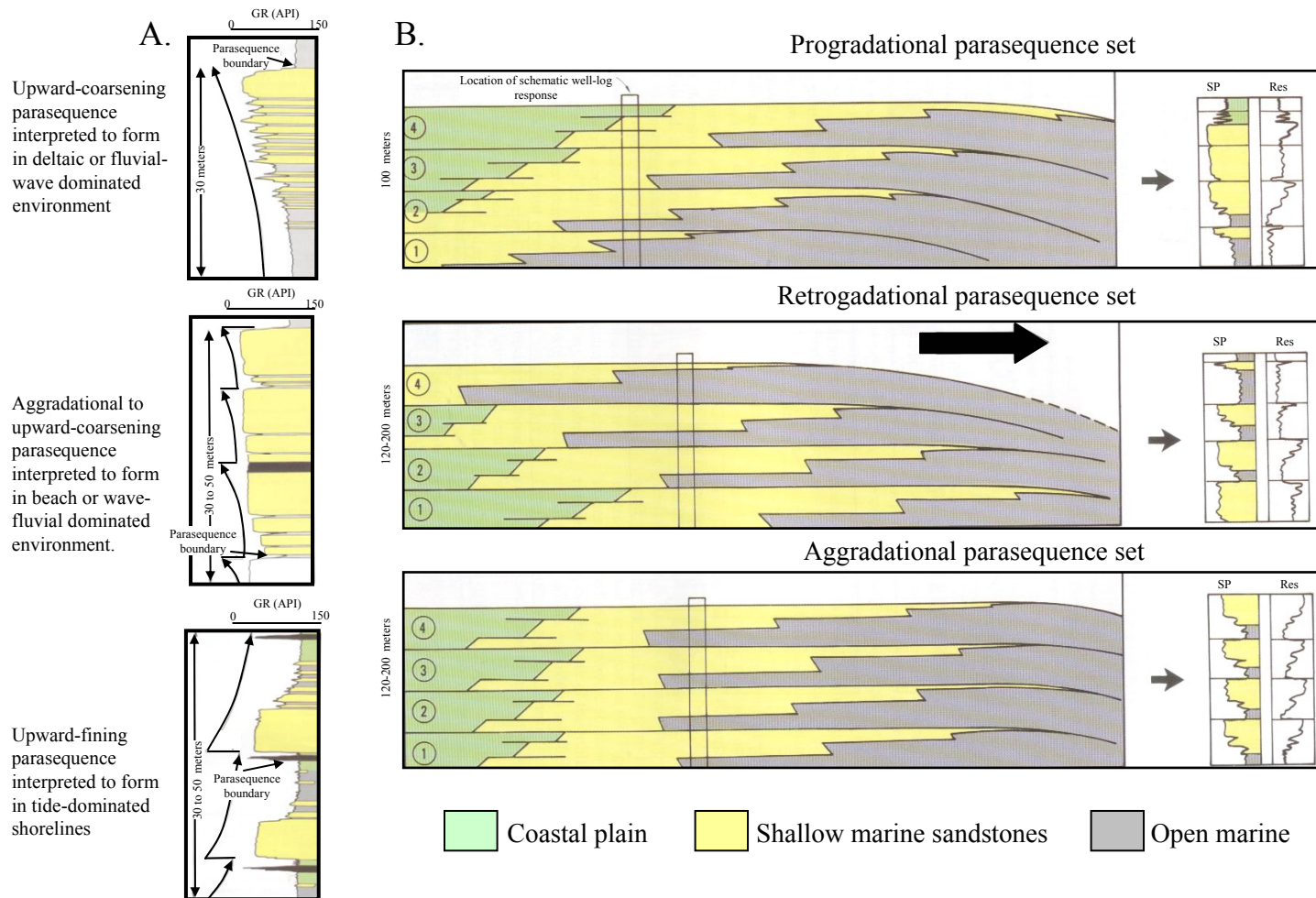


Figure 4.4. A) Log responses of parasequences. B) Stacking patterns in parasequence sets and well log expression. The log response illustrates deltaic and beach environments Modified from Van Wagoner et al., 1990.

Depositional sequence (sequence): A relatively conformable succession of genetically related strata bounded by unconformities and their correlative conformities (Vail et al., 1977).

Formation of stratigraphic sequences is the product of combining eustasy, sediment supply, and subsidence operating at different time scales. Identification of parasequences and parasequence sets can be done at the well log scale. Parasequences and parasequence sets represent the building blocks of depositional systems and the reservoirs (Van Wagoner et al, 1990) (Fig. 4.4). Vertical 1-D analysis of parasequences in well logs can be relatively simple, but 2-D analysis, (i.e., lateral correlations) is limited by the horizontal separation between wells. Figure 4.4 shows different log responses of parasequences and parasequence sets in a fluvial to marine setting (Van Wagoner et al, 1990). Stacking patterns are used to correlate the different parasequences that contain time and correlation lines defined by flooding surfaces.

The use of genetic sequences (Galloway, 1989) and sequences (Vail et al., 1977) depends on the kind of bounding surface to be used (i.e., maximum flooding surfaces or subaerial erosional sequence boundaries). Time duration of these sequences range from 0.5 to 3 my, and contain several parasequence sets. Maximum flooding surfaces form a regional characteristic surface in basins and usually give a good log response, whereas erosional sequence boundaries may record local expressions also dependant on a relative fall in sea level that exposes the shelf (Galloway, 1989). Erosional sequence boundaries are easy to recognize

when major tectonic events are present. These tectonic sequences are considered to be low frequency sequences (i.e., more than 3 my). These sequences can be called tectonosequences (equivalent to 2nd order sequences, Chapters 2 and 3) because of dominance of tectonics in controlling basin formation.

The Eocene section of the Maracaibo foreland basin is considered a tectonosequence (Lugo and Mann, 1995; Parnaud et al, 1995b, Chapter 3; Escalona and Mann, 2003b), which formed in an oblique collisional setting. Two major sequence boundaries bound the Eocene interval: the Paleocene and the Eocene unconformities (Chapters 2 and 3). Taking into account the high rates of subsidence, the recognition of continuous flooding events and the application of vertical stacking patterns, stratigraphic interpretation was done in the following manner:

1. Identification of the main bounding Eocene unconformities.
2. Identification of candidates for maximum flooding surfaces (i.e., genetic sequence interpretation).
3. Interpretation of parasequence sets.
4. Identification of candidates for sequence boundaries (i.e., sequence interpretation).

The first step is to interpret wells that penetrated the entire Eocene interval in the study area using core data and 1-D sequence stratigraphic analysis. The second step is to perform 2-D and 3-D sequence stratigraphic analysis by applying the pseudo-seismic transform technique. The third and final step is to use seismic

stratigraphy and mapping of the parasequence sets to build stratigraphic models and correlate these models with regional subsidence and seal level charts from previous workers.

4.4.3 Pseudo-seismic transform technique

In order to have a consistent sequence stratigraphic model and to maximize the use of the dense well database available (more than 300 wells), I applied the pseudo-seismic transform technique to display the log data. The pseudo-seismic transform technique of Carr et al. (1995) uses large numbers of well logs along with visualization techniques applied to 2-D and 3-D seismic data. Methods of conventional well log interpretation are usually time consuming for large numbers of wells. Correlation of several wells is limited to the number of wells that an interpreter can handle at the same time. Even computer stratigraphic interpretations become complex when using more than a dozen wells. In conventional methodology, the interpretation is done on a well to well basis and does not take advantage of the entire well data set. Seismic data allows a different approach: a single seismic line can have hundreds or even thousands of traces, and interpretation on either paper or a computer assisted program is quite standard procedure (Carr et al., 1995).

Ralph and Mitchum (1997) generated high resolution sequence stratigraphic well cross sections in shallow marine sandstones of the Carthage field, Texas. Their GR, SP and resistivity logs resemble high resolution inverted seismic traces. The pseudo-seismic transform is based on the observation that well

logs resemble seismic traces, where time represents depth, log amplitude represents seismic amplitude, and well location is related to a 2-D or 3-D seismic survey location that represents an area of the subsurface (bin). Thus, large volumes of well logs can be treated as seismic traces and interpreted using a seismic workstation program, increasing consistency and efficiency of interpretations.

Figure 4.5A shows a conventional well correlation based on well to well basis correlations. Figure 4.5B shows a single seismic line which display several seismic traces in a small area. In contrast to the well to well basis correlations in Figure 4.5A, pseudo-seismic cross sections in Figures 4.5C and D show how dozen of wells can be displayed using seismic visualization methods as in Figure 4.5B, and allow recognition of lateral and vertical stratigraphic and structural patterns. One of the most important steps is to define the datum on which the cross sections will be hung. Flooding surfaces represent the best markers for this purpose because of their lateral continuity and wide distribution, especially in tectonically complex areas such as the Maracaibo basin. Sequence boundaries, are very irregular erosional surfaces. Depending on the structural complexity of the study area, different flooding surfaces can be used as a datum for different stratigraphic levels. Sequence boundaries will record the ancestral topography upon which the different sequences were deposited.

PSEUDO-SEISMIC TRANSFORM CODE: A code to transform well log format (usually ASCII) to 3-D seismic data format (Segy) was written in Matlab

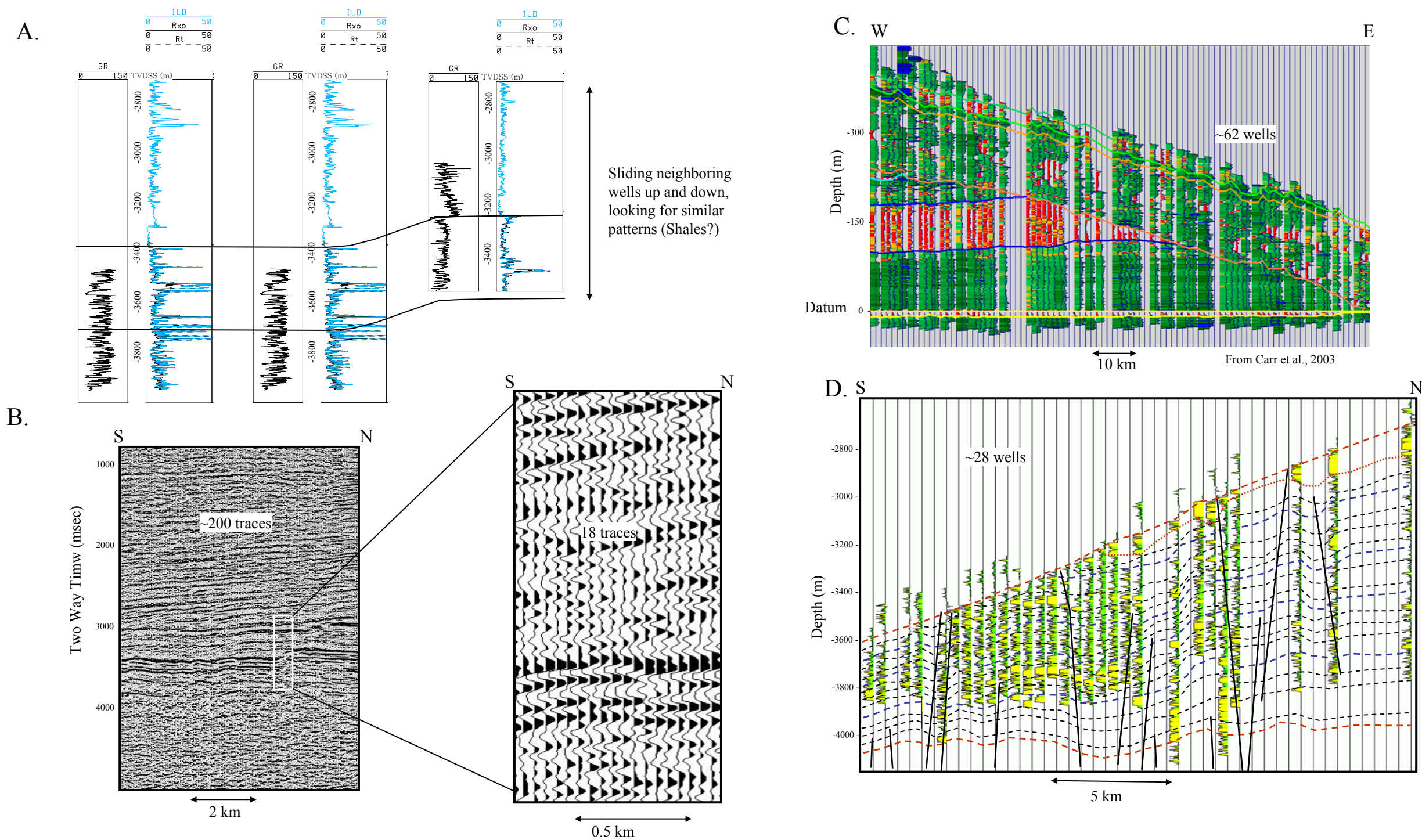


Figure 4.5. A) Conventional well-to-well log correlation, using GR and Resistivity logs. B) Example of a seismic line showing lateral continuity of reflections due to the amount of traces used. C) Stratigraphic pseudo-seismic section (modified from Carr et al., 1995). D) Structural pseudo-seismic section (this study).

in order to load the wells in seismic interpretation software including Seisworks from Landmark®, IEXS® from Geoquest, and Kingdom Suite®. Appendix 2 shows an example of this code for the 3-D pseudo-seismic lines used in this study. The code generates an empty matrix with the dimensions of the seismic line to be built (b=Y,X) and fills the matrix with well logs. The process is repeated as there are wells in the line. The last step is to output the matrix in Segy format and read it in into seismic interpretation software.

A “3-D seismic survey” was created in the seismic interpretation software in order to load the pseudo-seismic lines. Figure 4.6A shows a basemap with the location of the well data available. More than 300 wells are displayed. A 500 m² bin size was chosen for the 3-D grid in order to maximize the use of the wells and to take into account that well spacing is minimum 600 m for the Eocene reservoir area (Fig. 4.6B). The main objective is to make one well representative of each bin within the 3-D survey (500 m²). This objective requires that wells need to be relocated in the center of their corresponding bin. The well or a combination of the wells with best information is chosen to be the center of the bin.

For the stratigraphic interpretation, a 3-D pseudo-seismic cube using GR logs was built and loaded in Landmark software, Seisworks®. A color scheme was created, where yellow is low GR (sandstones) and dark green is high GR (shales) (Figure 4.4D). Other kinds of well logs are used to create different 3-D pseudo-seismic datasets, like deep resistivity to identify the presence of hydrocarbons (chapter 5). Volume of shale was not used because of graphic

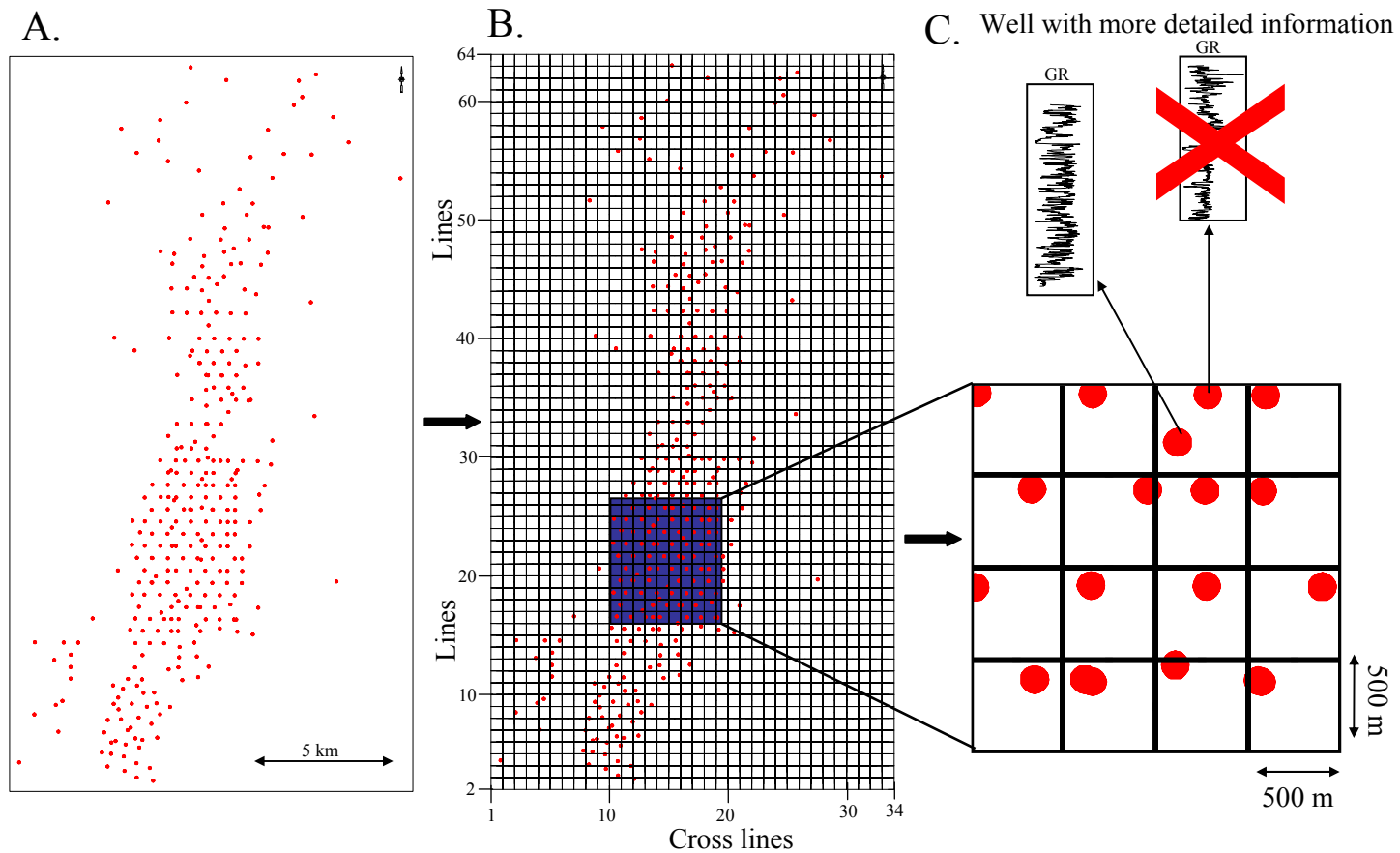


Figure 4.6. A) Well basemap. B) 3D pseudo seismic grid over the basemap showing direction of cross-lines and in-lines. C) Enlarged section of a part of the grid showing well selection for the 3D pseudo-seismic. One well will be representative of a 500 m² bin, and the other well will be discarded from the database.

limitations with the software and log shape preservation for facies characterization. One limitation using any well technique (conventional, pseudo-seismic, etc.) is that interpretations are biased by the spatial distribution of wells in the study area. In this study, wells form an elongate belt along an anticline. Lateral correlations outside this belt are poorly constrained and have to be tied to local and regional patterns.

4.4.4 Seismic interpretation

Conventional interpretation of 3-D seismic data began with generation of synthetic seismograms using well logs to provide correlations between seismic reflectors and well data, followed by correlation of the main, regionally continuous seismic reflections. An effort to correlate maximum flooding surfaces and unconformities from seismic data within the Eocene interval was not possible because of low vertical seismic resolution (~120 feet; ~40 m) and poor detailed correlation between the synthetic seismograms and the 3-D seismic data. The main maximum flooding surfaces and erosional sequence boundaries were projected among the discontinuous reflectors.

In order to improve the seismic interpretation and extract more stratigraphic information within the 3-D seismic cube, two non-conventional techniques were applied:

Seismic cube flattening (Fig. 4.7A): This technique consists of interpreting a good quality reflection from the 3-D seismic cube, and flattening the seismic cube relative to that reflection (i.e., as a stratigraphic section flattens a datum).

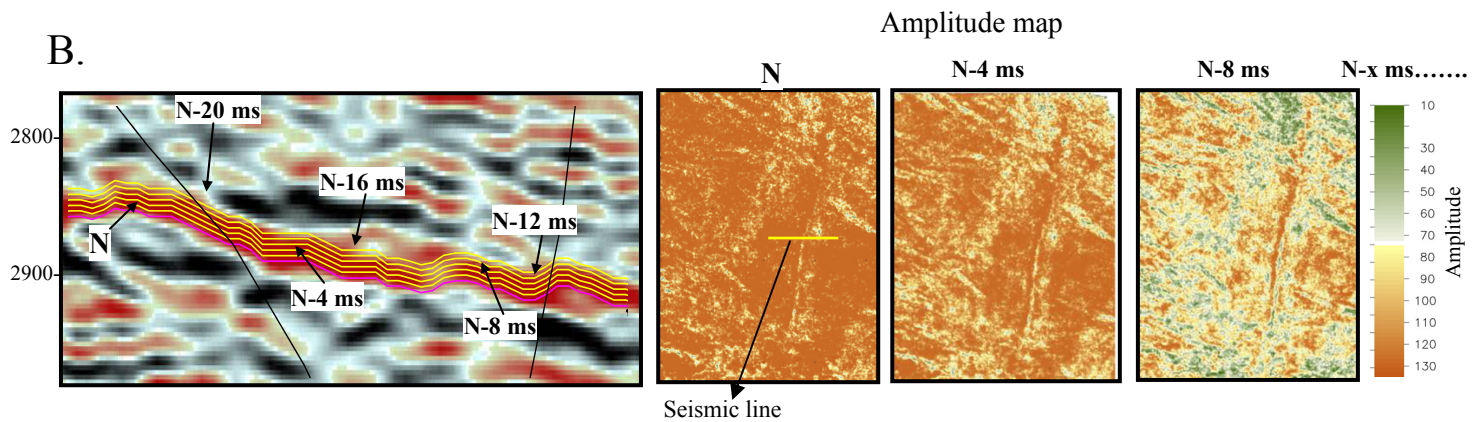
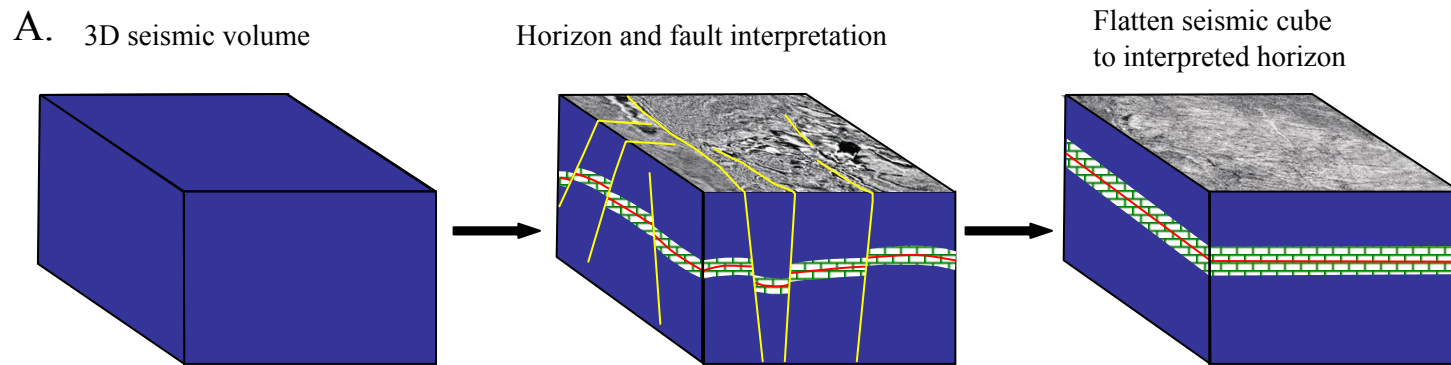


Figure 4.7. A) Methodology for seismic cube flattening and generation of seismic time slices. B) Methodology for generation of stratal slices relative to an interpreted horizon.

The main objective of flattening is to remove structural effects and generate seismic time slices which will be parallel to the datum. These surfaces represent pseudo-time lines relative to the datum and can highlight stratigraphic features (Fig 4.7A).

Stratal slices (Fig. 4.7B): The technique consists of generating horizons parallel to an interpreted horizon by adding or subtracting a constant time throughout the interpreted horizon. Extraction of amplitudes of the newly generated horizon will produce a horizon similar to the seismic cube flattening technique. Figure 4.7B shows stratal slices 4 ms (the data sample rate) apart from each other.

Another slicing technique is the proportional slice between two interpreted horizons (Zeng et al., 1998). All these techniques are based on the assumption that seismic reflectors follow chronostratigraphic surfaces (Zeng et al., 1998).

4.5 SEQUENCE STRATIGRAPHY

The main objective of sequence stratigraphic analysis is to identify and regionally correlate genetically stratigraphic units in the central Maracaibo basin within a chronostratigraphic framework. Identification of the stratigraphic units will incorporate understanding of the depositional systems and stratal geometry. Interpretation begins with a vertical one-dimensional analysis followed by two and three dimensional mapping of the genetic units.

4.5.1 One dimensional stratigraphic analysis

Figure 4.8 shows a comparison of type logs from previous 1-D stratigraphic analysis (Fig. 4.8A) and the 1-D stratigraphic analysis performed in this study (Fig. 4.8B). Major differences observed are the interpreted bounding surfaces and parasequence sets (Fig. 4.8). Previous interpretations proposed several intra-Eocene subaerial erosional surfaces (SB=sequence boundaries, Fig. 4.8A; PDVSA E&P and Veba Oil, 1998) defining depositional sequences. In this study, only one intra-Eocene subaerial surface was interpreted (SB41, Fig. 4.8B), and flooding surfaces are the main bounding surfaces of the stratigraphic units defining parasequence sets and genetic sequences (Fig. 4.8B). Stratigraphic 1-D analysis reveals the following characteristics:

- The Eocene tectonosequence is confined between two major unconformities: the basal Paleocene unconformity (Chapters 2 and 3) with an age of ~54 my (Fig. 4.8B) and the Eocene unconformity which separates middle Eocene (< 44 my) from early Miocene sedimentary rocks (~25.2 my; Rull, 2002).
- The Eocene tectonosequence is characterized by an aggradational succession of sandstones above the Paleocene unconformity followed by a major retrogradational succession of shales and sandstones with few progradational units and an aggradational succession of sandstones at the top (Fig. 4.8B).
- Four maximum flooding surfaces (MFS1 to MFS4) are interpreted from stacking patterns. These four surfaces define five genetic sequences (Galloway, 1989) (Fig. 4.8B). Genetic sequence 1 is bounded at the base by the

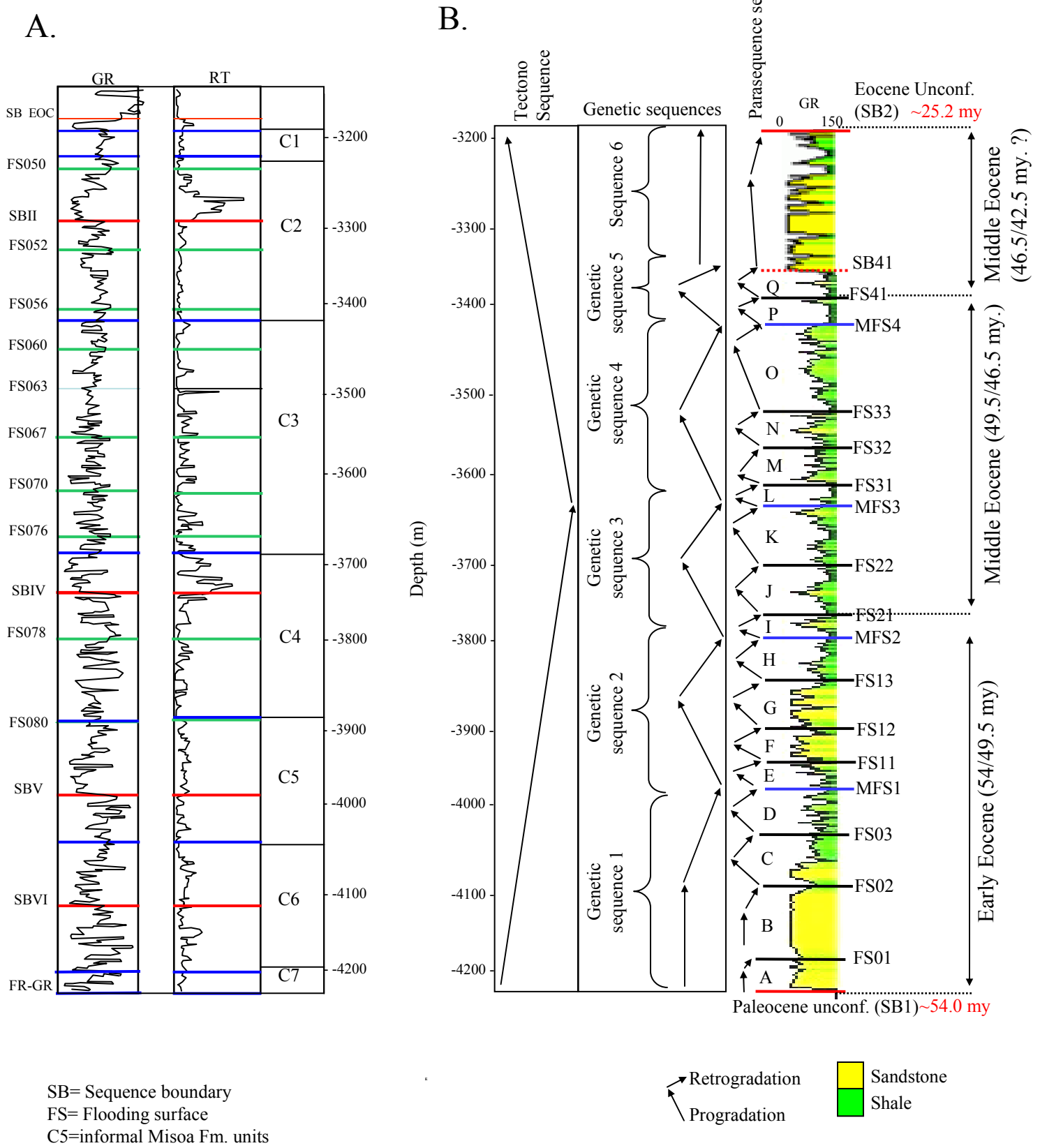


Figure 4.8. A) Type log of the study area with one-dimensional stratigraphic interpretation before this study, showing major bounding surfaces (modified from PDVSA E&P Occidente and Veba Oil, 1998), and B) Type log of the study area with one-dimensional stratigraphic interpretation from this study, showing the different levels of cyclicity, lithology, age of events, and name of interpreted sequences.

Paleocene unconformity (SB1), and sequence 5 is bounded at the top by the Eocene unconformity (SB2). These two unconformities are the boundaries of the Eocene tectonosequence (Chapters 2 and 3). Sequence 6 is interpreted at the top of the Eocene interval and is bounded by SB41 (subaerial erosional intra-Eocene surface) and the Eocene unconformity. This sequence is not present in all the wells.

- Progradational, aggradational or retrogradational units are bounded by flooding surfaces within each of the five genetic sequences (Fig. 4.8B). By definition, these units are parasequence sets, which include several parasequences that are bounded by marine flooding surfaces. Interpretation of parasequences was not performed due to uncertainties on the lateral facies variability within each parasequence set. As noted by Van Wagoner et al. (1990), identification of parasequences at the outcrop scale is possible, but lateral correlation may not be possible and becomes difficult when working with wells as lateral resolution is low. In the study area, seventeen parasequence sets are interpreted (A to Q, Fig. 4.8B) using major flooding surfaces (FS) or maximum flooding surfaces (MFS) within each genetic sequence. Also a sequence is interpreted in the upper part of the Eocene section (sequence R, Fig. 4.8B).

- In average, each genetic sequence consists of 3 to 4 parasequence sets, here called sets A to Q (Fig. 4.8B). Assuming linear interpolation between the few age control points and an average genetic sequence lasting from 1 to 3 my, the duration of parasequence sets is on the order of 300 to 900 ky.

4.5.2 Facies associations

In order to make 2-D and 3-D depositional system and facies interpretations within a 2-D and 3-D stratigraphic framework, a facies scheme was built to interpret for the Eocene interval. This step integrates core facies descriptions, GR log shape and 1-D sequence stratigraphic interpretation. The use of these facies associations gives a lateral and vertical predictive tool using "Walther's Law" (i.e., the lateral progression of environments is reflected in the vertical progression of facies) (Galloway, 1998).

Five main GR facies associations (table 4.1) were established; 1) blocky-fining upward, 2) spiky or mixed, 3) spiky-coarsening upward, 4) erratic and 5) blocky. These GR facies associations record environments that range from fluvial to marine on the Eocene Maracaibo shelf. The influence of tidal processes in the Eocene of the Maracaibo basin has been previously proposed by Maguregui (1990) and Ambrose et al., (1995) and has also been observed in core data from the study area (Figs. 4.2 and 4.3). Both of these studies agree that the Eocene consists of a succession of tide-dominated deltaic cycles and that the main lithofacies include distributary channel fills, tidal sand ridges, tidal channel fills, and prodelta shelf assemblages. Tide range was micro-to-meso tidal (0.5 to 3 m) and wave energy minor. Blocky-fining upward GR facies reflect the main sandy units in the early-middle Eocene interval and record the fluvial channel input to the shelf. Spiky GR facies show strong evidence of tidal influence and represent the transitional environments between middle-lower delta plain to shallow marine (shelf).

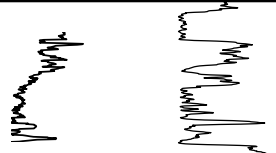
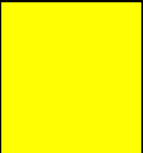
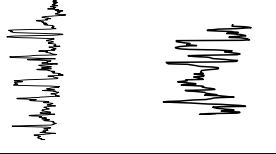
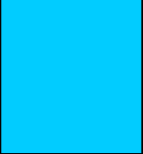
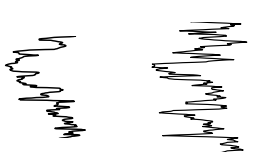
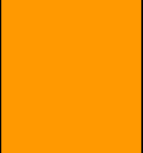
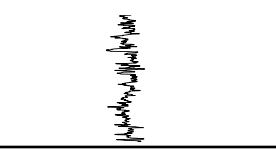
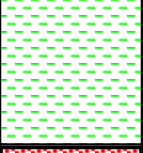
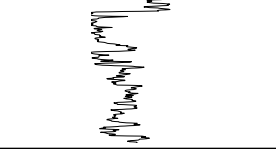
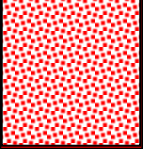
GR Facies associations	Color scheme	Description	Inferred facies and depositional system setting, based on core description	Sequence stratigraphic setting
		Blocky- fining upwards	Fluvial channel fill, distributary channel fill. Fluvial-dominated, tide influenced delta plain	Progradational system, possible erosive surface at the base
		Spike or mixed	Crevasse splay or tidal bar. Middle to lower delta plain	Transgression, possible ravinements surface at the base of main sandstone bodies
		Spike-coarsening upwards	Mouth bar, delta front or tidal bar	Progradation or retrogradation
		Erratic	Lower delta plain, shallow marine shelf	Transgression
		Blocky	Amalgamated fluvial channel fill	Progradation and retrogradation

Table 4.1. Gamma Ray facies associations for the study area

The upper interval is characterized by thick blocky sandstones. Core data are not available for this sequence (sequence 6). This amalgamated aggradational succession of sandstone seems to correlate with the initiation of tectonic rebound in the basin during the middle Eocene. The succession forms a sequence, because it is bounded by unconformities at the top and base (sequence 6, chapters 2 and 3).

4.5.3 Two-dimensional stratigraphic analysis

The application of the pseudo-seismic transform technique in generating two dimensional sections allows lateral correlation and interpretation of the sequence boundaries, maximum flooding surfaces, and flooding surfaces. Furthermore, lateral and vertical continuity of lithofacies associations is easily depicted using the proper datum within the Eocene tectonosequence.

Figures 4.9 and 4.10 show examples of 2-D stratigraphic analysis of cross-line 16 and in-line 25 respectively (see Fig. 4.6 for location). As observed in Figures 4.9B and 4.10B, the structural complexity within the Eocene section can obscure the lateral correlation of surfaces and the continuity of facies associations. Lateral correlation of surfaces was done interactively between structural sections (i.e. Figs. 4.9B and 4.10B) and stratigraphic sections (i.e. Figs. 4.9C and 4.10C), until the optimal correlation was found. The structural framework was imported from seismic interpretation (Chapters 2 and 3), and this framework was improved by utilizing the pseudo-seismic sections. The best datum was the maximum flooding surface MFS2 (Figs. 4.9C and 4.10C), because more than 95% of the wells penetrate and contain data for this surface. This maximum flooding surface

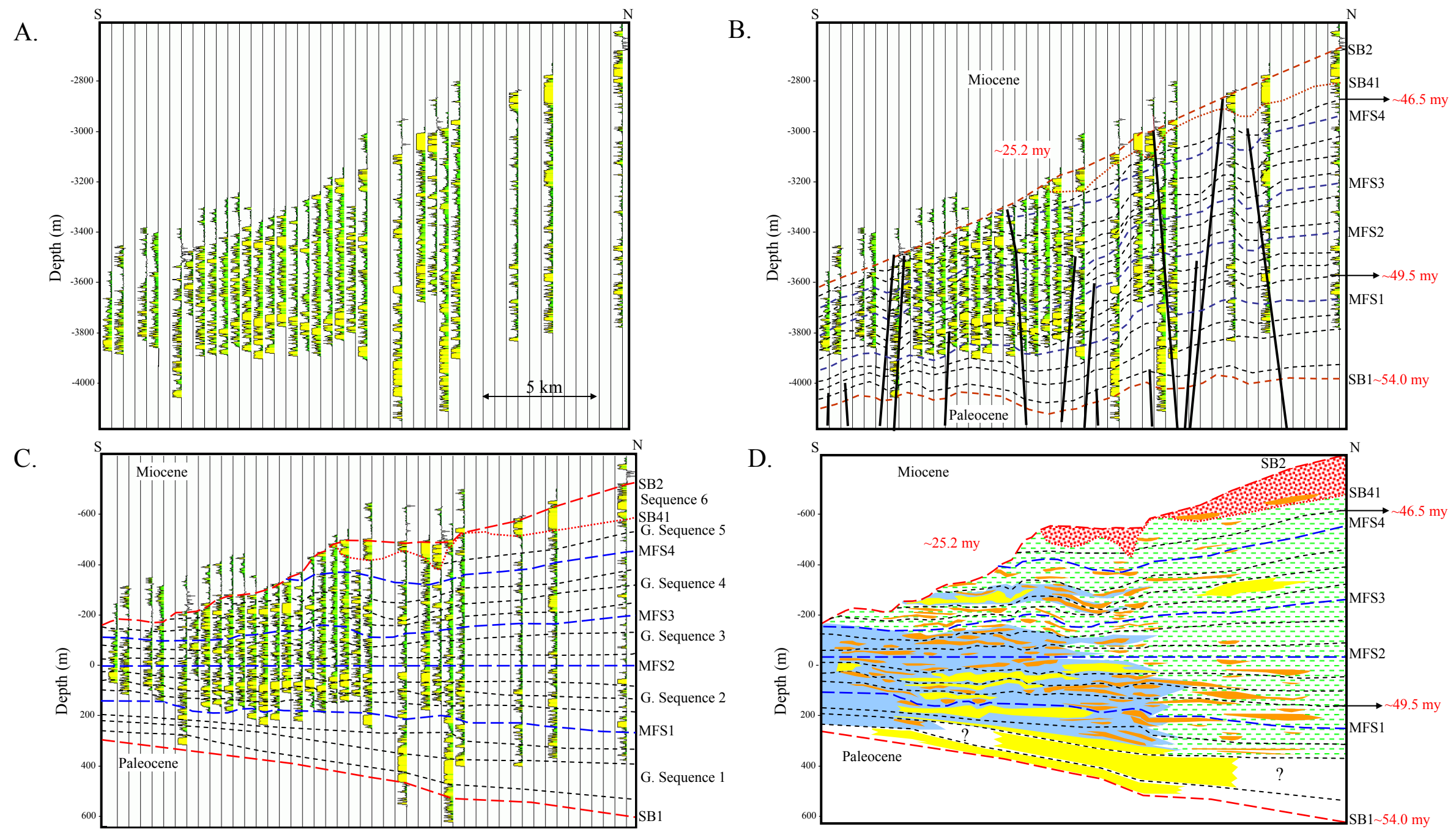


Figure 4.9. Pseudo-seismic N-S cross line 16: A) Uninterpreted. B) Structural interpretation and main surfaces. C) Stratigraphic interpretation with datum surface MFS2. D) Facies interpretation with datum on surface MFS2. Facies color scheme based on Table 4.1.

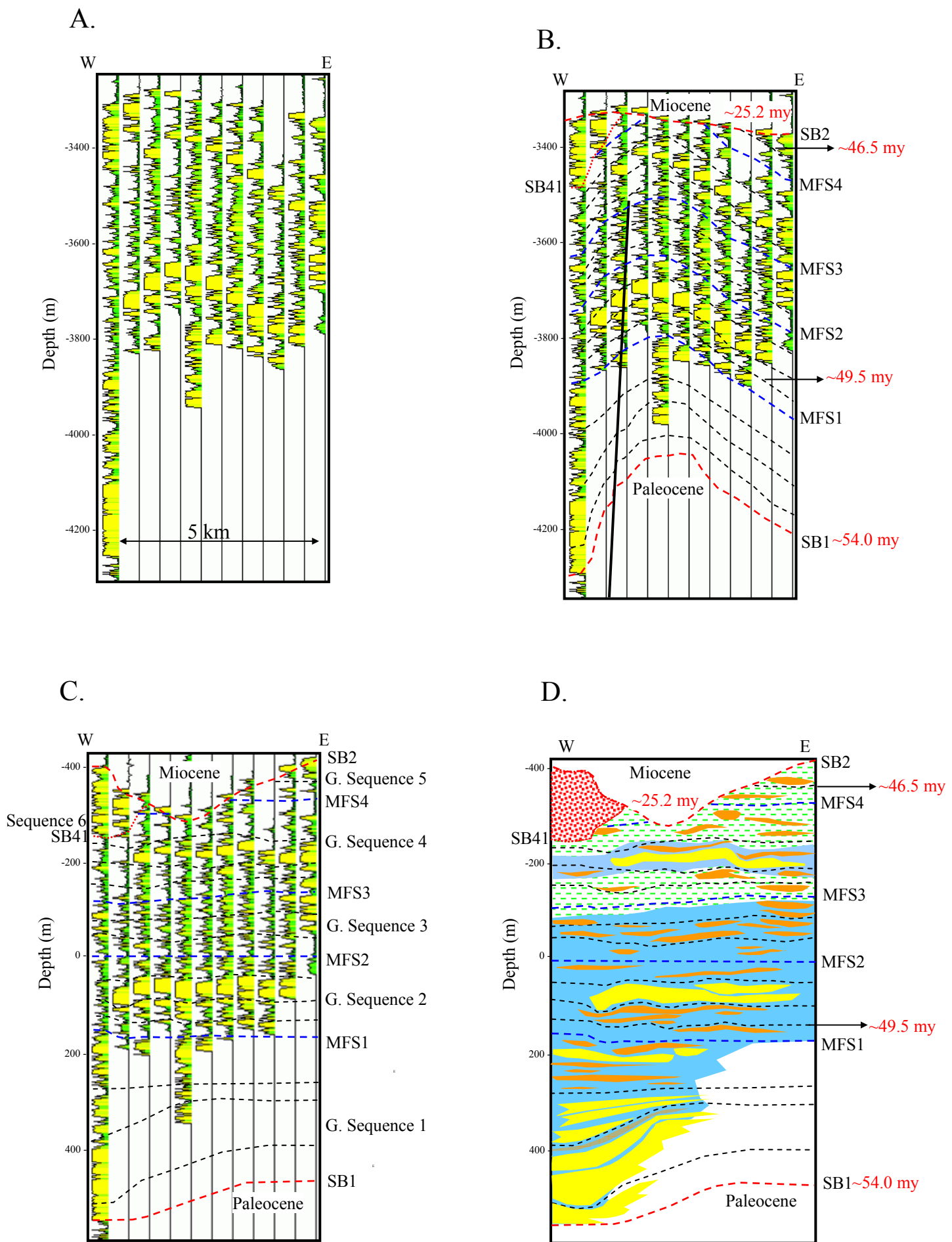


Figure 4.10. Pseudo-seismic E-W line 25: A) Uninterpreted; B) Structural interpretation and main surfaces; C) Stratigraphic interpretation with datum surface MFS2; and D) Facies interpretation with datum on surface MFS2. Facies color scheme based on Table 4.1.

is continuous and present throughout the study area. Stratigraphically the MFS2 is located in the middle of the Eocene interval and records a major flooding event in the area. Other maximum flooding surfaces were used to improve correlations locally.

- Stratigraphic interpretation of facies associations in two dimensions are based on the following observations: Thicknesses of parasequence sets, genetic sequences and sequences increase toward the north. Average thickness of parasequence sets is 50 m (~150 feet) in the south and 65 m (~200 feet) in the north.

- Stronger erosion affects the southern Eocene interval than the northern area. In general, the early-middle Eocene pinches out to the south against the forebulge and increases in thickness toward the basin located north from the Burro Negro fault (Chapter 2). Genetic sequence 5 and most of genetic sequence 4 are both eroded in the southern part of the study area (Fig. 4.9), whereas in the northern part genetic sequence 5 and sequence 6 are only partially eroded by the Eocene unconformity (Figs. 4.9 and 4.10).

- When structural highs are present in the study area, missing sections as a consequence of erosion at the Eocene unconformity become more numerous.

- A general retrogradational pattern of parasequence sets is interpreted for the Eocene tectonosequence (Figs. 4.9D and 4.10D). Shallow marine/shelf facies dominate the northern part of the area, whereas fluvial and tidally influenced facies (i.e., tidal bars) are more common in the southern part of the area.

- Maximum transgressions occurred during MFS3 and MFS4 (~47 and 46 my respectively, Figs. 4.9D and 4.10D). Facies are characterized by shallow marine facies and a few tidal bars in these intervals.

- Genetic sequence 1 is characterized by an aggradational pattern of amalgamated sandstones of ~3 my duration, overlying the Paleocene unconformity (4.9 my). Duration of parasequence sets are ~800 to 900 my.

- Regressive-transgressive cycles characterize genetic sequences 2 to 5. Genetic sequences 2 and 4 record the development of deltaic systems, whereas sequence 3 and 5 are mainly retrogradational with highly discontinuous sand bars. Average duration of genetic sequences are ~1 my, and parasequence sets are 400 ky.

- Sequence 6 is characterized by a thick package of amalgamated sandstones that incise genetic sequence 5 in an irregular manner below the Eocene unconformity (Fig. 4.9D). This sequence thickens abruptly to the north and west, and it is not present in most of the southern area.

4.5.4 Three dimensional stratigraphic analysis

Three-dimensional pseudo-seismic interpretation allows complete use of the well data in arbitrary directions (lines, crosslines and arbitrary lines); this analysis also includes cross validation of two-dimensional sections interactively. Analysis and mapping of parasequence sets throughout the study area were performed. Figure 4.11 shows a 3-D fence diagram where lateral and vertical continuity of the parasequence sets is observed. Three depositional episodes are

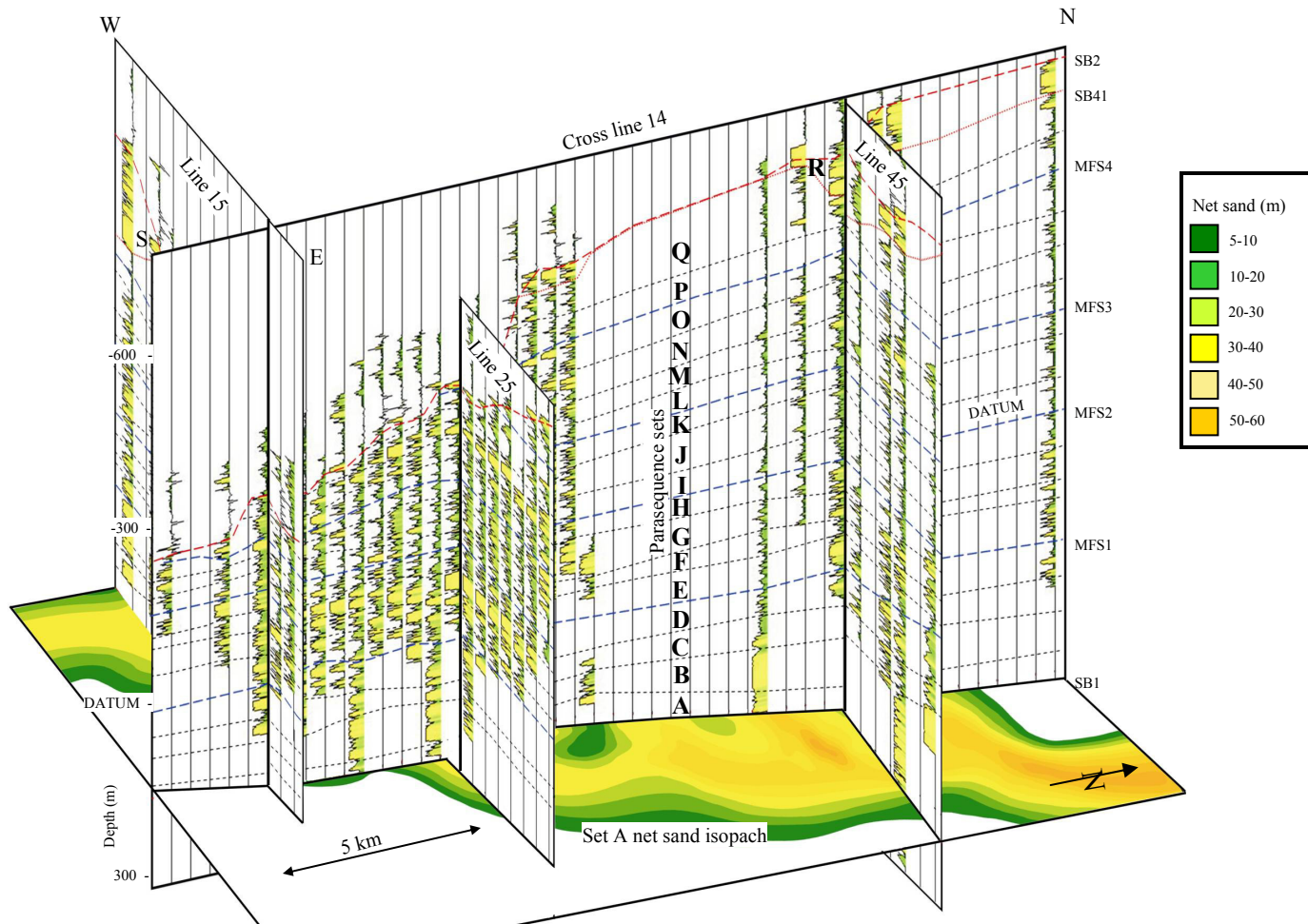


Figure 4.11. 3D pseudo-seismic fence diagram including crossline 14, in-lines 15, 25 and 45, and net sand isopach map of parasequence set A. Datum is MFS2.

interpreted in each crossline. Integrated with the fence diagram is a net sand isopach map of parasequence set A. Spatial analysis of stacking patterns of the parasequence sets reveals features already interpreted on the 2-D stratigraphic analysis: 1) an aggradational succession in genetic sequence 1 followed by regressive-transgressive cycles with major transgressions recorded by MFS3 and MSF4, 2) two main progradational sets (G and N) within these cycles, 3) the erosive character of sequence 6 which is laterally associated with the Eocene unconformity, and prominent erosion or missing section in the central and southern areas. Main progradational direction was N-NE, which is consistent with the regional depositional model during the early–middle Eocene (Maguregui, 1990; Parnaud et al., 1995b; Chapters 2 and 3).

Normal lateral and vertical successions of facies were interpreted within genetic sequences 1 to 5, and unconformable sequence boundaries are not observed. Figure 4.12 shows a facies interpretation of three crossline sections (11, 16 and 19; see Fig. 4.6 for location) with MFS2 taken as a datum. Facies interpretation shows the typical wedge shape of the early-middle Eocene foreland basin setting. The Eocene interval shows greatest erosion to the S-SW along crossline 11 (Fig. 4.12), where sections are missing down to the upper part of genetic sequence 3. Blocky sandstone facies of sequence 6 are thicker and more deeply incised in this area.

Fluvial-deltaic facies are mostly sandstone. These sandstone packages are observed in the aggradational succession of genetic sequence 1, in progradational sets F and G of genetic sequence 2, and set N of genetic sequence 4 (Figs. 4.11

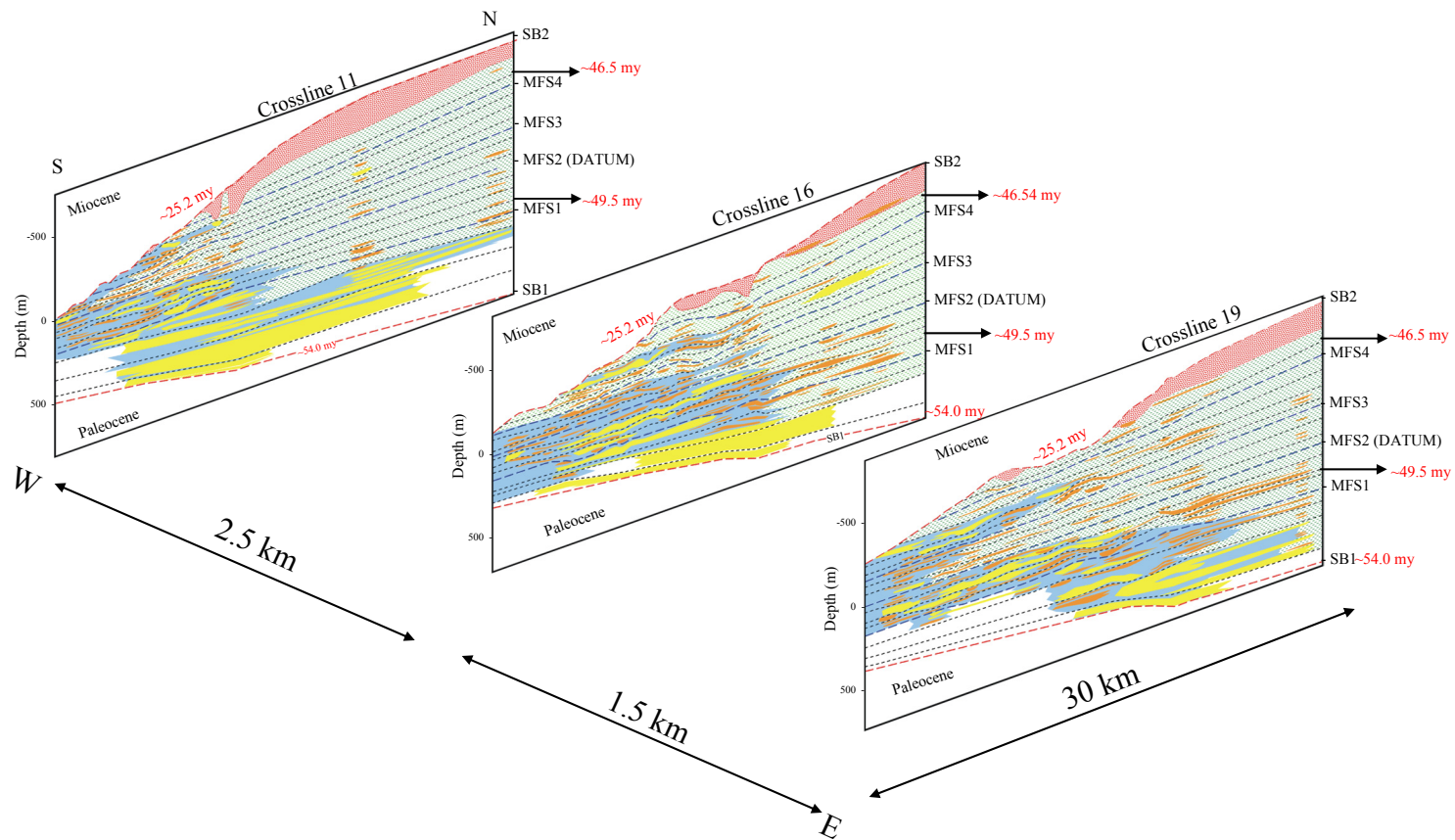


Figure 4.12. 3D pseudo-seismic facies interpretation illustrated by a fence diagram using crosslines 11, 16 and 19. Datum is given by MFS2.

and 4.12). Aggradational patterns of fluvial-deltaic facies are observed to the west, whereas progradation from S to N dominates in the center of the study area (Figs. 4.11 and 4.12). Marine influence dominates the central and northern study areas. Marine flooding was greater in the east for MFS1 and MFS2, whereas for MFS3 it was greater in the central-west areas (Fig. 4.12). Highly discontinuous sand bars are common in genetic sequences 2, 3 and 4. These sand bars tend to be more abundant in retrogradational sets, and thicker in progradational sets (Fig. 4.12, crosslines 16 and 19). Sand bars lengths vary from less than 1 km to more than 4 km and thicknesses range from few meters to 20 m (~60 feet, Figs. 4.11 and 4.12).

Net-to-gross and net sand maps were constructed for the parasequence sets (Figs. 4.13 to 4.16). High sandstone content is present in parasequence sets of genetic sequence 1, 2, 4 and sequence 6, whereas genetic sequences 3 and 5 are dominated by shale. Sand counting was done using the GR, where sandstones have values between 0 and 90 API units and shales have values higher than 90 API units.

GENETIC SEQUENCE 1 (Fig. 4.13): This sequence comprises sets A, B, C and D, and is the sandiest set in the Eocene interval of the study area. As described in 1-D and 2-D sequence stratigraphic analysis, the parasequence sets tend to be aggradational (Figs. 4.4, 4.8 and 4.9) and are characterized by high percentages of blocky sandstones reaching up to 100 m in thickness (Fig. 4.13). A general south to northeast sandstone trend is interpreted from maps, but may be biased by well distribution.

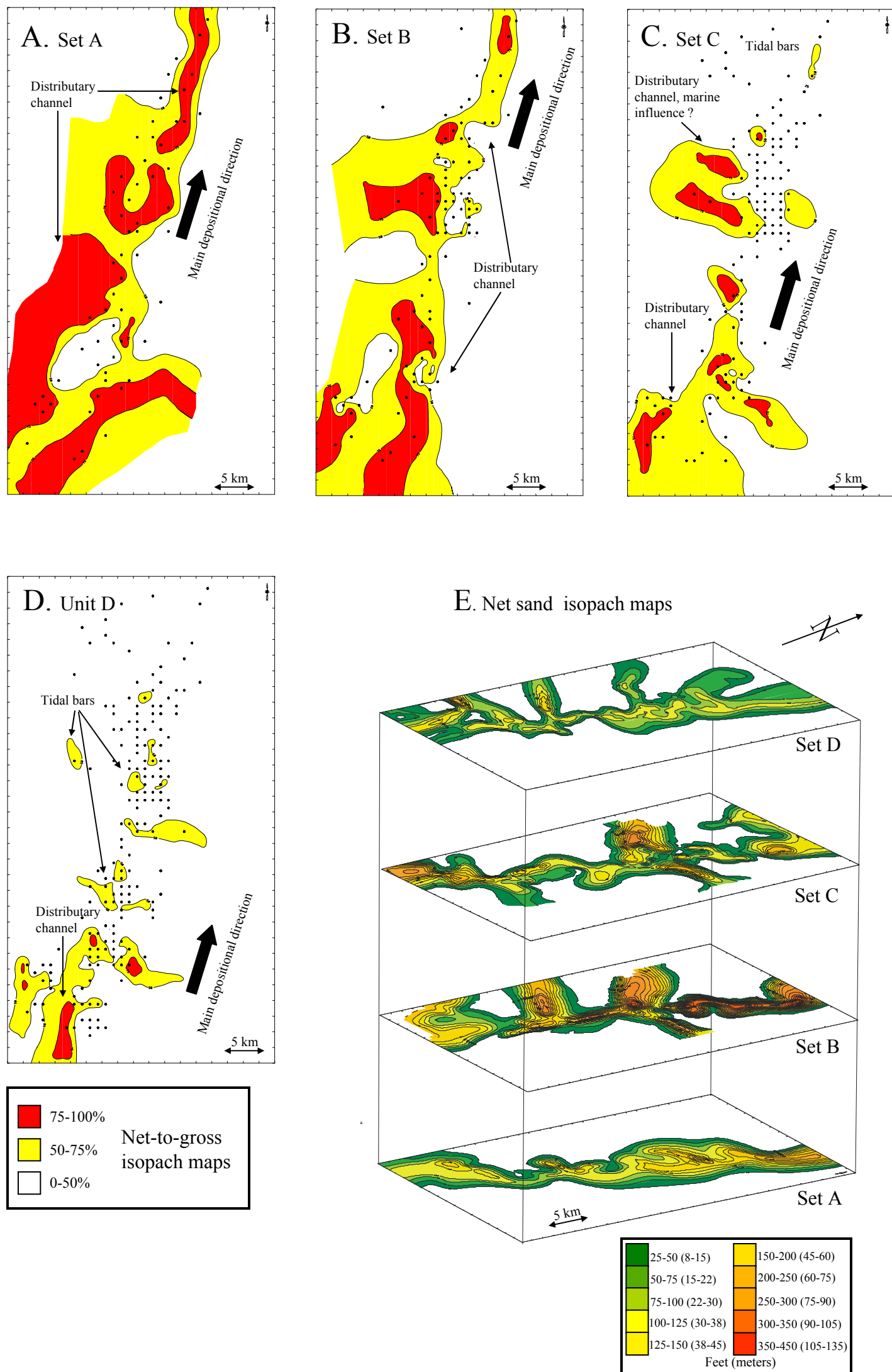


Figure 4.13. Parasequence sets net-to-gross maps. A) Set A. B) Set B. C) Set C. D) Set D; and E) net sand isopach fence maps of sets A, B, C and D (genetic sequence 1). This sequence has the greatest sandstone thickness, reaching up to 450 feet (~150 m) of thickness to the north of the study area.

Starting with set A, a main distributary channel complex is interpreted. To the northeast, shale percentage increases in the channel area (Fig. 4.13A). Set B (Fig. 4.12B) shows a similar trend as set A with the net-to-gross map, but the net sand isopach shows the main south-to-northeast channel splitting in several distributaries trending to the northwest and northeast (Fig. 4.13E). Maximum sandstone thickness is preserved within the main channel in the northeast area, similar to set A. Set C shows similar geometries as set B, but there is a decrease in the amount of sandstone (Fig. 4.13C). Major preservation occurs in the main channel to the south and lateral distributaries are located to the west and east in the central part of the area. Aggradational successions within the genetic sequence are less common in the northern areas of this set. Set D is strongly affected by marine flooding surface MFS1, and sandstone percentages in the northern area are less than 50% (Fig. 4.13D). North trending sand bars observed in the net to gross map form the dominant sand bodies within the distributary geometries interpreted from the net sand isopach (4.13E). Facies interpretation (Fig. 4.12) indicates an increase of marine influence during this set.

GENETIC SEQUENCE 2 (Fig. 4.14): This sequence comprises sets E, F, G and H. The entire succession of parasequence sets is a major regressive-transgressive cycle bounded by maximum flooding surfaces MFS1 and MFS2. As in genetic sequence 1, a southwest to north-east trend is inferred. However, sandstone percentages and thickness are less, suggesting more marine influence, and back stepping of deltaic facies (Fig. 4.14).

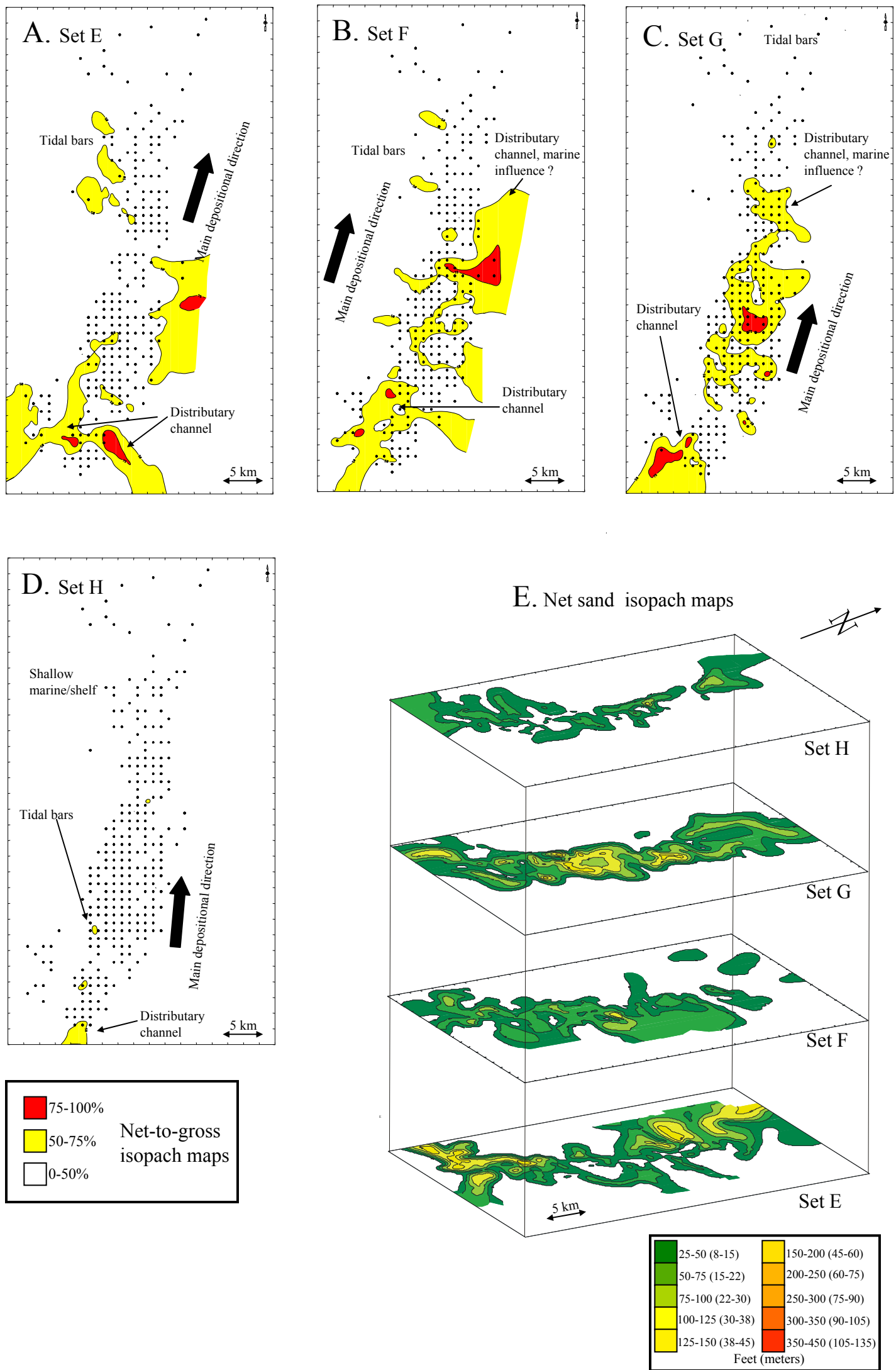


Figure 4.14. Parasequence sets net-to-gross maps. A) Set E. B) Set F. C) Set G. D) Set H; and E) net sand isopach fence maps of Set E, F, G and H (genetic sequence 2).

High percentages of sandstone (75-100%) are common in all the sequences, except set H. Set H has less than 50% with the exception of the southern area (Figs. 4.14D and E). This set is the major transgression event during the Eocene period in the area of study (genetic sequence 3), as interpreted from pseudo-seismic sections (Figs. 4.9 to 4.12). Sand bars oriented NW-SE are common in the central and northern areas and the bars are transitional between continental and marine facies. Set G (Fig. 4.14C) represents the maximum progradational set within the genetic sequence. Set G's depocenter was located in the center of the area. A southeast-northeast distributary system dominated by fluvial facies can be interpreted in sets F and G (Fig. 4.10 to 4.12). Progradation of fluvial facies within these two systems did not extend to the northern study area, as it did in genetic sequence 1. Fluvial facies are characterized by blocky sandstone GR patterns (Table 4.1; Fig. 4.9 to 4.12). Thinner sandstones (10-25 meters, Fig. 4.14) are characterized by spike GR response, indicative of sandy tidal bars and crevasse splays within the continental-marine transitional area (Table 4.1).

GENETIC SEQUENCE 4 (Fig. 4.15): This sequence comprises sets L, M, N and O. Erosion affects all of the sets in the central southern part of the study area. This regressive-transgressive cycle is less progradational than genetic sequence 2. However, a main distributary system is located in the southwestern part of the area (Fig. 4.15). Marine influence affects most of the central and northern areas, where elongated sand bars oriented mainly in a N-S direction are interpreted.

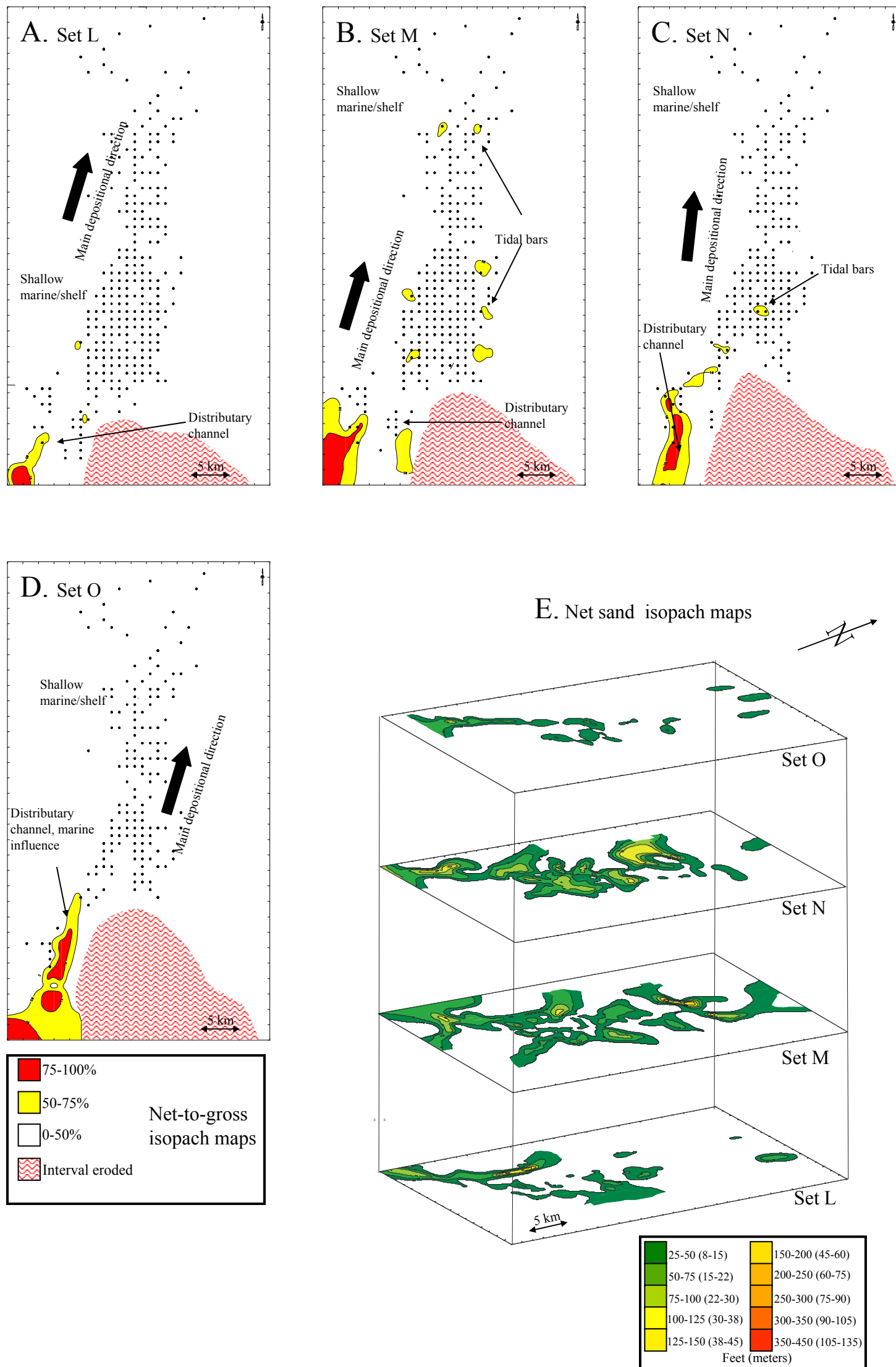


Figure 4.15. Parasequence sets net-to-gross maps. A) Set L. B) Set M. C) Set N. D) Set O; and E) net sand isopach fence maps of sets L, M, N and O (genetic sequence 4).

Sets L and O show sand bars that probably were controlled by tidal flow energy in the lower delta plain to shallow marine shelf settings. Some of the sand bars are isolated in the northern study area (Figs. 4.15A and D). Sets M and N are the main progradational systems within this genetic sequence. Although sandstone percentages are relatively low, a considerable amount of sand reached the central area, as observed from isopach maps (Figs. 4.15B, C and E).

This may be an indication that: 1) the dispersal system was sand poor (Fig. 4.3), 2) a decrease in the size of the depositional system from genetic sequences 1 and 2, and/or 3) increase of tidal influence (Fig. 4.3, table 4.1). Small distributaries seem to split to the NW and SE from the main SW-NE channel axis become sand bars to the north as observed in the net-to-gross maps in the central area (4.15E).

SEQUENCE 6 (Fig. 4.16): This sequence comprises set R and is characterized by sand percentages up to 100% and thickness of more than 150 meters (400 feet). Sequence 6 is mostly eroded or not present in the southern part of the study area, with the exception of the southwestern area and a smaller area to the southeast (Fig. 4.16). Sequence 6 is bounded at its base by the sequence boundary SB41, which incises set Q and part of set P of genetic sequence 5 (Fig. 4.9 to 4.12). At the top, sequence 6 is bounded by the Eocene unconformity. Major depositional trends of sequence 6 are mainly oriented to the northeast, with few trends to the east-west in the central and northern areas. Sub-division of parasequences sets was difficult because no age control or core data are available and stacking patterns are also difficult to identify.

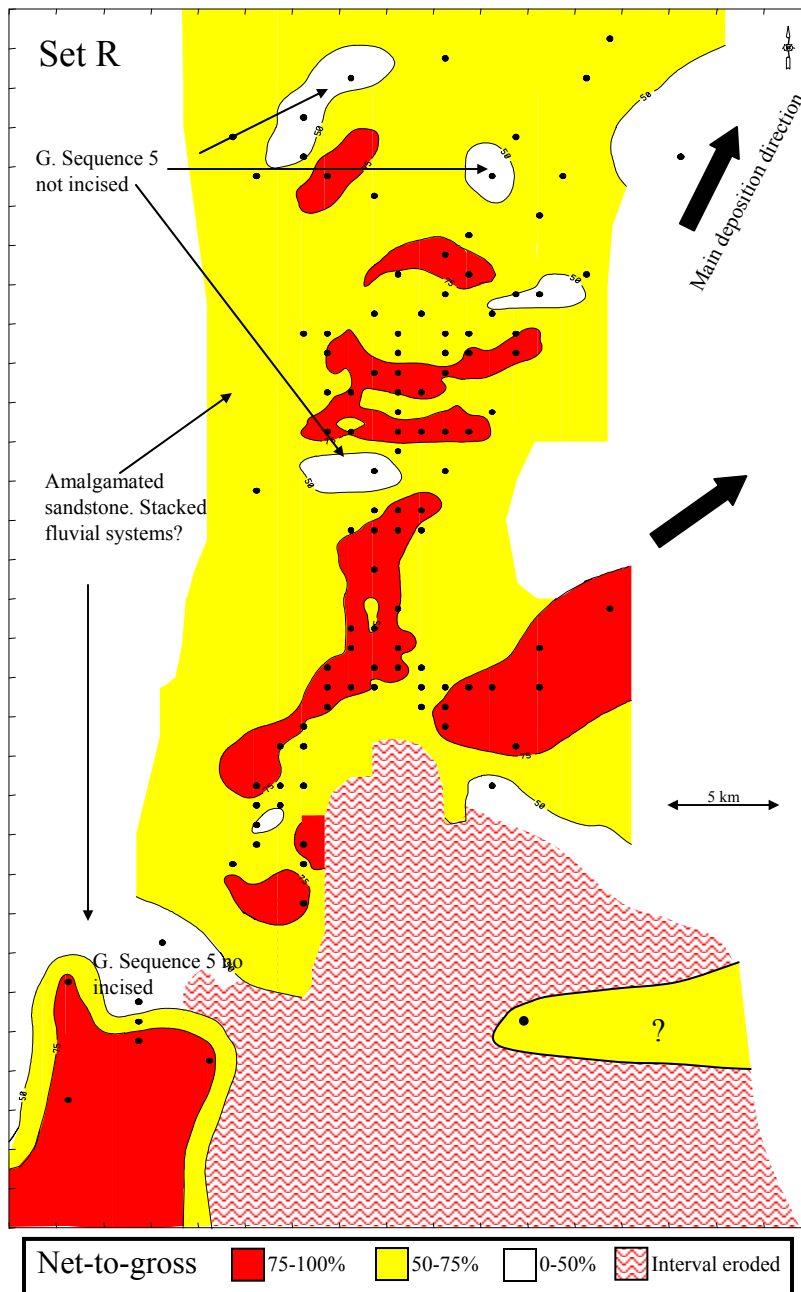


Figure 4.16. Sequence 6 net-to-gross map.

The erosive base of sequence 6 (set R), its aggradational pattern, and its absence in the southern area suggests that its formation was synchronous with the creation of the Eocene unconformity. Sediment was derived from the eroded highlands to the south during tectonic rebound (Villamil, 1999; Chapters 2 and 3). Depositional systems are interpreted as amalgamated fluvial systems that extend from the exposed highlands in the south toward the basin located in the northeast. Sequence 6 infilled the accommodation space produced on the shelf following the major Eocene transgression. Estuarine facies may have filled valley-shaped incisions during periods of transgression (Fig. 4.16).

4.5.5 Seismic stratigraphy

Several synthetic seismograms were generated using well logs from the study area (Fig. 4.17). A zero phase wavelet provided the best match between synthetic seismogram and seismic data with a dominant frequency of less than 30 Hz. Correlation between major surfaces identified in well data (e.g. flooding surfaces and sequence boundaries) was generally poor, except for the main tectonosequence boundaries. Poor correlation between both data may be due to logging problems. Well log data are sensitive to borehole shape. Caliper data in the study area reveals that most of the boreholes contain washouts and slumps (Fig. 4.17, caliper-CAL). Washouts can cause significant effects on log response, such as spikes in the sonic log affecting synthetic seismogram response.

Tectonosequence boundaries SB1 and SB2 are recognized throughout the Maracaibo basin, and well-to-seismic correlations of these boundaries are good.

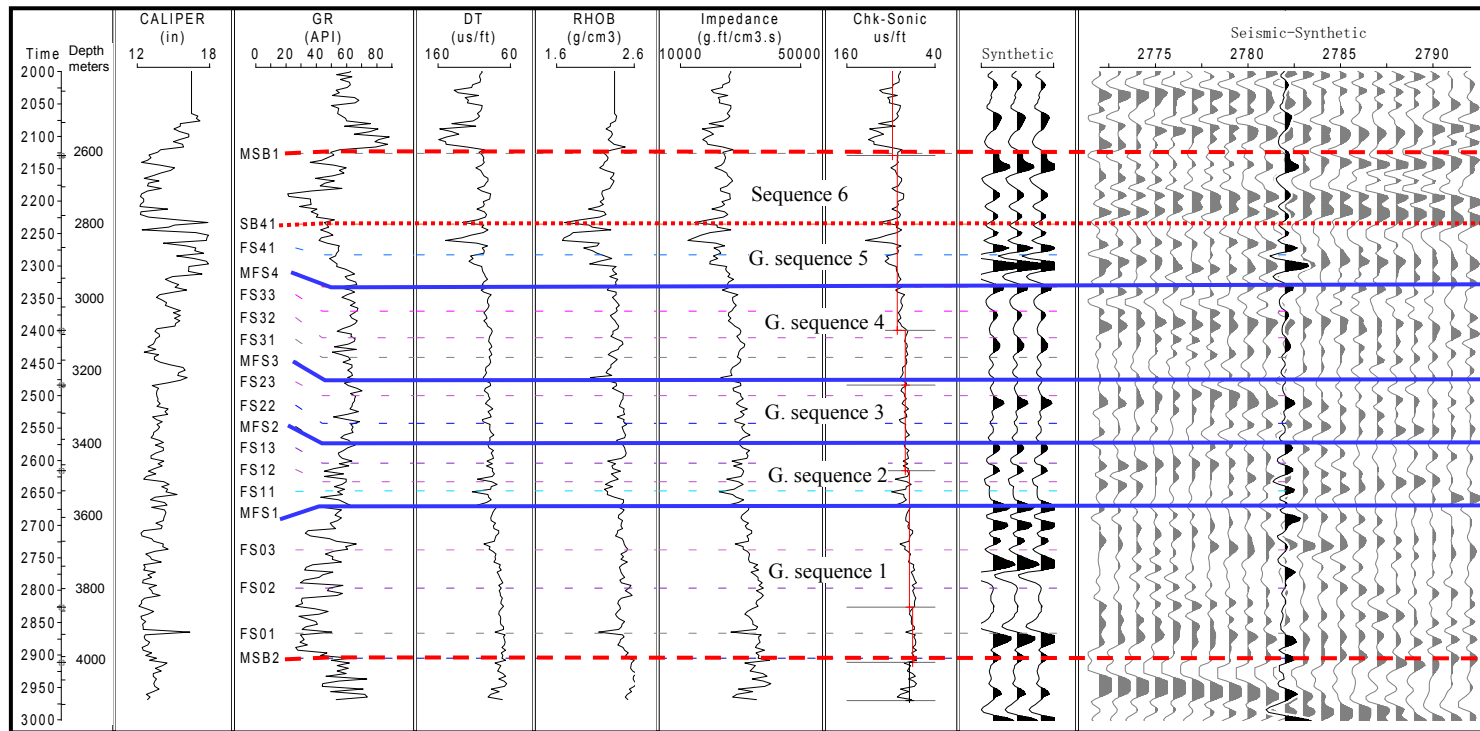


Figure 4.17. Example of a synthetic seismogram from well W26. Correlation between well logs and seismic data is poor, because inferior well bore conditions (see caliper) and resolution of 3-D seismic data. Main sequence boundaries and major flooding surfaces are shown.

Both surfaces create strong amplitude troughs in most of the synthetic seismograms, and show good continuity in seismic data (Figs. 4.17, 418A and 419B). These surfaces were used as control points to tie the synthetic seismograms with seismic data. Maximum flooding surfaces MFS1, MFS2 and MFS4 are characterized by troughs in the synthetic seismograms, whereas MFS3 is represented by a peak. Correlation with 3-D seismic data is of intermediate quality, because lateral stratigraphic variations (Fig. 4.17). Correlation of flooding surfaces, defining parasequence set on seismic data, was poor. Seismic reflections show high lateral variability and vertical resolution is in the range of the parasequence set thicknesses interpreted (~30-50 meters), generating wavelet interference in the seismic response (Brown, 1996).

After the main seismic events were identified from synthetic seismogram correlations, maximum flooding surfaces and sequence boundaries were interpreted from the 3-D seismic data. In addition, reflection characteristics within all sequences were interpreted in order to define the possible stratigraphic configurations using 3-D pseudo-seismic profiles. Figures 4.18 and 4.19 show examples of two seismic sections in the study area (Fig. 4.1 for location). Seismic horizon interpretation is correlated by synthetic seismograms. Main observations from the stratigraphic point of view are:

- The Eocene tectonosequence is interpreted as an asymmetric wedge that is thinning to the south, and thickening to the north (Chapters 2 and 3). Lap out is observed over the Paleocene unconformity (SB1) within genetic sequence 1 and truncations are interpreted below the Eocene unconformity (SB2). To the

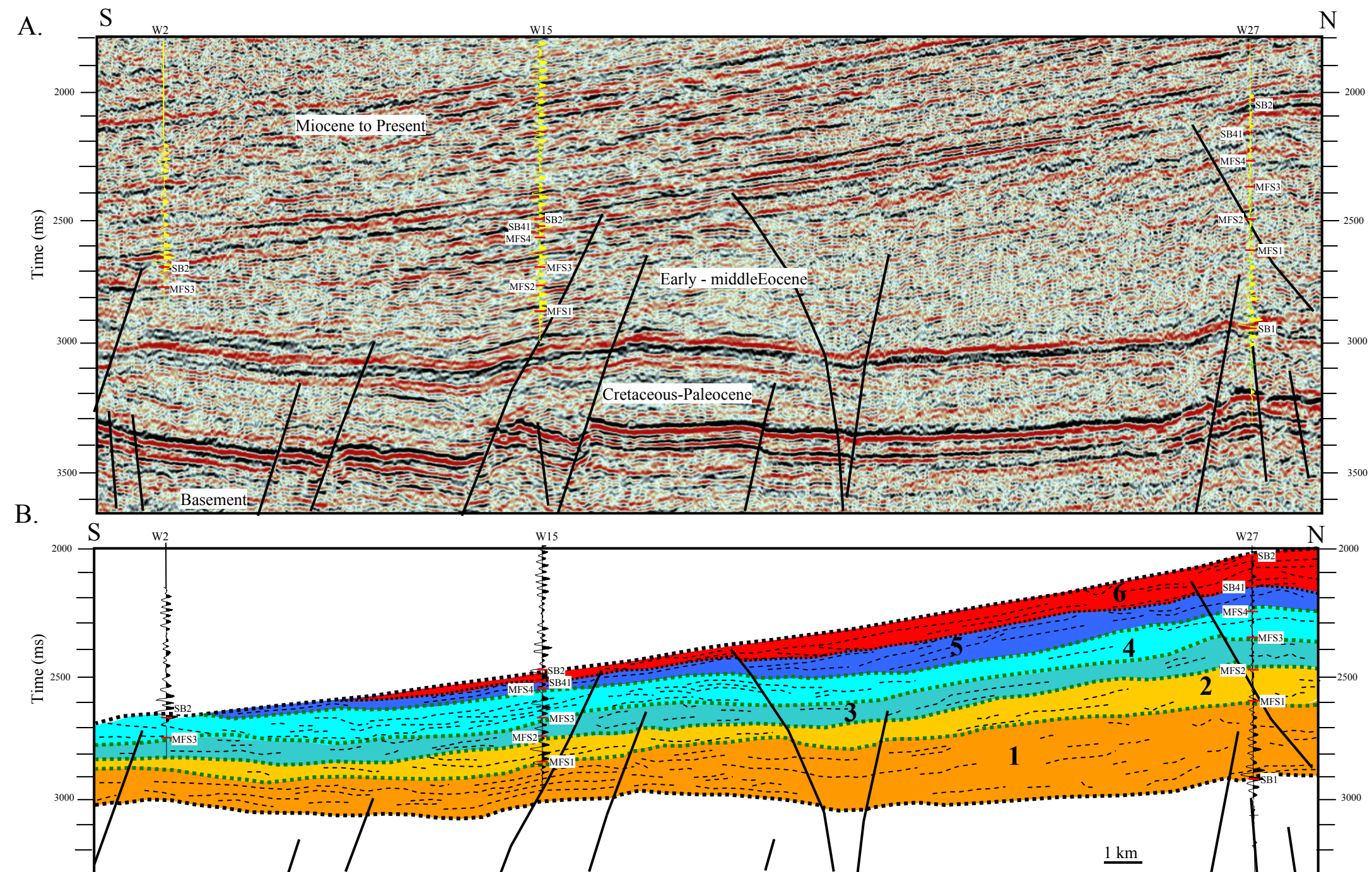


Figure 4.18. A) Uninterpreted seismic crossline. B) Interpreted seismic crossline showing different stratigraphic sequences. Reflections vary from sub-parallel to chaotic, and laterally discontinuous geometries are interpreted. Resolution of the seismic data does not allow detailed interpretation of stratigraphic sequences. A general divergent pattern is observed.

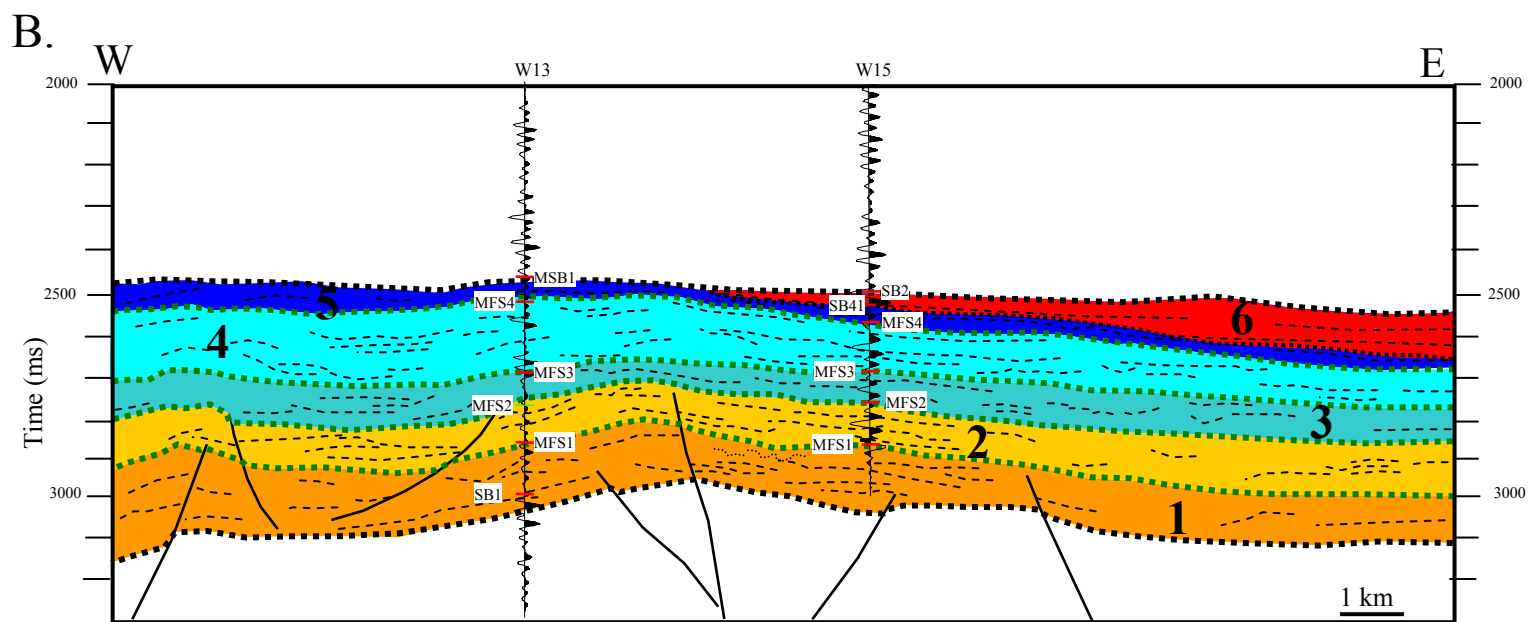
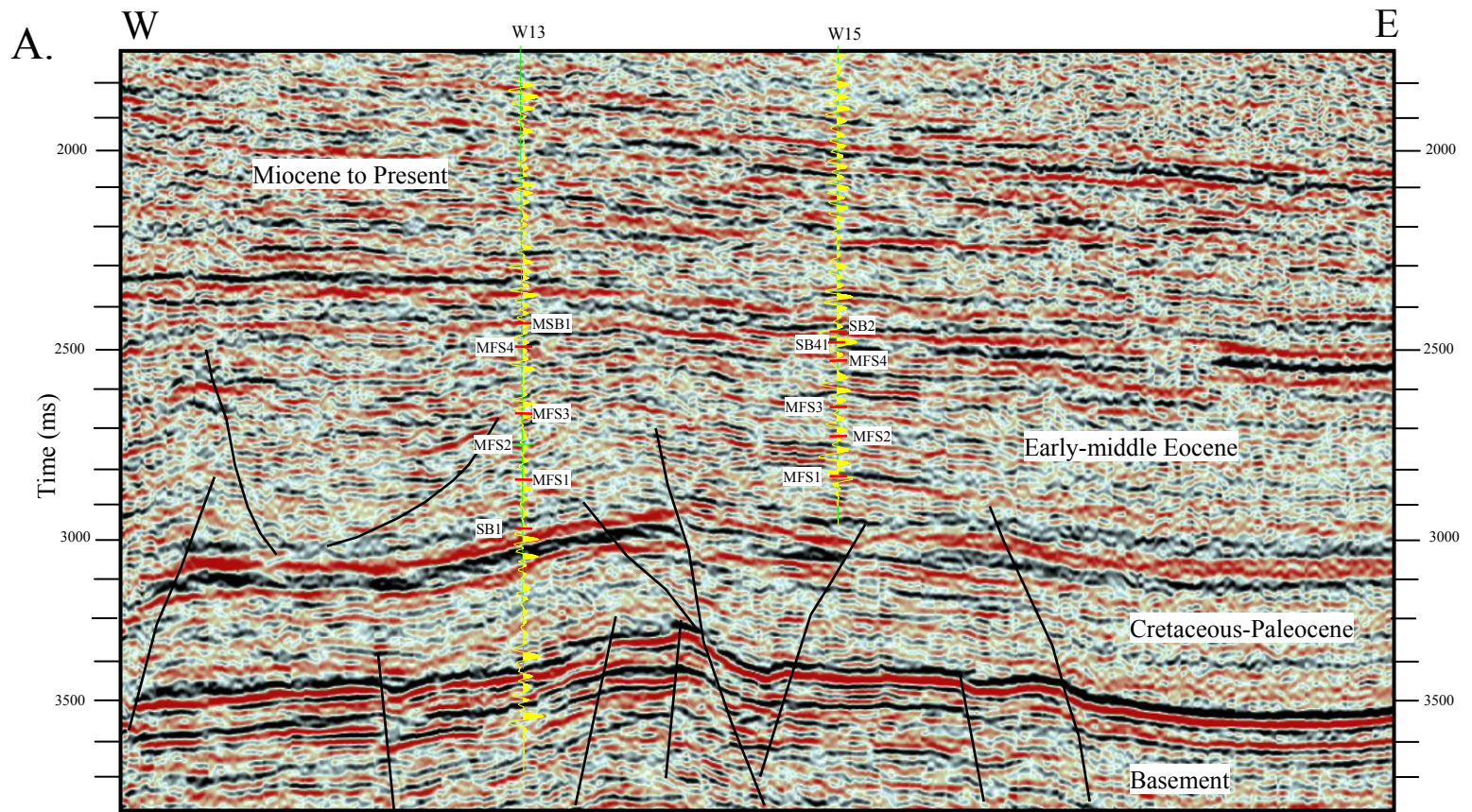


Figure 4.19. A) Uninterpreted seismic line. B) Interpreted seismic line showing different stratigraphic sequences. Reflections vary from sub-parallel to chaotic. Sequence 6 is interpreted to have erosional base characterized by strong reflections. Interpretation of parasequence sets is poor.

south, the Eocene unconformity (SB2) affects part of genetic sequence 4, most of genetic sequence 5 and the entire sequence 6 (Fig. 4.18).

- Reflections within the Eocene tectonosequence show a high lateral variability, making lateral correlation of individual surfaces difficult. However, maximum flooding surfaces and sequence boundaries are correlatable.

- Genetic sequences have a slight increase in thickness to the north as interpreted from well data (pseudo-seismic sections). Major thickening occurs in genetic sequence 1 and sequence 6. The general trend seems to be divergent and reflections within genetic sequences are discontinuous, sub-parallel and are characterized by terminations that occur in the direction of convergence (Fig. 4.18). This configuration may be the result of variations on the rate of deposition and/or progressive tilting of the depositional surface (Vail et al., 1977).

- Continuous reflections are observed in the south, whereas hummocky and chaotic reflection patterns are dominant in the north (Fig. 4.18).

- Reflection patterns suggest lateral variations of the depositional environments and lithologies. To the south fluvial and deltaic facies are dominant on well logs, whereas to the north, shallow marine/shelf facies are dominant on well logs (Figs. 4.9 to 4.12).

- A few channel-like and clinoform geometries are observed, but they usually are not continuous throughout the area. In general, clinoforms show a south-to-north prograding geometry and are interpreted as part of genetic sequences 4 (Fig. 4.18) and 6 (Figs. 4.18 and 4.19).

- Increase in thickness for most of the genetic sequences is observed to the west near the Icotea pull-apart basin (Fig. 4.19). These lateral variations in thickness suggest local increases in accommodation space on the Eocene Maracaibo shelf.

- Sequence 6 is characterized by high amplitude reflections, lap out terminations, truncations, and few clinofolds showing northward progradation. The basal sequence boundary (SB41), interpreted as a peak, becomes highly discontinuous to the north, where a few incised geometries are also interpreted. The upper part of genetic sequence 5 is eroded as a sub-parallel surface with increasing erosion toward the flanks of the anticline structure (Fig. 4.19).

Map view analysis using stratal slicing and seismic cube flattening was performed on the 3-D data. This technique was applied to the main surfaces (sequence boundaries and maximum flooding surfaces), and in all cases but one, no coherent result was obtained. As shown in the seismic interpretation (Figs. 4.18 and 4.19), most of the reflections within the Eocene interval of the study area are highly discontinuous and low quality, making slice interpretations difficult. The only surface that showed satisfactory results was the Paleocene unconformity (SB1), where both techniques gave similar results. This unconformity is one of the better seismic reflectors in the study area with good amplitude and continuity. Figure 4.20 shows the results obtained in large areas of the 3-D seismic data. Main observations include:

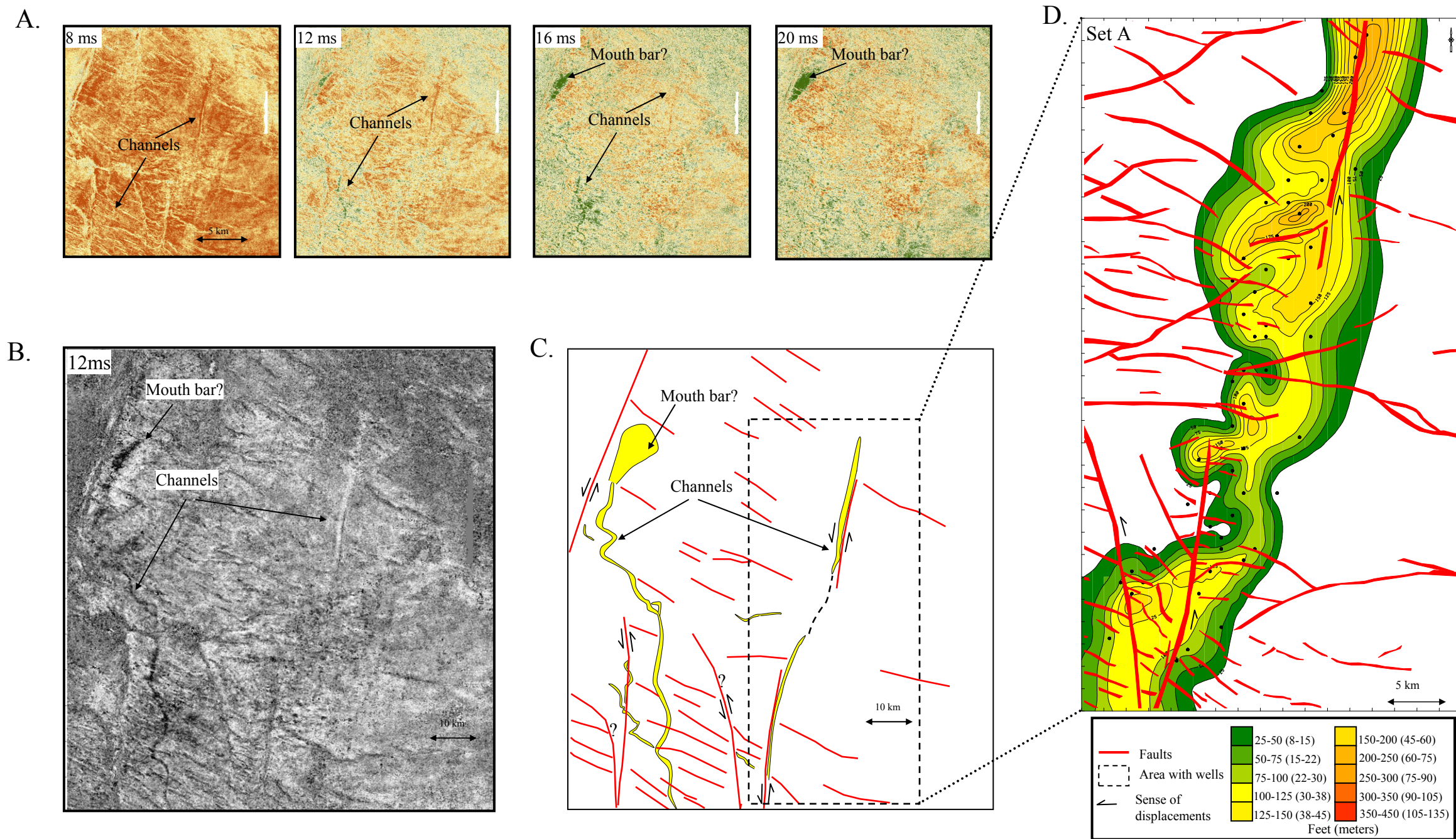


Figure 4.20. A) Partially interpreted seismic time slices flattened relative to SB1. Numbers in ms represent height above the unconformity SB1. B) Partially interpreted flattened time slice at 12 ms above SB1. C) Time slice interpretation: Incised channels in unit A over the basal Paleocene unconformity (SB1). The channel to the left cuts through the strike of the faults, and its depocenter is located in the Icoetea pull-apart basin (high amplitudes at the northern end of the channel); The channel on the right is controlled by N-NE trending strike-slip faults, which were active during the Eocene. D) Net sand isopach map of set A showing the N-NE faults controlling direction of the interpreted channel on the flattened times slice.

- At 8 ms above SB1, discontinuities related to faults are observed. These faults are interpreted using conventional seismic time slice methods at the Paleocene unconformity (Chapter 2).

- The succession of flattened seismic time slices relative to the Paleocene unconformity (Fig. 4.20A) show two channel systems at 8, 12 and 16 ms.

- The channel located to the west has low sinuosity and crosscuts the NW-SE striking faults (Fig. 4.20B). A high amplitude anomaly, interpreted at the northern end of the channel (Fig. 4.20A at 16 and 20 ms), suggests the location of the mouth bar. This amplitude anomaly is located in one of the depocenters of the Icoatea pull-apart basin (Chapter 2). This observation confirms the presence of an Eocene depocenter along with its syndepositional character. The sinuosity of the channel suggests either a mixed-load system (Galloway and Hobday, 1996), that the channel is deflected by NW-SE faults along its path to the depocenter, or tidal influence (Galloway and Hobday, 1996). This area is located west of the zone control by wells (Fig. 4.20B).

- The channel located to the east is straight and follows the strike of NE-SW strike-slip faults associated with the Icoatea pull-apart basin (Chapter 2). The channel is located in the area with well control (Figs. 4.1 and 4.20C), and have good correlation with set A. The isopach map of set A was used to guide the interpretation in this particular area. Width of channel from seismic data is smaller than the one interpreted using the well data which highlights the importance of well control. The straight character of the channel and the thick blocky sandstones suggest a bed load system (Galloway and Hobday, 1996).

- The strike of faults seems to control sediment paths and depocenters. Fault control is interpreted for the linear trends of two channels mapped from seismic data and isopach maps of parasequence sets (Figs. 4.20B, C and D).

- Other small channel-like features can be interpreted, but most of them closely follow fault strikes. This suggests that they are: 1) channels that follow the strike of the faults, like set A; 2) fault discontinuities; or 3) seismic artifacts (Fig. 4.20B).

4.6 REGIME VARIABLES

Understanding the control variables on the formation of stacking patterns and cycles in the stratigraphic record of a basin is a key step for spatial and temporal prediction of depositional systems. Three main variables have been proposed to be and the principal controls of sequence formation at different scales: eustatic sea level change, sediment supply and rate of basin subsidence. The interplay of these variables defines the stratigraphic architecture of the sediments that fill the accommodation space within the basin (Vail et al., 1977; Galloway, 1989; Emery and Myers, 1996). In order to understand the origin and stratigraphic architecture interpreted in the Maracaibo basin, these variables are discussed below.

4.6.1 Eustasy

Eustasy is defined as the absolute global change in sea-level relative to the center of the earth. Three main components of sea-level change are: glacial,

tectonic, and geoidal (Galloway, 1989). Furthermore, eustasy can vary either by changing the ocean basin volume or by changing ocean water volume (Pitman III, 1978). Ocean-basin volume changes are related to plate tectonic interactions, by changes in rate of basin subsidence due to tectonic events with duration of 3 to 50 my or opening and/or closing of ocean gateways (Pitman III, 1978). Also, it is generally accepted that water volume changes result from variations in the volume of continental ice caps. Volume of ice caps is affected by variations in the amount of solar distribution over the Earth's surface (Miall, 1997). Solar energy is controlled by the orbital oscillation of the Earth (i.e., called Milankovitch cycles) or by climatic and oceanic circulation changes (Miall, 1997). The duration of these cycles is in the order of 0.1 to 0.5 my. No single mechanism can explain cycles with duration of million years, although Vail et al. (1977) assume that it is due to glacial eustasy. Instead, cycles of this length probably are formed from the interplay between tectonics, eustasy and sediment supply.

The Paleocene, early and middle Eocene periods have generally been interpreted to be an ice-free period (Galloway, 1989; Miall, 1997; Abreu and Anderson, 1998). Several measurement techniques have been used to calculate the magnitude of eustatic changes in order to explain the short term variations in the stratigraphy record. Some of these methods include: 1) amount and location of sedimentary onlap onto the continental margins (Haq et al. (1988), 2) thickness of marine sedimentary cycles, 3) lithospheric stress (Cloetingh, 1986), 4) numerical simulations (Kendall and Lerche, 1988), and 5) variations in deep-ocean oxygen

isotopes (Abreu and Anderson, 1998). These methods are a proxy to estimate eustatic sea-level changes (Kendall and Lerche, 1988).

There is little knowledge about the effect of eustasy in the Eocene stratigraphic record of the Maracaibo basin. Previous works are based on the Haq et al. (1988) sea level chart (Lugo, 1991; Pinto, 1991). The Haq et al. (1988) sea level chart is based mainly on seismic interpretation of onlap in several passive margin sedimentary basins of the world and its reliability is arguable. In this study, sea-level proxy curves based on deep-ocean oxygen isotopes by Abreu and Anderson (1998) and transgressive-regressive facies cycles by Hardenbol et al. (1998) were used to estimate eustatic changes (Fig. 4.21). These curves are compared with the Haq et al. (1988) curve in Fig. 4.21.

The isotope oxygen data gives the most reliable record for sea-level proxies. For ancient records sea level is inferred from variations in O^{18} and O^{16} isotopes from unaltered successions of calcite in deep ocean basins. When the ocean is enriched in O^{18} due to growth of large ice sheets the $\delta^{18}O$ is heavy, whereas when melting of ice sheets occurs then the $\delta^{18}O$ is light. Nonetheless, these variations can also occur in minor amounts by changing water temperature and salinity of the oceans (Abreu and Anderson, 1998; Lear et al., 2000). Amplitude changes in the isotope record during middle Eocene correspond roughly to changes in sea-level magnitude of ~25 to 55 m (~70 to 150 feet) (Abreu and Anderson, 1998). Even smaller amplitude variations are expected to be observed for the early Eocene that is representative of a greenhouse period (Abreu and Anderson, 1998) (Fig. 4.21).

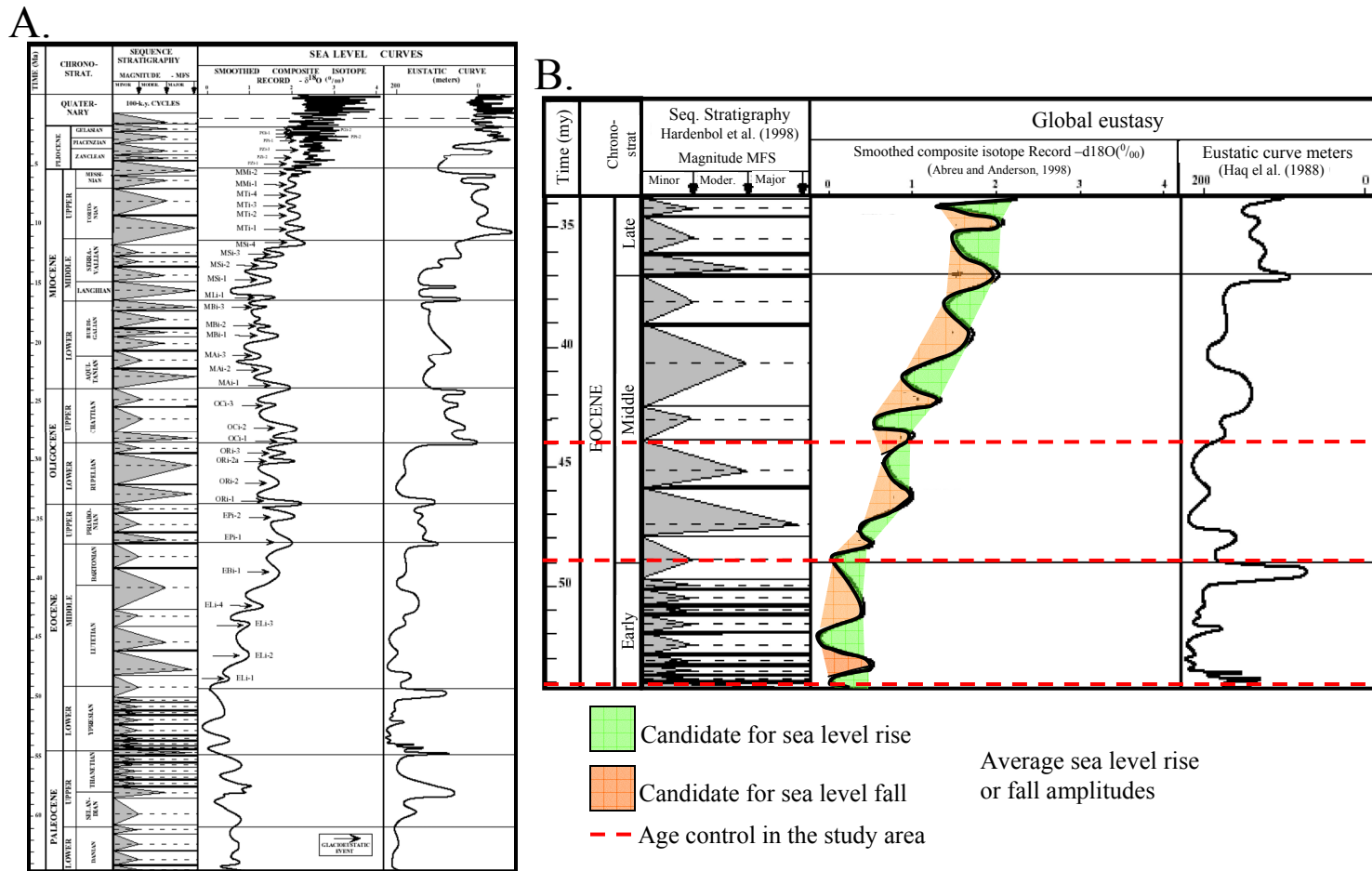


Figure 4.21. A) Composite sea level charts, including transgressive-regressive cycles of Hardenbol et al. (1998), composite oxygen isotope record of Abreu and Anderson (1998) and eustatic curve of Haq et al. (1988). (modified from Abreu and Anderson, 1998). B) Enlarged composite Eocene composite sea level charts from Fig. 4.21A.

The regressive-transgressive facies cycles of Hardenbol et al. (1998) is based on interpretation of facies stacking patterns and shelfal accommodation of European basins (compressional, extensional and passive margins), that are correlated in time using outcrop, well, core and seismic data. This method provides a qualitative indication of magnitude (minor, medium and major) of sea level changes controlled by tectono-eustatic effects, and gives an idea of stratigraphic architecture in other less studied basins.

For the Eocene, approximately 2 my duration cycles can be interpreted from the oxygen isotope record along with a general increase in O^{18} from the middle to late Eocene (Fig. 4.21). Candidates for maximum sea level fall, with amplitudes less than 55 m include: 53.5, 51, 48, 46, 44, 42, 39.5, 37 and 35 my. Candidates for maximum sea level rise, include: 54, 52.5, 49, 47, 45, 43, 41, 38, 36 and 34 my. These cycles show good correlation with the transgressive-regressive cycles of Hardenbol et al. (1998) during the middle and late Eocene, but the early Eocene, 0.5 to 1 my transgressive cycles are inferred. These higher frequency cycles probably indicate an increase in tectonic subsidence as proposed for the Eocene Maracaibo basin.

Major flooding events in the study area, interpreted from well cross sections and maps, assuming linear time scales between parasequences (Figs. 4.8 to 4.10), occur: 52, 50, 48.5, 47.6, and 46.5 my. Major progradational sets occur: 52.5, 50.8, 49, 47 and <44 (sequence 6) my. No correlation is obtained between events observed in the study area and the Abreu and Anderson (1998) or the Hardenbol et al. (1998) charts in Figure 4.21. Possible reason for this lack of

correlation are: 1) relative rise and fall of sea level were dominated by other regime variables (subsidence or sediment supply), 2) changes were the result of the combination between the three regime variables at any stratigraphic scale, and 3) ages assigned to events are poorly constraint in the study area.

4.6.2 Sediment supply

The rate of sediment supply controls the amount and location of accommodation space filling. Fluvial systems represent the major transporting mechanism from continents to basins. Other mechanisms of sediment redistribution to the basin include marine currents which can transport sediments for long distances along continental margins (Warne et al., 1999). Variations in climate, physiography, and basin configuration can considerably change rates of sediment supply to the basin in any time interval (Schumm, 1977; Galloway, 1996). The sediment variable is usually considered to be constant in sequence stratigraphic analysis, but it plays an important role in basin architecture and it is comparable with eustasy and subsidence in importance (Galloway, 1989). The amount of sediment discharge through time is usually unknown in ancient drainage systems.

Provenance study by Lugo (1991) in the Maracaibo basin indicated a southern cratonic source of sediments during the early-middle Eocene. Kasper and Larue (1986), Díaz de Gamero (1996), Driscoll and Diebold (1999) and Villamil (1999) have all proposed that the location of the north-flowing paleo-Orinoco River was located in the western Maracaibo basin during the Eocene, and

that the paleo-river progressively shifted eastward to its present position in northeastern South America.

Possibly significant amounts of clastic sediment supply from the proto-Orinoco river during the Eocene have not been recognized. Driscoll and Diebold (1999) have proposed that the 14-km-thick depocenter located in the Southern Caribbean deformed belt is filled with a large amount of Eocene sedimentary rock derived from the proto-Orinoco. Thick Eocene sedimentary rocks (>4 km) were recorded in the Maracaibo basin. Regional paleogeographic maps by Villamil (1999) show N-S oriented depocenters from southern Colombia to western Venezuela. These depocenters were fed by the Guyana shield to the east and south, and by uplift of the Colombian Andes to the west. A large paleodrainage system with high rates of denudation seems to have existed through the Eocene. A possible estimate of sediment supply can be given by present-day rates for the Orinoco River. The river is one of the largest drainage basins in the world with an estimate of 150 to 212 millions tons/yr of sediment discharge (Warne et al., 1999).

4.6.3 Subsidence

The main objective of back stripping analysis is to calculate tectonic subsidence by removing the effects of sediment loading, compaction, and eustasy. These methods will reveal the tectonic mechanism that controls basin subsidence (Miall, 1997). Determination of the type of tectonic activity and timing are important in defining the evolution of the basin and its infilling.

Figure 4.22 shows subsidence plots in the Maracaibo basin constructed by Lugo (1991). These plots show an increase in subsidence rates during the Eocene for the northern and northeastern parts of the Maracaibo basin. Calculated subsidence rates in the study area for the Eocene are: 55 m/my (~200 feet/my) between 54 and 48 my, and 95 m/my (~300 feet/my) between 48 and 40 my. From 40 to 25 my, uplift occurred with an equivalent magnitude to the amount of previous foreland related subsidence. Uplift explains the loss of ~20 my missing sedimentary record at the Eocene unconformity in the study area.

The Maracaibo basin was formed as a foreland basin during the Eocene during oblique collision between the Caribbean and South American plates (Lugo and Mann, 1995; Chapter 2). As revealed by subsidence plots (Lugo, 1991; Fig. 4.22), outcrop (Mathieu, 1989), and seismic lines (Escalona and Mann, 2003a), the major depocenter during this time developed in the northwestern area of the basin. Therefore, the Eocene sequence is classified as a tectonosequence, where subsidence was controlled by plate tectonic interaction. Subsidence history during the Eocene Maracaibo shelf can be summarized as follows (Fig. 4.23):

1. **LATE PALEOCENE ~ 60 MY** (Fig. 4.23A): The Maracaibo basin was a passive margin that underwent tectonic loading from the north-northwest as the Caribbean plate approached western Venezuela. The shelf edge was located along the Burro Negro fault (Chapter 2) and subsidence rates increased along this depositional structural boundary (Fig. 4.22; wells C, D and F).

2. **EARLY EOCENE ~54 MY** (Fig. 4.23B): Tectonic loading continued from the north, inducing higher subsidence rates on most of the shelf (Fig. 4.22,

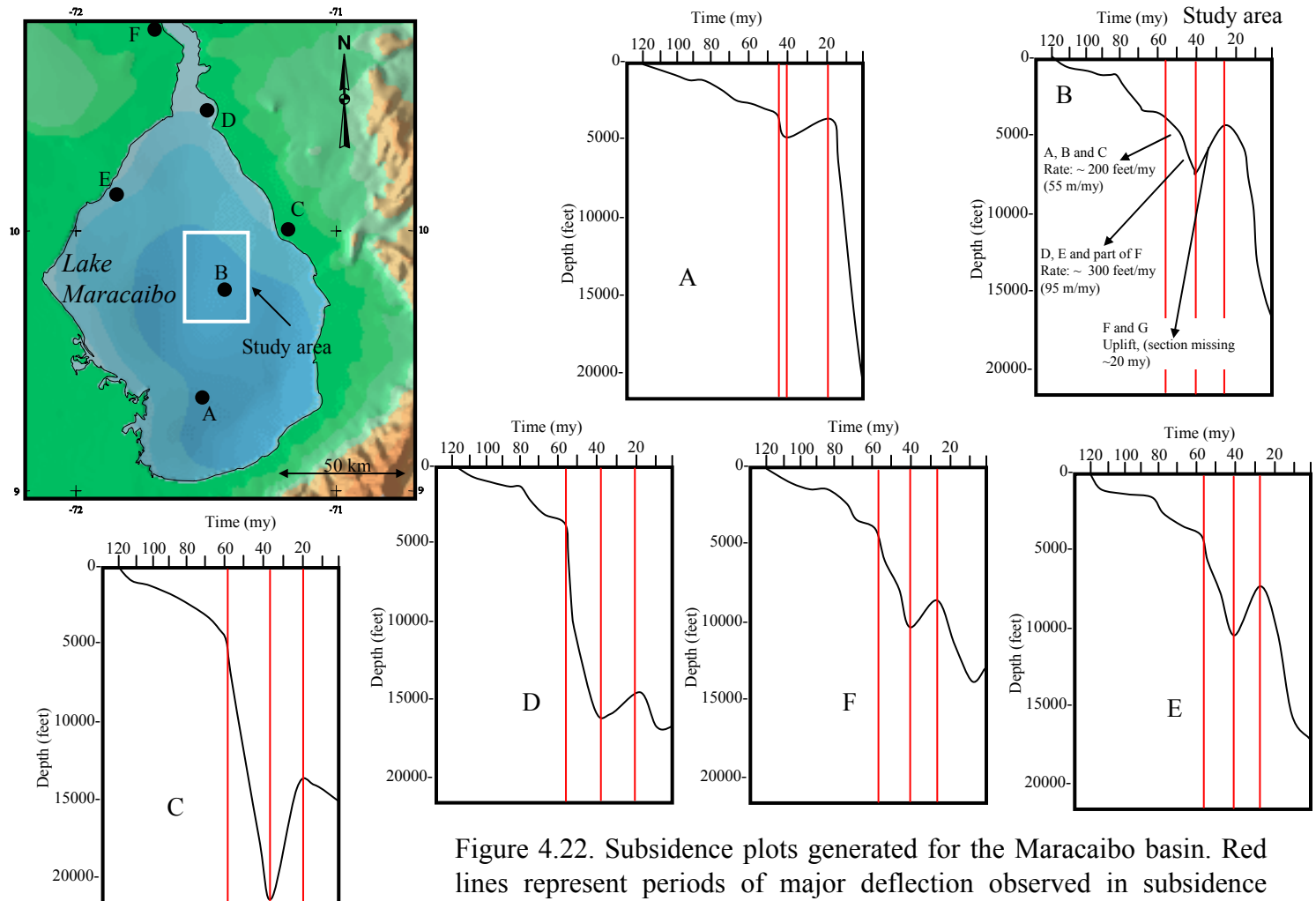


Figure 4.22. Subsidence plots generated for the Maracaibo basin. Red lines represent periods of major deflection observed in subsidence curves during the Paleogene (modified from Lugo, 1991).

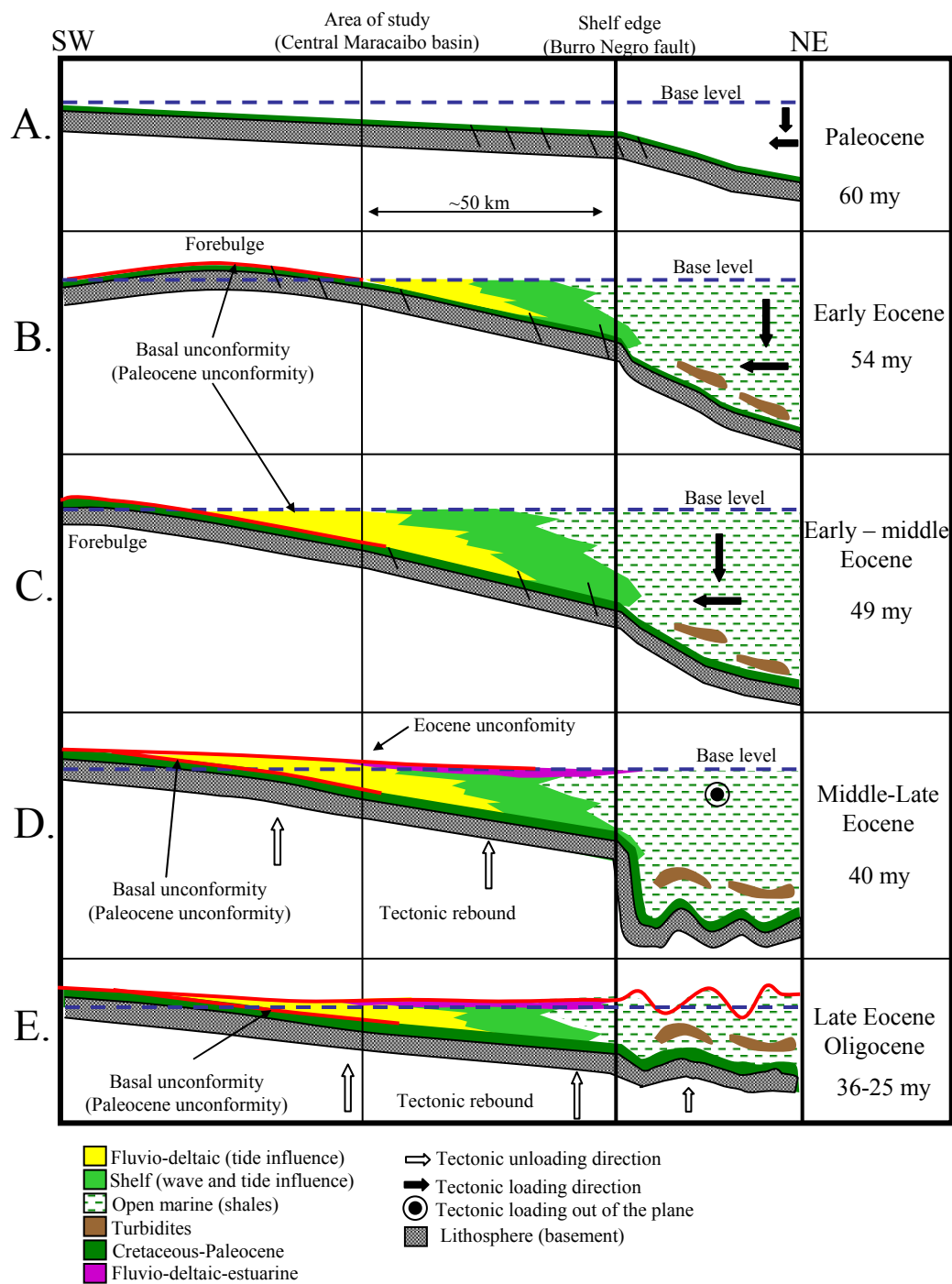


Figure 4.23. Subsidence evolution of the Maracaibo basin during the Paleogene and its effect on stratigraphic architecture.

well B). Flexural loading induced the formation of a forebulge to the south (Chapter 2). The Paleocene platform was exposed forming the Paleocene unconformity (SB1). Clastic input began to infill the basin in large amounts and turbidites were deposited in the deep Maracaibo basin northeast of the Burro Negro fault (Trujillo Formation, Mathieu, 1989).

3. **EARLY-MIDDLE EOCENE ~49 MY** (Fig. 4.23C): Tectonic loading reached its climax with an increase in subsidence rates for the entire basin (up to 65 m/my on the shelf and more than 150 m/my in the main depocenter; Fig. 4.22). Progressive migration of the forebulge southward occurred and clastic sediments onlap the Paleocene unconformity. High rates of subsidence induced retrogradation of the Eocene tectonosequence. The forebulge was uplifted and is estimated to have been 20 to 40 times smaller in magnitude than the subsidence of the basin, depending on thickness, density, continuity of the lithosphere, and tectonic loading (Crampton and Allen, 1995). For the Maracaibo basin a maximum of 10 m/my uplift represents a good estimate for the Eocene forebulge, considering subsidence rates of ~150 m/my in the main depocenter.

4. **MIDDLE-LATE EOCENE ~40 MY** (Fig. 4.23D): Tectonic loading moved eastward (Chapter 2). The lithosphere responded by tectonic rebound characterized by uplift rates of 60 m/my (~200 feet/my). Rebound affected the entire Eocene Maracaibo shelf (Fig. 4.22). Formation of the Eocene unconformity was induced by the tectonic rebound, and generated higher rates of erosion to the south (forebulge).

5. *LATE EOCENE-OLIGOCENE ~35-25 MY* (Fig. 4.23E): By this time period the entire basin was subaerially exposed (Chapters 2 and 3), and erosion cannibalized a large amount of sediments (more than 30% to the south, Figs. 4.9 and 4.10).

Generally, the Eocene tectonosequence is driven by tectonic subsidence, and formation of bounding unconformities. Migration of the forebulge and changes in tectonic loading in the main basin depocenter through time controlled the asymmetric wedge shape of the basin.

4.7 COMPARISON WITH OTHER AREAS OF THE MARACAIBO BASIN

Previous sequence stratigraphic analysis of the Maracaibo basin are based either on regional tectonosequence evolution (Audemard, 1991; Lugo and Mann, 1995; Parnaud et al., 1995b), or focused on detailed, reservoir-scale studies (Maguregui, 1990; Ambrose and Ferrer, 1997; Raeuchle et al., 1997; Hamilton et al., 1998). There are few published studies on the age of stratigraphic units. Instead, units are correlated using the standard lithostratigraphic system (i.e., CX sands and BX sands; González de Juana, 1980). Regional sequence stratigraphic interpretation of units by age and surfaces that integrate most of the wells in the Maracaibo basin remains to be done. Information, integration, and interpretation are needed in order to build a consistent and predictable stratigraphic model, which allows a better understanding of the evolution of the Maracaibo basin, and the distribution of its reservoirs.

Figure 4.24 shows a comparison of two parasequence sets sand isopach maps in the study area with equivalent units interpreted by Ambrose et al. (1995) (Fig. 4.24A) and Maguregui (1990) (Fig. 4.24B). Age of parasequence sets in the study area is subject to linear interpolation using few palynology markers. Lateral time correlation with other areas is based on the vertical location within the stratigraphic column and because no age control is available for these interpretations. Furthermore, Maguregui (1990) and Ambrose et al. (1995) based their stratigraphic framework on continuous shale markers that were inferred to represent regional flooding surfaces. They proposed tide-dominated depositional systems, whose main lithofacies include distributary channels, tidal sand bars, tidal channels, and shelf assemblages.

Set G (~49 my, genetic sequence 2) is compared with the upper C4X sandstones of Ambrose et al. (1995) located 15 km north of the study area (Fig. 4.24A). Similar sandstone thickness is interpreted from both areas and a NE-depositional trend is observed, suggesting the same depositional pattern toward the deep basin in both systems. The area studied by Ambrose et al. (1995) seems to be continuous and fed by a system located to the southwest of the study area. This is indicative of a more complex tide dominated deltaic network in the Maracaibo shelf, as proposed by Maguregui (1990).

Sequence 6 (set R, < 44 my) is correlated with interval A of Maguregui (1990). Interval A is a possible sub-unit of set R, located a few km NE of the study area (Fig. 4.24B). Sequence 6 was not subdivided in the study area because of its thickness. Its blocky-coarsening upward amalgamated character (probably

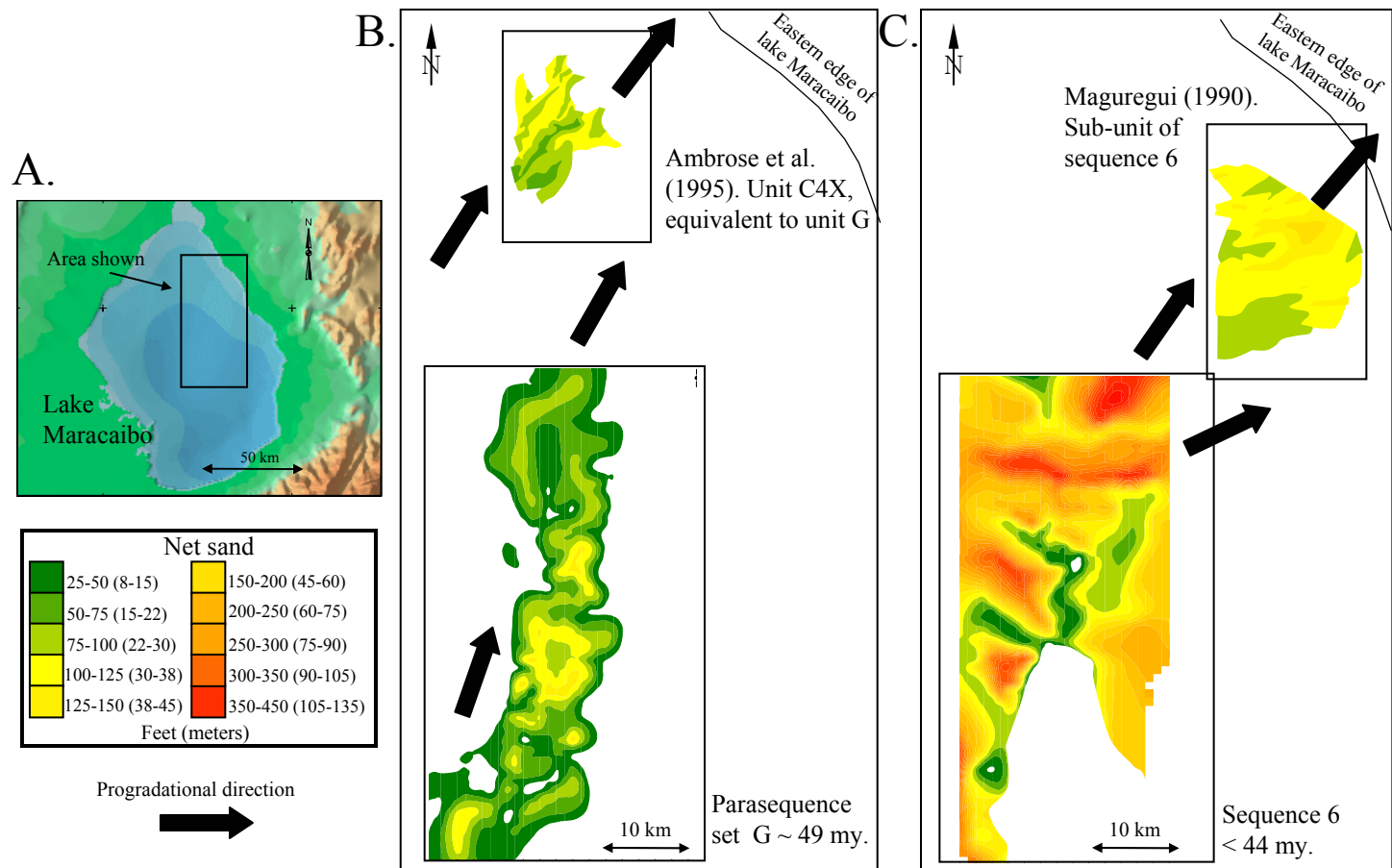


Figure 4.24. A) Comparison of parasequence set units in the area of study with other studies in Lake Maracaibo. B) Net sand map of parasequence set G compared with equivalent unit C4X mapped by Ambrose et al. (1995). C) Net sand map of sequence 6 compared with sub-unit A of Maguregui (1990)

related to bed load fluvial systems) makes it difficult to subdivide in subunits. A similar NE trend can be interpreted for sandstones of sequence 6 in the northeast part of study area and the sandstones interpreted by Maguregui (1990). Fluvial facies in the study area pass laterally into deltaic systems to the NE, interpreted by Maguregui (1990) as intervals A to G (BX sands).

4.8 ORINOCO DELTA ANALOG (EASTERN VENEZUELA)

The Orinoco delta is located in eastern Venezuela and represents a triangular to trapezoidal depocenter of approximately 22,000 km² (Figs. 4.25A and B). At a regional scale, the delta is located in a foreland setting (Eastern Venezuela Basin, Di Croce et al., 1999), with the Serranía del Interior and Trinidad to the north and the Guayana shield to the south (Fig. 4.25A). Tectonic transpression is controlling the region and it is related to the collision between the Caribbean and South America plates. To the NW, transpressional structures are interpreted trending NW and NE (Warne et al., 1999).

The fluvial network of the delta comprises six major distributaries radiating from the apex to the coast, and comprises a suite of depositional environments including: distributaries, swamps and marshes, and tidal channels (Figs. 4.25C and D). Distributary channels tend to be straight and widening to the coast in a funnel shape (Figs. 4.25B, C and D). Tidal fluctuations are mesotidal and affect the main distributary channel up to 100 km upstream. Wave energy is

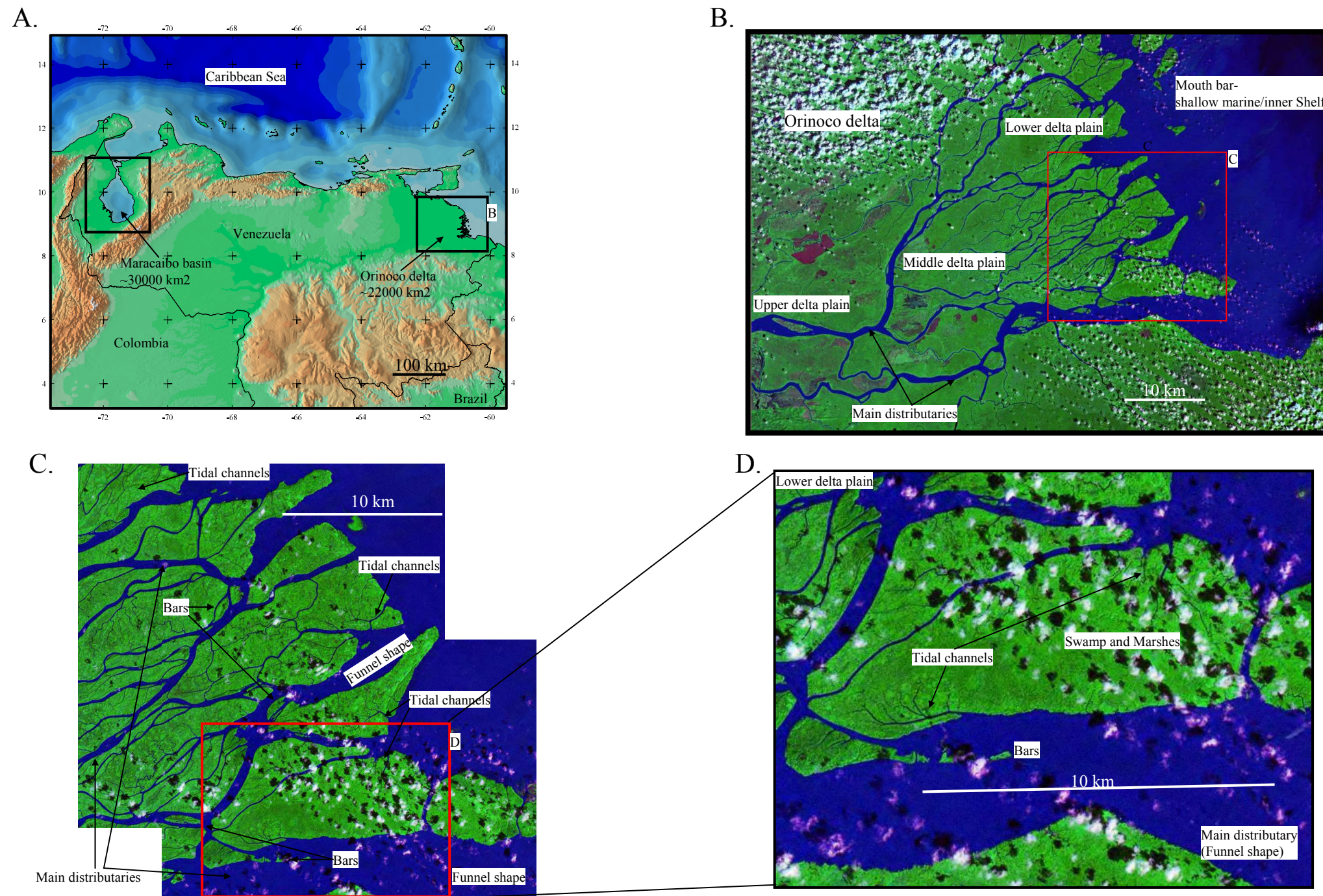


Figure 4.25. Orinoco delta physiography: A) Location of the Orinoco delta with respect to the Maracaibo basin; B) Orinoco delta, major distributaries, and sub-zones distribution; C) Main depositional systems and geometries of an area of the Orinoco delta; and D) Funnel shape and main depositional system in the main distributary channel. Source of satellite images: Nasa at <http://zulu.ssc.nasa.gov/mrsid/>.

minimal because of the wide, shallow water Orinoco shelf (~100 km wide and maximum 100 m deep) (Warne et al., 1999).

The Orinoco delta represents an excellent analog for the fluvial-deltaic system interpreted in the Maracaibo basin during the Eocene because of its scale, and structural and stratigraphic setting (Fig. 4.25A). Understanding the configuration of the different depositional systems in this modern deltaic system is a key for interpreting and understanding the geometries, scales and processes that formed ancient systems in the Maracaibo basin. The Eocene of the Maracaibo basin is interpreted to have a broad shallow shelf (>100 km; Maguregui, 1990; Chapter 2) with tidal and fluvial influence. These characteristics are also observed in the modern Orinoco delta.

The geometries and distribution of facies in the Maracaibo basin were compared with those in the Orinoco delta. The study area represents a small area of the Eocene Maracaibo shelf (Figs. 4.26 A, B and C). Main observations that reflect the four principal depositional systems of the Orinoco delta with the parasequence sets of the study area include (Fig. 4.26C):

- Set A resembles a fluvial-dominated channel system of the upper Orinoco delta, where the main distributary is straight with crevasse splays and levees. Cross-stratification is a common feature.
- Set D shows similar geometry of distributary channels located in the middle delta plain, where processes have marine influence. The main distributary channel splits in several channels, where channels are more sinuous and becoming

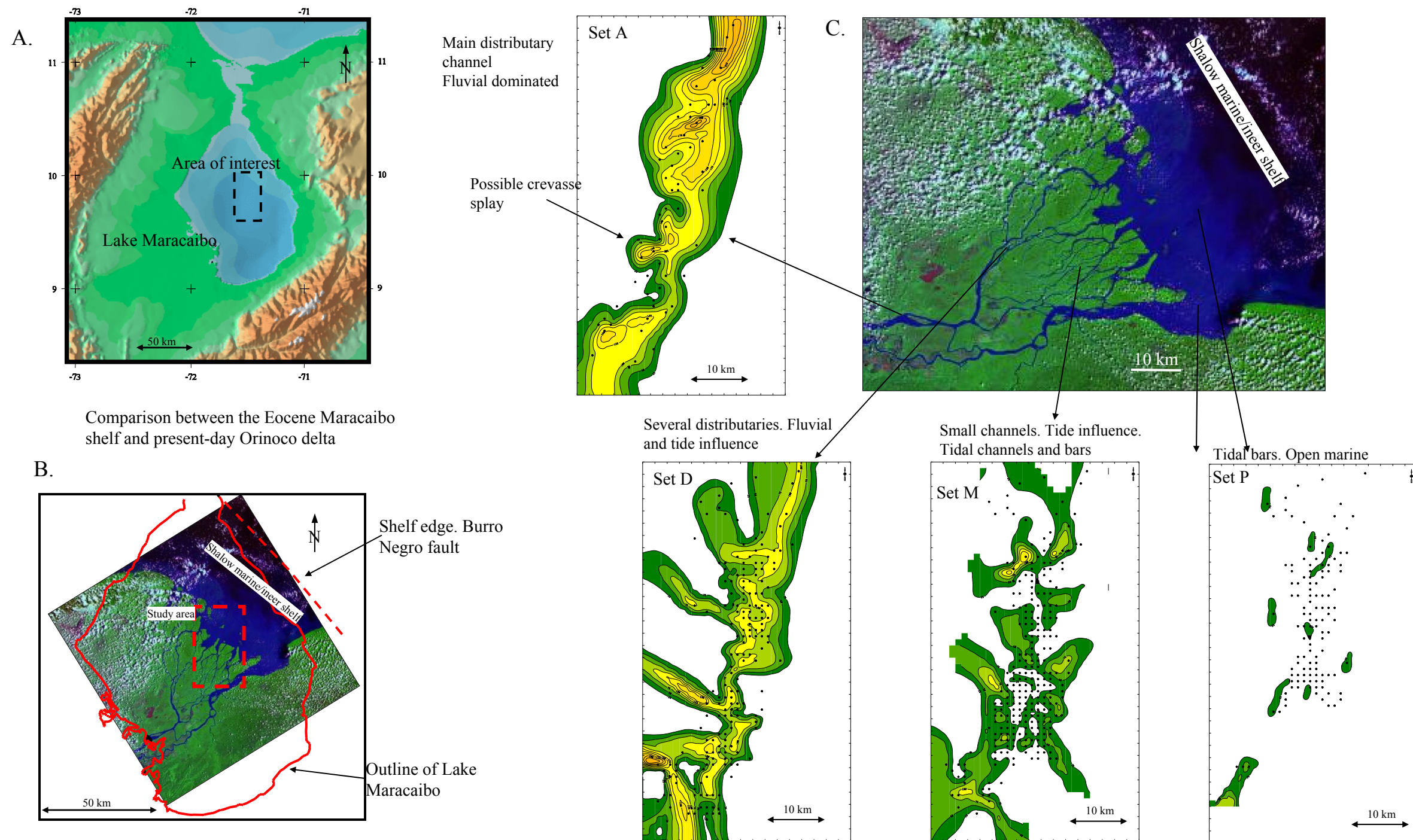


Figure 4.26. Comparison of depositional systems of the Orinoco delta with depositional systems interpreted in the study area. Source of satellite images: Nasa at <http://zulu.ssc.nasa.gov/mrsid/>.

again less sinuous closer to the coast. Tidal channels and sand bars islands are evident and are surrounded by swamps (Fig. 4.25C and 4.26C).

The lower delta plain of the Orinoco delta is controlled by tides, but also by fluvial processes. Peat is a common feature and swamps and marshes are cut by a complex network of tidal channels. Large, dip-elongated tidal sand bars are observed along the main distributaries characterized by a funnel shape due to tide influence (Warne et al., 1999). Set M shows similar geometries to this system, suggesting tidal sand bars and tidal channels as main facies, with small sand-to-shale ratios. Bars are oriented to the NE, which is inferred to be the main depositional dip for the Maracaibo basin (Fig. 3.25D and 4.26C).

- Low sand to shale ratio is typical of the nearshore and inner shelf of the Orinoco delta, and coasts are basically mud-flat and mangrove swamps. Also, distributaries mouth bars widen due to tidal and marine influence. Parasequence set P seems to resemble the mouth bar to outer shelf transition, where open marine processes rework most sand from the mouth bar to the basin (4.26C).

- Tide influence is observed from shelf to the middle-upper delta plain, up to ~100 km upstream in the Orinoco delta. Tide influence in the Maracaibo basin is interpreted for most of the Eocene facies suggesting a similar range of influence. Sediment dispersal processes, facies, and geometries in the Eocene of the Maracaibo basin shelf needs regional mapping of parasequences, in order to have a better comparison model with modern analogs, and to have a complete understanding of the entire system from source to deep basin.

4.9 SUMMARY AND DISCUSSION: INTEGRATED EVOLUTION OF THE STUDY AREA

The stratigraphic evolution of the Maracaibo basin during the Eocene is controlled by the oblique collision between the Caribbean plate and passive margin of South America in western Venezuela, and to a much lesser degree by sediment supply and eustasy. The general retrogradational pattern interpreted from well data (Figs. 4.9 to 4.12) and from analysis of subsidence plots (Lugo, 1991; Fig. 4.22) leads to the conclusion that subsidence controls the long term relative sea level change. Changes in the stratigraphy was characterized by increasing accommodation space between 55-95 m/my (~200 to 280 feet/my) during the early Eocene and most of the middle Eocene, and by decreasing accommodation space at similar subsidence rates during the late Eocene and Oligocene (Fig. 4.22).

High frequency cycles, including genetic sequences and parasequence sets, seem to be controlled by a combination of eustasy and sediment supply. However, small changes in the oxygen isotope record (Abreu and Anderson, 1998) and the lack of major continental ice caps during the early-middle Eocene greenhouse period suggest that eustasy played a minor role in high frequency cycles observed in the Maracaibo basin. Lateral and vertical continuity of facies associations in the study area does not indicate any major erosional surfaces within the genetic sequences. This observation is supportive of the idea that the Eocene Maracaibo shelf was never subaerially exposed and also supports my inference that rates of sea level fall were smaller than subsidence rates (i.e., less than 55m/my; Abreu and Anderson, 1998). There is no good correlation between

major sea level falls shown in the sea-level charts (Hardenbol et al.; 1998) and the age of Eocene progradational units in the Maracaibo basin.

Instead, sediment supply seems to have had a strong influence over the observed high frequency cycles. The area of western South America was an active tectonic margin during the Eocene and it is likely that tectonics was an important control on morphology, paleodrainage and sediment supply. Climate control has also played a major role on sediment discharge as it does in other subtropical regions like the Orinoco delta (Villamil, 1999; Warne et al, 1999). Another possible cause of high frequency sea level fluctuations was intraplate stresses related to tectonic loading as proposed by Cloetingh (1986). Cloetingh (1986) proposes that fluctuations of relative sea level can be in the order of 10 m cause by sediment loading and thermal contraction on passive margin, or greater than 50 m cause by active tectonic plate boundaries on a million year cycles.

Figure 4.27 A to G summarizes the stratigraphic evolution of the study area, as interpreted from the 3-D pseudo-seismic data, seismic data and analysis of regime variables. Aggradational and progradational units composed of distributary channels and deltas characterize the lower Eocene (Figs 4.27A and B). These systems are the product of slight shallowing of the Eocene Maracaibo basin shelf and formation of a forebulge to the south. Tides and fluvial processes are dominant, and tidal influence is enhanced by the shallow, broad shelf. A succession of regressive-transgressive cycles with a general retrogradational pattern is characteristic of most of the middle Eocene (Figs. 4.27 C to E). Few, highly prograding units are observed (sets M and N, Fig. 4.27D) and were formed

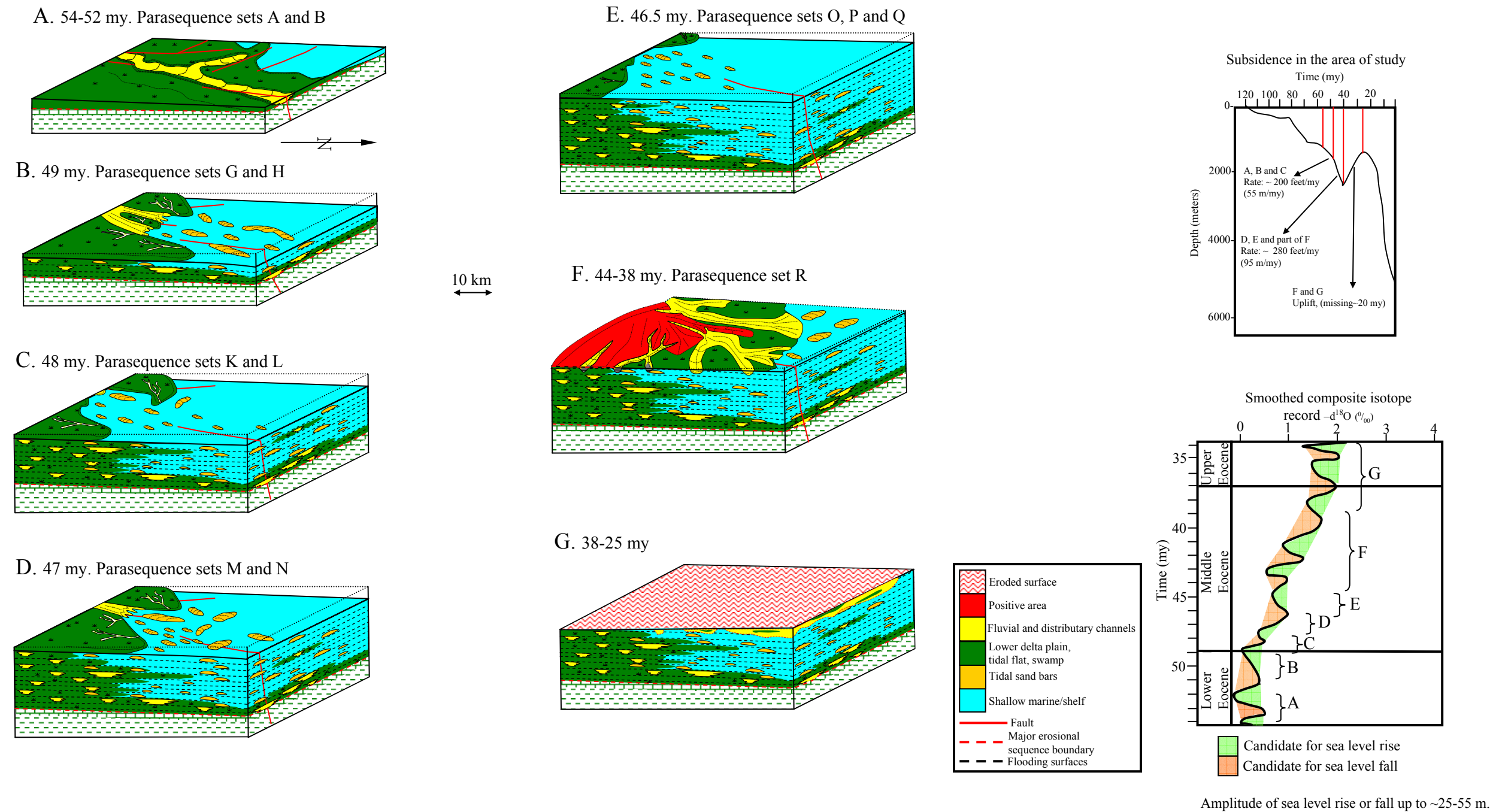


Figure 4.27. Evolution of the study area from the Eocene to the Oligocene. Interplay among subsidence (modified from Lugo, 1991) and eustatic sea level history (modified from Abreu and Anderson, 1998).

by a possible regional increase in sediment supply. A long term transgression induced by tectonics produced back-stepping of the forebulge and continental facies (Fig. 4.23B and C), contributing to an increase in marine influence and tidal energy in the shallow Eocene Maracaibo shelf.

By the end of the middle Eocene (~40 my), tectonic loading ceased, and lithospheric rebound affected the basin. Rebound produced migration of the shoreline to the northeast and incision of the upper part of older Eocene units in a complex network of fluvial systems (Figs. 23D and 4.27F). The deltaic system migrated to the northeast near the shelf edge (study area of Maguregui, 1990, Fig. 4.24B). In this shelf edge setting eustasy and sediment supply played a major role in controlling high frequency cycles of the basin. During the late Eocene and Oligocene periods, most of the Maracaibo shelf was exposed by a combination of tectonic rebound (Fig. 4.22) and higher amplitudes of sea level fall due to increase in volume of continental ice caps (Abreu and Anderson, 1998) (Fig. 4.27G).

Active faulting during the Eocene controlled the orientation of main distributary channels and localized intra-shelf depocenters like the Icotea pull-apart basin (Chapter 2). Thickening of genetic sequence 1, and sequence 6 toward the west suggest that the Icotea pull-apart basin was mostly filled during these periods of deposition (Figs. 4.10, 4.13 4.20).

4.10 CONCLUSIONS

Sequence stratigraphic interpretation of a representative area of the Maracaibo Eocene foreland basin using an integrated methodology including a

dense well data base, core, 3-D seismic, previous works and modern depositional system analogs yields to the following conclusions:

- The stratigraphic architecture of the Maracaibo basin during the Eocene was controlled by tectonic subsidence and to a lesser degree by sediment supply. Eustasy does not play an important role during the early Eocene and for most of the middle Eocene.

- Continuous shale markers and stacking patterns were used to interpret five genetic sequences. These genetic sequences were subdivided into seventeen parasequence sets throughout the whole area. A sequence bounded by erosional surfaces was interpreted within the Eocene tectonosequence, at the upper section of the interval.

- The lack of sequence boundaries reveals that the Eocene Maracaibo shelf was not subaerially exposed during the early and middle Eocene. Instead, this period was dominated by a long term retrogradational stacking patterns.

- The area is interpreted as a transitional environment from delta plain to shelf, where fluvial and tidal processes dominate facies architecture. Main facies interpreted include: distributary channels, crevasse splays, tidal bars and shallow marine facies. Sediments were transported from S-SW to the NNE

- The vertical stratigraphic succession is characterized by an aggradational package, followed by regressive-transgressive cycles in a retrogradational trend, and ending with the Eocene unconformity. Associated with the Eocene unconformity an aggradational cycle, suggest a shift of the shoreline to the NE, of an exposed platform to the south.

- The application of the 3-D pseudo-seismic transform technique resulted in an excellent visualization and interpretation methodology when working with a dense well database. The technique improved lateral and vertical correlations, allowed better understanding of the stratigraphy of the area, and provided more reliable 3-D geological interpretations.

- Comparison of facies architecture with modern depositional environments aids understanding ancient systems.

CHAPTER 5

Reservoir properties

5.1 INTRODUCTION

Understanding reservoir architecture is fundamental for optimizing hydrocarbon production. Eocene elastic rocks of the Maracaibo basin contain one of the most prolific reservoirs in the world for light and medium oil. These Eocene reservoirs are characterized by complex stratigraphic and structural compartments.

Structural traps are controlled by a variety of features, including normal faults, inverted faults on the flexed continental plate (Harding and Tuminas, 1989, Chapters 2 and 3), folds within the foreland basin itself, and strike-slip faults forming N-S anticlines (Chapter 3). All trap types were charged with hydrocarbons from underlying Cretaceous source rocks (Zambrano et al., 1971; González de Juana et al., 1980). Stratigraphic traps are found in heterogeneous, mixed fluvial and tidal-dominated deltaic systems defining regressive-transgressive cycles on the Eocene Maracaibo shelf (Maguregui, 1990; Ambrose et al., 1995; Chapter 4). Major reservoir facies are stacked distributary channels and tidal bars with lateral variability depending on the stratigraphic unit to which they belong (Chapter 4).

Reservoirs in central Lake Maracaibo have been producing since the late 1960's. More than 1.5 billion barrels of medium oil have been produced from the

Eocene interval. Current production from the Eocene reservoirs is about ~50,000 barrels a day with a recovery factor of less than 30% (PDVSA E&P Occidente and Veba Oil, 1998). More than 400 wells produce from the Eocene in central Lake Maracaibo where well spacing is a minimum 600 m radius by government regulations. Prediction of reservoir facies, their connectivity and petrophysical properties in the interwell areas are very unreliable. As a result, it becomes difficult to define new development areas solely from well control, and the success of offset wells and recovery projects is not as high as expected.

Three dimensional seismic data in the study area have been used to continuously depict the structural framework. Stratigraphic interpretations have been difficult because of the low vertical resolution of the seismic data (~40 m, ~120 feet; Gil and Trautnitz, 1995). Seismic amplitude interpretations seem to show correlation between stratigraphic attributes and seismic response. León (1997) and Escalona and MacDonalds (1998) found that crossplots of Eocene sandstone units show a direct relationship between reflection amplitude and net oil sandstone thickness and porosity for thin beds. International Reservoir Technologies, Inc. (1997) also identified a tentative seismic amplitude correlation with net sandstone thicknesses for thin beds.

To gain a better understanding of the reservoir architecture, the aim of this study is to provide an overview of the distribution of Eocene reservoirs in the central Lake Maracaibo area and to determine if correlations between seismic amplitudes and petrophysical properties exist. The objective is to determine if the spatial continuity of the 3-D seismic data can be used in combination with the

vertical resolution of the well data to predict reservoir properties in interwell areas, mainly in thin layered and unexplored reservoirs. This analysis is based upon the high resolution stratigraphic framework built in Chapter 4, which used more than 300 wells, covering most of the study area.

5.2 COMMENTS ON PETROLEUM SYSTEMS

Figure 5.1 shows the distribution of hydrocarbons reservoirs in the Maracaibo basin (Zambrano et al. 1971). Most reservoirs are located along and between the Icotea and Pueblo Viejo faults south of the Burro Negro fault zone. Distribution of the source rocks, migration paths and trapping of hydrocarbons in the basin are the result of the structural and stratigraphic evolution of the basin. Hydrocarbon reservoirs are Cretaceous, Eocene and Miocene in age.

Figure 5.2 is a transverse E-W interpreted seismic line in the central Maracaibo basin showing the main features of the petroleum system from Cretaceous source rock to Eocene and Miocene reservoirs.

SOURCE ROCKS: Hydrocarbon source rocks in the Maracaibo basin are Cretaceous carbonates of the La Luna Formation (Albian-Coniacian) and, in lesser amount, Eocene and Miocene shales (Zambrano et al., 1971; Young et al., 1977). Hydrocarbon generation most likely occurred during the Paleogene, when Cretaceous rocks were deeply buried and reached the thermal maturation window (Zambrano et al., 1971; G3nzales de Juana et al., 1980) (see subsidence plots in Fig. 4.22). Tectonic Miocene inversion of the Maracaibo basin deeply buried Eocene and Miocene rocks to the southern part of the basin (Maracaibo syncline,

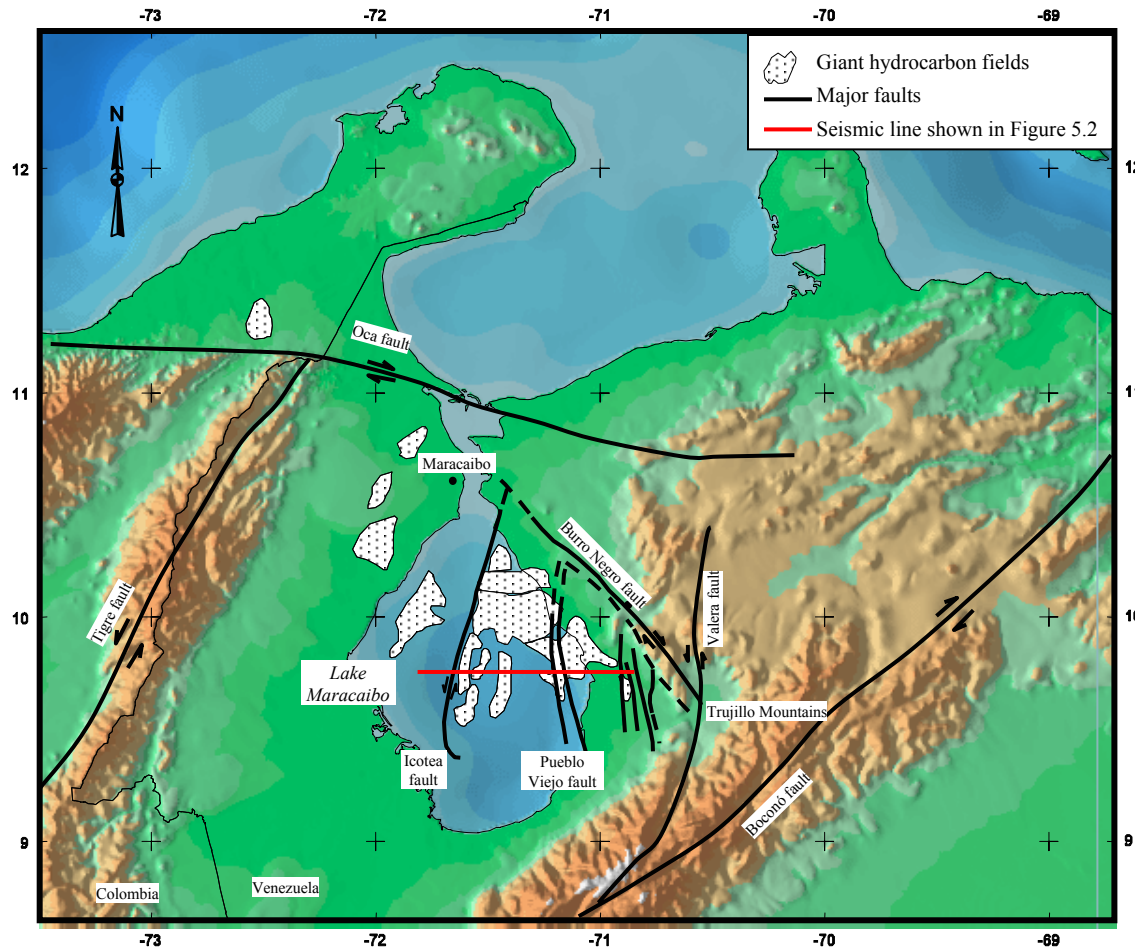


Figure 5.1. Giant hydrocarbon oil fields in the Maracaibo basin and major faults. Most oil fields are located along major strike-slip faults (i.e. Icoitea and Pueblo Viejo faults; modified from Zambrano et al. 1971). The seismic line corresponds to a transverse line in the central Maracaibo basin discussed in chapter 2.

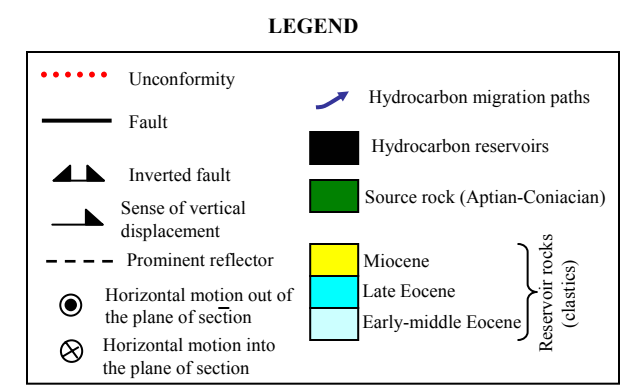
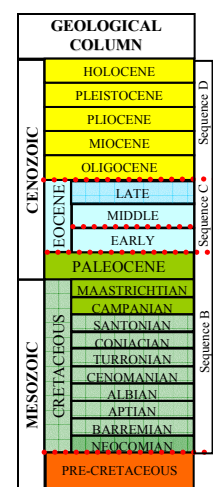
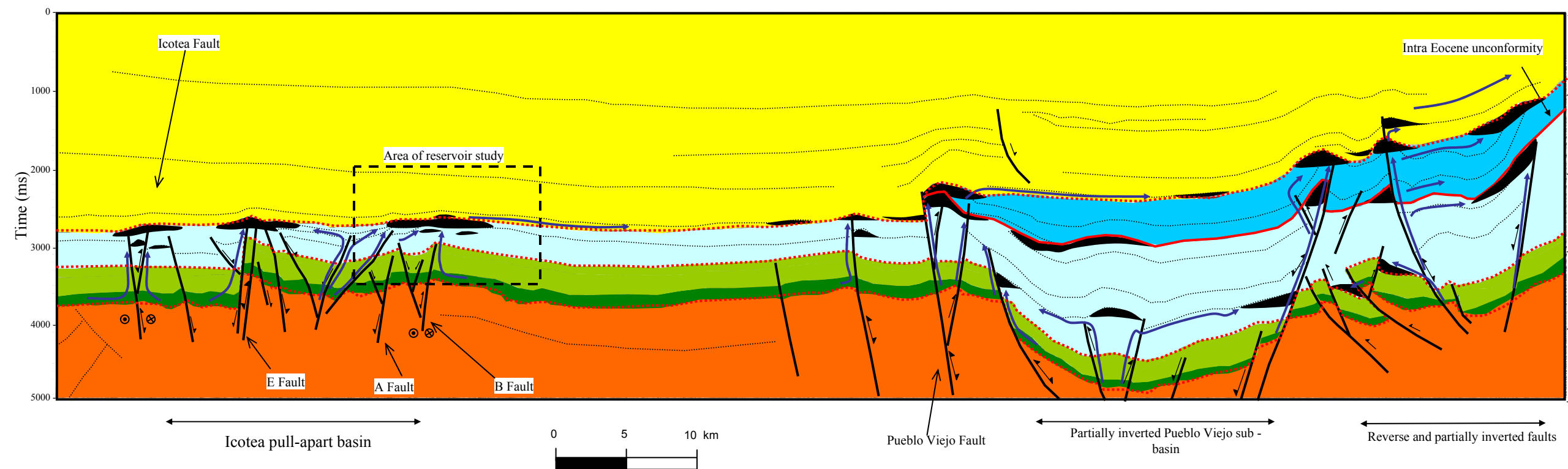


Figure 5.2. Profile derived from interpreted E-W seismic line in Figure 3.6. The section shows the main structural and stratigraphic features of the Maracaibo Basin and its petroleum system (see Fig. 5.1 for location). Migration paths from source to reservoir are localized along major faults in the basin (e.g. Icoatea fault, Pueblo Viejo, A, B and E faults). Hydrocarbon reservoirs are mostly located in structural highs beneath the Eocene unconformity, and in the Miocene along the north and eastern flanks of the Maracaibo syncline.

Castillo, 2001) creating an alternative post-Eocene period for hydrocarbon generation on Eocene and Miocene shales (Gonzales de Juana et al., 1980).

MIGRATION AND TRAPPING: Hydrocarbon migration and trapping occurred at least in two main phases:

Paleogene oblique collision between the Caribbean and South American plates (Chapters 2 and 3): During this period an asymmetric wedge of fluvial-deltaic Eocene rocks was deposited in a foreland basin. Pull-apart basins controlled by reactivated Jurassic N-S trending faults within the Maracaibo basin were formed (e.g., Icotea and Pueblo Viejo sub-basins). These faults served as vertical pathways for hydrocarbon migration from the Cretaceous source rocks to Eocene reservoirs (Boesi, 1978; Fig. 5.2). Also, vertical displacement of major faults allowed lateral contact between Cretaceous source rocks and Eocene reservoir rocks, contributing to increase hydrocarbon migration (Fig. 5.2).

Hydrocarbon traps are associated with anticlines formed during creation of the pull-apart basins structures beneath the Eocene unconformity and compartmentalized by NW-SE striking faults (Chapter 2 and 3). Regional N-NE dip of the basin also contributed to oil migration updip to better quality fluvial and deltaic reservoir facies (Chapter 4) and trapping against the Eocene unconformity in the central Maracaibo basin (Figs. 2.6, 4.9 and 4.12).

Post Eocene inversion: This phase of basin development was characterized by uplift of the Sierra de Perijá and the Mérida Andes, formation of the N-S Maracaibo syncline (Castillo, 2001), and inversion of Eocene structures in the central basin. Hydrocarbon migration occurred along fault zones at the Eocene

unconformity, or where post-Eocene reservoir rocks are in contact with Eocene reservoirs, allowing updip migration to Miocene reservoirs. In contrast to the Eocene, the Miocene depocenter was located to the south of the Maracaibo basin and continental facies pinch out to the NE, forming a major stratigraphic trap (Figs. 2.6 and 5.2). Hydrocarbons are mainly trapped in a few inverted structures (Fig. 5.2) and stratigraphic wedges out to the NE (Figs. 2.6 and 5.2) or escaped to the surface, forming seeps to the east and west of the Maracaibo syncline (Zambrano et al., 1971; G3nzales de Juana et al., 1980; Fig. 5.2).

5.3 MAIN RESERVOIRS IN CENTRAL LAKE MARACAIBO

Hydrocarbon in the Eocene reservoirs in the study area has API gravity between 20 and 30, and is classified as medium oil. The reservoirs are located on structural highs and in parasequence sets with high sandstone content. The structural highs were formed by strike-slip and inversion of N-NE-striking normal faults. NNW-SSE normal faults separate the anticline in different blocks, with the lowest structure located in the central part of the study area (Fig. 5.3).

Figure 5.3 shows six maps of the most prolific units in the area. These maps combine the structural map of the upper bounding flooding surface of the respective genetic unit, net sand isopach of the reservoir interval, and areas with hydrocarbons based on a cutoff of 15 ohm.m in the deep-resistivity log. A bottom aquifer is the main drive mechanism for the reservoirs (PDVSA E&P Occidente and Veba Oil, 1998). Structural lows to the east and west tend to be wet reservoirs

outside the main anticline areas, and also to the south for the deeper genetic units (i.e. genetic sequence 1).

Most of the oil production is located in the central and southern area in parasequence sets F, G and N, where a combination of structural highs and thick sandstone packages occur. To the north these sets are less productive, probably due to an increase in shale content related to an increase of tidal influence (Chapter 4). Oil is most likely to be concentrated in the main continuous distributary channel facies and sand bars.

The southern and central areas have been intensely drilled over the main anticline structure. Pay zones are generally perforated when resistivities of the sandstones are greater than 15 ohm.m. The northern area and flanks of the main anticline are poorly drilled and open the opportunity for more infill drilling and stratigraphic traps in the central-west part of the study area (Fig. 5.3).

5.4 HIGH RESOLUTION SEQUENCE STRATIGRAPHIC CORRELATION

The GR pseudo-seismic data provides a visualization technique to interpret the continuity of the reservoirs in the study area. The sequence stratigraphic framework is based upon the stratigraphic correlation built using a dense well data base and on mapping of different parasequence sets (Chapter 4). In addition to the GR pseudo-seismic data, a deep-resistivity pseudo-seismic data set was built in order to interpret the lateral and vertical distribution of hydrocarbons within the different sets. Resistivity logs used include induction (i.e. ILLD) and resistivity logs (i.e. LLD, LL8). One of the main problems found in the

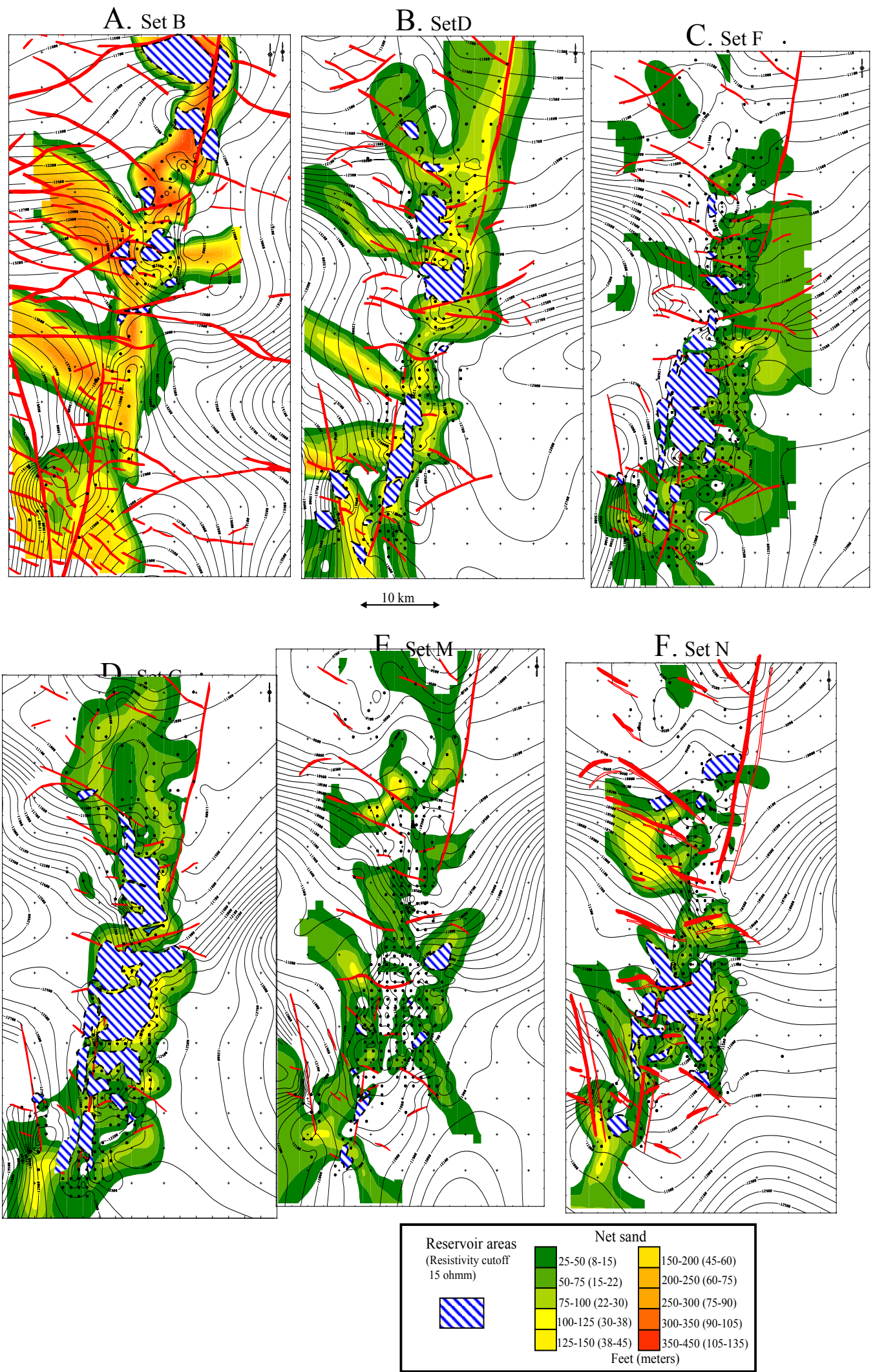


Figure 5.3. Central Lake Maracaibo structural maps of indicating net sand distribution and areas with high resistivity values: A) Set B; B) Set D; C) Set F; D) Set G; E) Set M; and F) Set N.

generation of the deep-resistivity, pseudo-seismic data is the variability of the magnitude of resistivity measurements, which can range from less than 1 ohm.m to more than 2000 ohm.m, depending in the logging tool used. For the study area a cut-off of 15 ohm.m was defined to be the most appropriate value for hydrocarbon detection (PDVSA E&P Occidente and Veba Oil, 1998). Resistivities between 15 to 200 ohm.m were displayed for visualization purposes in the pseudo-seismic data.

Figures 5.4 and 5.5 show structural pseudo-seismic line 25 and crossline 17, respectively (the pseudo-seismic display of well logs is discussed in detail in chapter 4). In both sections, the main reservoirs are located in parasequence sets F, G and N, where high resistivity values are observed ($>>15$ ohm.m). The main reservoirs are distributary channels, trending from S-SW to the N-NE over the Eocene Maracaibo shelf (Chapter 4). Hydrocarbons are present on structural highs, as observed in Figure 5.4. Toward the E and W flanks of the structure, aquifers are present in different sets. A bottom aquifer is interpreted from Figure 5.5, where the oil-water contact can be located between -3800 to 3870 m (-12500 to 12700 feet) (depending upon drilled year and reservoir compartment of the wells). This bottom aquifer explains why reservoirs of genetic sequence 1 show hydrocarbons to the north (Fig. 5.5), whereas to the south sets underneath set F (genetic sequence 2) are wet (stratigraphic higher sets).

Structurally and stratigraphically complex hydrocarbon traps occur in the central and northern areas, where highly discontinuous sand bodies are observed (Figure 5.5). This observation suggests: 1) a complex hydrocarbon migration

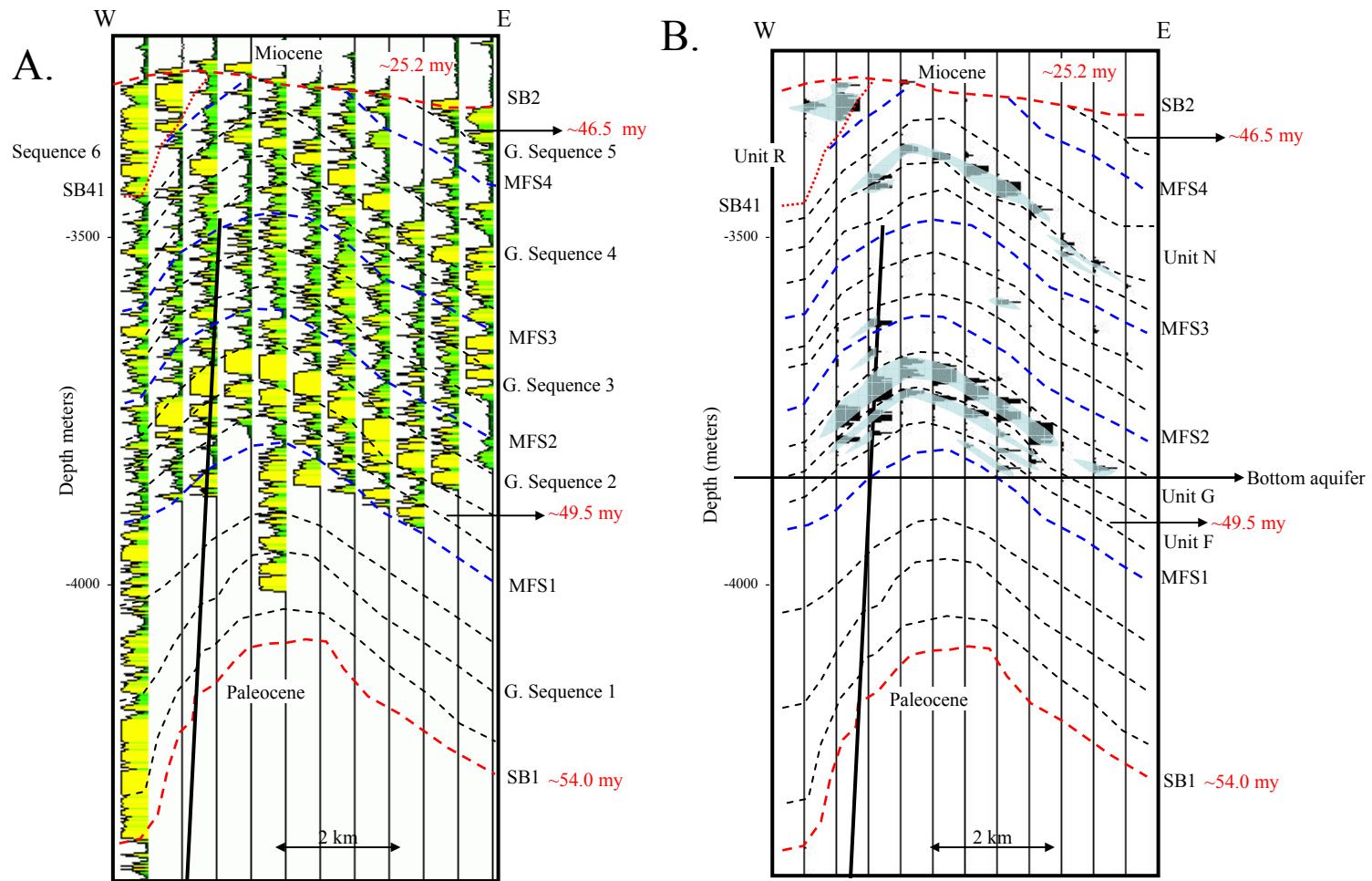


Figure 5.4. A) Structural GR pseudo-seismic line 25. B) Structural deep-resistivity pseudo-seismic line 25. See Figure 4.1 for location.

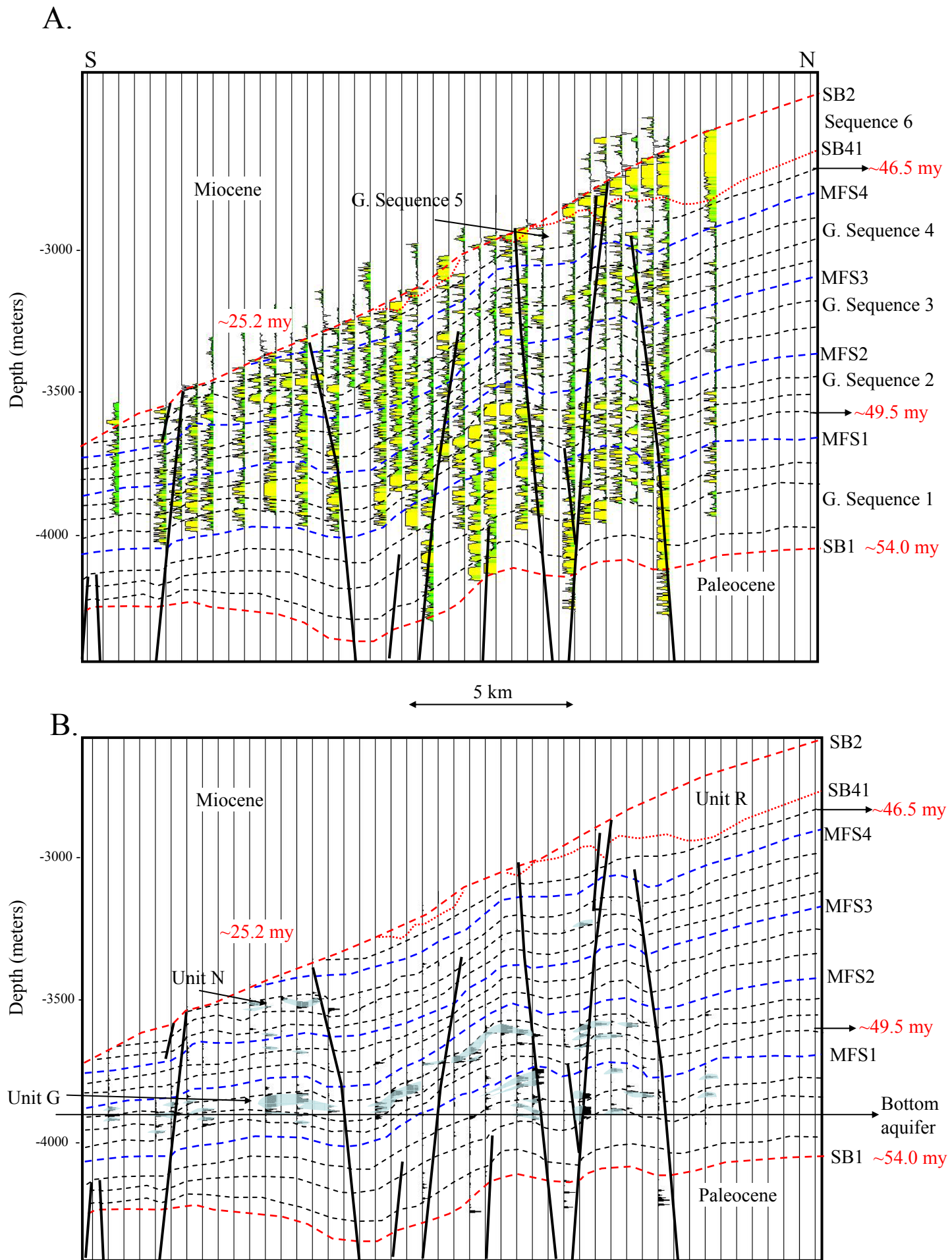


Figure 5.5. A) Structural GR pseudo-seismic cross line 17. B) Structural deep-resistivity pseudo-seismic cross line 17. See Figure 4.1 for location.

pathway allowing trapping in certain isolated stratigraphic or structural traps, but leaving areas at the same set or same structural level wet; and 2) genetic sequences above genetic sequence 1 shows an increase in shale content (i.e., erratic facies, more marine influence) leading to a reduction in the connectivity of the sand bodies (sand bars), an increase in capillary pressure and more variability in permeability. In such genetic sequences, it is common to interpret different aquifers for each reservoir. Likewise reservoirs can be found off structural highs, as in genetic sequence 4 (parasequence sets M and N, Fig. 5.3).

5.5 WELL AND SEISMIC DATA CORRELATION

Prediction of the continuity and petrophysical properties of the reservoirs is difficult in interwell correlations in areas where reservoir heterogeneity is high (Tyler; 1988). Prediction on heterogeneous tide-influence facies is very poor between neighboring wells and even poorer in new development areas (Maguregui, 1990; Ambrose et al., 1995).

Seismic data can be helpful to enhance interpretation of interwell and new development areas when seismic vertical resolution is good. In the best case, petrophysical properties of reservoirs correlate with seismic properties.

5.5.1 Petrophysical properties of the reservoirs

Little core data are available from 9 wells in the study area (Fig. 4.1). Conventional analysis was performed on most of these core data. This analysis was done by the Instituto de Investigaciones Petroleras de La Universidad del

Zulia and S.A. Consultores C.S.C, where permeability and porosity were measured. Using these data, petrophysical properties were assigned to each facies association to estimate reservoir quality.

Figure 5.6 shows an example of an analysis performed in Well W12. Permeability and porosity are displayed in depth and compared with the GR (Fig. 5.6A). GR facies associations were extracted from log data, in addition to the corresponding permeability and porosity of the stratigraphic set. Porosity versus permeability plots were generated for potential correlations between these properties (Fig. 5.6B).

Average porosity for the different stratigraphic sets, independent of age and facies, is around 20%. Permeability shows more variability, and is different for each facies and parasequence set. Reasonable correlations with porosity can be inferred (an increase in porosity represents an increase in permeability and vice versa). Permeability calculated in the lab was Klinkenberg permeability or corrected gas permeability, which is the most representative of reservoir condition, rather than air permeability. For spiked or mixed GR facies (crevasse splay, tidal bars) permeability ranges from 260 to 420 md. Blocky to fining upwards GR facies permeability (fluvial channels, distributaries) range from 500 to 700 md (with maximum up to 2500 md). Blocky to spiked-coarsening upwards GR facies (channels) show the lowest permeability, with average of 160 md. The best quality reservoirs are distributary channels and fluvial channels in genetic sequence 1 and parasequence sets G and N, followed by tidal sand bars.

5.5.2 Acoustic properties of well and seismic data: Implications for interwell correlation using seismic data

To determine a plausible correlation between well and seismic data, seismic properties, synthetic seismograms (sonic and density from well data) and cross-plots were analyzed (Torres-Verdin et al., 1999).

Seismic properties and synthetic seismograms

Synthetic seismograms were built and compared with the seismic data (i.e. Figures 5.7 and 5.8). The main objective was to extract the seismic properties (frequency, wavelet and phase) and compare the seismic response with the acoustic response observed in the wells for the Eocene tectonosequence.

The seismic data available for the project is sampled at 4 ms, amplitude range of 8 bit display, and a frequency band of 8-55 Hz. The dominant frequency is between 25 to 30 Hz (Fig. 5.7C). Using an average velocity for the interval of interest between 3600 to 3900 m/sec (12000 to 13000 feet/sec) (taken from sonic logs), the limit of separability or vertical resolution (Sheriff and Geldart, 1995; Brown, 1996) is approximately 40 m (120 feet) (Fig. 5.7C). Unfortunately no pre-stack seismic data or stacked seismic data at 16 bit was available, thus reducing the probability for interpreting stratigraphic features either from amplitude analysis or by improving seismic quality through reprocessing.

Figures 5.7A and 5.8A show synthetic seismograms for two wells in the study area. A reasonable match between seismic and well data is found for the main reflection events. The best wavelet extracted from the seismic used in the synthetic seismograms for the frequency band of interest was a near zero-phase

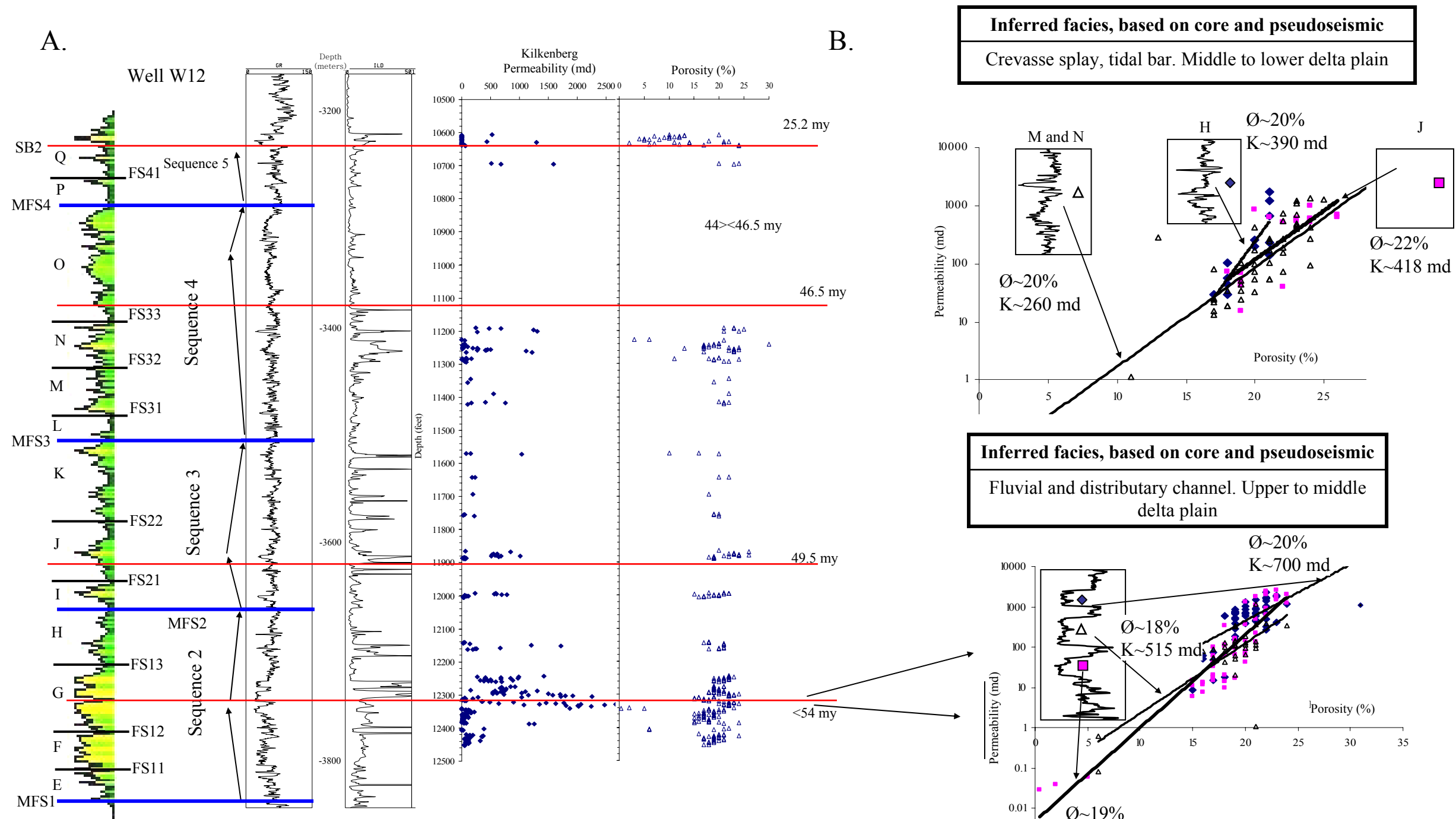
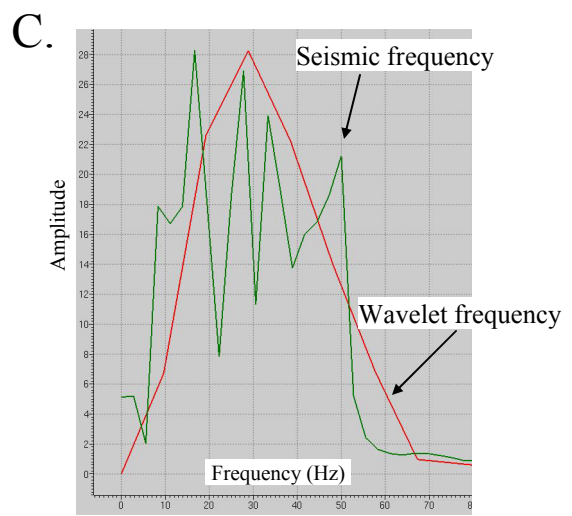
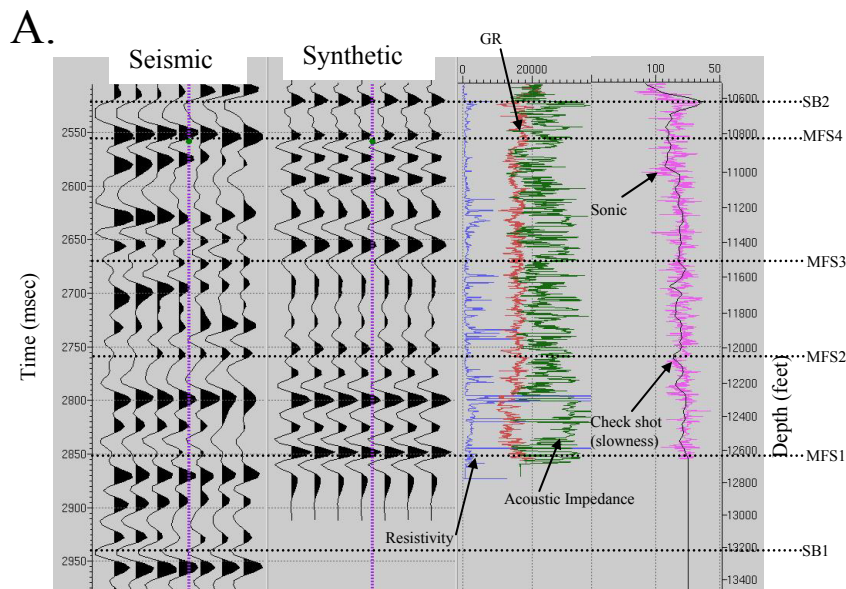


Figure 5.6. Facies petrophysical properties from core data in well W12. Crevasse splays and tidal bars have an average of 20% porosity and 300 md. Fluvial channels and distributaries have an average of 19% porosity and permeability varies from 160 to 700 md (Instituto de Investigaciones Petroleras de la Universidad del Zulia, 1991)

wavelet shown in Figures 5.7B and 5.8B. Acoustic impedance (green), gamma ray (red) and resistivity (blue) logs reveal that most of the reservoirs have thicknesses no greater than 30 m (100 feet), which is below the vertical resolution of the seismic data. Top and base of set R (between SB2 and SB41) is the stratigraphic set which thickness is greater than the vertical resolution (Figs. 5.7A and 5.8A). Few hydrocarbons have been discovered for this set. For quality control between the synthetic seismogram and the seismic data correlation, frequencies of both data were compared (Figs. 5.7C and 5.8C). Also, the sonic logs were compared with the slowness log extracted from the checkshot survey logs. In general, both analyses show good quality and correlation with the data, but seismic resolution does not have enough resolution to characterize the individual reservoirs.

Crossplots

Acoustic impedance (product of density and velocity, Figs. 5.7A and 5.8A) varies with rock properties including: lithology, porosity, fluid, compaction, and fluid pressure (Jason Geosystems BV, 1997). Crossplots between acoustic impedance, density and gamma ray shown in Figure 5.9 reveal the different acoustic properties of the genetic sequences. The main objective of this aspect of the study is to evaluate if the acoustic impedance is able to differentiate lithology and fluid content. Two wells are displayed in Figure 5.9 (wells W12 and W16) showing their acoustic and lithologic response for the different genetic sequences



Limit of separability = $\lambda/4 = t/2 = (V/4F) = \sim 40 \text{ m (120 feet)}$

V = Average velocity of the Eocene $\sim 4 \text{ km/sec} \sim 12000\text{-}13000 \text{ feet/sec}$
 F = Average maximum amplitude of the Eocene $\sim 28\text{-}35 \text{ Hz}$

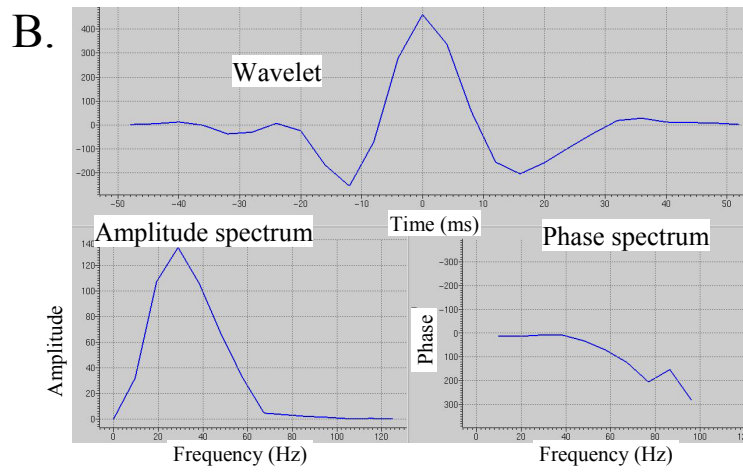


Figure 5.7. A) Synthetic seismogram of well W12. B) Extracted wavelet, frequency and phase from the seismic data in the neighborhood of well W12 in the Eocene interval. Dominant frequency 28-30 Hz. C) Quality control between the seismic data and the extracted wavelet.

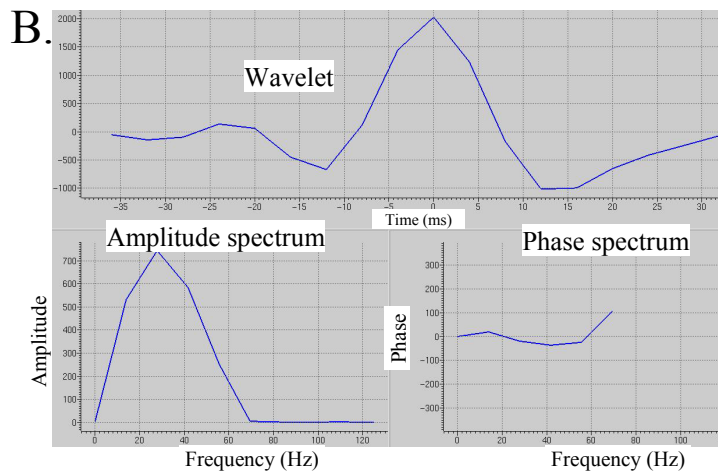
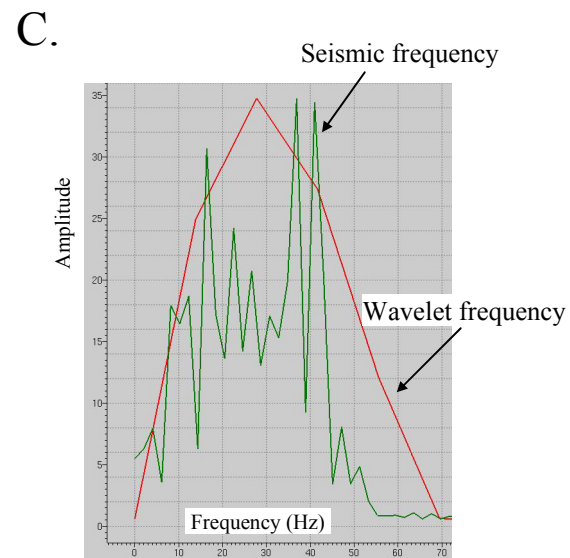
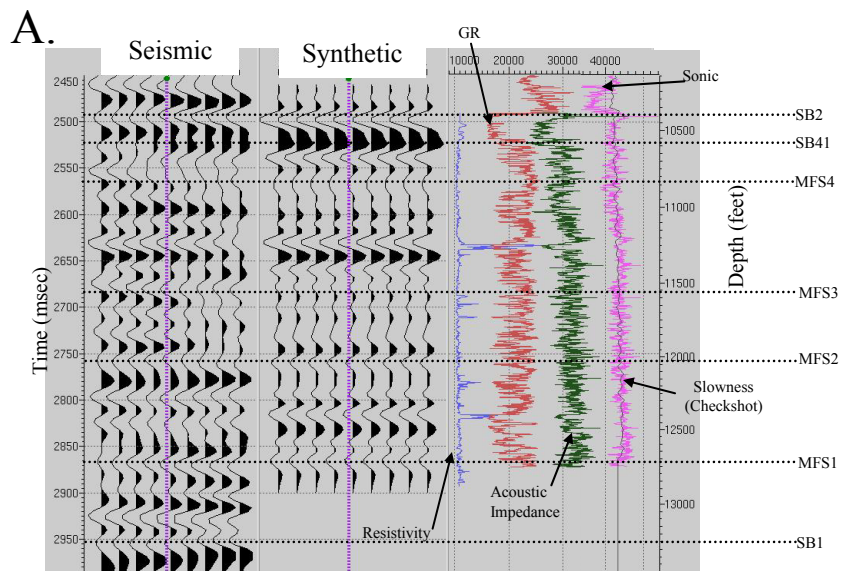


Figure 5.8. A) Synthetic seismogram of well W16. B) Extracted wavelet, frequency and phase from the seismic data in the neighborhood of well W12 in the Eocene interval. Dominant frequency 28-30 Hz. C) Quality control between the seismic data and the extracted wavelet.

interpreted in the study area. These two wells are located no more than 4 km apart (Fig. 4.1). Main observations from the crossplots include:

1. In general, reservoir sandstones can be differentiated from shales by the acoustic impedance, as shown by the polygonal areas, representing highlighted intervals in the logs. However, partial overlap between both lithologies occurs.

2. Well W12 sandstone (low GR, yellow and red colors) shows high acoustic impedance and density values for all genetic sequences (Fig. 5.9A and 5.9B), except for genetic sequence 4, where sandstones with hydrocarbons (high resistivity) can be differentiated from wet sandstones by their low acoustic impedance (yellow highlight in the well logs, 5.9B).

3. In contrast, well W16 show low acoustic impedance and density values for all sandstones in the genetic sequences independent of fluid (Figs. 5.9C and 5.9D). For genetic sequence 2, acoustic impedance of sandstones is similar to the acoustic impedance of the shales making them difficult to differentiate lithology on the logs (5.9D).

Seismic and well data resolution implications

As interpreted from crossplots, acoustic impedance can discriminate lithology from the genetic sequences, and in some cases fluid, as the case of genetic sequence 4 (Fig. 5.9B). In order to have a definitive answer regarding the question of whether seismic data can resolve lithology and reservoirs, the well log resolution has to be downscaled to the seismic resolution. The objective is to

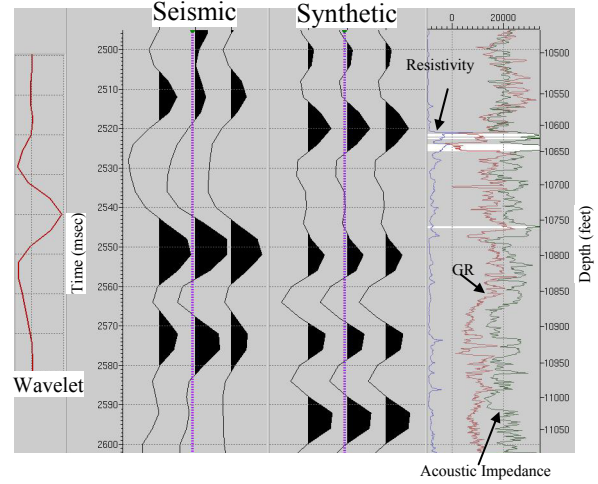
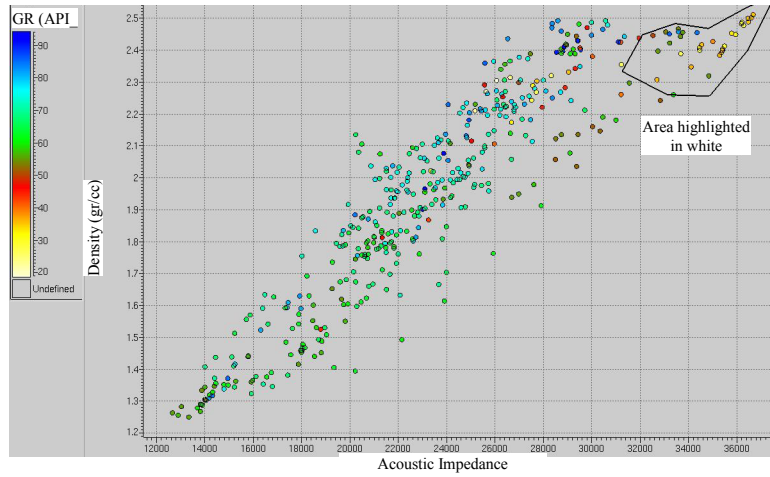
analyze whether the new lower acoustic impedance resolution can separate shales from sandstones and hydrocarbon for water. This process consists in applying a high frequency band limiting filter to the well logs (seismic band frequency between 8-50 Hz, Figs. 5.7 and 5.8).

Figure 5.10 shows a comparison between crossplots at well log resolution and the crossplots from log data at seismic resolution. The low frequency crossplots cannot differentiate the lithology, as the shales and sandstones are mixed on the plot. The low frequency acoustic impedance and GR logs cannot resolve the thickness of the sandstones. The signature of acoustic impedance in separating lithologies is lost as vertical resolution decrease and becomes difficult to impossible to interpret stratigraphic features at the reservoir scale using the seismic data. The lack of higher frequency content in the seismic data reduces its capabilities to resolve most of the Eocene reservoirs.

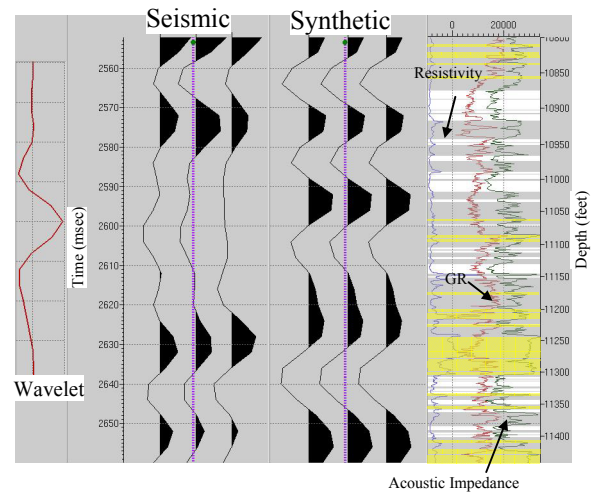
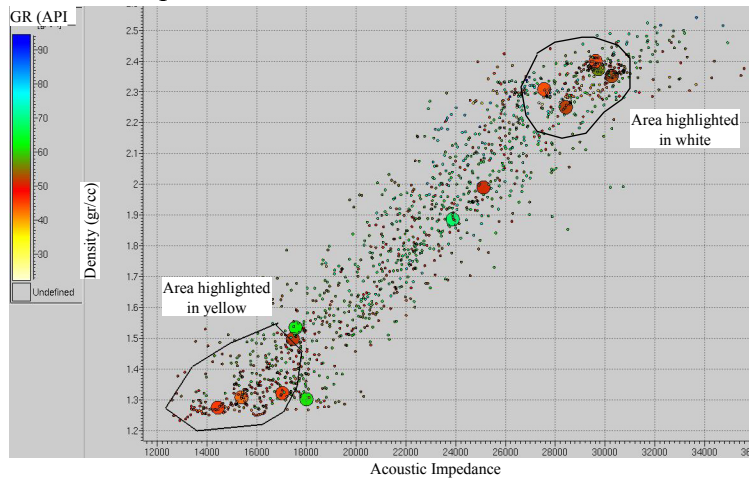
Tuning

The tuning thickness is the bed thickness where amplitude reaches the maximum value due to constructive interference between wavelets from top to bottom of the bed (Brown, 1996). For beds thinner than the tuning thickness, the wavelet stays the same, but its amplitude decreases. This relationship serves to correlate the amplitude value with the sand thickness (for thin sands) and can also be helpful in defining the spatial continuity of the depositional systems and their reservoir properties. The applicability of this attribute is limited by the level of noise present in the data, defining what is called the “limit of visibility” (Brown, 1996). In general, amplitudes respond to changes in the thickness of the rocks and

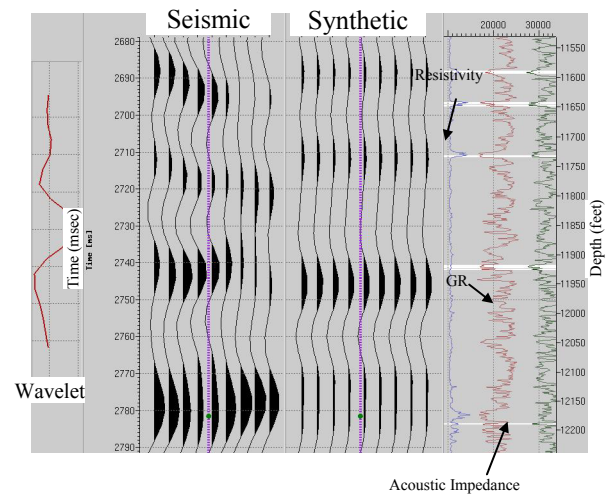
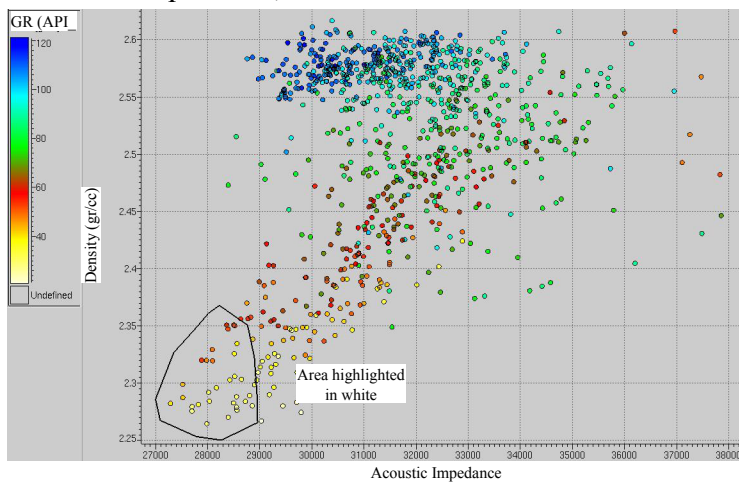
A. Genetic sequence 5, well W12



B. Genetic sequence 4, well W12



C. Genetic sequence 3, well W16



D. Genetic sequence 2, well W16

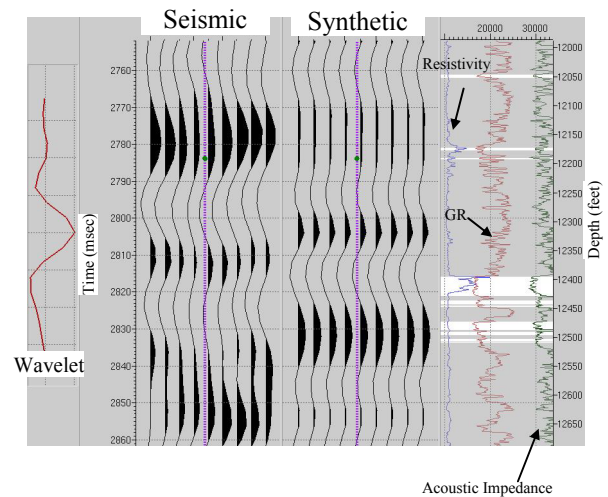
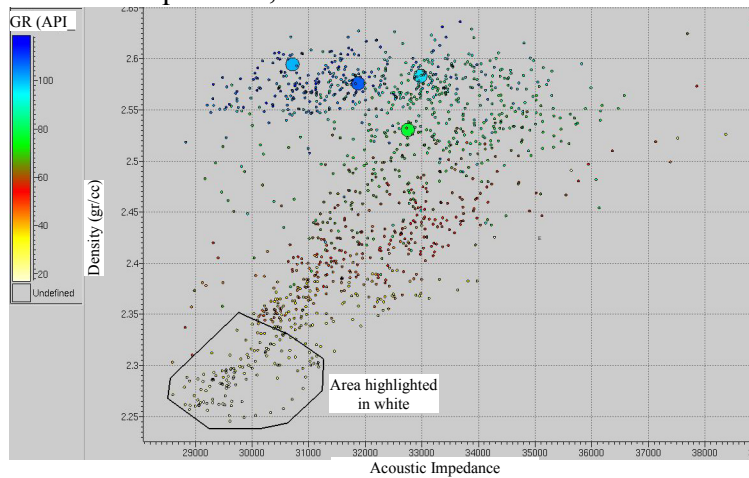
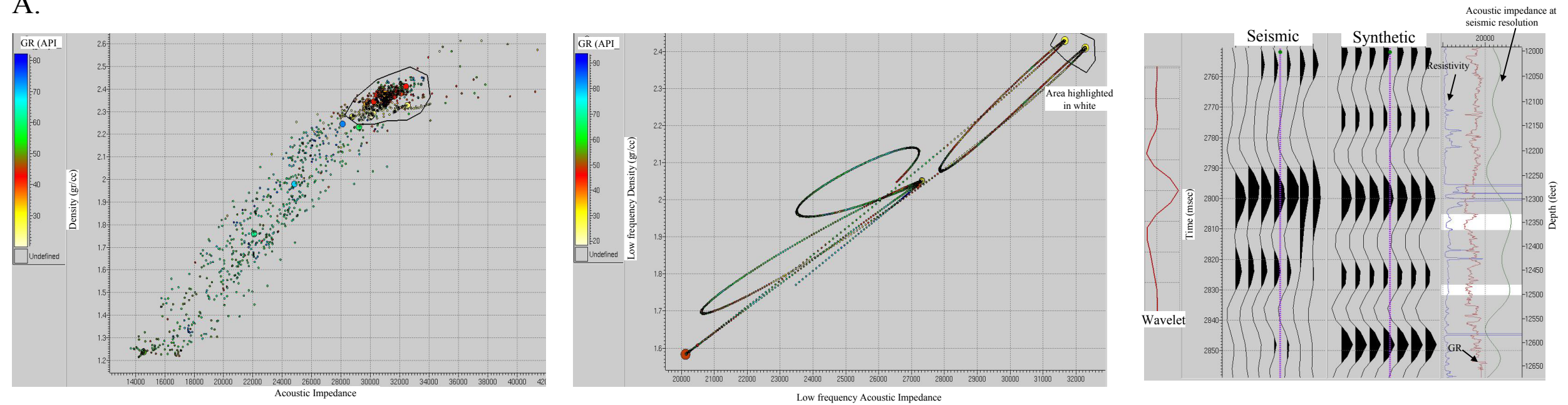


Figure 5.9. A) Crossplot and synthetic seismogram of genetic sequence 5 in well W12. B) Crossplot and synthetic seismogram of genetic sequence 4 in well W12. C) Crossplot and synthetic seismogram of genetic sequence 3 in well W16. D) Crossplot and synthetic seismogram of genetic sequence 4 in well W16.

A.



B.

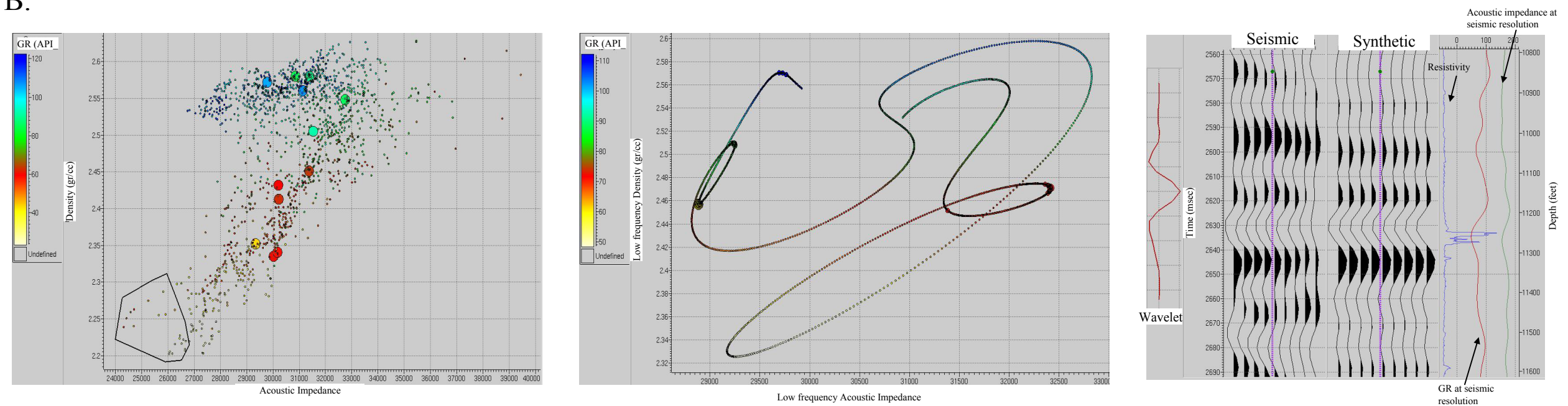


Figure 5.10. A) Crossplots at well and seismic resolution and synthetic seismogram of genetic sequence 2 in well W12. GR and acoustic impedance logs are displayed with the seismic frequency. B) Crossplots at well and seismic resolution and synthetic seismogram of genetic sequence 4 in well W16. GR and acoustic impedance logs are displayed with the seismic frequency.

their internal properties. Because the resolution of the seismic data is low (~ 40 m; 120 feet), interpretation has to be done below the tuning thickness in order to apply the correlation between amplitudes and reservoir properties.

An example of amplitude versus thickness is shown in Figure 5.11. The reservoir is located in set M, and was penetrated by three wells (Fig. 5.11A). Initial oil production was more than 1000 barrels of hydrocarbon per day in each well (Escalona and MacDonalds, 1998). An attempt to follow the top and base reflection was done, and amplitude was extracted (Figs. 4.11B and C). A crossplot between thickness and amplitudes from the top of the reservoir show an incipient correlation, suggesting that all wells are in the interference zone between top and base reflection (i.e., below the vertical resolution). Maximum interference is interpreted to be at 25 m (~70 feet) thickness (Fig. 4.11D).

The value of tuning thickness interpreted from Figure 5.11 is smaller than the average vertical resolution calculated for the Eocene in Fig. 5.7 ($70 < 120$ feet). This value difference might indicate vertical resolution variability in the Eocene interval or that more data is needed to better constraint the tuning thickness calculated. This methodology failed as more wells were added and showed sparse correlation, probably as a consequence of: 1) acoustic changes in the reservoirs (i.e. acoustic impedances variability observed in wells W12 and W16), 2) high signal to noise ratio, 3) thin discontinuous reservoirs, and 4) amplitudes affected by beds above and below the zone of interest. This suggests that tuning may work in small areas and when true-amplitude information is preserved in order to correlate reservoir thicknesses below the limit of resolution.

Stratal slices

This technique involved generation of horizons parallel to an interpreted horizon by adding or subtracting a constant time throughout the interpreted horizon. Extraction of amplitudes of the newly generated horizon will produce a horizon similar to the seismic cube flattening technique, which will represent a pseudo-time line relative to the horizon of origin. Another slicing technique is the proportional slice, where proportional slices are produced between two interpreted horizons. All these techniques made the assumption that seismic reflectors follow chronostratigraphic surfaces (Zeng et al., 1998).

Figure 5.12 shows an example of stratal slices where the northern part of the main distributary channel of parasequence set A can be interpreted. The slice at 8 ms above the Paleocene unconformity (SB1) (Fig. 5.12D) is able to resolve the central part of the channel, because its thickness is greater than the vertical seismic resolution (40 m; ~120 feet). When thickness becomes less than the vertical seismic resolution, the channel is not shown. This technique worked effectively at this interval, because the Paleocene unconformity is a good quality reflection. In other intervals, no coherent image was obtained because reflections are highly discontinuous.

The main reservoir in parasequence set A is located in a structural high along a N-NE-striking fault (western side of the fault, Fig. 5.12A). Another compartment is located in the northeastern side of the fault (Fig. 5.12A). The channel follows the strike of the fault on its western side, and in the area where

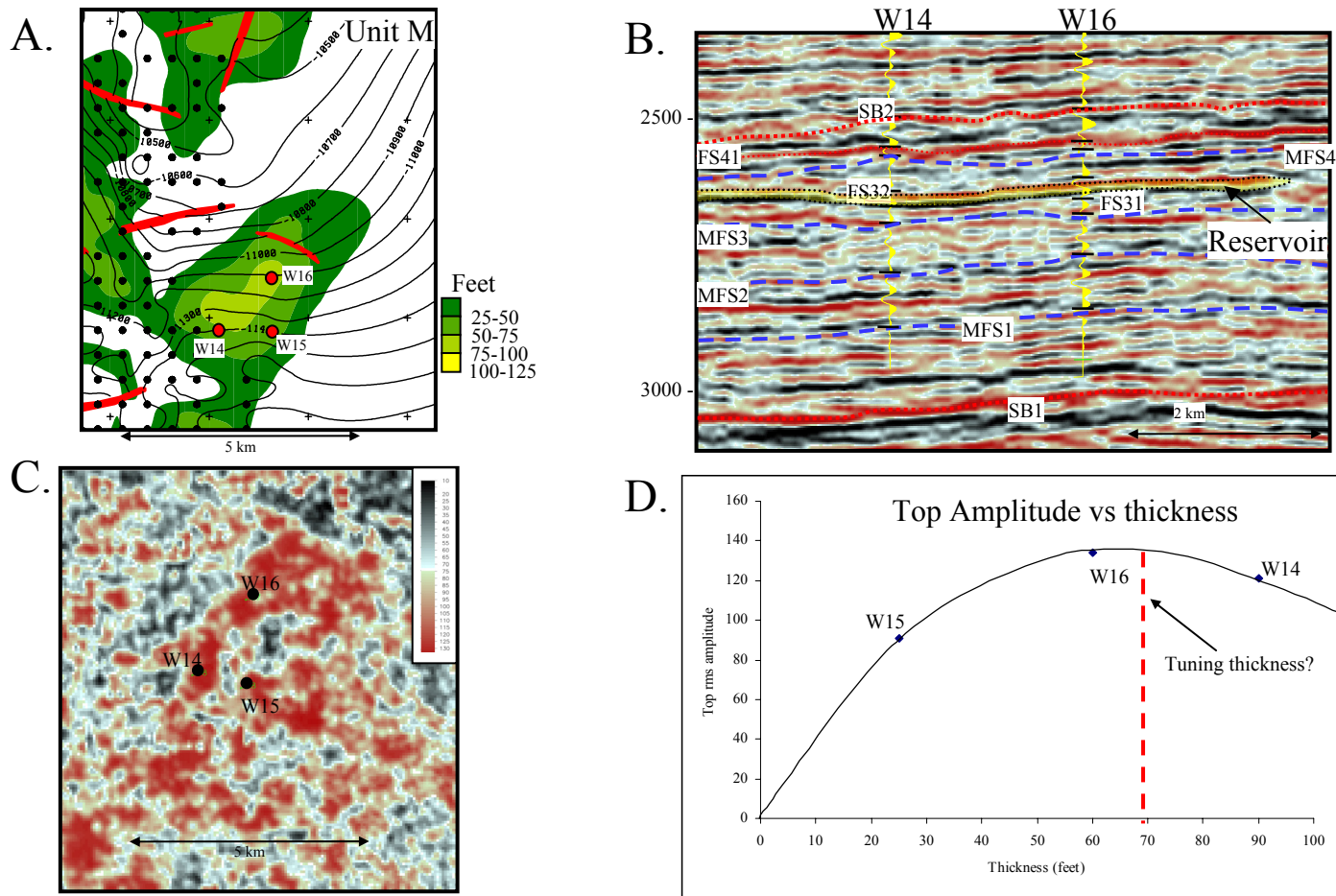


Figure 5.11. A) Net sand map of parasequence set M in the neighborhood of wells W14, W15 and W16. B) Seismic line showing the possible reservoir. C) Amplitude map of the top of the reservoir. D) Sandstone thickness vs. amplitude showing possible tuning thickness for the interval.

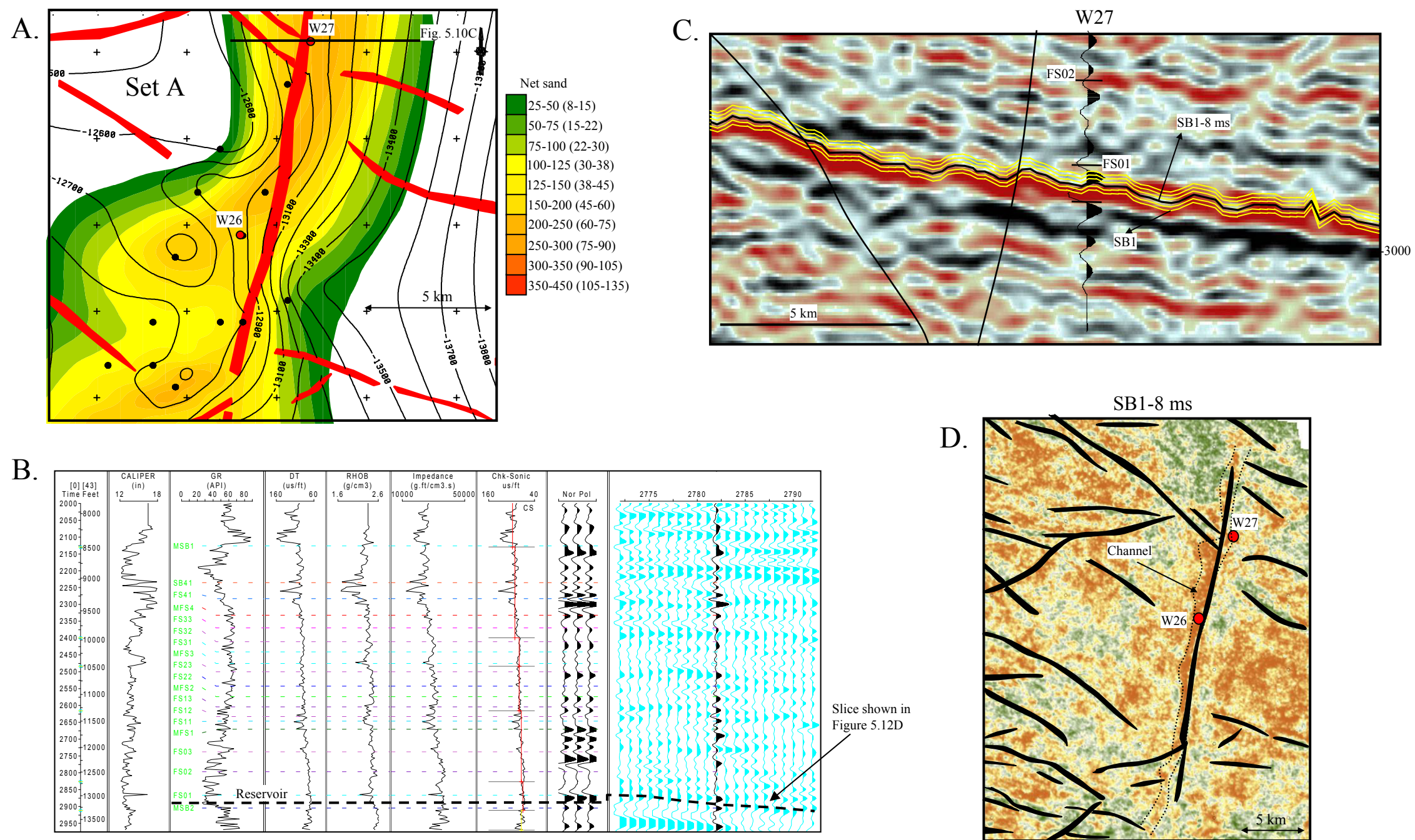


Figure 5.12. A) Net sand map of parasequence set A in the neighborhood of Wells W26 and W27. B) Synthetic seismogram of well W27, showing the main reservoir. C) Seismic interpretation of the reservoir using stratal slices. D) Slice 8 ms above the Paleocene unconformity (SB1) showing the main channel interpreted from well data.

well W27 is located it crossed to the eastern side as interpreted from the net sand map. Wells W26 and W27 penetrated more than 30 m (100 feet) of net pay sandstone. Other areas of this parasequence set are wet.

5.6 CONCLUSIONS

After an intensive analysis of the petrophysical properties of the rock record in the Eocene tectonosequence, spatial distribution of the reservoirs, and the properties of the 3-D seismic data available in the study area, the main conclusions of this chapter include:

- Reservoir occurrence is mainly in distributary channels and sand bar facies, which represent good quality fluid flow units (porosity ~20%, and permeability dependent on facies with range from 160 to 700 md).
- Reservoirs in genetic sequence 1 and 2 are affected by a bottom aquifer, and hydrocarbon is trapped on the structural highs. For genetic sequence 4, a more complex interplay between stratigraphy and structure forms isolated traps.
- Lithology and fluid content can sometimes be differentiated by acoustic impedance in well logs. The seismic data are unable to resolve the lateral and vertical continuity of the reservoirs.
- The noisy character of the reflections, the low vertical resolution and the lithologic heterogeneities reduce the utility of horizon amplitude extraction and application of alternative techniques as stratal slices in the interval of study.

- Reprocessing the 3-D seismic survey with full dynamic range of the recovered data, or acquisition of a higher resolution 3-D seismic survey in the area, is recommended. There is a good correlation between acoustic properties of the logs and the seismic data, but higher dominant frequency (~50 Hz) and data quality are needed to be able to image the reservoirs that are in the range of 10 meters and up in thickness.

CHAPTER 6

Conclusions

Integration of the different scales of geological observations, from regional to reservoir scale, using subsurface data, yielded a consistent geological model of the Eocene clastic sedimentary rocks of the Maracaibo basin, western Venezuela. The model links the tectonic evolution of the basin during oblique collision between the Caribbean and the South American plates, with the structural and stratigraphic architecture interpreted in central Maracaibo basin. Tectonic subsidence and fault reactivation are responsible for the complexity of the Petroleum systems in the basin. Individual conclusions are:

1. Interpretation of 2-D and 3-D seismic data in central and eastern Maracaibo basin show two major deformational events during the oblique collision between the Caribbean and the South American plates in the Paleogene:
1) During the late Paleocene-early Eocene, a foreland basin, whose depocenter was located north and northeast of the basin with a forebulge located in the southern part of the basin.; and 2) during the middle-late Eocene strike-slip motion through a lateral ramp fault controlled the middle-late Eocene depocenters and directed the thrust front toward the SE, ending the foreland basin stage in most of the Maracaibo basin. The Burro Negro fault is interpreted as the lateral ramp fault, in addition to has been the shelf edge of the Maracaibo basin during the Paleogene. The fault separates the Maracaibo basin into an uncollided zone to the southwest, from a collided zoned to the northeast.

2. In the Eocene Maracaibo shelf, three different fault trends contributed to the formation of the Icotea pull-apart basin. The three fault trends within the study area include: 1) N-NE faults (*i.e.* Icotea fault). These are pre-existing Jurassic faults reactivated as strike-slip faults with left-lateral and reverse movement during the Paleocene-Eocene. Strike-slip displacement was driven by NW-SE directed oblique collision of the Caribbean plates against northern South America plate. 2) NW-SE-striking faults. These faults formed during the late Paleocene from downward flexure of the central Maracaibo basin. Strike-slip movement along the N-NE-striking faults locally reactivated these faults as normal faults to form the Icotea pull-apart basin. 3) NE-SW-striking faults. These normal faults formed during pre-Cretaceous rifting between North America and South America, and were reactivated during late Paleocene-Eocene.

3. The Icotea fault is classified as an intraplate fault (Sylvester, 1988) restricted to the crust, transferring horizontal slip to other N-NE faults, as a result of differential continental blocks movement, caused by convergence. Normal displacement is localized on pre-existing NW-SE-striking faults formed by 0.5 km of plate flexure. Within the Icotea pull-apart basin normal displacement on 23 basin transverse faults was measured in a range between 0.8 and 2.25 km.

4. Sequence stratigraphic interpretation reveals that the Eocene stratigraphic framework was controlled by tectonic subsidence and secondarily by sediment supply. Eustasy does not play an important role during the early Eocene and most of the middle Eocene greenhouse period. Five genetic sequences and one depositional sequence were interpreted within the Eocene tectonosequence.

These sequences were subdivided in eighteen parasequence sets (sets) and mapped throughout the whole study area. The lack of unconformable sequence boundaries reveals that the Eocene Maracaibo basin shelf was not exposed during the early and most of the middle Eocene. Fluvial, delta, delta plain and shallow marine depositional systems dominated. Fluvial systems nourished the basin from the SSW to the NNE, interacting with tidal processes in the transitional environments of the delta plain and inner shelf. The application of the 3-D pseudo-seismic transform technique to a dense well database resulted in an excellent visualization and interpretation methodology. This methodology improved lateral and vertical correlations, creating more reliable 3-D stratigraphic interpretations where 3-D seismic resolution is poor.

5. Reservoirs in central Lake Maracaibo are concentrated in distributary channel and sand bar facies located mainly in structural highs formed by left-lateral strike-slip faults. These facies represent good quality fluid flow units (porosity ~20%, and permeability dependent on facies, ranging from 160 to 700 md).

6. Lithology and fluid content sometimes can be differentiated by the acoustic impedance in the well logs, but the low vertical resolution of the seismic data is unable to image the lateral and vertical continuity of the reservoirs. The discontinuous character of reflections in the interval of study reduces the utility of horizon amplitude extraction and application of alternative techniques such as stratal slices.

FUTURE WORK

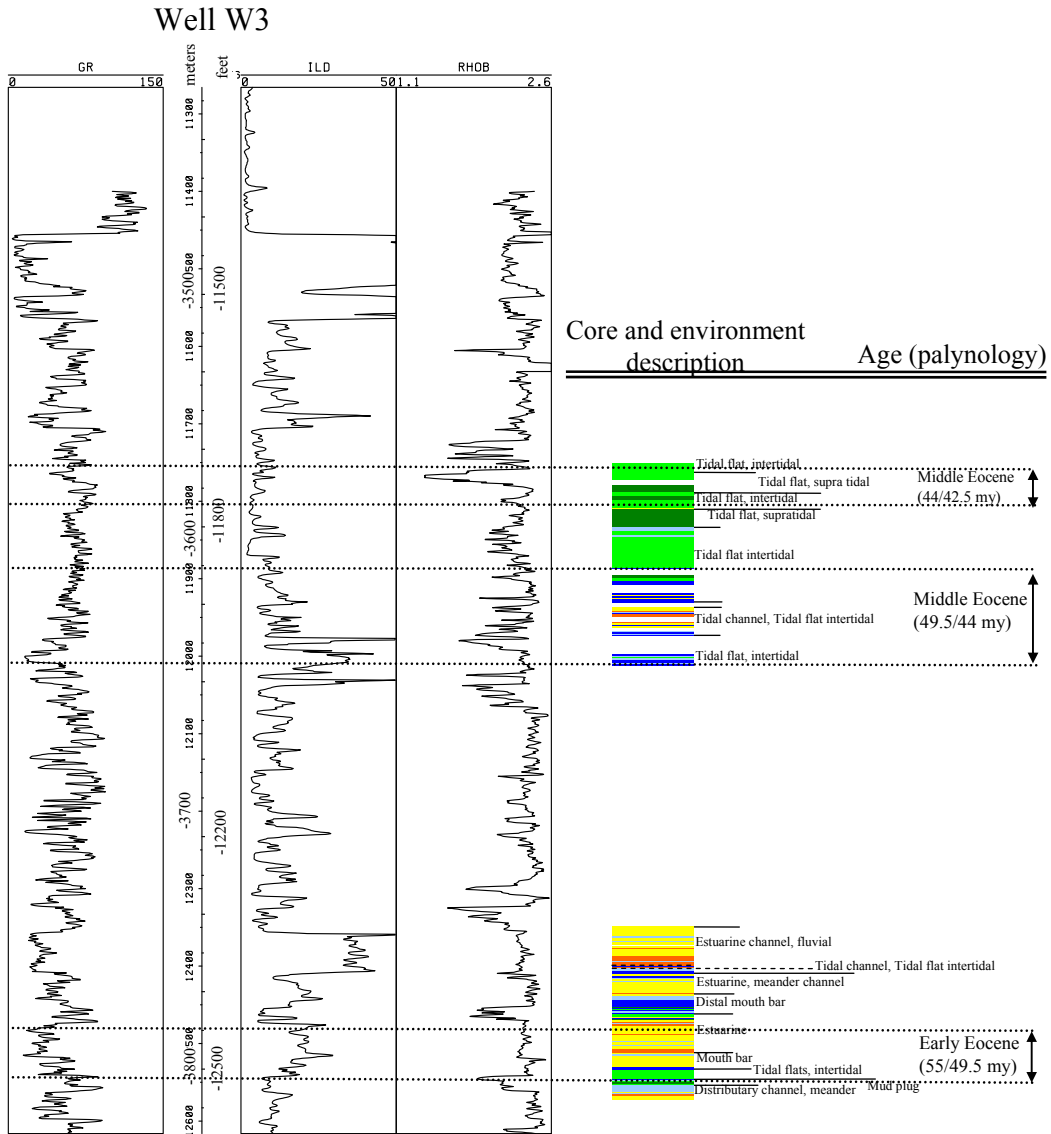
After more than 50 years of hydrocarbon exploration and production in the Maracaibo basin, a large amount of data including core, thousands of wells, and enormous quantities of 2-D and 3-D seismic data sets has been collected. Despite these data, high-resolution structural and stratigraphic integration of interpretations of the different production blocks, shelf-to-basin correlations and modern studies using surrounding outcrops have not been done. It is important to unify these data sets and provide an integrated geological model of this mature basin in order to increase its hydrocarbon production in coming years.

Detailed structural mapping can be performed using merged 3-D seismic data which now covers more than 30% of the basin. Seismic time slice interpretation, described in Chapter 3, provides an accurate regional to local picture of basin configuration and evolution for different tectonosequences. Detailed sequence stratigraphic mapping of regional chronostratigraphic surfaces allow stratigraphic definition of the different depositional systems.

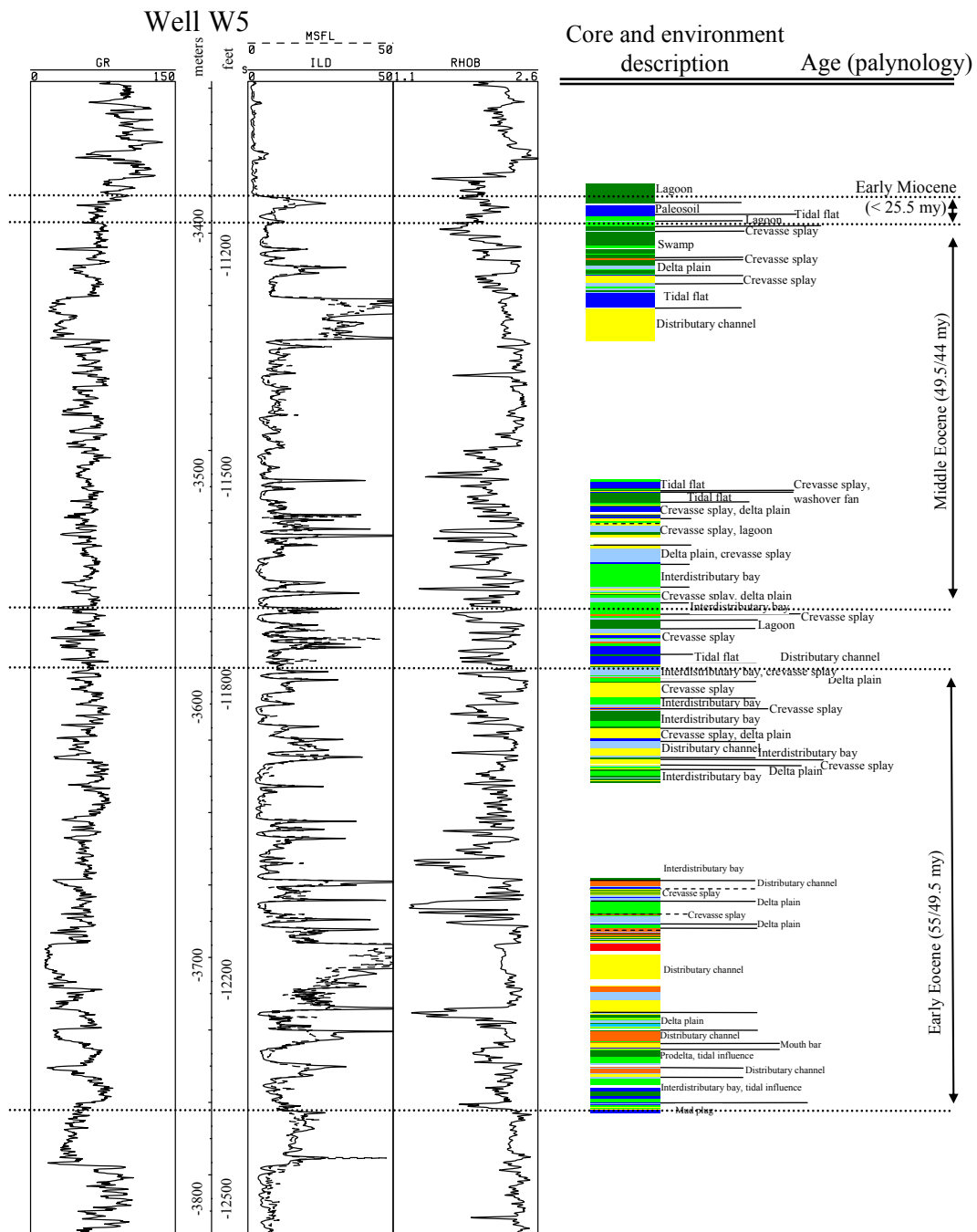
Future studies need to include the area north of the Burro Negro and Oca faults (Fig. 2.2). Few studies have been done in the area, and these areas represent part of the main depocenters during the Paleogene (González de Juana et al., 1980; Stephan, 1985; Mathieu, 1989; Lugo and Mann, 1995). The connection between the Maracaibo basin depocenter and the deep offshore basins, like the Venezuela and Grenada basin, require regional studies of their tectonic and stratigraphic evolution. These areas will become increasingly important as exploration move offshore in search of new giant oil fields.

Appendices

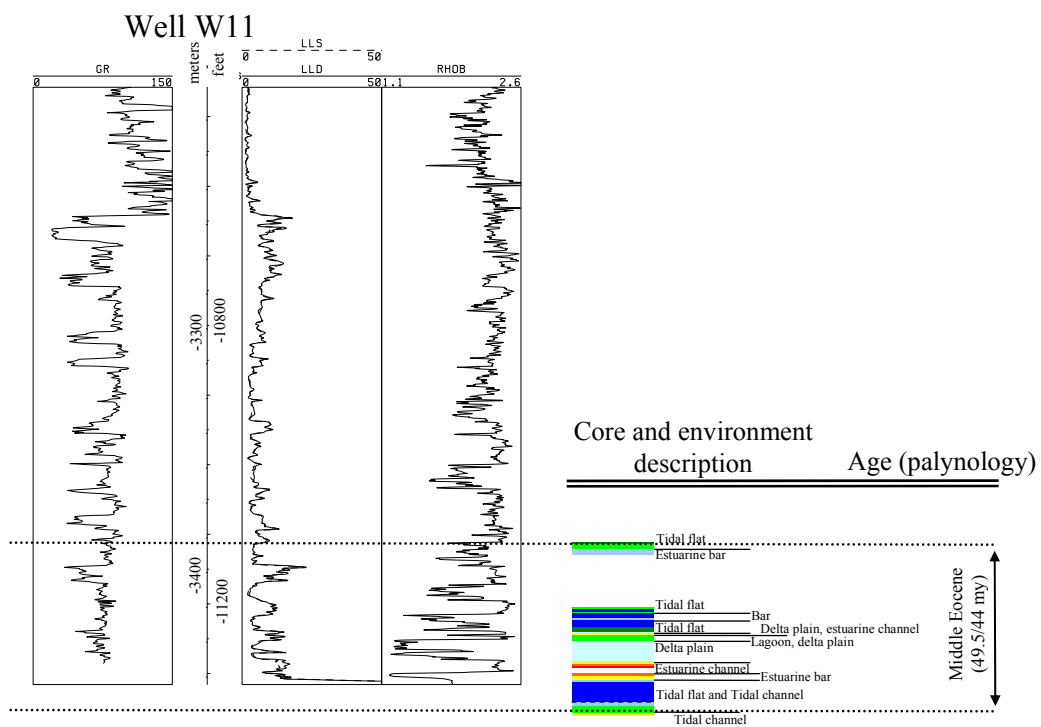
Appendix 1: Core data



Appendix 1.1. W3 well log (GR-gamma ray, ILD-deep induction and RhoB-density) with facies and environment descriptions (modified from S.A. Consultores CSC, 1989)

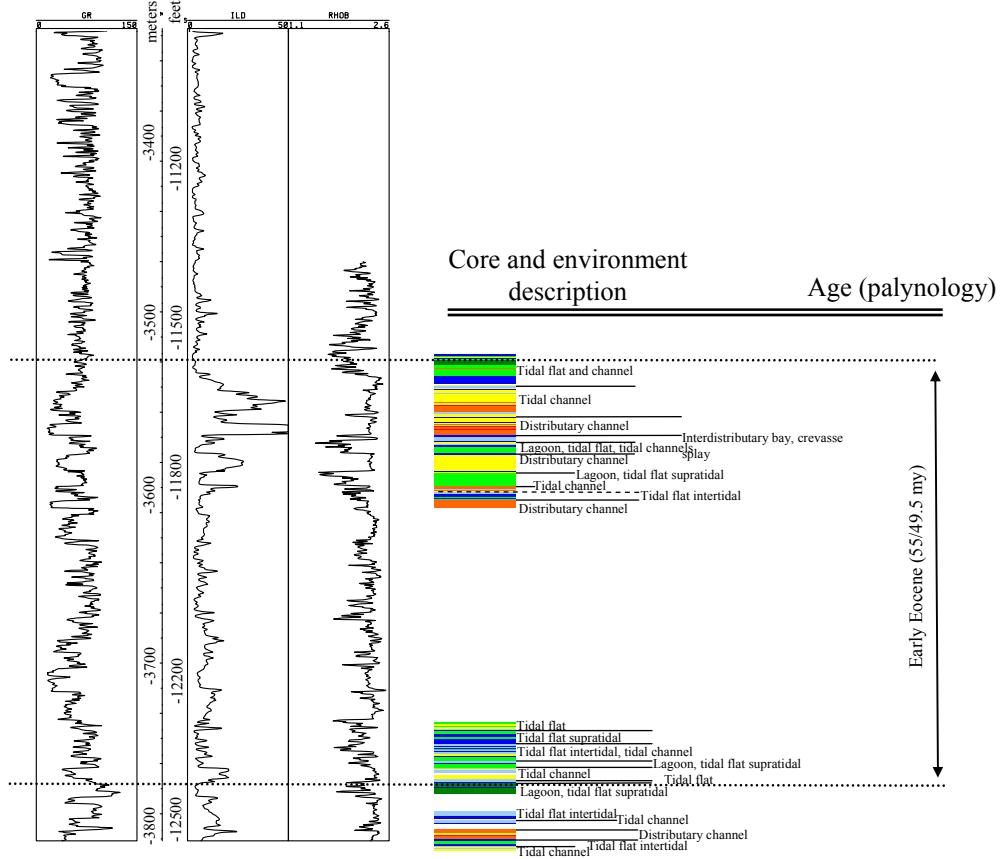


Appendix 1.2. W5 well log (GR-gamma ray, ILD-deep induction and RhoB-density) with facies and environment descriptions (modified from S.A. Consultores CSC, 1993)

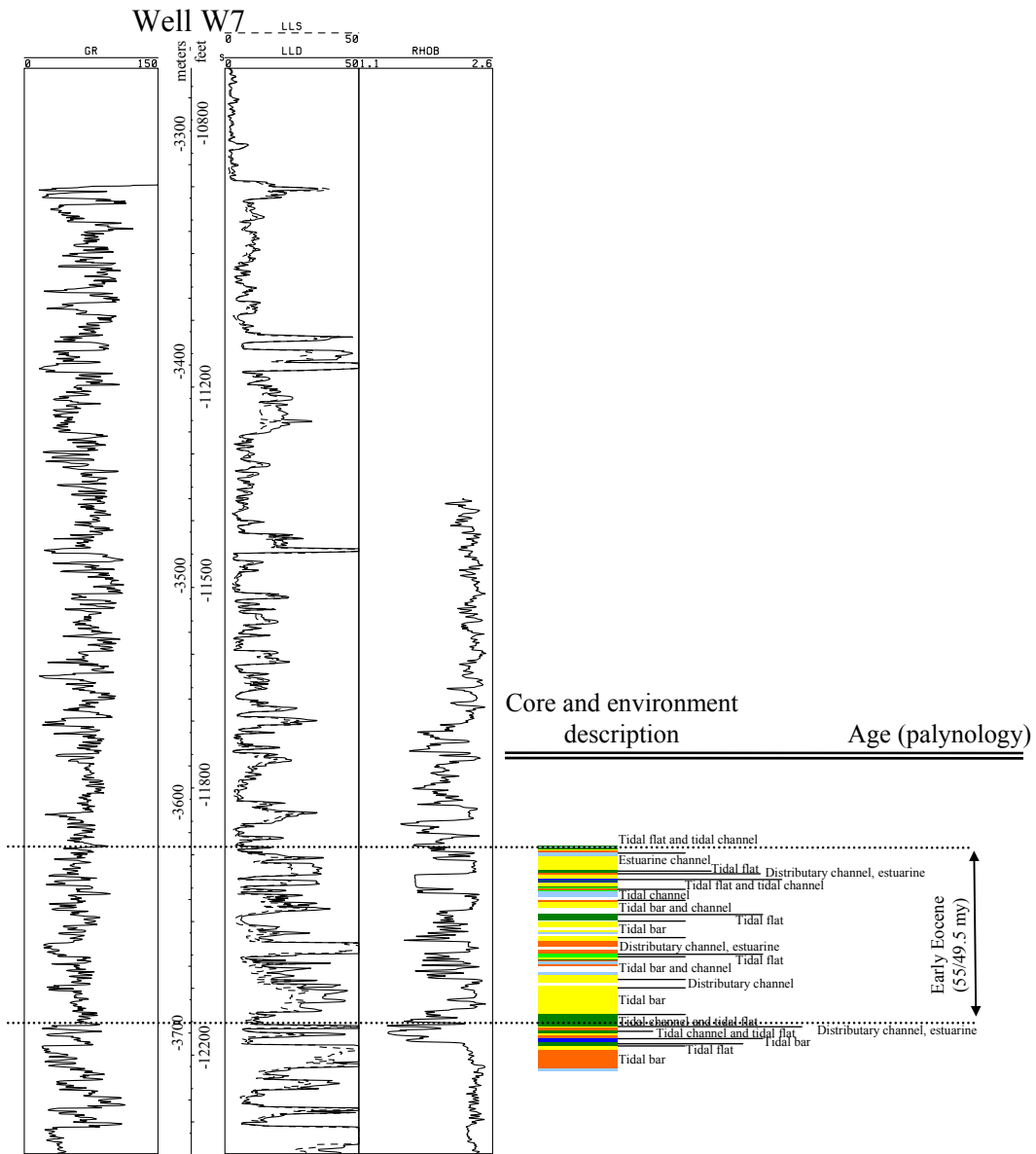


Appendix 1.3. W11 well log (GR-gamma ray, ILD-deep induction and RhoB-density) with facies and environment descriptions (modified from S.A. Consultores CSC, 1991)

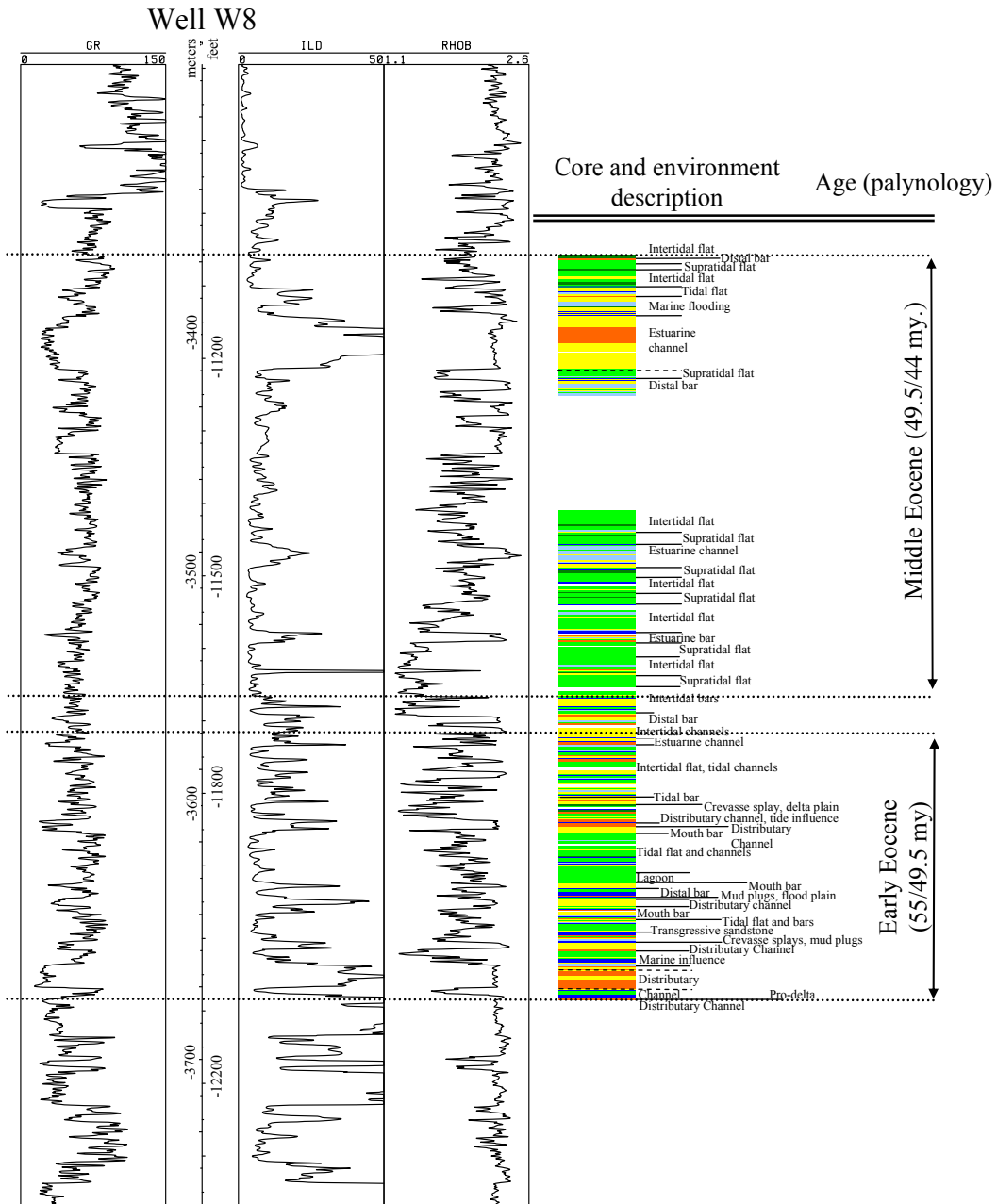
Well W18



Appendix 1.4. W18 well log (GR-gamma ray, ILD-deep induction and RhoB-density) with facies and environment descriptions (modified from S.A. Consultores CSC, 1991)



Appendix 1.5. W7 well log (GR-gamma ray, ILD-deep induction and RhoB-density) with facies and environment descriptions (modified from S.A. Consultores CSC, 1996)



Appendix 1.6. W11 well log (GR-gamma ray, ILD-deep induction and RhoB-density) with facies and environment descriptions (modified from S.A. Consultores CSC, 1991)

APPENDIX 2: CODE FOR PSEUDO-SEISMIC TRANSFORM IN MATLAB

Code to convert Las format to Segy format and create. 3D pseudo-seismic.

The transform is done one seismic line at the time.

```
%Line 5= Line name
%matrix containing 34 columns=seismic traces on a line
b=zeros(17000,34);
%1 well
[logmat, lognmem, logdesc, wellname, wellid, loc, nullval, dpthunits,
...kb,tops,ztops,lasheader] = readlas('well1.las');
%Counter
h=1;
% Substitute values on empty trace of the Line that corresponds with the
well position, just in the area where there is well information
f=size(logmat);
m=(logmat(1,2))*(-1);
n=f(1,1);
for i=m:(m+n-1)
    k=logmat(h,3);
    b(i,1)=k;
    h=h+1;
end
```

```

%2 well
[logmat, logmnem, logdesc, wellname, wellid, loc, nullval, dpthunits, ...
    kb,tops,ztops,lasheader] = readlas('well2.las');
%Counter
h=1;
% Substitute values on the empty trace of the Line that corresponds with
the well position, just in the area where there is well information
f=size(logmat);
m=round((logmat(1,2))*(-1));
n=f(1,1);
for i=m:(m+n-1)
    k=logmat(h,3);
    b(i,9)=k;
    h=h+1;
end

filename='Vsh5.sgy'
line_name=5
seis=b;
x=[222250:500:238750];
t=[0:1:17000];
nullval=0.0;
xs=x;

```



```
xr=x;  
a=ones(1,34);  
yr=a.*1071250;  
ys=yr;  
ntr=1;  
offs=zeros(1,34);  
selevs=offs; relevs=offs;  
sdepths=offs;  
cdps=a;
```

```
code=writesegy(filename,line_name,seis,x,t,nullval,ntr,...  
                xs,ys,xr,yr,offs,selevs,relevs,sdepths,cdps)
```

References

- Abreu, V. and Anderson, J., 1998, Glacial eustasy during the Cenozoic: Sequence stratigraphic implications. *American Association of Petroleum Geologists Bulletin*, v. 82, p. 1385-1400.
- Allen, P. A. and Homewood, P., 1986, Foreland basins: An introduction. *In*: Allen, P. A. and Homewood, P., eds., *Foreland basins*, International Association of Sedimentologists, Special Publication 8, p. 3-12.
- Ambrose, W, Ferrer, E., Dutton, S., Wang, F., Padron, A., Carrasquel, W., Yeh, J. and Tyler, N., 1995, Production optimization of tide-dominated deltaic reservoirs of the lower Misoa Formation (Lower Eocene), LL-652 Area, Lagunillas field, Lake Maracaibo, Venezuela. The University of Texas at Austin, Bureau of Economic Geology, internal report n. 226, 46 p.
- Ambrose, W. and Ferrer, E., 1997, Seismic stratigraphy and oil recovery potential of tide-dominated depositional sequences in the lower Misoa Formation (Lower Eocene), Lagunillas field, Lake Maracaibo, Venezuela. *The Leading Edge*, v. 16, p. 1331-1334.
- Aslan, A., Warne, A. G., White, W. A., Guevara, E. H., Smyth, R. C., Raney, J. A. and Gibeaut, J. C., 2001, Mud volcanoes of the Orinoco delta, eastern Venezuela. *Geomorphology*, v. 41, p. 323-336.
- Audemard, F., 1991, Tectonics of western Venezuela: (unpublished Ph.D. dissertation) Rice University, Houston, 245 p.
- Audemard, F. A., Bousquet, J. and Rodríguez, J. A., 1999, Neotectonic and paleoseismicity studies on the Urumaco fault, northern Falcón basin, northwestern Venezuela. *Tectonophysics*, v. 308, p. 23-35.
- Aydin, A. and Nur, A., 1985, The types and role of stepovers in strike-slip tectonics. *In*: Biddle, K. and Christie-Blick, N., eds., *Strike-slip deformation, basin formation, and sedimentation*, Tulsa, Society of Economic Paleontologists and Mineralogists, Special Publication 37, p. 35-44.
- Babb, S. and Mann, P., 1999, Structural and sedimentary development of a Neogene transpressional plate boundary between the Caribbean and South America plates in Trinidad and the Gulf of Paria. *In*: Mann, P., ed.,

- Caribbean Basins. *Sedimentary Basins of the World*, 4, Amsterdam, Elsevier, p. 495-557.
- Barber, A. J., Tjokrosoepoetro and Charlton, T. R., 1986, Mud volcanoes, shale diapirs, wrench faults, and melanges in accretionary complexes, eastern Indonesia. *The American Association of Petroleum Geologists Bulletin*, v. 70, p. 1729-1741.
- Bartok, P., 1993, Pre-breakup geology of the Gulf of Mexico-Caribbean; its relation to Triassic and Jurassic rift systems of the region. *Tectonics*, v. 12, p. 441-459.
- Bates, R. L. and Jackson, J. A., eds., 1984, *Dictionary of geological terms*: New York, Doubleday, 571 p.
- Ben-Avraham, Z. and Zoback, M., 1992, Transform-normal extension and asymmetric basins: An alternative to pull-apart models. *Geology*, v. 20, p. 423-426.
- Boesi, T., 1978, Resumen sobre el origen de las acumulaciones de hidrocarburos en la Fm. Misoa, area del lago de Maracaibo. Informe privado. Maraven, S.A.
- Boesi, T., and Goddard, D., 1991, A new geological model related to the distribution of hydrocarbon source rocks in the Falcón basin, northwestern Venezuela. *In*: Biddle, K., ed., *Active margin basins*, The American Association of Petroleum Geologists, Memoir 52, p. 303-319.
- Borges, R., 1984, Mapa geológico estructural de Venezuela (1:250000): Ministerio de Energía y Minas, Caracas, Venezuela
- BP, 2002, Statistical review. http://www.bp.com/downloads/1087/statistical_review.pdf (accessed April, 2003)
- Bradley, D and Kidd, W., 1991, Flexural extension of the upper continental crust in collisional foredeeps. *Geological Society of America Bulletin*, v. 103, p. 1416-1438.
- Brown, A., ed., 1996, *Interpretation of Three-Dimensional Seismic Data*, Tulsa, The American Association of Petroleum Geologists, Memoir 42, 424 p.
- Burke, K., 1988, Tectonic evolution of the Caribbean. *Annual Review of Earth and Planetary Sciences*, v. 16, p. 201-230.

- Carr, t., Hopkins, J., Feldman, H., Feltz, A., Doveton, J. and D. Collins, 1995, 2-D and 3-D Pseudo-seismic transform of wireline logs: A seismic approach to petrophysical sequence stratigraphy. <http://www.kgs.ukans.edu/PRS/publication/carr.html> (accessed December, 2002)
- Carter, R., Van Gils, J. L., Walton, W., Fah, Y. and Buk, S., 1997, Application of a new high resolution sequence stratigraphy for reservoir modeling studies of the upper Miocene deltaic reservoirs of the Champion field, offshore Brunei Darussalam. *In: 18th Annual Research Conference, Shallow Marine and Nonmarine Reservoirs*, p. 67-91.
- Castillo, M. V., 2001, Structural analysis of Cenozoic fault systems using 3D seismic data in the southern Maracaibo basin, Venezuela: (unpublished Ph.D. dissertation) The University of Texas at Austin, Austin, 189 p.
- Chatellier, J-Y, Mendez, M., Hague, P. and Navarro, A., 1998, Shale mobility in western Venezuela, implications for maturity studies and prospectivity. *In: AAPG Annual Convention Expanded Abstract*.
- Christie-Blick, N. and Biddle, K., 1985, Deformation and basin formation along strike-slip faults. *In: Biddle, K. and Christie-Blick, N., eds., Strike-slip deformation, basin Formation, and sedimentation, Tulsa, Society of Economic Paleontologists and Mineralogists, Special Publication 37, p. 1-34.*
- Cloetingh, S., 1986, Intraplate stresses: A new element in basin analysis. *In: Kleinspehn, K. and Paola, C., eds., New Perspectives in Basin Analysis, Spring-Verlag, New York, p. 205-230.*
- Colmenares, L. and Zoback, M., in press, Stress field and seismotectonics of northern South America. *Geology*.
- Cooper, M. A., Williams, G. D., De Gracainsky, P. C., Murphy, R.W., Needham, T., De Paor, D., Stoneley, R., Todd, S. P., Turner, J. P. and Ziegler, P. A., 1989, Inversion tectonics - A discussion. *In: Cooper, M. A. and Williams, G. D., eds., Inversion Tectonics, Geological Society, Special Publication 44, p. 335-347.*
- Cooper, M., Addison, F., Alvarez, R., Hayward, A., Howe, S., Pulham, A. and Taborda, A., 1995, Basin development and tectonic history of the Llanos basin, Colombia. *In: Tankard, A., Suarez, S. and Welsink, H., eds., Petroleum basins of South America, The American Association of Petroleum Geologists, Memoir 62, p. 659-665.*

- Crampton, S. L. and Allen, P. A., 1995, Recognition of forebulge unconformities associated with early stage foreland basin development: Example from the north Alpine foreland basin. *The American Association of Petroleum Geologists Bulletin*, v. 79, p. 1495-1514.
- CSC, S.A Consultores, 1990, Estudio sedimentológico de núcleos del pozo W8 Campo Centro Lago. Lagoven S.A., 137 p.
- CSC, S.A Consultores, 1991a, Estudio sedimentológico de núcleos del pozo W11 Campo Centro Lago. Lagoven S.A., 24 p.
- CSC, S.A Consultores, 1992, Estudio sedimentológico de núcleos del pozo W12 Campo Centro Lago. Lagoven S.A., 107 p.
- CSC, S.A Consultores, 1993, Estudio sedimentológico de núcleos del pozo W5 Campo Centro Lago. Lagoven S.A., 107 p.
- CSC, S.A. Consultores, 1989, Estudio sedimentológico de núcleos del pozo W3 Campo Centro Lago Estado Zulia. Lagoven, S.A., 69 p.
- CSC, S.A. Consultores, 1991b, Estudio sedimentológico de núcleos del pozo W18 Campo Centro Lago Estado Zulia. Lagoven, S.A., 45 p.
- CSC, S.A. Consultores, 1996, Estudio sedimentológico de núcleos del pozo W7 Campo Centro Lago Estado Zulia. Lagoven, S.A., 37 p.
- Di Croce, J., 1995, Eastern Venezuela basin: Sequence stratigraphy and structural evolution: (unpublished Ph.D. dissertation) Rice University, Houston, 245 p.
- Di Croce, J., Bally, A. and Vail, P., 1999, Sequence Stratigraphy of the eastern Venezuela basin. *In: Mann, P., ed., Caribbean Basins. Sedimentary Basins of the World*, 4, Amsterdam, Elsevier, p. 419-476.
- Díaz de Gamero, M. L., 1996, The changing course of the Orinoco river during the Neogene: a review. *Palaeogeography, Palaeoclimatology, Palaeoecology*, v. 123, p. 385-402.
- Driscoll, N. W. and Diebold, J. B., 1999, Tectonic and stratigraphic development of the eastern Caribbean: New constraints from multichannel seismic data. *In: Mann, P., ed., Caribbean Basins, Sedimentary Basins of the World*, 4, Amsterdam, Elsevier Science B. V., p. 591-626.

- Duerto, L., 1998, Principales zonas triangulares de Venezuela: (unpublished M.Sc. thesis) Universidad Central de Venezuela, Caracas, 176 p.
- Emery, D. and Myers, K. J., 1996, Sequence Stratigraphy, Blackwell Science Ltd, 297 p.
- Erlich, R. and Barret, S., 1992, Petroleum Geology of eastern Venezuela foreland basin. *In*: Macqueen, R. and Leckie, D., eds., Foreland basins and fold belts, The American Association of Petroleum Geologists, Memoir 55, p. 341-362.
- Escalona, A. and MacDonalds, C., 1998, 3D characterization of the upper member C2X, east flank of the north dome, Centro Lago field, Lake Maracaibo. *The Leading Edge*, v. 17, p. 1748-1752.
- Escalona, A. and Mann, P., 2003a, Paleogene depocenter along the NE margin of the Maracaibo basin: Structure along an exhumed Eocene age lateral ramp fault in western Venezuela. *In*: AAPG Annual Meeting Expanded Abstracts.
- Escalona, A. and Mann, P., 2003b, Three-dimensional structural architecture and evolution of the Eocene pull-apart basin, central Maracaibo basin, Venezuela. *Marine and Petroleum Geology*, v. 20, p. 141-161.
- Galloway, W., 1989, Genetic stratigraphic sequences in basin analysis I: Architecture and genesis of flooding-surface bounded depositional units. *The American Association of Petroleum Geologists Bulletin*, v. 73, p. 125-142.
- Galloway, W., 1998, Clastic depositional systems and sequences: Applications to reservoir prediction, delineation, and characterization. *The Leading Edge*, v. 17, p. 173-180.
- Galloway, W. and Hobday, D., 1996, Terrigenous clastic depositional systems, Berlin, Springer, 489 p.
- Garfunkel, Z. and Ben-Avraham, Z., 1996, The structure of the Dead Sea basin. *Tectonophysics*, v. 266, p. 155-176.
- Gil, J. and Trautnitz, M., 1995, Center Lake integrated study 3D seismic interpretation. Lagoven, Unidad Occidente, Proyecto Centro Lago, 32 p.

- Giles, K. and Dickinson, W., 1995, The interplay of eustasy and lithospheric flexure in forming stratigraphic sequence in foreland settings: An example from the Antler foreland, Nevada and Utah. *In: Dorobek, S. and Ross, G., eds., Stratigraphic evolution of foreland basins, Society of Economic Paleontologists and Mineralogists, Special Publication 52, p. 187-211.*
- Gölke, M. and Cloetingh, S., 1994, Finite-element modelling of pull-apart basin formation. *Tectonophysics, v. 240, p. 45-57.*
- González de Juana, C., Iturralde, J. and Picard, X, 1980a, Geología de Venezuela y de sus Cuencas Petrolíferas, v. I and II: Caracas, Ediciones Foninves, 407 p.
- Gradstein, F., Agterberg, F., Ogg, J. Hardenbol, J., Van Veen, P., Thierry, J. and Huang, Z., 1995, A Triassic, Jurassic and Cretaceous time scale. *In: Kent, W., Aubry, M. and Hardenbol, J., eds., Geochronology, time scales and global stratigraphy correlation, Society of Economic Paleontologists and Mineralogists, Special Publication 54, p. 95-126.*
- Hamilton, D., Fouad, K., Barba, R. Jr., Holtz, M. and Fimlay, C., 1998, Characterization of reservoirs in the Tertiary section of Block B in the south of Lake Maracaibo. *The Leading Edge, v. 17, p. 1754-1758.*
- Haq, B., Hardenbol, J. and Vail, P., 1988, Mesozoic and Cenozoic chronostratigraphy and cycles of relative sea level change. *In: Wilgus, C., Hastings, B., Kendall, C., Posamentier, H., Ross, C. and Van Wagoner, J., eds., Sea level changes: An integrated approach, Society of Economic Paleontologists and Mineralogists, Special Publication 42, p. 3-17.*
- Hardenbol, J., Thierry, J., Farley, M., de Graciansky, P-C and Vail, P., 1998, Mesozoic and Cenozoic sequence chronostratigraphic framework of European basins. *In: De Graciansky, P-C, Hardenbol, J., Jaquin, T. and Vail, P., eds., Mesozoic and Cenozoic sequence stratigraphic of European basins, Society of Economic Paleontologists and Mineralogists, 60, p. 3-13.*
- Harding, T. and Tuminas, A., 1989, Structural interpretation of hydrocarbon traps sealed by basement normal block faults at stable flank of foredeep basins and at rift basins. *The American Association of Petroleum Geologists Bulletin, v. 73, p. 812-840.*
- Harding, T., Vierbuchen, R. C. and Christie-Blick, N. H., 1985, Structural styles, plate tectonic settings, and hydrocarbon traps of divergent (transtensional)

- wrench faults. *In*: Biddle, K. and Christie-Blick, N., eds., Strike-slip deformation, basin formation and sedimentation, Tulsa, Society of Economic Paleontologists and Mineralogists, Special Publication 37, p. 51-77.
- Hempton, M. and Neher, K., 1986, Experimental fracture, strain and subsidence patterns over *en echelon* strike-slip faults: Implications for the structural evolution of pull-apart basins. *Journal of Structural Geology*, v. 8, p. 597-605.
- Hippolyte, J., Badescu, D. and Constantin, P., 1999, Evolution of the transport of the Carpathian belt during its collision with the east European platform. *Tectonics*, v. 18, p. 1120-1138.
- Instituto de Investigaciones Petroleras de la Universidad del Zulia, 1991, Análisis convencionales, pozo: W12. Lagoven, S.A., internal report n. ST-126-91, 37 p
- International Reservoir Technologies, Inc., 1997, Integrated reservoir study of Block VIII, Center Lake Maracaibo. Phase I report and phase II proposal. Maraven, S.A. (Filial de Petróleos de Venezuela), 57 p.
- Jason Geosystems, BV, 1997, Introduction to trace-based inversion and modeling, training manual. Jason Geoscience Workbench.
- Kasper, D. A. and Laure, D. K., 1986, Paleogeographic and tectonic implications of quartzose sandstones of Barbados. *Tectonics*, v. 5, p. 837-854.
- Kellogg, J. N., 1984, Cenozoic tectonic history of the Sierra de Perijá, Venezuela-Colombia, and adjacent basins. *In*: Bonini, W.E., Hargraves, R. B. and Shagam, R., eds., The Caribbean-South American plate boundary and regional tectonics, Geological Society of America, Memoir 162, p. 239-261.
- Kendall, C. and Lerche, I., 1988, The rise and fall of eustacy. *In*: Wilgus, C., Hastings, B., Kendall, C., Posamentier, H., Ross, C. and Van Wagoner, J., eds., Sea level changes; an integrated approach, Society of Economic Paleontologists and Mineralogists, Special Publication 42, p. 3-17.
- Krause, H., 1971, La Falla de Icotea en los Bloques I de las concesiones de la Compañía Shell de Venezuela en el Lago de Maracaibo. *In*: III Jornadas Técnicas de Petróleo, Maracaibo, Venezuela, p. 20.

- Lear, C., Elderfield, H. and Wilson, P., 2000, Cenozoic deep-sea temperatures and global ice volumes from Mg/Ca in benthic foraminiferal calcite. *Science*, v. 287, p. 269-272.
- León, P., 1997, Seismic and geological characterization of the middle Eocene Misoa formation, Centro Lago field, Maracaibo basin, Venezuela: (unpublished M.Sc. thesis) The University of Texas at Austin, Austin, 82 p.
- León, P., Camposano, C., Moya, M. and Brink, G., 1999, Extensional and compressional structural influence upon the stratigraphic framework of Eocene and Oligocene sequences, South Lake Maracaibo basin, Venezuela. The American Association of Petroleum Geologists Annual Meeting, Expanded Abstracts, p. A79.
- Linzer, H., Ratschbacher, L. and Frisch, W., 1995, Transpressional collision structures in the upper crust: The fold-thrust belt of the Northern Calcareous Alps. *Tectonophysics*, v. 242, p. 41-61.
- Lowell, J., 1995, Mechanism of basin inversion from worldwide examples. *In*: Buchanan, J. and Buchanan, P., eds., Basin inversion, Geological Society, Special Publication 88, p. 39-57.
- Lugo, J., 1991, Cretaceous to Neogene tectonic control on sedimentation: Maracaibo basin, Venezuela: (unpublished Ph.D. dissertation) The University of Texas at Austin, Austin, 219 p.
- Lugo, J. and Mann, P., 1995, Jurassic-Eocene tectonic evolution of Maracaibo basin, Venezuela. *In*: Tankard, A., Suarez, S. and Welsink, H., eds., Petroleum basins of South America, The American Association of Petroleum Geologists, Memoir 62, p. 699-725.
- Maguregui, J. A., 1990, Evolution and reservoir rock properties of middle Eocene tide-dominated deltaic sandstones in eastern Lagunillas field, Maracaibo basin, Venezuela: (unpublished M.Sc. thesis) The University of Texas at Austin, Austin, 172 p.
- Mann, P., 1999a, Tectonic and exploration significance of lateral ramp faults in the circum-Caribbean region. American Association of Petroleum Geologists Annual Meeting, Expanded Abstract, p. A88.
- Mann, P., 1999b, Caribbean sedimentary basins: Classification and tectonic setting from Jurassic to present. *In*: Mann, P., ed., Caribbean Basins.

- Sedimentary Basins of the World, 4, Amsterdam, Elsevier Science B. V., p. 3-31.
- Mann, P. and Burke, K., 1984, Neotectonics of the Caribbean. *Reviews of Geophysics and Space Physics*, v. 22, p. 309-362.
- Mann, P., Gahagan, L. and Gordon, M., in press, Tectonic setting of the world's giant oil fields. *In: Halbouty, M., ed., Giant Oil Fields of the Decade, 1999-2000, AAPG Memoir.*
- Mann, P., Hempton, M. R., Bradley, D. C. and Burke, K., 1983, Development of pull-apart basins. *Journal of Geology*, v. 91, p. 529-554.
- Mann, P., Taylor, F. W., Lawrence, R. and Ku, T., 1995, Actively evolving microplate formation by oblique collision and sideways motion along strike-slip faults: An example from the northeastern Caribbean plate margin. *Tectonophysics*, v. 246, p. 1-69.
- Mathieu, X., 1989, La Serranía de Trujillo-Ziruma aux confins du bassin de Maracaibo, de la Sierra du Falcón et de la Chaîne Caraïbe. Lithostratigraphie, tectonique (surface-subsurface) et évolution géodynamique: (unpublished Ph.D dissertation) L'Université de Bretagne Occidentale, Bretagne, 264 p.
- McClay, K. and Dooley, T., 1995, Analogue models of pull-apart basins. *Geology*, v. 23, p. 711-714.
- Miall, A., 1997, *The geology of stratigraphic sequences*: Berlin, Springer-Verlag, 433 p.
- Muessig, K. W., 1984, Structure and Cenozoic tectonics of the Falcón basin, Venezuela, and adjacent areas. *In: Bonini, W.E., Hargraves, R. B. and Shagam, R., eds., The Caribbean-South American plate boundary and regional tectonics, Geological Society of America, Memoir 162, p. 217-230.*
- Munro, S., 1985, Lake Maracaibo revisited. *In: VI Congreso Venezolano de Geología*, p. 2540-2551.
- Munro, S. E. and Smith, F. D. Jr., 1984, The Urica fault zone, northeastern Venezuela. *In: Bonini, W.E., Hargraves, R. B. and Shagam, R., eds., The Caribbean-South American plate boundary and regional tectonics, Geological Society of America, Memoir 162, p. 213-215.*

- Nasa, <http://zulu.ssc.nasa.gov/mrsid> (accessed March, 2003)
- Naylor, M., Mandl, G. and Sijpesteijn, C. H. K., 1986, Fault geometries in basement induced wrench faulting under different initial stress states. *Journal of Structural Geology*, v. 8, p. 737-752.
- Parnaud, Y., Gou, Y., Pascual, J., Capello, M. A., Truskowski, I. and Passalacqua, H., 1995b, Stratigraphic synthesis of Western Venezuela. *In: Tankard, A., Suarez, S. and Welsink, H., eds., Petroleum basins of South America*, The American Association of Petroleum Geologists, Memoir 62, p. 681-698.
- Parnaud, Y., Gou, Y., Pascual, J., Truskowski, I., Gallango, O. and Passalacqua, H., 1995a, Petroleum geology of the central part of the Eastern Venezuela basin. *In: Tankard, A., Suarez, S. and Welsink, H., eds., Petroleum basins of South America*, The American Association of Petroleum Geologists, Memoir 62, p. 741-756.
- PDVSA E&P Occidente and Veba Oil, 1998, Estudio integrado Centro Lago-Miembro C4X. Volumen I: Modelo estático. PDVSA E&P Occidente, Unidad de Explotación Centro Lago, 75 p.
- Pérez, O., Bilham, R., Bendick, R., Velandia., J., Hernandez, C., Hoyer, M. and Kozuch, M., 2001, Velocity field across the southern Caribbean plate boundary and estimates of Caribbean-South American plate motion using GPS geodesy 1994-2000. *Geophysical Research Letters*, v. 28, p. 2987-2990.
- Pindell, J. and Kennan, L., in press, Processes and events in the terrane assembly of Trinidad and Eastern Venezuela. *In: Special Publication of the Geological Society of Trinidad and Tobago*.
- Pindell, J., Higgs, R. and Dewey, J., 1998, Cenozoic palinspatic reconstruction, paleogeographic reconstruction and hydrocarbon setting of the northern margin of South America. *Paleogeographic evolution and non-glacial eustasy, Northern South America*, Society for Sedimentary Geology, 45-85.
- Pindell, J.L. and Barret, S. F., 1990, Geological evolution of the Caribbean region: A plate tectonic perspective. *In: Dengo, G. and Case, J. E., eds., The Caribbean Region, The Geology of North America: The Geology of North America*, p. 405-432.

- Pinto, J., 1991, Sequence stratigraphic interpretation of upper Paleocene-middle Eocene rocks: Block III, Lake Maracaibo: (unpublished M.Sc. thesis) The University of Texas at Austin, Austin, 150 p.
- Pitman III, W. C., 1978, Relationship between eustacy and stratigraphic sequences of passive margins. *Geological Society of America Bulletin*, v. 89, p. 1389-1403.
- Raeuchle, S., Ambrose, W., Saleem, A., Casas, J., Salamanca, L., Muñoz, P. and León, A., 1997, Integrated reservoir study, lower Eocene Misoa reservoirs, Lagunillas field, Lake Maracaibo, Venezuela. *The Leading Edge*, v. 16, p. 1335-1337.
- Ralph, A. and Mitchum, R., 1997, Sequence stratigraphy controls on Cotton Valley tight gas sandstones, Carthage field, Panola county, Texas. *In: 18th Annual Research Conference, Shallow Marine and Nonmarine Reservoirs*, p. 409-425.
- Reading, H., 1980, Characteristics and recognition of strike-slip fault systems. *In: Ballance, P. and Reading, H., eds., Sedimentation in oblique-slip mobile zones, Special Publication of the International Association of Sedimentologists*, 4, p. 7-26.
- Renz, O., 1981, Venezuela. *In: Reymont, R. A. and Bengtson, P., eds., Aspects of Mid-Cretaceous Regional Geology*, New York, Academic Press, p. 197-220.
- Rod, E., 1956, Strike-slip faults of northern Venezuela. *The American Association of Petroleum Geologists Bulletin*, v. 40, p. 457-476.
- Rodgers, D., 1980, Analysis of pull-apart basin development produced by *en echelon* strike-slip faults. *In: Ballance, P. and Reading, H., eds., Sedimentation in oblique-slip mobile zones, Special publication of the International Association of Sedimentologists*, 4, p. 27-41.
- Roure, F., Colleta, B., De Toni, B., Loureiro, D., Passalacqua, H. and Gou, Y., 1997, Within-plate deformations in the Maracaibo and east Zulia basins, western Venezuela. *Marine and Petroleum Geology*, v. 14, p. 139-163.
- Rull, V., 2002, High-impact palynology in petroleum geology: Applications from Venezuela (northern South America). *American Association of Petroleum Geologists Bulletin*, v. 86, p. 279-300.

- Ryan, H. F. and Coleman, P. J., 1992, Composite transform-convergent plate boundaries: Description and discussion. *Marine and Petroleum Geology*, v. 9, p. 89-97.
- Sandwell, D. and Smith, W., 1997, Marine gravity anomaly from Geosat and ERS 1 satellite altimetry. *Journal of Geophysical Research*, B, v. 102, p. 10039-10054.
- Schubert, C., 1982, Neotectonics of Boconó fault, western Venezuela. *Tectonophysics*, v. 85, p. 205-220.
- Schubert, C., Sifontes, R., Padron, V., Velez, J. and Loiza, P., 1979, Formación la Quinta (Jurásico) Andes Merideños: Geología de la sección tipo. *Acta Científica Venezolana*, v. 30, p. 42-55.
- Schumm, S. A., 1977, *The fluvial system*: New York, Wiley-Interscience, 338 p.
- Sheriff, R. and Geldart, L., 1995, *Exploration Seismology*, Cambridge University Press, 592 p.
- Stephan, J. F., 1977, El contacto Cadena Caribe-Andes Merideños entre Carora y el Tocuyo (edo. Lara): Observaciones sobre el estilo y la edad de las deformaciones Cenozoicas en el occidente Venezolano. *In: V Congreso Geológico Venezolano*, p. 789-815.
- Stephan, J. F., 1985, Andes et Chaîne Caraïbe sur La Transversal de Barquisimeto (Venezuela), Evolution géodynamique. *In: Géodynamique des Caraïbes, Symposium*, p. 505-529.
- Sylvester, A. G., 1988, Strike-slip faults. *Geological Society of America Bulletin*, v. 100, p. 1666-1703.
- Taboada, A., Rivera, L., Fuenzalida, A., Cisternas, A., Philip, H., Bijwaard, H., Olaya, J. and Rivera, C., 2000, Geodynamics of the northern Andes: Subductions and intracontinental deformation (Colombia). *Tectonics*, v. 19, p. 787-813.
- Thomas, W. A., 1990, Controls on locations of transverse zones in thrust belts. *Eclogae geol.*, v. 83, p. 727-744.
- Torres-Verdin, C., Victoria, M., Merletti, G. and Pendrel, J., 1999, Trace-based and geostatistical inversion of 3-D seismic data for thin-sand delineation:

- An application in San Jorge basin, Argentina. *The Leading Edge*, v. 18, p. 1070-1077.
- Trenkamp, R., Kellogg, J., Freymueller, J. and Mora, H., 2002, Wide plate margin deformation, southern Central America and northwestern South America, CASA GPS observations. *Journal of South American Earth Sciences*, v. 15, p. 151-171.
- Tyler, N., 1988, New oil from old fields. *Geotimes*, July 1983, p. 8-10.
- Vail, P. R., Mitchum, R. M. Jr., Todd, R. G. and Sangree, J. B., 1977, Seismic stratigraphy and global changes of sea level. *In: Payton, C. E., ed., Seismic stratigraphy-application to hydrocarbon exploration*, The American Association of Petroleum Geologists, Memoir 26, p. 49-212.
- Van Veen, F., 1972, Ambientes sedimentarios de las formaciones Mirador y Misoa del Eoceno inferior y medio en la cuenca del lago de Maracaibo. *Boletín de Geología Publicación Especial*, Caracas, Venezuela, v. 5, p. 1073-1104.
- Van Wagoner, J., Mitchum, R., Champion, K. and Rahmanian, V., 1990, Siliciclastic sequence stratigraphy in well logs, cores, and outcrops: concepts for high resolution correlation of time and facies: *Methods in Exploration series*, v. 7, The American Association of Petroleum Geologists, 55 p.
- Villamil, T., 1999, Campanian-Miocene tectonostratigraphy, depocenter evolution and basin development of Colombia and western Venezuela. *Palaeogeography, Palaeoclimatology, Palaeoecology*, v. 153, p. 239-275.
- Warne, A., Aslan, A., White, W., Gibeaut, J., Tremblay, T., Smyth, R., Guevara, E., and others, 1999, Geo-environmental characterization of the Delta del Orinoco, Venezuela. The University of Texas at Austin, Bureau of Economic Geology, Center for space Research and PDVSA/DAO.
- Wheeler, C. B., 1963, Oligocene and Lower Miocene stratigraphy of western and northeastern Falcón basin, Venezuela. *The American Association of Petroleum Geologists Bulletin*, v. 47, p. 35-68.
- White, T., Furlong, K. and Arthur, M., 2002, Forebulge migration in the Cretaceous Western Interior basin of the central United States. *Basin Research*, v. 14, p. 43-54.

- Wilcox, R., Ronald, E., Harding, T. P. and Seely, D. R., 1973, Basic wrench tectonics. *The American Association of Petroleum Geologists Bulletin*, v. 57, p. 74-96.
- Wood, R., Pettinga, J. R., Bannister, S., Lamarche, G. and McMorran, T.J., 1994, Structure of the Hanmer strike-slip basin, Hope fault, New Zealand. *Geological Society of America Bulletin*, v. 106, p. 1459-1473.
- Worrall, D. M. and Snelson, S., 1989, Evolution of the northern Gulf of Mexico, with emphasis on Cenozoic growth faulting and the role of salt. *In: Bally, A. and Palmer, A., eds., The Geology of North America; An Overview: The Geology of North America*, The Geological Society of America, v. A, p. 97-138.
- Xiao, H. and Suppe, J., 1992, Origin of rollover. *The American Association of Petroleum Geologists Bulletin*, v. 76, p. 509-529.
- Young, A., Monaghan, P. and Schweisberger, R. T., 1977, Calculation of ages of hydrocarbon oils-Physical chemistry applied to petroleum geochemistry I. *The American Association of Petroleum Geologists Bulletin*, v. 61, p. 573-600.
- Zambrano, E., Vásquez, E., Duval, B., Latreille, M. and Coffinieres, B., 1971, Síntesis paleogeográfica y petrolera del occidente de Venezuela. *In: Cuarto Congreso Geológico Venezolano*, p. 483-552.
- Zeng, H., Backus, M., Barrow, K. and Tyler, N., 1998, Stratal slicing, part I: Realistic 3-D seismic model. *Geophysics*, v. 63, p. 502-513.

Vita

Alejandro Escalona was born in Caracas, Venezuela on February 7, 1973, to Cesar Alberto Escalona and Maria Edilia Varela de Escalona. After graduating from the Colegio Santiago de Leon de Caracas, he attended the Universidad Central de Venezuela, where he graduated in 1995 with a BS in geophysical engineer.

In 1995, he began work with PDVSA as a reservoir engineer and production geophysicist for oil fields in the central Maracaibo basin, Venezuela. In 1997, he became a lecturer in geophysics at the Universidad del Zulia in Maracaibo, and in 1999 he became a lecturer in geophysics at the Universidad Central de Venezuela in Caracas. In the spring of 2000, he entered the Department of Geological Sciences of the University of Texas at Austin to pursue a Ph.D. degree in Geological Sciences. During his Ph.D. studies, he was a teaching assistant for several graduate-level courses and was a graduate research assistant at the BEG and UTIG. He married Sylvia Nordfjord, another Ph.D. student in the geology, in April, 2003.

Permanent address: Av. Rómulo Gallegos, Res. Parque Sebucán, Apto. 71, Caracas, Venezuela.

This dissertation was typed by Alejandro Escalona. All figures were created by the author in Landmark Graphics Corporation® and Microsoft Office®.